REPUBLIQUE DU CAMEROUN
Paix-Travail-Patrie
****
UNIVERSITE DE YAOUNDE I
****
CENTRE DE RECHERCHE ET DE FORMATION DOCTORALE EN SCIENCES, TECHNOLOGIES ET GEOSCIENCES
****
UNITE DE RECHERCHE ET DE FORMATION DOCTORALE PHYSIQUES ET APPLICATIONS
****
DEPARTEMENT DE PHYSIQUE
****
P.O Box: 812, Yaoundé
Email: crfd_stg@uy1.uninet.cm

REPUBLIC OF CAMEROON
Peace-Work-Fatherland
****
UNIVERSITY OF YAOUNDE I
****
POSTGRADUATE SCHOOL FOR SCIENCE, TECHNOLOGY AND GEOSCIENCE
****
RESEARCH AND POSTGRADUATE TRAINING UNIT FOR PHYSICS AND APPLICATIONS
****
DEPARTMENT OF PHYSICS
****
P.O Box: 812, Yaounde
Email: crfd_stg@uy1.uninet.cm

LABORATORY OF MECHANICS, MATERIALS AND STRUCTURES

SPATIOTEMPORAL DYNAMICS OF LIGHT BULLETS IN A NONLOCAL OPTICAL FIBER

THESIS

Submitted and defended publicly in fulfillment of the requirements for the degree of **Doctor of Philosophy** in Physics

Speciality: **Mechanics, Materials and Structures**
Option: **Fundamental Mechanics and complex systems**

Written and Presented by:
KABADIANG NGON Ghislaine Flore
Registration number: **09W0916**
M. Sc. in Physics

Under the supervision of

KOFANE Timoléon Crépin
Professor,
University of Yaounde I

Year 2025

UNIVERSITE DE YAOUNDE I
UNIVERSITY OF YAOUNDE I

FACULTE DES SCIENCES
FACULTY OF SCIENCE

DEPARTEMENT DE PHYSIQUE
DEPARTMENT OF PHYSICS

ATTESTATION DE CORRECTION DE LA THESE DE DOCTORAT/Ph.D

Nous, Professeurs **BOUETOU BOUETOU Thomas, DJUIDJE KENMOE Germaine** et Professeur **BEN-BOLIE Germain Hubert**, respectivement Examinateurs et Président du jury de la thèse de Doctorat/Ph.D de Madame **KABADIANG NGON Ghislaine Flore**, Matricule **09W0916**, préparée sous la direction du Professeur **KOFANE Timoléon Crépin,** intitulée « **Spatiotemporal dynamics of light bullets in a nonlocal optical fiber** », soutenue le **vendredi 31 octobre 2025**, en vue de l'obtention du grade de Docteur/Ph.D en Physique, spécialité Mécanique, Matériaux et Structures, option Mécanique Fondamentale et Systèmes Complexes, attestons que toutes les corrections demandées par le Jury de soutenance ont été effectuées.

En foi de quoi, la présente attestation lui est délivrée pour servir et valoir ce que de droit.

Fait à Yaoundé le 05 NOV 2025

Examinateurs

Pr BOUETOU BOUETOU Thomas

Pr DJUIDJE KENMOE Germaine

Le Président du Jury

Pr BEN-BOLIE Germain Hubert

Le Chef de Département de Physique

UNIVERSITE DE YAOUNDE I * FACULTE DES SCIENCES * DEPARTEMENT DE PHYSIQUE
Le Chef de Département

Ben-Bolie Germain Hubert
Professeur

ANNÉE ACADEMIQUE 2025/2026

(Par Département et par Grade)

DATE D'ACTUALISATION 24 Septembre 2025

ADMINISTRATION

1. **DOYEN :** OWONO OWONO Luc Calvin, *Professeur*
2. **VICE-DOYEN / DPSAA :** NDJIGUI Paul-Désiré, *Professeur*
3. **VICE-DOYEN / DSSE :** NYEGUE Maximilienne Ascension, *Professeur*
4. **VICE-DOYEN / DRC :** NOUNDJEU Pierre, *Maître de Conférences*
5. **Chef Division Administrative et Financière :** NDOYE FOE Florentine Marie Chantal, *Maître de Conférences*
6. **Chef Division des Affaires Académiques, de la Recherche et de la Scolarité DAARS :** AJEAGAH Gideon AGHAINDUM, *Professeur*

1- DÉPARTEMENT DE BIOCHIMIE (BC) (44)

N°	NOMS ET PRÉNOMS	GRADE	OBSERVATIONS
1.	BIGOGA DAIGA Jude	Professeur	En poste
2.	KANSCI Germain	Professeur	En poste
3.	MBACHAM FON Wilfred	Professeur	En poste
4.	NJAYOU Frédéric Nico	Professeur	*Chef de Département*
5.	NGUEFACK Julienne	Professeur	En poste
6.	NJAYOU Frédéric Nico	Professeur	En poste
7.	OBEN Julius ENYONG	Professeur	En poste
8.	ACHU Merci BIH	Maître de Conférences	En poste
9.	BEBEE Fadimatou	Maître de Conférences	En poste
10.	BEBOY EDJENGUELE Sara N.	Maître de Conférences	En poste
11.	FONKOUA Martin	Maître de Conférences	En poste
12.	AKINDEH MBUH NJI	Maître de Conférences	En poste
13.	ATOGHO Barbara MMA	Maître de Conférences	En poste
14.	AZANTSA KINGUE GABIN BORIS	Maître de Conférences	En poste
15.	BELINGA née NDOYE FOE F. M. C.	Maître de Conférences	*Chef DAF / FS*
16.	DAKOLE DABOY Charles	Maître de Conférences	En poste
17.	DONGMO LEKAGNE Joseph Blaise	Maître de Conférences	En poste
18.	DJUIDJE NGOUNOUE Marceline	Maître de Conférences	En poste
19.	DJUIKWO NKONGA Ruth Viviane	Maître de Conférences	En poste
20.	EFFA ONOMO Pierre	Maître de Conférences	*VD/FS/Univ Ebwa*
21.	EWANE Cécile Annie	Maître de Conférences	En poste
22.	KENGNE NOUEMSI Anne Pascale	Maître de Conférences	En poste
23.	KOTUE TAPTUE Charles	Maître de Conférences	En poste
24.	LUNGA Paul KEILAH	Maître de Conférences	En poste
25.	MANANGA Marlyse Joséphine	Maître de Conférences	En poste
26.	MBONG ANGIE M. Mary Anne	Maître de Conférences	En poste
27.	MOFOR née TEUGWA Clotilde	Maître de Conférences	*Doyen FS / UDs*
28.	NANA Louise épouse WAKAM	Maître de Conférences	En poste
29.	NGONDI Judith Laure	Maître de Conférences	En poste
30.	Palmer MASUMBE NETONGO	Maître de Conférences	En poste
31.	PECHANGOU NSANGOU Sylvain	Maître de Conférences	En poste
32.	BAKWO BASSOGOG Christian Bernard	Chargé de Cours	En poste
33.	ELLA Fils Armand	Chargé de Cours	En poste
34.	EYENGA Eliane Flore	Chargée de Cours	En poste
35.	FOUPOUAPOUOGNIGNI Yacouba	Chargé de Cours	En poste
36.	KOUOH ELOMBO Ferdinand	Chargé de Cours	En poste
37.	MADIESSE KEMGNE Eugenie Aimée	Chargée de Cours	En poste
38.	MANJIA NJIKAM Jacqueline	Chargée de Cours	En poste
39.	MBOUCHE FANMOE Marceline J.	Chargée de Cours	En poste
40.	OWONA AYISSI Vincent Brice	Chargé de Cours	En poste

41.	WILFRED ANGIE ABIA	Chargé de Cours	En poste
42.	WOGUIA Alice Louise	Chargée de Cours	En poste

2- DÉPARTEMENT DE BIOLOGIE ET PHYSIOLOGIE ANIMALES (BPA) (50)

1.	AJEAGAH Gideon AGHAINDUM	Professeur	*DAARS/FS*
2.	DJIETO LORDON Champlain	Professeur	En poste
3.	DZEUFIET DJOMENI Paul Désiré	Professeur	En poste
4.	ESSOMBA née NTSAMA MBALA	Professeure	*CD et Vice Doyen/FMSB/UYI*
5.	KEKEUNOU Sévilor	Professeur	*Chef de Département*
6.	MEGNEKOU Rosette	Professeure	En poste
7.	NJAMEN Dieudonné	Professeur	En poste
8.	NOLA Moïse	Professeur	En poste
9.	TCHUEM TCHUENTE Louis Albert	Professeur	*Inspecteur de service / Coord.Progr./MINSANTE*
10.	ZEBAZE TOGOUET Serge Hubert	Professeur	En poste

11.	ALENE Désirée Chantal	Maître de Conférences	*Vice Doyen/ Uté Ebwa*
12.	ATSAMO Albert Donatien	Maître de Conférences	En poste
13.	BILANDA Danielle Claude	Maître de Conférences	En poste
14.	DJIOGUE Séfirin	Maître de Conférences	En poste
15.	GOUNOUE KAMKUMO Raceline épse FOTSING	Maître de Conférences	En poste
16.	JATSA BOUKENG Hermine épse MEGAPTCHE	Maître de Conférences	En Poste
17.	KANDEDA KAVAYE Antoine	Maître de Conférences	En poste
18.	LEKEUFACK FOLEFACK Guy B.	Maître de Conférences	En poste
19.	MAHOB Raymond Joseph	Maître de Conférences	En poste
20.	MBENOUN MASSE Paul Serge	Maître de Conférences	En poste
21.	MOUNGANG Luciane Marlyse	Maître de Conférences	En poste
22.	NOAH EWOTI Olive Vivien	Maître de Conférences	En poste
23.	MONY Ruth épse NTONE	Maître de Conférences	En Poste
24.	MVEYO NDANKEU Yves Patrick	Maître de Conférences	En poste
25.	NGUEGUIM TSOFACK Florence	Maître de Conférences	En poste
26.	NGUEMBOCK	Maître de Conférences	En poste
27.	TADU Zephyrin	Maître de Conférences	En poste
28.	TAMSA ARFAO Antoine	Maître de Conférences	En poste
29.	TOMBI Jeannette	Maître de Conférences	En poste
30.	YEDE	Maître de Conférences	En poste

31.	AMBADA NDZENGUE GEORGIA ELNA	Chargée de Cours	En poste
32.	BASSOCK BAYIHA Etienne Didier	Chargé de Cours	En poste
33.	ETEME ENAMA Serge	Chargé de Cours	En poste
34.	FEUGANG YOUMSSI François	Chargé de Cours	En poste
35.	KENGNE Alvine Christelle Epse FOKAM	Chargée de Cours	En poste
36.	FOSSI TANKOUA Olivia Epse DJEUTCHOUANG SAYANG	Chargée de Cours	En poste
37.	GONWOUO NONO Legrand	Chargé de Cours	En poste
38.	KOGA MANG Dobara	Chargé de Cours	En poste

39.	LEME BANOCK Lucie	Chargée de Cours	En poste
40.	MAPON NSANGOU Indou	Chargé de Cours	En poste
41.	METCHI DONFACK Mireille Flaure EPSE GHOUMO	Chargée de Cours	En poste
42.	NDENGUE Jean De Matha	Chargé de Cours	En poste
43.	NGOUATEU KENFACK Omer Bébé	Chargé de Cours	En poste
44.	NJUA Clarisse YAFI	Chargée de Cours	*Cheffe Div. U. Bamenda*
45.	NWANE Philippe Bienvenu	Chargé de Cours	En poste
46.	YOUNOUSSA LAME	Chargé de Cours	En poste
47.	ZEMO GAMO Franklin	Chargé de Cours	En poste

48.	KODJOM WANCHE Jacguy Joyce	Assistante	En poste

3- DÉPARTEMENT DE BIOLOGIE ET PHYSIOLOGIE VÉGÉTALES (BPV) (37)

1.	AMBANG Zachée	Professeur	*Chef de Département*
2.	BIYE Elvire Hortense	Professeure	En poste
3.	DJOCGOUE Pierre François	Professeur	En poste
5.	NDONGO BEKOLO	Professeur	En poste

7.	ANGONI Hyacinthe	Maître de Conférences	En poste
8.	DJEUANI Astride Carole	Maître de Conférences	En poste
9.	MAHBOU SOMO TOUKAM Gabriel	Maître de Conférences	En poste
10.	MALA Armand William	Maître de Conférences	En poste
12.	NGALLE Hermine BILLE	Maître de Conférences	En poste
13.	NGONKEU MAGAPTCHE Eddy L.	Maître de Conférences	*CT/MINRESI*
14.	TONFACK Libert Brice	Maître de Conférences	En poste
16.	ONANA Jean Michel	Maître de Conférences	En poste

17.	DIDA LONTSI Sylvere Landry	Chargé de Cours	En poste
18.	GONMADGE Christelle	Chargé de Cours	En poste
19.	MAFFO MAFFO Nicole Liliane	Chargé de Cours	En poste
20.	MANGA NDJAGA JUDE	Chargé de Cours	En poste
21.	NNANGA MEBENGA Ruth Laure	Chargée de Cours	En poste
22.	NOUKEU KOUAKAM Armelle	Chargée de Cours	En poste
23.	NSOM ZAMBO EPSE PIAL Annie Claude	Chargée de Cours	*En détachement/UNESCO MALI*
24.	GODSWILL NTSOMBOH NTSEFONG	Chargé de Cours	En poste
25.	KABELONG BANAHO Louis-Paul-Roger	Chargé de Cours	En poste
26.	KONO Léon Dieudonné	Chargé de Cours	En poste
27.	LIBALAH Moses BAKONCK	Chargé de Cours	En poste
28.	LIKENG-LI-NGUE Benoit C	Chargé de Cours	En poste
29.	TAEDOUNG Evariste Hermann	Chargé de Cours	En poste
30.	TEMEGNE NONO Carine	Chargée de Cours	En poste
31.	BOLIE Hubert	Assistant	En poste
33.	MACHE NKOUANDEU Pasma	Assistante	En poste
34.	MAFFO FOKOU Adèle	Assistante	En poste
35.	METSEBING Blondo-Pascal	Assistant	En poste
36.	NTONMEN YPNKEU Amandine Flore	Assistante	En poste
37.	ONANA EBODE Clotaire	Assistant	En poste

4- DÉPARTEMENT DE CHIMIE INORGANIQUE (CI) (28)

1.	GHOGOMU Paul MINGO	Professeur	*Ministre Chargé de Mission PR*
2.	NANSEU NJIKI Charles Péguy	Professeur	En poste
3.	NDIFON Peter TEKE	Professeur	*CT MINRESI*
4.	NGOMO Horace MANGA	Professeur	*Vice Chancelor/UB*
5.	NJIOMOU C. épse DJANGANG	Professeur	En poste
6.	NJOYA Dayirou	Professeur	En poste

7.	ACAYANKA Elie	Maître de Conférences	En poste
8.	EMADAK Alphonse	Maître de Conférences	En poste
9.	KAMGANG YOUBI Georges	Maître de Conférences	En poste
10.	KEMMEGNE MBOUGUEN Justin C.	Maître de Conférences	En poste
11.	KENNE DEDZO GUSTAVE	Maître de Conférences	En poste
12.	MBEY Jean Aimé	Maître de Conférences	En poste
13.	NDI Julius NSAMI	Maître de Conférences	*Chef de Département*
14.	NEBAH Née NDOSIRI Bridget NDOYE	Maître de Conférences	*Sénatrice/SENAT*
15.	NYAMEN Linda Dyorisse	Maître de Conférences	En poste
16.	PABOUDAM GBAMBIE AWAWOU	Maître de Conférences	En poste
17.	TCHAKOUTE KOUAMO Hervé	Maître de Conférences	En poste
18.	BELIBI BELIBI Placide Désiré	Maître de Conférences	*Chef Service/ ENS Bertoua*
19.	CHEUMANI YONA Arnaud M.	Maître de Conférences	En poste
20.	KOUOTOU DAOUDA	Maître de Conférences	En poste

21.	MAKON Thomas Beauregard	Chargé de Cours	En poste
22.	NCHIMI NONO KATIA	Chargée de Cours	En poste
23.	NJANKWA NJABONG N. Eric	Chargé de Cours	En poste
24.	PATOUOSSA ISSOFA	Chargé de Cours	En poste
25.	SIEWE Jean Mermoz	Chargé de Cours	En Poste
26.	BOYOM TATCHEMO Franck W.	Assistant	En Poste
27.	DANTIO NGUELA Christian Brice	Assistant	En poste
28.	LEKENE NGOUATEU Reine	Assistant	En poste

6- DÉPARTEMENT DE CHIMIE ORGANIQUE (CO) (33)			
1.	Alex de Théodore ATCHADE	Professeur	*DEPE/Univ. Bertoua*
2.	NGOUELA Silvère Augustin	Professeur	*Chef de Département/UDS*
3.	PEGNYEMB Dieudonné Emmanuel	Professeur	*Recteur UBertoua/ Chef de Département*
4.	MKOUNGA Pierre	Professeur	En poste
5.	AMBASSA Pantaléon	Maître de Conférences	En poste
6.	EYONG Kenneth OBEN	Maître de Conférences	*Director/HTTTC/UBda*
7.	FOTSO WABO Ghislain	Maître de Conférences	En poste
8.	KAMTO Eutrophe Le Doux	Maître de Conférences	En poste
9.	KENMOGNE Marguerite	Maître de Conférences	En poste
10	MVOT AKAK CARINE	Maître de Conférences	En poste
11	NGOMO Orléans	Maître de <conférences	En poste
12	NGO MBING Joséphine	Maître de Conférences	*Chef de Cellule MINRESI*
13	NGONO BIKOBO Dominique Serge	Maître de Conférences	*Chef Div./MINESUP*
14	NOTE LOUGBOT Olivier Placide	Maître de Conférences	*Dir ENS/Uté Bertoua*
15	NOUNGOUE TCHAMO Diderot	Maître de Conférences	En poste
16	TABOPDA KUATE Turibio	Maître de Conférences	En poste
17	TAGATSING FOTSING Maurice	Maître de Conférences	En poste
18	OUAHOUO WACHE Blandine M.	Maître de Conférences	En poste
19	ZONDEGOUMBA Ernestine	Maître de Conférences	En poste
20.	MELONG Radius	Chargé de Cours	En poste
21.	MESSI Angélique Nicolas	Chargé de Cours	En poste
22.	MUNVERA MFIFEN Aristide	Chargé de Cours	En poste
23.	NGNINTEDO Dominique	Chargé de Cours	En poste
24.	NONO NONO Éric Carly	Chargé de Cours	En poste
25.	OUETE NANTCHOUANG Judith Laure	Chargée de Cours	En poste
26.	SIELINOU TEDJON Valérie	Chargé de Cours	En poste
27.	TCHAMGOUE Joseph	Chargé de Cours	En poste
28.	TSAFFACK Maurice	Chargé de Cours	En poste
29.	TSAMO TONTSA Armelle	Chargée de Cours	En poste
30.	TSEMEUGNE Joseph	Chargé de Cours	En poste
31.	NDOGO ETEME Olivier	Assistant	En poste
32.	NGUEMDJO CHIMEZE Valery Wilfried	Assistant	En poste

6- DEPARTEMENT DES ENERGIES RENOUVELABLES (ER) (1)			
1.	BODO Bertrand	Professeur	*Chef de Département*

7- DÉPARTEMENT D'INFORMATIQUE (INF) (22)			
1.	ATSA ETOUNDI Roger	Professeur	*Chef de Division des SI/MINESUP*
2.	FOUDA NDJODO Marcel Laurent	Professeur	*Inspecteur Général Académique/ MINESUP*
3.	NDOUNDAM René	Professeur	En poste
4.	ABESSOLO ALO'O Gislain	Maître de Conférences	*CT1/MINFOPRA*
5.	MELATAGIA YONTA Paulin	Maitre de Conférences	En poste
6.	TSOPZE Norbert	Maître de Conférences	En poste

6.	AMINOU HALIDOU	Chargé de Cours	*Chef de Département*
7.	DJAM Xaviera YOUH - KIMBI	Chargée de Cours	En Poste
8.	DOMGA KOMGUEM Rodrigue	Chargé de Cours	En poste
9.	EBELE Serge Alain	Chargé de Cours	En poste
10.	EKODECK Stéphane Gaël Raymond	Chargé de Cours	En poste
11.	HAMZA Adamou	Chargé de Cours	En poste
12.	JIOMEKONG AZANZI Fidel	Chargé de Cours	En poste
13.	KOUOKAM KOUOKAM E. A.	Chargé de Cours	En poste
15.	MESSI NGUELE Thomas	Chargé de Cours	*Chef de Département/Génie Info./U Ebolowa*
16.	MONTHE DJIADEU Valery M.	Chargé de Cours	En poste
17.	NZEKON NZEKO'O Armel Jacques	Chargé de Cours	En poste
18.	OLLE OLLE Daniel Claude Georges Delort	Chargé de Cours	*Directeur Adjoint ENSET Ebolowa*
19.	TAPAMO Hyppolite	Chargé de Cours	En poste

20.	BAYEM Jacques Narcisse	Assistant	En poste
21.	MAKEMBE. S. Oswald	Assistant	*Directeur CUTI*
22.	MAXWELL NDOGNKON MANGA	Assistant	En poste
23.	NDOM Francis Rollin	Assistant	En poste
24.	NGUIMEYA TSOFACK Baudoin	Assistant	En poste
24.	NKONDOCK. MI BAHANACK. N.	Assistant	En poste

8- DÉPARTEMENT DE MATHÉMATIQUES (MA) (34)

1.	AYISSI Raoult Domingo	Professeur	*Chef de Département/D. ENSPY*

2.	KIANPI Maurice	Maître de Conférences	En poste
3.	MBANG Joseph	Maître de Conférences	En poste
4.	MBEHOU Mohamed	Maître de Conférences	*Chef de Division/ENSPY*
5.	MBELE BIDIMA Martin Ledoux	Maître de Conférences	En poste
6.	NOUNDJEU Pierre	Maître de Conférences	*VDRC/FS/UYI*
7.	TAKAM SOH Patrice	Maître de Conférences	En poste
8.	TCHAPNDA NJABO Sophonie B.	Maître de Conférences	*Directeur/AIMS Rwanda*
9.	TCHOUNDJA Edgar Landry	Maître de Conférences	En poste

10.	AGHOUKENG JIOFACK Jean Gérard	Chargé de Cours	*Chef Cellule MINEPAT*
11.	BOGSO ANTOINE Marie	Chargé de Cours	En poste
12.	BITYE MVONDO Esther	Chargé de Cours	En poste
13.	CHENDJOU Gilbert	Chargé de Cours	En poste
14.	DJIADEU NGAHA Michel	Chargé de Cours	En poste
15.	DOUANLA YONTA Herman	Chargé de Cours	En poste
16.	KIKI Maxime Armand	Chargé de Cours	En poste
17.	KOKOMO AYISSI Eric Brice	Chargé de Cours	En poste (transfert de l'université de Douala)
18.	LOUMNGAM KAMGA Victor	Chargé de Cours	En poste
19.	MBAKOP Guy Merlin	Chargé de Cours	En poste
20.	MBATAKOU Salomon Joseph	Chargé de Cours	En poste
21.	MENGUE MENGUE David Joël	Chargé de Cours	*Chef Dpt /ENS Université d'Ebolowa*
22.	MBIAKOP Hilaire George	Chargé de Cours	En poste
23.	NGUEFACK Bertrand	Chargé de Cours	En poste
24.	NIMPA PEFOUKEU Romain	Chargée de Cours	En poste
25.	OGADOA AMASSAYOGA	Chargée de Cours	En poste
26.	POLA DOUNDOU Emmanuel	Chargé de Cours	*En stage*
27.	TENKEU JEUFACK Yannick Léa	Chargé de Cours	En poste
28.	TCHEUTIA Daniel Duviol	Chargé de Cours	En poste
29.	TETSADJIO TCHILEPECK M. Eric.	Chargé de Cours	En poste

30.	EBODE ATANGANA Pie Désiré	Assistant	En poste
31.	FOKAM Jean Marcel	Assistant	En poste
32.	GUIDZAVAI KOUCHERE Albert	Assistant	En poste
33.	MAMA ASSANDJE Prosper	Assistant	En poste

34.	MANN MANYOMBE Martin Luther	Assistant	En poste
35.	MEFENZA NOUNTU Thiery	Assistant	En poste
36.	NYOUMBI DLEUNA Christelle	Assistant	En poste

9 - DÉPARTEMENT DE MICROBIOLOGIE (MIB) (24)

1.	ESSIA NGANG Jean Justin	Professeur	*Chef de Département*
2.	KOUITCHEU MABEKU Epse KOUAM Laure Brigitte	Professeure	En poste
3.	MUNE MUNE Martin Alain	Professeur	En poste
4.	NYEGUE Maximilienne Ascension	Professeure	*Vice-Doyen / DSSE*
5.	SADO KAMDEM Sylvain Leroy	Professeur	En poste
6.	ASSAM ASSAM Jean Paul	Maître de Conférences	*Doyen/FASA/UDs*
7.	BOUGNOM Blaise Pascal	Maître de Conférences	En poste
8.	NJIKI BIKOÏ Jacky	Maître de Conférences	En poste
9.	TCHIKOUA Roger	Maître de Conférences	*Chef de Service de la Scolarité*
10	EHETH Jean Samuel	Chargé de Cours	En poste
11	ESSONO Damien Marie	Chargé de Cours	En poste
12	EZO'O MENGO Fabrice Télésfor	Chargé de Cours	En poste
13	LAMYE Glory MOH	Chargé de Cours	En poste
14	MEYIN A EBONG Solange	Chargée de Cours	En poste
15	MONI NDEDI Esther Del Florence	Chargée de Cours	*Cheffe de service/DAAC/UYI*
16	NKOUDOU ZE Nardis	Chargé de Cours	En poste
17	NKOUE TONG Abraham	Chargé de Cours	En poste
18	NGOUENAM Romial Joël	Chargé de Cours	En poste
19	NJAPNDOUNKE Bilkissou	Chargé de Cours	En poste
20	TAMATCHO KWEYANG Blandine Pulchérie	Chargée de Cours	En poste
21	SAKE NGANE Carole Stéphanie	Chargée de Cours	En poste
22	TOBOLBAÏ Richard	Chargé de Cours	En poste
23	ZO'O EZO'O Fabrice Télesfor	Assistant	En poste
24	MAYI Marie Paule Audrey	Assistante	En poste

10. DEPARTEMENT DE PHYSIQUE (PHY) (45)

1.	BEN- BOLIE Germain Hubert	Professeur	*Chef de Département*
2.	BIYA MOTTO Frédéric	Professeur	*DG/HYDRO Mekin*
3.	DJUIDJE KENMOE ép. ALOYEM	Professeur	En poste
4.	EKOBENA FOUDA Henri Paul	Professeur	*Vice-Recteur. Uté Ngaoundéré*
5.	ESSIMBI ZOBO Bernard	Professeur	En poste
6.	EYEBE FOUDA Jean sire	Professeur	En poste
7.	FEWO Serge Ibraïd	Professeur	En poste
8.	HONA Jacques	Professeur	En poste
9.	NANA ENGO Serge Guy	Professeur	En poste
10.	NANA NBENDJO Blaise	Professeur	*Chef de Département/Uni. Bertoua*
11.	NDJAKA Jean Marie Bienvenu	Professeur	*Chef de Département/UIT Bois*
12.	NJANDJOCK NOUCK Philippe	Professeur	En poste
13.	SAIDOU	Professeur	*Chef de centre/IRGM/MINRESI*
14.	SIEWE SIEWE Martin	Professeur	En poste
15.	SIMO Elie	Professeur	En poste
16.	TABOD Charles TABOD	Professeur	*Doyen FS/Univ/Bda*
17.	TCHAWOUA Clément	Professeur	En poste
18.	WOAFO Paul	Professeur	En poste
19.	ZEKENG Serge Sylvain	Professeur	En poste
20.	VONDOU Derbetini Appolinaire	Professeur	En poste

21.	ENYEGUE A NYAM épse BELINGA	Maître de Conférences	*Cheffe de Div./ENSPY*
22.	FOUEJIO David	Maître de Conférences	*Chef Cell/MINADER*
23.	MBINACK Clément	Maître de Conférences	En poste
24.	MBONO SAMBA Yves Christian U.	Maître de Conférences	En poste
25.	MELI'I Joelle Larissa	Maître de Conférences	En poste
26.	MVOGO ALAIN	Maître de Conférences	En poste
27.	NDOP Joseph	Maître de Conférences	En poste
28.	WAKATA née BEYA Annie Sylvie	Maître de Conférences	*Secrétaire Générale /UYII*
29.	WOULACHE Rosalie Laure	Maître de Conférences	*Absente de son poste*
30.	ABDOURAHIMI	Chargé de Cours	En poste
31.	AYISSI EYEBE Guy François Valérie	Chargé de Cours	En poste
32.	CHAMANI Roméo	Chargé de Cours	En poste
33.	DJIOTANG TCHOTCHOU Lucie Angennes	Chargée de Cours	En poste
34.	EDONGUE Hervais	Chargé de Cours	En poste

35.	KAMENI NEMATCHOUA Modeste	Chargé de Cours	En poste
36.	LAMARA Maurice	Chargé de Cours	En poste
37.	NGA ONGODO Dieudonné	Chargé de Cours	En poste
38.	OTTOU ABE Martin Thierry	Chargé de Cours	Chef de Div./DIPD/UYI
39.	SOUFFO TAGUEU Merimé	Chargé de Cours	En poste
40.	TCHAPET NJAFA Jean-Pierre	Chargé de Cours	Chef Ser. Adj./FLASH/UYI
41.	TEYOU NGOUPO Ariel	Chargé de Cours	En poste
42.	TOGUEU MOTCHEYO Alain Bertrand	Chargé de Cours	En poste
43.	WANDJI NYAMSI William	Chargé de Cours	En poste
44.	ETEME Armand Sylvin	Assistant	En poste
45.	NGO MOUELLAS épouse LOTHIN	Assistante	En poste
46.	TCHODIMOU Carole	Assistant	En poste
47.	SOUFFO TAGUEU Merimé	Assistant	En poste

11- DÉPARTEMENT DE SCIENCES DE LA TERRE (ST) (34)

1.	BISSO Dieudonné	Professeur	*Chef de Département*
2.	EKOMANE Emile	Professeur	*Chef Div./Uté Ebolowa*
3.	GANNO Sylvestre	Professeur	En poste
4.	NDJIGUI Paul-Désiré	Professeur	*Vice-Doyen /DPSAA*
5.	NGUEUTCHOUA Gabriel	Professeur	*CEA/MINRESI*
6.	NGOS III Simon	Professeur	En poste
7.	NKOUMBOU Charles	Professeur	En poste
8.	ONANA Vincent Laurent	Professeur	*Chef de Département/Uté. Eb.*
9.	YENE ATANGANA Joseph Q.	Professeur	*Chef Div. /MINTP*
10.	TCHOUANKOUE Jean Pierre	Professeur	En poste

11.	Elisé SABABA	Maitre de Conférences	En poste
12.	EYONG John TAKEM	Maître de Conférences	En poste
13.	FUH Calistus Gentry	Maître de Conférences	*Sec. D'Etat/MINMIDT(ai)*
14.	MAMDEM TAMTO Lionelle Estelle, épouse BITOM	Maitre de Conférences	En poste
15.	MBIDA YEM	Maître de Conférences	En poste
16.	MBESSE Cécile Olive	Maitre de Conférences	En poste
17.	METANG Victor	Maître de Conférences	En poste
18.	NGO BIDJECK Louise Marie	Maître de Conférences	En poste
19.	NJILAH Isaac KONFOR	Maître de Conférences	En poste
20.	NTSAMA ATANGANA Jacqueline	Maître de Conférences	En poste
21.	TCHAKOUNTE Jacqueline épse NUMBEM	Maître de Conférences	*Chef. Cell /MINRESI*
22.	TCHAPTCHET TCHATO De P.	Maître de Conférences	En poste
23.	TEMGA Jean Pierre	Maître de Conférences	En poste
24.	ZO'O ZAME Philémon	Maître de Conférences	*DG/ART*

25.	ANABA ONANA Achille Basile	Chargé de Cours	En poste
26.	KOAH NA LEBOGO Serge P.	Chargé de Cours	En poste
27.	NGO BELNOUN Rose Noël	Chargée de Cours	En poste
28.	NGO'O ZE ARNAUD	Chargé de Cours	En poste
29.	NOMO NEGUE Emmanuel	Chargé de Cours	En poste
30.	TEHNA Nathanaël	Chargé de Cours	En poste
31.	TENE DJOUKAM Joëlle Flore, épouse KOUANKAP NONO	Chargée de Cours	En poste
32.	FEUMBA Roger	Chargé de Cours	En poste
33.	MBANGA NYOBE Jules	Chargé de Cours	En poste

Dedication

To my beloved husband, **Pierre Marius NGATAT TCHATA**,

and my parents, **Yves** & **Sygnone FRANCO** and **AMBASSA ASSIENE Dieudonné**,

with love and gratitude.

Acknowledgments

My sincere gratitude is extended to all those who, near and far, have played a part in supporting me during my doctoral years and contributed to the completion of this document, either directly or indirectly.

First of all, I am grateful to **GOD ALMIGHTY** for the breath of life, for the strength and motivation to keep going through all these years of research, "*for it is **God** which worketh in me both to will and to do of his good pleasure*".

Next, I would like to thank the **members of the JURY** for the honor of attending this defense and judging this scientific work.

I would also like to express my sincere gratitude to Professor **KOFANE Timoléon Crépin**, my thesis supervisor. I had the opportunity to work with you since my Master's degree, which was a very good start in scientific research. I would not have had the privilege to appreciate this subject if you had not thought it through, reflected on it and proposed it. Professor KOFANE Timoleon Crepin, with these few words I would like to express my gratitude for your inspiration and dedication to research, which inspire me so much. I am very grateful for your invaluable advice, continuous support and patience.

Furthermore, I wish to acknowledge the valuable support of Professor **BEN-BOLIE Germain Hubert**, Head of the Department of Physics, for his administrative contribution and encouragement.

I am equally grateful to Professor **NDJAKA Jean Marie Bienvenu**, Professor **TCHAWOUA Clément**, Professor **Thomas BOUETOU BOUETOU**, Professor **WOAFO Paul**, Professor **Conrad B. TABI**, Professor **Serge Ibraïd FEWO**, Professor **Germaine DJUIDJE**, Professor **Martin SIEWE SIEWE**, Professor **MBANE BIOUELE**, Professor **MVOGO alain**, Dr. **Dieudonné NGA ONGODO** , and **all the other teachers in the Physics Department**, who have contributed to my progress by teaching, supporting, advice and intellectual contribution.

My sincere thanks are also intended to the members of our Laboratory of Mechanics, Materials and Structures of the University Yaounde I and my other classmates for their contributions. I would particularly like to name Dr. **DJOKO Martin**, Dr. **DJAZET Alain**, Dr. **AMBASSA OTSOBO Jenny Alban**, for playing a very important accompanying role since I started this thesis.

I am deeply indebted to my parents **Sygnone FRANCO**, **Yves FRANCO** and **AMBASSA ASSIENE Dieudonné** for their unfailing support and encouragement. To my brothers and sisters, especially the eldest,

Professor **ASSIENE NGON Patrick Henri** and his wife Dr. **ASSIENE MBENA KAMGA Tatiana**. To my elder sister **MEKO NGON Francine Hortense** and her husband **TOUKOULOU Pierre Severin**. To the youngest, **KOFANE NGON Moise** and **AMBASSA AMBASSA Franck Dieudonné**.

To my uncle **ASSA KOFANE Raphael**.

To the **ASSIENE** and **KOFANE** families.

To my parents and family in law the **TCHATA's** family for their support.

My heartfelt thanks also go to all my brothers and sisters in Christ, especially to **Mr** & **Mrs NDJIGUI** (Georges and Mathilde), **Mr** & **Mrs LANGKEU NDJIKAM** (Francis and Eveline), **Mr** & **Mrs YOUNG** (Leonard and Florence), **Mr** & **Mrs MOUBEKE** (Moussa and Regine), **Mr. NANGUE** Maurice, **Mr** & **Mrs MEDI** (Jonathan and Josiane), **Mr** & **Mrs BEB** (Julien and grâce), **Mr** & **Mrs BEBEY** (Jacques and Pauline), **Mr** & **Mrs BASSANG-NA** (Roger and Edwige), **Mr** & **Mrs NKONO** (Ernest and Jeannine), **Mrs BESSEM** Margaret, **Mrs ATALA** Sylvie, **Mr. BILÉ** Cédric, **Mr** & **Mrs EVINA**, **Mr** & **Mrs LOBE** (Orphée and Nicole), **Mr** & **Mrs VUNDA MANSONI** (Faustin and Carole), **Mr** & **Mrs BOLOKO**, **Mr** & **Mrs KEMOUGNE** (David and Charlotte), all the branch coordinators in Douala, the **TOGO 2024** advanced-class Group V, the TOGO 2024 advanced-class Group Cameroon, the **Advanced Group Cameroon** July 2025, and my fellowship household, for their love and support.

Words fail me when it comes to thanking my adorable husband **Pierre Marius NGATAT TCHATA**, for his unconditional love. Not a day goes by that I don't thank God for giving me such an understanding and caring husband. Despite life's ups and downs, during this PhD project, your love was strong enough to withstand any adversity and support me. Thank you, my husband.

Throughout this work, you have given me peaks of joy and valleys of love. Without his love and support, the completion of this work would never have been possible. Our wonderful **daughter NZIA TCHATA LOÏS ZARA** was born during these years of research and the joy of receiving her has motivated me to keep going.

Finally, I wish to extend my sincere apologies to anyone I may unintentionally omitted. Your support and encouragement have been deeply appreciated and will never be forgotten.

Contents

List of abbreviations

Acronym	Meaning
LBs:	Light Bullets
LB:	Light Bullet
GVD:	Group Velocity Dispersion
SPM:	Self-Phase Modulation
MI:	Modulation Instability
EDFA:	Erbium-Doped Fiber Amplifier
EDFAs:	Erbium-Doped Fiber Amplifiers
CGL:	Complex Ginzburg-Landau
CCGLE:	Cubic Complex Ginzburg-Landau Equation
CQ:	Cubic-Quintic
CQCGLE:	Cubic-Quintic Complex Ginzburg-Landau Equation
(1+1)-D:	(1+1)-Dimensional
(2+1)-D:	(2+1)-Dimensional
(3+1)-D:	(3+1)-Dimensional
SMF:	Single Mode Fiber
MMF:	Multimode Fiber
STIN:	Step-Index

Acronym	Meaning
GRIN:	Graded-Index
LED:	Light-Emitting Diode
PMD:	Polarization Mode-Dispersion
SBS:	Stimulated Brillouin Scattering
SRS:	Stimulated Raman Scattering
FWM:	Four-Wave Mixing
XPM:	Cross-Phase Modulation
OC:	Optical Connection
OT:	Optical Transmitter
OR:	Optical Receiver
ONN:	Optical Network Nodes
SNR:	Signal-to-Noise Ratio
PD:	Photodetector
SOA:	Semiconductor Optical Amplifiers
RA:	Raman Amplifiers
ReDFA:	Rare-earth Doped Fiber Amplifiers
NLSE:	Nonlinear Schrödinger Equation
RK:	Runge-Kutta
RK4:	Fourth-Runge-Kutta
MRK4:	Fourth-Runge-Kutta Method
SSFM:	Split-Step Fourier Method
FODEs:	First-Order Differential Equations

List of Figures

Abstract

Starting from Maxwell's theory of electromagnetic waves, we derived extended (3+1)-D cubic and cubic-quintic complex Ginzburg-Landau equations that describe the spatiotemporal dynamics of dissipative light bullets in optical fiber amplifiers under the interplay between dopants and a spatially nonlocal nonlinear response.

Derived model equations include the effects of gain saturation, gain dispersion, fiber dispersion, fiber nonlinearity, atomic detuning, diffractive transverse effects, and nonlocal nonlinear response. To gain physical insight into relevant light bullet parameters, including the amplitude, temporal and spatial pulse widths, and position of the pulse maximum, unequal wavefront curvatures, chirp parameters, and phase shift, we derived a system of eight coupled ordinary differential equations for each model equation using the variational approach based on the Euler-Lagrange equations. Moreover, in the context of the Routh-Hurwitz stability criterion, we first construct a Jacobi determinant, and then verify the necessary and sufficient conditions for stability by examining the characteristic polynomial equation derived from the determinant.

Numerical studies are then conducted on the obtained variational equations, using the fourth-order Runge-Kutta method for the spatial evolution and the split-step Fourier method for the temporal evolution.

Keywords: *Spatiotemporal dynamics, cubic nonlinearity, cubic-quintic nonlinearity, light bullets, nonlocality, doped nonlocal optical fiber, variational approach, Routh-Hurwitz stability criterion, Fourth-order Runge-Kutta method, split-step Fourier method.*

Résumé

À partir de la théorie des ondes électromagnétiques de Maxwell, nous dérivons des équations cubiques et cubiques-quintiques de Ginzburg-Landau étendues en (3+1)-D, qui décrivent la dynamique spatio-temporelle des balles de lumière dissipatives dans les amplificateurs à fibre optique, sous l'action des dopants et d'une réponse non linéaire spatialement non locale. Les équations modèles dérivées incluent les effets de saturation du gain, de dispersion du gain, de dispersion de la fibre, de nonlinéarité de la fibre, de désaccord atomique, d'effets transversaux diffractifs et de réponse nonlinéaire nonlocale.

Pour obtenir un aperçu physique des paramètres pertinents des balles de lumière, qui comprennent l'amplitude, les largeurs d'impulsion temporelle et spatiale, la position du maximum d'impulsion, les courbures inégales du front d'onde, les paramètres de chirp et le déphasage, nous dérivons un système de huit équations différentielles ordinaires couplées pour chaque équation modèle en utilisant l'approche variationnelle basée sur les équations d'Euler-Lagrange. De plus, dans le contexte du critère de stabilité de Routh-Hurwitz, nous construisons d'abord un déterminant de Jacobi, puis nous vérifions les conditions nécessaires et suffisantes pour la stabilité en examinant l'équation polynomiale caractéristique dérivée du déterminant.

Des études numériques sont finalement menées sur les équations variationnelles obtenues, en utilisant la méthode de Runge-Kutta de quatrième ordre pour l'évolution spatiale et la méthode de Fourier à pas fractionné pour l'évolution temporelle.

***Mots clés**: Dynamique spatio-temporelle, non-linéarité cubique, non-linéarité cubique-quintique, balles de lumière, nonlocalité, fibre optique dopée nonlocale, approche variationnelle, critère de stabilité de Routh-Hurwitz, méthode de Runge-Kutta de quatrième ordre, méthode de Fourier à pas fractionné.*

General Introduction

The spatiotemporal dynamics of light bullets is a broad and complex research area that has attracted considerable attention over the past decade.

Spatiotemporal dynamics encompasses both temporal and spatial effects, which, in the context of optical fibers, describe the propagation of optical pulses under appropriate conditions. The solutions resulting are called optical solitons.

Optical solitons have promising potential to become principal information carriers in telecommunication due to their capability of propagating long-distance signals without attenuation and without changing their shapes. One of the primary goals in the field of soliton physics is the generation of light fields that are localized in all three dimensions of space as well as in time, which we will refer to as (3+1)-D spatiotemporal solitons or light bullets (LBs).

LBs can also be called dissipative solitons in the case of dissipative systems, i.e. systems that require a continuous supply of matter and/or energy. Dissipative solitons are self-organizing structures in space and time, resulting from a double equilibrium. On the one hand, the simultaneous balance between diffraction and group velocity dispersion (GVD) by the transverse self-focusing and nonlinear self phase-modulation (SPM) in the longitudinal direction, respectively [1]. On the other, the balance between gains and losses [2].

Considerable attention is being paid theoretically and experimentally to analyze the dynamics of spatial optical solitons in materials exhibiting local nonlinear and nonlocal nonlinear responses [3-4].

The local nonlinearity of optical media is usually approximated by a local function of the light intensity implying that the change in refractive index at a given spatial location depends solely

on the light intensity at that location. In contrast, nonlocal nonlinearity means that the change of the refractive index in a particular point is determined by the light intensity not only in the same point but also in its vicinity.

Recent findings indicate that nonlocality can lead to new effects, such as strong modifications to modulational instability (MI) [5-6], suppression of beam collapse [7], dramatic change of the soliton interaction [8, 9], formation of multi-soliton bound states [10], stabilization of spatially localized vortex solitons [11], symmetry breaking azimuthal instability [12, 13] as well as stabilization of different nonlinear structures such as ringlike clusters of many solitons [14] and modulated localized vortex beams or azimuthons [15].

When transmitting information over long distances via optical fibers, it is essential to deal with the attenuation issue, as it reduces the energy of the soliton propagating in the fiber. The soliton then undergoes broadening as reduced peak power weakens the SPM effect necessary to counteract the GVD.

The first solution found and approved by scientists and laboratories in the 1990s involved periodically restoring the soliton signal using repeaters or electrical regenerators.

Regenerators, consisting of a receiver-transmitter combination, were placed at specific intervals between the initial optical transmitter and the final receiver. Some laboratories were moving away from this method due to its prohibitive costs, highlighting the need for more affordable alternatives.

An alternative they adopted was the deployment of optical amplifiers that could directly regenerate the optical soliton signal without the need to convert it into an electrical signal.

Doping optical fibers with rare earth ions, such as Neodymium, Erbium, Praseodymium, and Ytterbium, introduced additional energy and matter, resulting in doped fiber amplifiers. The most prominent type of doped fiber amplifier is the erbium-doped fiber amplifier (EDFA)[16-17].

On the other hand, there are interesting studies on the pulse propagation problem in doped fiber amplifiers within the rate equation approximation. The governing equations for these studies are the complex Ginzburg-Landau (CGL) equations and their variants: the complex cubic Ginzburg-Landau equation (CCGLE) and the complex cubic-quintic Ginzburg-Landau equation (CQCGLE) [18-22]. CCGLE and CQCGLE can account for the inherent phenomena in optical fibers, including dispersion, attenuation, diffraction, nonlinearities, and external dissipative effects such as losses

and gains. These factors are essential for localized structures, or solitons, in optical fibers [1].

In some previous studies [23-29], multidimensional spatiotemporal optical solitons, i.e., both (2+1)-dimensional [(2+1)-D] and (3+1)-dimensional [(3+1)-D] dissipative optical bullets were considered using the (2+1)-D and (3+1)-D family of CGL equations. Stable spatiotemporal dissipative solitons have been documented in various forms, stationary stable and pulsating solutions, double, quadruple, sixfold, eightfold, and tenfold bullet complexes, self-trapped necklace-ring, ring-vortex solitons, uniform ring beams, spherical and rhombic distributions of LBs, fundamental and cluster solitons, respectively.

Recently, the stability diagram from the Lenz transformation and the linear stability analysis have revealed that higher values of the quintic nonlocality contributed to the reduction of the MI in weakly CQ nonlocal nonlinear media [30]. Recent findings have indicated that the instability regions from the pure quartic MI gain in weakly nonlocal birefringent fibers were more expanded due to nonlocality, which, via direct numerical illustrations, showed the emergence of Akhmediev breathers [27,31,32].

For a nonlinear saturable media with competing nonlocal nonlinearity, the quenching effect of the nonlocal nonlinearity on the MI has been corrected, especially when the saturable index and the nonlocality range were well-balanced [33].

So, questions naturally arise: can we prevent both attenuation and collapse in optical fiber propagation by combining doping effects with spatial nonlocality?

Or is it possible to simultaneously manage the doping parameters and the spatial nonlocality coefficient in fiber-optic propagation to counteract attenuation and avoid collapse?

The primary goal of the present Ph.D thesis is to investigate (3+1)-D dissipative LBs in fiber amplifiers under the interplay between dopant and a spatially nonlocal nonlinear response, which, to the best of our knowledge, has not yet been proposed in the literature. We mainly focus on the localized Gaussian solution in the form of three-dimensional traveling waves.

The remaining part of this thesis is organized as follows.

Chapter I covers a review of the literature on the history, structure, classification, and properties of optical fibers, highlighting spatiotemporal dissipative LBs and the influence of the spatially nonlocal response on their propagation through optical fibers.

In **chapter II**, we deal with Models and Methods: we derive the extended (3+1)-D nonlocal

CCGLE and CQCGLE, governing the dynamics of the dissipative LBs in a doped and weakly nonlocal nonlinear medium.

The dynamic characteristics of the dissipative LBs, which include the amplitude, temporal and spatial pulse widths, and position of the pulse maximum, unequal wavefront curvatures, chirp parameters, and the phase shift in specially designed media, are studied using the variational technique.

In **chapter III**, we present the results and discussion: we establish the stability criterion for steady-state solutions of the (3+1)-D nonlocal CCGLE and the (3+1)-D nonlocal CQCGLE , fixing a domain of dissipative LB parameters. Following this, we carry out direct integrations with the Runge-Kutta and the split-step Fourier methods, showing stable self-organized dissipative spatiotemporal LBs.

Chapter I

Literature Review

1.1 Introduction

This chapter covers the history, structure, classification, and properties of optical fibers. We discuss the evolution of optical fibers from their use by the ancient Greeks to the 21th century. We show that optical fibers consist of three main parts: the core, the cladding, and the coating buffer. Each part contributes to the proper confinement and guidance of light. Furthermore, optical fibers can be divided into two categories based on the refractive index and the paths the optical signal can take during propagation: Single Mode Fiber (SMF) and Multimode Fiber (MMF).
It is important to note that for the formation of (3+1)-D dissipative optical solitons, commonly referred to as LBs, it is generally necessary to supply external energy to the SMF. The balance is thus not only between linear and nonlinear effects but also between gains and losses. This type of double compensation plays a crucial role in the design of optical amplifiers. Therefore, we aim to investigate whether combining this double compensation with weak spatial nonlocality could enhance the robustness of LBs and prevent collapse.

1.2 Generality on optical fibers

1.2.1 History and physical structure of optical fibers

1.2.1.1 A brief history of optical fibers

The first steps in the transport of light using glass tubes were observed in ancient times when the ancient Greeks used them for decorative purposes. Little by little, the use of glass tubes became known to venetian craftsmen, who innovated by inventing ornamental glass. Years later,

research on total internal reflection by Jean-Daniel Colladon in 1841, Jacques Babinet in 1842, and John Tyndall in 1854 [34], were to be the precursors for the actual invention of the optical fiber.

John Tyndall discovered something that would become a foundation for the other research works in fiber optics. He based his experiment on a jet of water flowing from one container to another one and proved that light, thanks to internal reflections, could travel along water following a specific path. At the same time, he showed that it was possible to tilt a light signal. The results of this research led to a number of inventions, including Alexander Graham Bell's photophone in 1880. This photophone enabled light to be transmitted over a distance of 200 meters [35].

In the same vein, in the 1950s, Abraham Van Heel and Harold Hopkins invented the fiberscope for transporting images using fiber optics. A similar discovery had been made in 1927 by Baird and Hansell. Their research focused on the transport of television images by optical fiber. Their results had not emerged like those of Van Heel and Harold Hopkins. Nevertheless, in the years that followed, in 1953 to be precise, Narinder Singh Kapany, an Indian-American physicist, succeeded in demonstrating, for the first time, with the same Harold Hopkins, the transmission of images on optical fiber bundles. This work was based on John Tyndall's experiments [36]. In 1956, he, Narinder Singh, coined the term fiber optics, which today refers to the field of applied science and engineering concerned with the design and application of optical fibers.

In 1960, an electrical engineer and physicist named Charles Kuen Kao revolutionized the transport of information in telecommunications thanks to certain physical properties of glass he had discovered [37, 38]. His work paved the way for the transmission of light by optical fiber over long distances, at high speed and with very low attenuation. In 1970, an American multinational technology company, Corning Glass, successfully developed Charles Kuen Kao's work and made fiber usable for telecommunications. As a result of the information traffic generated by activities such as e-commerce on the Internet, computer networks, multimedia, voice, data and video, the need to use optical fiber has increased dramatically.

1.2.1.2 Physical structure of optical fibers

An optical fiber is a cylindrical dielectric waveguide in the form of a filament, essentially made of glass or silica plastic. It exploits the phenomenon of total internal reflection along its optical

axis to guide light and transmit information. This information is transmitted in the form of an optical pulse from one point to another at high speed, over long distances and with low loss.

As mentioned above, an optical fiber can be made of plastic, but also of unhardened glass which can easily be bent and moulded. Whether plastic or glass, they consist of three main parts. From the inside to the outside we have the core, the cladding and the coating buffer [39] as illustrated in Figure 1.1.

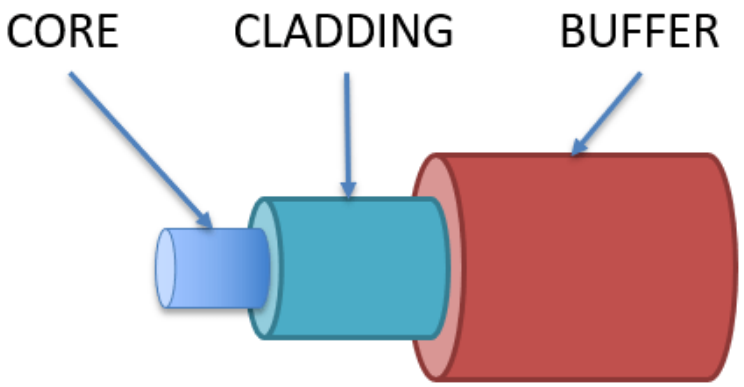

Figure 1.1: Optical fiber's profile

The core is where the light is confined and guided along the optical axis. The core is made of fused silica, a glassy material with very low loss (about 0.2 dB/km) in the near infrared region around 1.5 μm. Dopants such as phosphorus and germanium are added during the manufacturing process to increase the core refractive index denoted n_1. This refractive index is a few millimetres higher than that of the cladding.

The cladding surrounds the core to protect it from damage. Dopants such as fluorine and boron trioxide are incorporated into the low-grade silica that makes up the cladding, reducing its refractive index n_2.

The coating buffer : the role of the coating buffer is to protect the fiber from mechanical pressure and environmental stress. It consists of polyuterine polymer or PVC. Thanks to its high resistance to tearing, grease and abrasion, it protects the core from electromagnetic interference and radio frequencies.

It is important to note that the slight and appropriate refractive index difference between the core and cladding is in accordance with Descartes' law. For light to be well guided into the core, the refractive index of the core must be greater than that of the cladding. The cladding is therefore there to counteract the fact that light is confined to the core. If the refractive index of the cladding was much higher, the light would come from the outside and dissipate without returning to the core, and we would observe a large attenuation. The difference is therefore important to allow total internal reflection to take place. According to Descartes' law, when a light ray passes from one medium to another with a lower index of refraction, it can be reflected. Total reflection occurs when the angle of incidence of the light ray is greater than the critical angle and there is no loss [40].

Reflection and refraction at the boundary of two media are illustrated in Figure 1.2, which shows the case $n_1 > n_2$ [41].

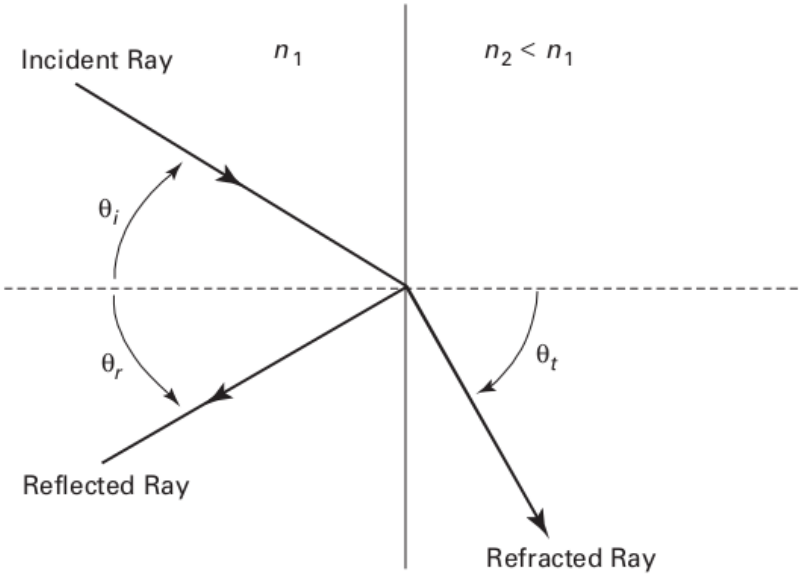

Figure 1.2: Snell-Descartes law [41].

The parameter θ_i represents the angle of incidence, θ_r corresponds to the angle of reflection, and θ_t is the angle of the transmitted ray (angle of refraction). The relations between θ_i, θ_r, and θ_t are given by:

$$\theta_r = \theta_i, \tag{1.1}$$

and

$$n_1 sin\theta_i = n_2 sin\theta_t. \tag{1.2}$$

It can be seen from Eq. (1.2) that there is a critical angle θ_c, given as

$$\theta_c = sin^{-1}(n_2/n_1). \tag{1.3}$$

The angle θ_c, the critical angle, is the specific angle of incidence in the core that results in an angle of refraction of $\pi/2$ radians at the core-cladding interface. This condition is the threshold for total internal reflection.

The following Figure 1.3 shows the ray propagation in a step-index fiber and illustrates guided and unguided rays. At angles of incidence greater than θ_c, all the energy is totally reflected, resulting in a guided ray. These rays, guided through the core of the fiber, carry the optical signal.

A ray entering the fiber at a sufficiently small angle of incidence, shown in the figure as the acceptance cone, is totally reflected, bouncing back and forth between the internal walls of the fiber as it propagates, whereas a ray incident outside the acceptance cone is partially refracted at each bounce [40].

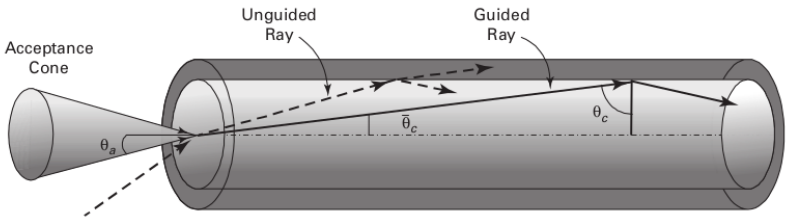

Figure 1.3: Ray propagation in a step-index fiber (From [Saleh+91, Figure 8.1-3a]. Copyright c 1991. Reprinted by permission of John Wiley and Sons, Inc.)

For rays entering the fiber from the air, the largest possible angle of incidence for guided rays is the acceptance angle θ_a, which is equal to

$$\theta_a = sin^{-1}\left(\sqrt{(n_1^2 - n_2^2)}\right). \tag{1.4}$$

The numerical aperture NA of the fiber is defined as:

$$NA = sin\theta_a = \sqrt{(n_1^2 - n_2^2)}. \tag{1.5}$$

The numerical aperture increases with the fractional refractive index change, $\Delta = (n_1 - n_2)/n_1$. In a typical cladded fiber, we have $\Delta \ll 1$; thus, only a narrow cone of light is accepted as a guided ray. However, in an uncladded fiber, both Δ and NA are large.

The guiding properties of an optical fiber are characterized by a dimensionless parameter defined as:

$$V = a(\omega/c)(n_1^2 - n_2^2)^{1/2}, \tag{1.6}$$

where a is the core radius and ω is the frequency of light. The parameter V determines the number of modes supported by the fiber. For example, if $V < 2.405$, this indicates that the optical fiber can support only one mode. Such fibers are called single mode optical fibers. They are more commonly used than other types of optical fibers, as we will see in the following subsection.

1.2.2 Optical fiber classification and properties

1.2.2.1 Optical fibers classification

Optical fibers are divided into two categories based on their refractive index and mode: SMF and MMF. The mode simply refers to the path that the optical signal can take as it propagates through the optical fiber.

- **The SMF** uses a single path for transmission of electromagnetic wave whose wavelength is between 1330 and 1550 nm with a large bandwidth and low losses. The SMF core size is between 8 and 9 μm. It can support speeds up to 10G (gigabits per second) and distances up to about 10 km.

The main characteristic of the SMF is the step change in refractive index from the core of the fiber to the cladding surface, which allows only one mode of light to propagate through the fiber. Such fibers are used in miniaturized optical scanners to extend a high-resolution image, in a scanning fiber optic microscope, acting as a spatial filter or as a pinhole detector, in laser light illumination and in the collection of the reflected light.

Mollenauer et *al.* [42] showed that SMF with low loss (with a wavelength of 1550 nm) and with negative GVD, provide a stable, simple, and well characterized medium for solitons. Furthermore, the experiment made by Nakatsuka et *al.* [43] showed that it is also possible to have a stable soliton in SMF under positive GVD.

- **The MMF** can be classified into step-index (STIN) multimode fibers and graded-index

(GRIN) multimode fibers. The STIN is described by a uniform refractive index, while the GRIN is described by radially varying refractive index. The MMF is designed for less bandwidth-intensive applications for short distances and can transmit more than one mode of electromagnetic wave with a wavelength between 800 and 1300 nm. Standard MMF core sizes are 50 μm and 62.5 μm. Information traveling as a light pulse in multimode fiber follows multiple paths through the core. Therefore, it is subject to modal dispersion. This is good for short distances but causes distortion over long distances. For this reason, SMF is suitable for long distance and in comparison with MMF, allows avoiding unclear and incomplete data transmission for a certain distance.

It is worth mentioning that SMF has a much smaller core than MMF, and this makes it better comparable to the MMF. In fact, the smaller the core, the tighter the total internal reflections on a more direct path. As a result, the optical signal can be of good quality and travel longer distances. In addition, SMF is used for higher bandwidth requirements and uses a laser as its light source, while MMF uses a light-emitting diode (LED) as its light source and has less bandwidth-intensive applications.

Figure 1.4 shows the refractive index profile and ray transmission in STIN: the case of SMF and the MMF, respectively. The refractive index profile and ray transmission in a multimode GRIN is shown in Figure 1.5.

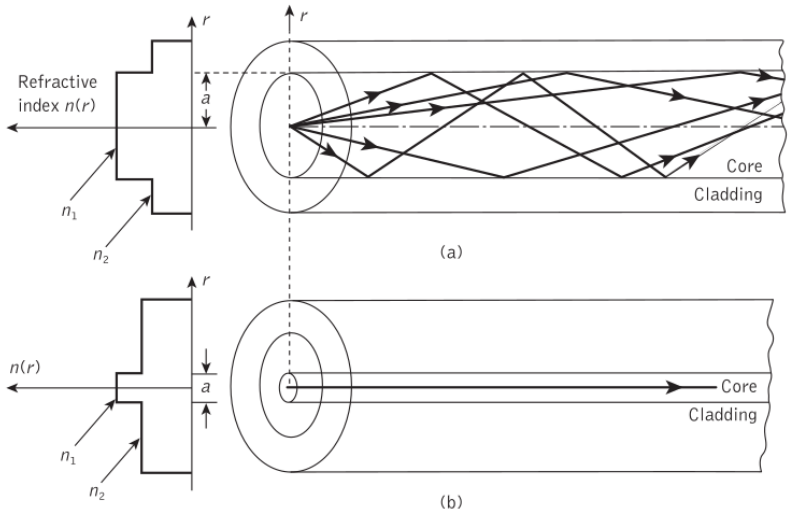

Figure 1.4: The refractive index profile and ray transmission in step index fibers: (a) multimode step index fiber; (b) single-mode step index fiber [44].

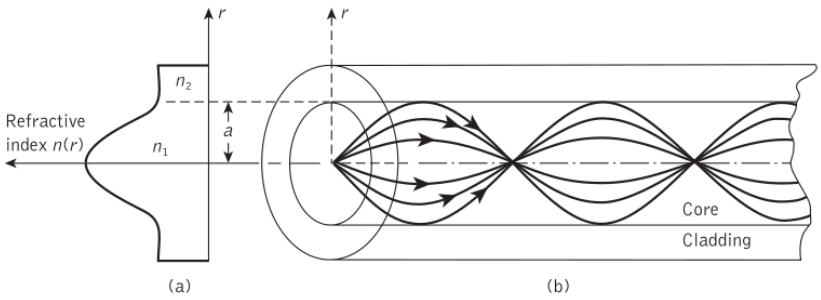

Figure 1.5: The refractive index profile and ray transmission in a multimode graded index fiber [44].

1.2.2.2 Optical fibers properties

An optical fiber can transmit light or an information-carrying signal when the linear and nonlinear effects produced within it are well balanced. Although the balance of all these linear and nonlinear effects is adapted to the signal to be transmitted, the transmission distance can be limited if we restrict ourselves to considering only these effects. It is therefore generally necessary to supply to the optical fiber external energy, and one way of doing this is to dope it. From this moment on, the balance is no longer ensured only by linear and nonlinear effects but also by the balance between gains and losses.

In the following, we will take a brief look at the different types of linear and nonlinear effects inside the optical fiber.

Three major linear effects occur in optical fibers, namely the dispersion effect, the attenuation effect and the diffraction effect.

(a) Dispersion

Dispersion tends to spread out temporally and distort the signal or light pulse as it travels through the fiber. Without good compensation, dispersion limits transmission distances and thus limits the speed at which information can be transmitted. There are typically two types of dispersion, modal dispersion and chromatic dispersion. The former occurs only in multimode fibers, while the latter occurs in all types of fibers.

• **Modal Dispersion** applies to multimode fibers, where the path (mode) of each ray travels at different speeds. The high order modes take much longer to propagate through the fiber, while the low order modes propagate much faster. This process causes a distortion, which results in modal

dispersion. However, to reduce modal dispersion, we can use a GRIN multimode fiber instead of the STIN. Light rays in GRIN multimodes also travel in different modes, but the modal dispersion is greatly reduced because of the different light propagation speeds. One way to avoid modal dispersion is to use single mode, since only one mode is extended and the light enters along the fiber axis. A particular form of modal dispersion is polarization mode-dispersion

Polarization mode-dispersion (PMD) is a special form of modal dispersion. It is an inherent linear effect in optical fiber due to the glass manufacturing process, and sometimes caused by fiber cabling, installation and the operating environment of the cable. This type of dispersion is the result of the polarization dependence of the propagation characteristics of light rays in optical fibers. In fact, light is an electromagnetic wave represented by perpendicular axes, namely the electromotive force and magnetomotive force. In addition, light is also an energy wave or energy region in optical fiber. When the energy within the two axes is transmitted at different speeds, we end up with a PMD.

• **Chromatic Dispersion** is due to the fact that different wavelengths are propagate at different speeds in the fiber, since the refractive index of glass fiber is a wavelength-dependent quantity. Thus, a signal propagating in an optical fiber will undergo a more or less significant temporal dispersion depending on its central wavelength and its temporal width. It is the combination of material and waveguide dispersion effects.

Material Dispersion occurs when the refractive index of the fiber core material is a function of frequency. Because the fiber has different refractive index characteristics at different wavelengths, each wavelength travels through the fiber at a different speed. Thus, some wavelengths arrive before others and a signal pulse is spread out.

Waveguide dispersion occurs due to the dependence of the mode propagation constant on the signal wavelength and the fiber parameters such as the core radius and the refractive index difference between the core and the cladding.

The chromatic dispersion effect can be evaluated using the Taylor series expansion of the mode

propagation constant β around the central frequency ω_0 or central frequency of the pulse spectrum [45]:

$$\beta(\omega) = \frac{\omega}{c} n_{eff}(\omega) = \beta_0 + \beta_1(\omega - \omega_0) + \frac{1}{2!}\beta_2(\omega - \omega_0)^2 + \frac{1}{3!}\beta_3(\omega - \omega_0)^3 + \frac{1}{24!}\beta_4(\omega - \omega_0)^4..., \quad (1.7)$$

where $\beta_0 = \beta(\omega_0) = \frac{\omega_0}{c} n_{eff}(\omega_0)$ and $\beta_m = \left(\frac{d^m \beta}{d\omega^m}\right)_{\omega=\omega_0}$ for $m = 0, 1, 2, 3, 4, ...$

The β_m terms are generally expressed in ps^m/km.

Regarding the quantities β_1 and β_2, the underlying physical meaning is quite intuitive. The term β_1 is related to the group velocity v_g of the pulse and is given by:

$$\beta_1 = \frac{1}{v_g} = \frac{n_{eff}(\omega_0)}{c} + \frac{\omega}{c}\frac{dn_{eff}}{d\omega} \mid_{\omega_0}, \quad (1.8)$$

whith n_{eff} representing the effective index.

β_2 is responsible for the temporal broadening of the pulse and reflects the dispersion of the group velocity:

$$\beta_2 = \frac{d\beta_1}{d\omega} = -\frac{1}{v_g^2}\frac{dv_g}{d\omega} = \frac{1}{c}\left(2\frac{dn_{eff}}{d\omega} + \omega\frac{d^2 n_{eff}}{d\omega^2}\right). \quad (1.9)$$

The quantity $\beta_2(\omega)$ which is the chromatic dispersion derived from $\beta(\omega)$, is generally defined by the dispersion parameter D, expressed in $ps/nm/km$. The correlation between D and β_2 is given by [45]:

$$D(\lambda) = -\frac{2\pi c}{\lambda^2}\beta_2(\lambda) = -\frac{\lambda}{c}\frac{d^2 n_{eff}}{d\lambda^2}. \quad (1.10)$$

The dispersion length is given by:

$$L_{Disp} = T_0^2/|\beta_2|, \quad (1.11)$$

where T_0 is the half-width of the pulse measured at $1/e$ of the maximum intensity.

The dispersion slope which characterizes the evolution of D, is then defined by:

$$S_D(\lambda) = \frac{dD}{d\lambda}. \quad (1.12)$$

In standard silica fibers, β_2 changes sign from positive to negative as the wavelength of light increases beyond 1.3 μm. Therefore, two dispersion regimes are defined: the normal GVD regime, or positive GVD, when D is negative (or $\beta_2 > 0$), and the anomalous GVD regime, or negative GVD, when D is positive ($\beta_2 < 0$). In the normal dispersion regime, low frequency spectral components propagate faster than high frequency components. In the anomalous dispersion regime,

the opposite is true, high frequency spectral components propagate faster than low frequency components. The magnitude of β_2 can be controlled by shifting the wavelength at which β_2 changes sign. Dispersion-shifted fibers used for optical communications are designed to have $\beta_2 = 0$ near 1.5 μm. It is possible to design fibers so that β_2 is relatively small over a wide range of wavelengths from 1.3 to 1.6 μm. Such fibers are called dispersion-flattened fibers.

Fiber dispersion is not always bad for transmission signals in fiber optics. In fact, it results in stable light propagation when well balanced with nonlinear effects.

(b) Attenuation

Attenuation is the loss of signal strength during transmission. Measured in decibels (dB), it is 0.36 dB/km at a wavelength of 1310 nm and $0.22dB/km$ at a wavelength of 1550 nm. When signals are transmitted as light pulses from one point to another through an optical fiber over a long distance, uncontrolled attenuation causes the signal to become inconsistent. Amplification is therefore required. Repeaters are often used and placed so that each time the signal weakens, it is amplified and regenerated. As we can see, attenuation is the opposite of amplification. We will see in the following section that due to the expensive price of repeaters, other alternatives have been found to overcome the attenuation problem.

Attenuation is due to external or internal factors such as material absorption, Rayleigh scattering, and waveguide imperfections.

- **Material absorption**: light is absorbed by the residual OH^+ and the dopants used to modify the refractive index, and then it is converted to heat by molecules in the glass. The OH^+ absorption occurs at discrete wavelengths and around 1000 nm, 1400 nm, and above 1600 nm (see Figure 1.6).

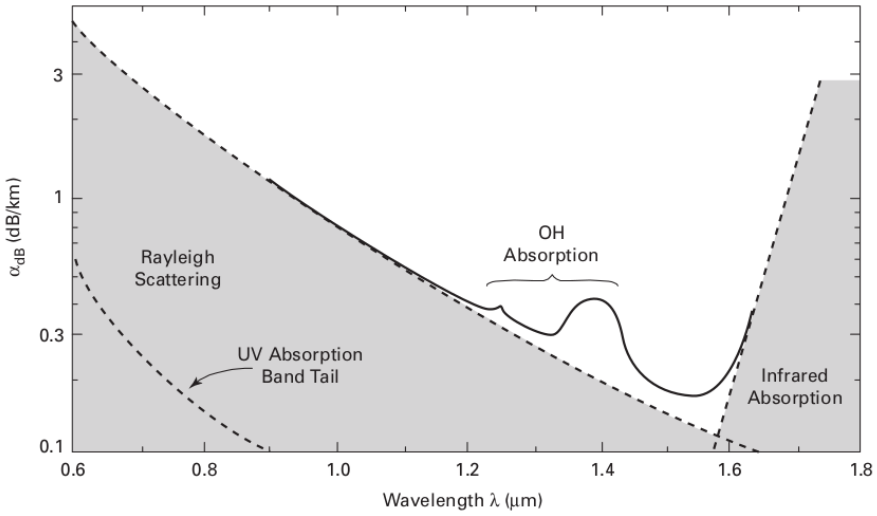

Figure 1.6: Attenuation as a function of wavelength (From [Saleh+91, Figure 8.3-2]. Copyright c 1991. Reprinted by permission of John Wiley & Sons, Inc.) [41]

• **Rayleigh scattering** occurs because the medium is not absolutely uniform. Light scattered at angles outside the numerical aperture of the fiber is absorbed by the cladding or transmitted back toward the source. Scattering is also a function of wavelength, proportional to the inverse fourth power of the wavelength ($1/\lambda^4$) of the light, so it is the dominant loss factor at the short wavelengths. Thus, if you double the wavelength of light, you reduce the scattering losses by 2 to the 4th power, or 16 times. Therefore, for long distance transmission, it is advantageous to use the longest practical wavelength to minimize attenuation. Combined with infrared absorption, Rayleigh scattering limits the optical spectrum to a range of about 800 to 1700 nm, excluding the OH^+ attenuation peaks. The Rayleigh scattering formula for a single component glass is given by [44]:

$$\gamma_R = \frac{8\pi^3}{3\lambda^4} n^8 p^2 \beta_c K T_F, \tag{1.13}$$

where γ_R is the Rayleigh scattering coefficient, λ is the optical wavelength, n is the refractive index of the medium, p is the average photoelastic coefficient, β_c is the isothermal compressibility at a fictive temperature T_F, and K is Boltzman's constant. The fictive temperature is the temperature at which the glass reaches a state of thermal equilibrium and is closely related to the annealing temperature. In addition, the Rayleigh scattering coefficient is related to the transmission loss

factor and the transmissivity of the fiber $\mathscr{L}$ by the following correlation:

$$\mathscr{L} = exp(-\gamma_R L), \tag{1.14}$$

where L isthe length of the fiber.

- **Waveguide imperfections** are caused by manufacturing imperfections, small bends and distortions in the fibers. Normally, these contribute to a relatively small additional loss component. The simplest way to express these losses is through a relation of the form [41]:

$$dP/dz = -\alpha P, \tag{1.15}$$

where P is the optical power propagating down the fiber at some point, and α is a positive attenuation coefficient. Integrating Eq. (1.15) allows to obtain:

$$P_R = e^{-\alpha} P_T, \tag{1.16}$$

with P_T, the power launched into the fiber and P_R, the power received at the end of a fiber of length L. The attenuation coefficient is then expressed as:

$$\alpha_{dB} = -\frac{10}{L} log_{10} \frac{P_R}{P_T}, \tag{1.17}$$

where L is in units of kilometers.

(c) Diffraction

Optical beams have an inherent tendency to spread out when propagating in a homogeneous medium. However, beam diffraction can be compensated for by beam refraction if the refractive index in the beam region is increased [46]. Optical fiber is an excellent waveguide that can provide such an environment, resulting in stable light propagation. Diffraction and nonlinear refraction are well balanced so that the light is confined in the transverse direction of the optical fiber, forming a spatial optical soliton.

Nonlinear effects are typically grouped into two categories. The first categories are the scattering effects, such as stimulated Brillouin scattering (SBS) and stimulated Raman scattering (SRS).

The second categories are the Kerr effects, namely four-wave mixing (FWM), self-phase modulation (SPM) and cross-phase modulation (XPM).

The response of any dielectric to light becomes nonlinear for intense electromagnetic fields. In the transparent region of optical fibers, the lowest order nonlinear effects originate from the third order susceptibility $\chi^{(3)}$ [46]. The real part of $\chi^{(3)}$ leads to the Kerr effects such as SPM, XPM, and FWM, while the imaginary part leads to the scattering effects such as SBS and SRS [45].

(d) SBS and SRS

In each of these two scattering effects, light interacts with the fiber medium, producing inelastic collisions in which the wavelength of the scattered photon is longer than that of the incident photon, i.e., energy is lost. In each case, a signal present at the wavelength of the scattered photons can produce stimulated emission of another photon at the same wavelength and hence amplification [4].

• **SBS** can be thought of as the modulation of light by thermal molecular vibrations within the fiber [44]. The scattered light appears as upper and lower sidebands separated from the incident light by the modulation frequency. The incident photon in this scattering process produces a phonon of acoustic frequency and a scattered photon. This results in an optical frequency shift that varies with the scattering angle, because the frequency of the sound wave varies with the acoustic wavelength. The SBS is significant only above a threshold power density given by [44]:

$$P_B = 4.4 \times 10^{-3} d^2 \lambda^2 \alpha_{_{dB}} \nu \text{ watts.} \tag{1.18}$$

Eq. (1.18) expresses the threshold optical power that must be injected into a SMF before SBS occurs. In this equation, d and λ are the fiber diameter and the operating wavelength, respectively, both measured in micrometer. α_{dB} is the fiber attenuation in decibels per kilometer defined in a previous paragraph, and ν is the source bandwidth in gigahertz.

• **SRS** is similar to SBS except that a high-frequency optical phonon is generated in the scattering process instead of an acoustic phonon [44]. It involves the transfer of the power pump, called the pump frequency ω_p, from the highest frequency wave, called the anti-Stokes ω_a, to the lower frequency wave, called the Stokes ω_s. The energy difference that is absorbed by the diffuser center can be used advantageously for optical amplification. By pumping an optical fiber at the frequency

ν, the Stokes wave is generated at $\nu - \omega_s$, and its intensity increases exponentially according to the following equation [40]:

$$I_s(t) = I_s(0)exp(g_r cL), \tag{1.19}$$

where I_p designates the pump intensity, g_r is the Raman gain, L is the propagation length, Ω_s corresponds to maximum efficiency. The threshold optical power for SRS in a long single-mode fiber is given by:

$$P_R = 5.9 \times 10^{-2} d^2 \lambda^2 \alpha_{_{dB}} \nu \text{ watts.} \tag{1.20}$$

In Figure 1.7., we can see the spectrum of the scattered light showing the inelastic scattering processes, not drawn to scale because the intensities of the anti-Stokes Raman lines are much smaller than those of the Stokes Raman lines [44].

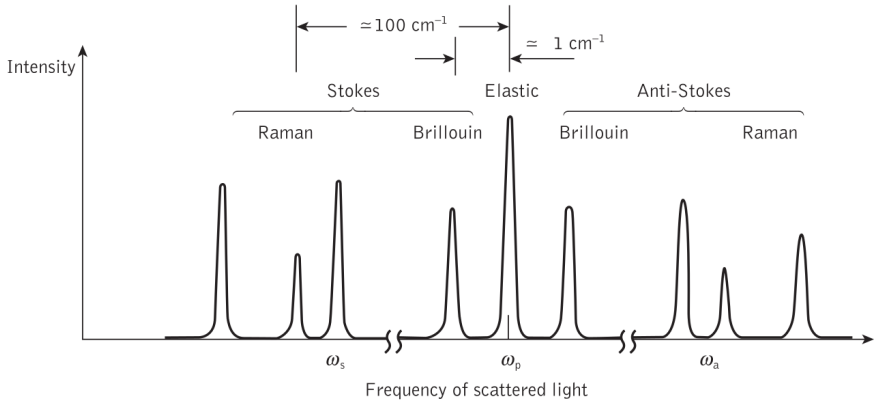

Figure 1.7: Spectrum of scattered light showing the inelastic scattering processes [44].

(e) FWM

FWM and phase modulation effects can be explained in terms of a nonlinear dependence of the polarization P on the optical field E, leading to nonlinear refraction. In silica glass, there is a small cubic term in this nonlinearity which is related to a third order nonlinearity susceptibility $\chi^{(3)}$. The cubic relation between P and E can be expressed as a square-law nonlinearity in the refractive index:

$$n(\omega, |E|^2) = n_0 + n_2|E|^2, \tag{1.21}$$

where n_0 represents the linear frequency-dependent part of n that take into account the material

dispersion, and n_2 accounts for various nonlinear effects.

(f) SPM

This phenomenon was observed in a 1978 experiment and is caused by an intensity-dependent phase shift, since the signal modulates its own phase. Its magnitude can be obtained by noting that the phase of an optical field changes during transmission through the fiber by [40]:

$$\psi = (n + n_2 I)k_0 L, \tag{1.22}$$

where k_0 is the wavenumber given by $k_0 = \omega_0/c = 2\pi/\lambda$. The parameter c represents the light celerity, ω_0 is the carrier frequency, λ is the wavelength, L is the fiber length, and I is the intensity of the light.

The nonlinear phase shift resulting from the SPM is:

$$\psi_{NL} = n_2 k_0 L I. \tag{1.23}$$

Silica glass is a relatively weak nonlinear medium with a measured value of $n_2 \approx 2.7 \times 10^{-20} m^2/W$. This value can vary depending on the density of the dopants. However, even though n_2 is relatively small compared to most other nonlinear media, the nonlinear phase shift ψ_{NL} can become large because the intensity I is enhanced by orders of magnitude in optical fibers. Moreover, relatively low losses in fibers can maintain this intensity over long lengths ($\sim 10km$), and, if fiber losses are periodically compensated by the use of optical amplifiers, the interaction length L can exceed thousands of kilometers.

Note that, a temporally varying phase shift implies that the carrier frequency over the pulse differs from its central value ω_0. We then have a frequency shift $\delta\vartheta(t)$, called frequency chirp, which is itself time-dependent:

$$\delta\vartheta(t) = -\frac{\delta\psi_{NL}}{\delta t}, \tag{1.24}$$

where the minus sign is due to the choice $exp(-i\omega_0 t)$.

(g) XPM

XPM is a similar effect to SPM except that overlapping but distinguishable pulses, possessing, for example, different wavelengths or polarizations, are involved. In this case, variations in the intensity of one pulse will modulate the refractive index of the fiber, causing phase modulation of

the overlapping pulse(s) [44]. XPM is exhibited as a crosstalk mechanism between channels when either intensity modulation is used in dispersive optical fiber transmission or, alternatively, when phase encoding is employed [48].

1.2.3 Optical amplifiers: the case of erbium-doped fiber amplifiers

1.2.3.1 Optical amplifiers

An optical amplifier is used to increase the strength of the signal without changing its shape. It is a necessary device for an optical connection (OC). The OC includes an optical transmitter (OT) and an optical receiver (OR) connected by an optical path consisting of optical fiber links passing through one or more optical network nodes (ONN). In addition, optical amplifiers require three essential components for proper signal regeneration (see Figure 1.8). These components are the power amplifier, the line amplifier, and the preamplifier.

- **The power amplifier** is used to increase the strength of the signal before it is launched over the line. This part is located in the optical transmitter.

- **For the line amplifier**, it is placed at a strategic point along the transmission link between fiber sections to emit a signal and then compensate for the fiber attenuation.

- **The preamplifier** is used for receiver sensitivity in fiber optic transmission links and is located in an optical receiver. In this case, the signal level at the input of an optical receiver is increased by the preamplifier, which serves to improve the signal-to-noise ratio (SNR) at the input of the photodetector (PD) and the electrical detector [41].

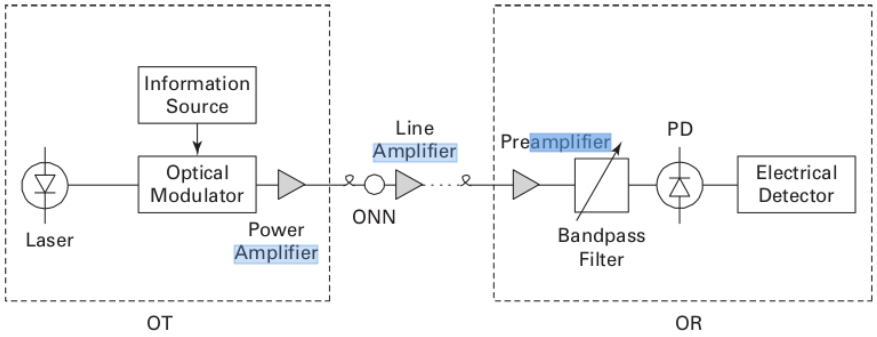

Figure 1.8: A point-to-point optical connection [41].

Attenuation has long been a real problem with optical fibers. As we said, the word attenuation refers to the loss of signal strength due to external or internal factors. Before optical amplifiers, regenerators were used every 120 km on optical fibers to regenerate and amplify the signal strength weakened by attenuation. However, these regenerators were so expensive that researchers considered another alternative, leading to the advent of optical amplifiers. Regenerators were therefore completely replaced in transoceanic systems, and optical amplifiers were installed every 45 to 85 km [48]. In addition, optical amplifiers were also used in terrestrial systems to improve existing installations [49]. They were therefore a perfect alternative to replace the expensive and limited electronic repeaters used previously.

There are many types of optical amplifiers, namely semiconductor optical amplifiers (SOA), Raman amplifiers (RA), and rare-earth doped fiber amplifiers (ReDFA). The latter is the one that has attracted the most attention from researchers in recent years.

1.2.3.2 Erbium-doped fiber amplifiers

ReDFA bring together a large family of dopants. These include praseodymium, neodymium, ytterbium, thulium, and erbium. The Erbium-doped fiber amplifier (EDFA) has been successfully used in many underwater and terrestrial systems because it has properties suitable for the 1550 nm window in optical fibers where low attenuation exists [50]. Other properties are high gain [51,52], high saturation output power [53], polarization-independent gain [54], low noise and low insertion loss.

In fields such as telecommunications, signals at a fiber window of 1550 nm are amplified by

passing them through a short section of optical fiber through which the energy source, the pump light, also propagates. The core of this special section contains the rare-earth element erbium, which acts as a storage medium for the transfer of energy from the pump to the signal. In the fiber amplifier section, the erbium core has a refractive index profile and composition tailored for optimal amplifier performance.

EDFA operates via a three metastable energy level system, the levels E_1, E_2 and E_3, as shown in Figure 1.7. below.

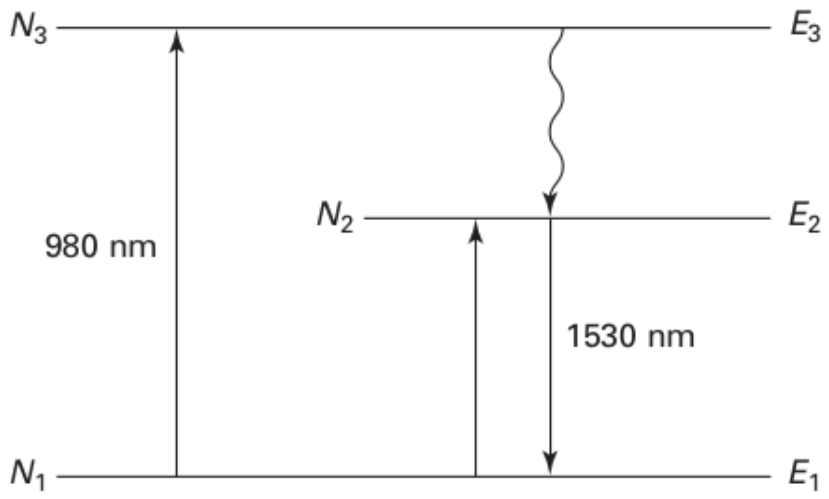

Figure 1.9: The erbium-ion described with the energy level diagram [41].

The population fractional densities of the three energy levels are denoted by N_1, N_2, and N_3, respectively. If the condition $N_1 > N_2 > N_3$ is satisfied, the system is in thermal equilibrium, i.e. no pump or signal is present. In contrast, when pump and signal are present, these population fractional densities change as ions move back and forth between levels, accompanied by the emission or absorption of photons at frequencies determined by the energy level difference [41]. The wavelength λ for each transition is given by the quantum relation $\lambda = hc/\Delta E$, where c is the light celerity, h is Planck's constant, and ΔE is the difference in energy levels. Each transition is actually associated with a band of wavelengths rather than a single line.

For practical optical fiber communication systems, the EDFA must be pumped by semiconductor laser diodes at 980 nm, and 1480 nm. Therefore, two pump wavelengths are typically used for EDFAs: 980 and 1480 nm.

Light at a wavelength of 980 nm is absorbed by erbium ions (E_r^{+3}), raising it to a higher energy

level E_3, which rapidly decays non-radiatively to a long-lived metastable state E_2. The rate at which these transitions occur is proportional to $N_1 P_p$, where P_p is the power of the pump. The metastable state can also be populated by pumping the upper edge of the band at 1480 nm. From this storage state, deexcitation will occur radiatively, emitting a photon around 1530 nm. This process does not occur spontaneously, since the lifetime τ in the metastable state E_2 is very long, as we said before. It is much more likely that the emission is stimulated by a traveling signal around 1530 nm, which provides signal amplification. The combination of long lifetime and absence of lower energy states makes the erbium system extremely efficient for amplification of telecommunication signals [52].

The mathematical expression describing the doping effect is [18]:

$$\chi_a(\omega) = \frac{g_p}{k_0} \frac{(\omega - \omega_a)T_2 - i}{1 + (\omega - \omega_a)^2 T_2^2}, \tag{1.25}$$

where $\chi_a(\omega)$ is the atomic susceptibility governing the response of the dopant in the optical fiber. The peak gain corresponds to $g_p = \sigma(N_2 - N_1)$. The parameter σ is a transition cross section, while N_1 and N_2 are the atomic population fractional densities for the lower and upper energy levels of the two-level system. ω_a is the atomic resonance frequency, and T_2 is the relaxation time. Furthermore, one can expand the function $\chi_a(\omega)$ in Taylor series up to the fourth order in the vicinity of the carrier frequency ω_0 and find [18,55]:

$$\begin{aligned}\chi_a(\omega) = \frac{g_p}{k_0}\Bigg[\frac{\delta - i}{1+\delta^2} + \frac{1-\delta^2+2i\delta}{(1+\delta^2)^2}(\omega-\omega_0)T_2 + \frac{\delta(\delta^2-3)+i(1-3\delta^2)}{(1+\delta^2)^3}(\omega-\omega_0)^2T_2^2 \\ + \frac{6\delta^2-\delta^4-1+i(4\delta^3-4\delta)}{(1+\delta^2)^4}(\omega-\omega_0)^3T_2^3 \\ + \frac{\delta^5-10\delta^3+5\delta-i(5\delta^4-10\delta^2+1)}{(1+\delta^2)^5}(\omega-\omega_0)^4T_2^4\Bigg],\end{aligned} \tag{1.26}$$

where $\delta = (\omega_0 - \omega_a)T_2$ is the detuning parameter.

1.3 Light bullets

Although history mentions Russell as the ancestor or father of the "soliton" concept since he first observed it in a water channel in 1834 [56], the existence of the optical soliton was first predicted

theoretically by the Japanese scientist Hasegawa in 1973 [57, 58]. Optical solitons are localized optical structures or light pulses propagating in nonlinear optical media. We can observe either spatial optical solitons, temporal optical solitons, or spatiotemporal optical solitons, depending on whether these localized structures are confined in space and/or time.

Spatiotemporal optical solitons are cases of solitons confined simultaneously in space and time. When confined in three dimensions (x, y, z) as well as in time t, spatiotemporal optical solitons have a bullet shape and are called LBs [59].

1.3.1 Temporal optical solitons

Depending on whether the localized structures or light pulses are spatially or temporally confined, we can observe either a spatial optical soliton or a temporal optical soliton. In this section, we deal with temporal optical solitons. They keep their shape during propagation due to the balance between the GVD and the SPM caused by the Kerr nonlinearity.

In 1973, Hasegawa and Tappert predicted the existence of stable temporal solitons in optical fibers [57,58]. And years later, in 1980 to be precise, Mollenauer et *al.* [60] made an experimental observation.

How do each of these effects, GVD and SPM, affect the proper stable propagation of optical time solitons? The GVD leads to a broadening of the optical pulse propagating in the optical fiber, and the parameter used in the optical fiber to represent it is β_2. On the other hand, SPM induces a varying refractive index of the medium due to the optical Kerr effect, which will cause a phase shift in the pulse, leading to a change in the frequency spectrum or chirp ϑ of the pulse. The nonlinear phenomenon of SPM will impose a chirp on the optical pulse such that $\vartheta > 0$. For a good expectation, the GVD parameter is set to $\beta_2 < 0$ when operating near 1.55 μm, which is the best wavelength range of silica fibers. Since the GVD parameter β_2 and the chirp ϑ are set so that they have opposite signs, the condition $\beta_2\vartheta < 0$ is satisfied for stable propagation of the optical temporal soliton inside the optical fiber.

Such solitons can be modeled by the Nonlinear Schrödinger Equation (NLSE)[2]:

$$\frac{\partial\phi}{\partial z} + \beta_1\frac{\partial\phi(z,t)}{\partial t} + i\frac{\beta_2}{2}\frac{\partial^2\phi(z,t)}{\partial t^2} = iq|\phi|^2\phi(z,t), \tag{1.27}$$

with

$$\beta_1 = 1/v_g. \tag{1.28}$$

In Eq. (1.27), β_1 and β_2 correspond to the first and second order dispersion, respectively. The term β_2 represents the GVD parameter, since it takes the dispersion into account. The parameter $\phi(z,t)$ represents the temporal optical pulse. In Eq. (1.28), v_g is the group velocity associated with the pulse.

To get the (1+1)-dimensional [(1+1)-D] NLSE, we need to change the variables as follows:

$$\tau = (t - \beta_1 z)/T_0,\ \mathrm{Z} = z/L_{Disp}, \qquad \Phi(Z,\tau) = \sqrt{|q + |L_{Disp}}\phi(z,t), \tag{1.29}$$

where $L_{Disp} = T_0^2/|\beta_2|$ corresponds to the dispersion length, T_0 is a temporal scaling parameter.

The (1+1)-D NLSE for the cubic nonlinearity is then written as given below:

$$\frac{\partial\Phi(Z,\tau)}{\partial Z} - \frac{s}{2}\frac{\partial^2\Phi(Z,\tau)}{\partial\tau^2} \pm |\Phi|^2\Phi(Z,\tau) = 0, \tag{1.30}$$

where the $\pm$ signs depend on the sign of the nonlinear refractive index parameter n_2; the minus sign is chosen in the case of self-defocusing ($n_2 < 0$), and the positive sign in the case of self-focusing. The parameter $s = sign(\beta_2)$ takes into account either for the normal GVD regime or for the anomalous GVD regime.

1.3.2 Spatial optical solitons

Spatial optical solitons are localized structures confined in transverse space. This propagation occurs without change or distortion when the balance between linear diffraction and nonlinear self-focusing is precisely achieved. Linear diffraction tends to expand or spread the light pulse, while nonlinear self-focusing tends to contract the light pulse [2].

There are many types of spatial optical solitons, depending on the physical mechanism producing the nonlinear effect. These include [61, 2] Kerr solitons, Kerr-like solitons, photorefractive solitons, quadratic solitons, nematicons [62, 63], etc. Our present study deals with Kerr solitons.

Theoretical and experimental work on spatial optical solitons predates that on temporal optical solitons. However, the consistency between theory and experiment with respect to spatial optical solitons came many years later, in 1985 to be precise, after the progress in consistency for temporal optical solitons had been made [64]. Many extensive studies have been done on spatial solitons, and the one worth mentioning here is the work of Kelley [65]. In his work, he proved that the self-trapping mode of the (2+1)-D beam in the Kerr self-focusing nonlinear medium is unstable and there will surely appear a catastrophic collapse: the beam diameter will tend to zero and the beam intensity will be infinite.

Similarly, Bergé's work [66] states that (2+1)-D spatial solitons (self-formed cylindrical beams) in media with Kerr (cubic, or $\chi^{(3)}$) nonlinearity are unstable, unlike their (1+1)-D counterparts. This is due to the fact that two-dimensional fluctuations can disrupt the equilibrium between the nonlinearity and diffraction in this case. In particular, an increase in intensity leads to self-focusing of the cylindrical beam, which further increases the intensity and the corresponding intensity-dependent correction of the refractive index, which leads to even stronger focusing and an increase in intensity, and so on. This self-accelerating process of nonlinear self-focusing is called beam collapse.

However, years later it was shown that a saturable nonlinearity could prevent the catastrophic collapse and the formation of self-trapped (2+1)-D beams [67, 68]. In addition, many other studies have highlighted nonlinear nonlocality as a factor capable of suppressing the catastrophic collapse of (2+1)-D beams [69-72].

Figure 1.10 below illustrates the lens analogy for spatial solitons. Diffraction acts as a concave lens, while the nonlinear medium acts as a convex lens. A soliton is formed when the two lenses balance each other so that the phase front remains plane [2].

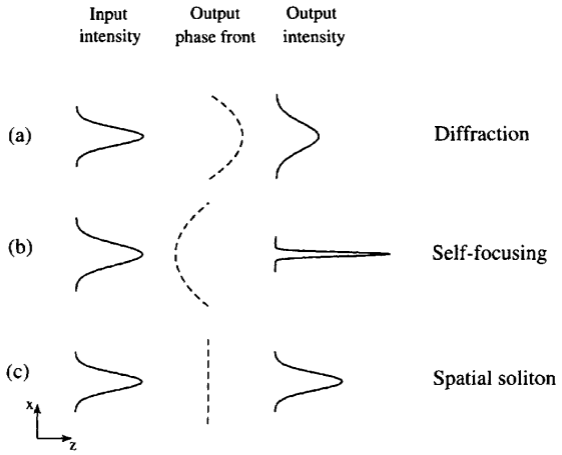

Figure 1.10: Schematic illustration of the lens analogy for spatial solitons [2].

When the nonlinear and diffractive effects are included and the envelope ϕ is assumed to vary with z on a scale much longer than the wavelength λ, the paraxial approximation, so that the second derivative $d^2\phi/dz^2$ can be neglected, the following scaled (2+1)-D NLSE is obtained in the case of cubic Kerr nonlinearity

$$i\frac{\partial\phi}{\partial Z} + \frac{1}{2}\left(\frac{\partial^2\phi}{\partial X^2} + \frac{\partial^2\phi}{\partial Y^2}\right) \pm |\phi|^2\phi(X, Y, z) = 0, \tag{1.31}$$

where $X = x/w_0$, $Y = y/w_0$, $Z = z/L_{diff}$, $\phi = (k_0|n_2|L_{diff})^{1/2}A$, where n_2 is the nonlinear part of the refractive index that depends on the beam intensity. The signs of $\pm$ depend on the sign of the nonlinear refractive index parameter n_2; the minus sign is chosen in the case of self-defocusing ($n_2 < 0$), and the positive sign in the case of self-focusing. The parameter w_0 is a transverse scaling parameter related to the input beam width, $L_{diff} = \beta_0\omega_0^2$ is the diffraction length, also called the Rayleigh range. The coefficient β_0 is the propagation constant with respect to the optical wavelength. The coordinate Z is the axis along which the beam is assumed to propagate, and X and Y are the spatial coordinates along which the beam diffracts. The parameter A is the amplitude.

As we mentioned above, self-dimensionality (2+1) trapped beam, could propagate stably and not be subject to catastrophic collapse due to many factors such as saturable nonlinearity and nonlocal nonlinearity. In the same way, we need additional perturbations for the soliton to move without distortion in three dimensions.

1.3.3 Light bullets as (3+1)-D spatiotemporal optical dissipative solitons

The concept of spatiotemporal dynamics in optical fibers includes both temporal and spatial effects that describe the propagation of the optical pulse under appropriate conditions. The solutions resulting from spatiotemporal dynamics are localized structures that remain confined in both time and space. They are called spatiotemporal optical solitons. In the case where the aforementioned confinement is in three dimensions (x, y, z) as well as in time t, the spatiotemporal optical solitons, have a ball shape, hence they are called LBs, a term coined by Silberberg [59]. We have often referred to them as spatiotemporal optical dissipative solitons or dissipative LBs [2], since the existence of LBs also require disturbances such as dissipation, including the supply of matter or energy. The concept of "dissipative solitons" could be applied to biology and even medicine, and thus not only to physical systems [73]. Optical dissipative LBs achieve confinement in three dimensions when, in addition to balancing nonlinearities and transversely broadening due to spatial diffraction as well as longitudinally (temporally) broadening due to GVD, gains and losses are well balanced. For dissipative systems, (1+1)-D and (2+1)-D problems have been studied extensively [2, 63]. However, less systematic work has been done in the case of (3+1)-D systems.

Figure 1.11 is an illustration of the formation of a spatiotemporal optical solitons due to the simultaneous equilibrium of diffraction and dispersion by nonlinear self-focusing [1].

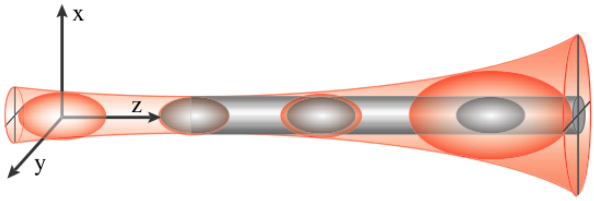

Figure 1.11: Illustration of the formation of a spatiotemporal soliton [1].

Spatiotemporal dynamics of optical solitons in a dissipative system can be described by a (D+1)-dimensional CQCGLE [74]

$$i\frac{\partial\phi}{\partial z} + \Delta\phi + |\phi|^2\phi + \nu|\phi|^4\phi = Q, \tag{1.32}$$

where ϕ is the normalized complex envelope of the optical field and $\Delta\phi = r^{1-D}\partial/\partial r(r^{D-1}\partial\phi/\partial r)$

is the D-dimensional Laplacian describing beam diffraction and/or anomalous group velocity dispersion. The term D accounts for the transverse dimension $1, 2, 3$, ν is the CQ nonlinearity. Dissipative terms are contained in the parameter Q, which is given by

$$Q = i\delta\phi + i\epsilon|\phi|^2\phi + i\mu|\phi|^4\phi + i\beta\Delta\phi. \tag{1.33}$$

The ϵ and μ parameters are the cubic and quintic gain-loss terms, respectively. The coefficient δ is the linear gain or loss depending on the sign. The last term β is the parabolic gain if β is greater than zero ($\beta_0 > 0$).

1.4 Spatially nonlocal nonlinear response in a doped optical fiber

Spatial nonlocality means that the light-induced refractive index change of a material at a given location is determined not only by the light intensity at that location, but also in a certain neighborhood of that location [75,76]. For a thorough understanding of the spatially nonlocal nonlinear response in a doped optical fiber, one should have a general idea of spatial nonlocality.

1.4.1 Spatial nonlocality overview

There are many forms of normalized nonlocal response, namely the exponential, the rectangular, the cylindrical, the Lorentzian, the periodic, and the Gaussian nonlocal functions, just to name a few [77-81].

Regarding the exponential nonlocal function, the following equation is a good description,

$$R(x, y) = (2\sigma)^{-1} exp(-|x + y|\sigma), \tag{1.34}$$

where $R(x, y)$ is the real, localized and symmetric function representing the profile of the nonlocal response. The parameter σ is the characteristic width chosen in such a way that

$$\int_{-\infty}^{\infty}\int_{-\infty}^{\infty} R(x, y)dxdy = 1. \tag{1.35}$$

The rectangular profile for the nonlocal response function extended to two dimensions is given as,

$$R(x,y) = \frac{1}{2\sigma}, -\sigma \leq x^2 + y^2 \leq \sigma \tag{1.36}$$

$$= 0, \text{otherwise.} \tag{1.37}$$

The following equation gives the cylindrical nonlocal response function:

$$R(x,y) = \frac{1}{2\sigma}, 0 \leq \sqrt{x^2 + y^2} \leq \sigma \tag{1.38}$$

$$= 0, \text{otherwise.} \tag{1.39}$$

The Lorentzian nonlocal response function is described by:

$$R(x,y) = \left[\pi\sigma\left(1 + \frac{(x+y)^2}{\sigma^2}\right)\right]^{-1}. \tag{1.40}$$

The periodic nonlocal response function is specified as

$$R(x,y) = \frac{1}{2\sigma} sin\left(\frac{|x+y|}{\sigma}\right). \tag{1.41}$$

For the purpose of our study, the Gaussian form has attracted our attention. Such a nonlocal response function can be generally described by [82]:

$$R(r - r') = \left(\pi\sigma^2\right)^{-1} e^{-(r-r')/\sigma^2}, \tag{1.42}$$

where r is the radius of the local points (x, y), with $r = \sqrt{x^2 + y^2}$, and r' is the radius of the neighborhood, given by $r' = \sqrt{x'^2 + y'^2}$.

The relation between the width of the response function and the width of the intensity profile divides the degree of nonlocality into four types, namely local, weak, general and strong nonlocal response [83,84].

- **Local** , appears when the degree of nonlocality is zero ($\sigma = 0$).
- **Weak nonlocality** occurs when $\sigma \ll 1$.
- **General nonlocality** corresponds to the case where $\sigma = 1$.

• **Strong nonlocality** is observed when the degree of nonlocality tends to plus infinity ($\sigma \to +\infty$).

In one dimension, the width of the response function $R(x)$ relative with respect to the width of the intensity profile $I(x,z)$ determines the degree of nonlocality. Figure 1.12 shows the different nonlocality ranges for a one-dimensional nonlocal response function [83].

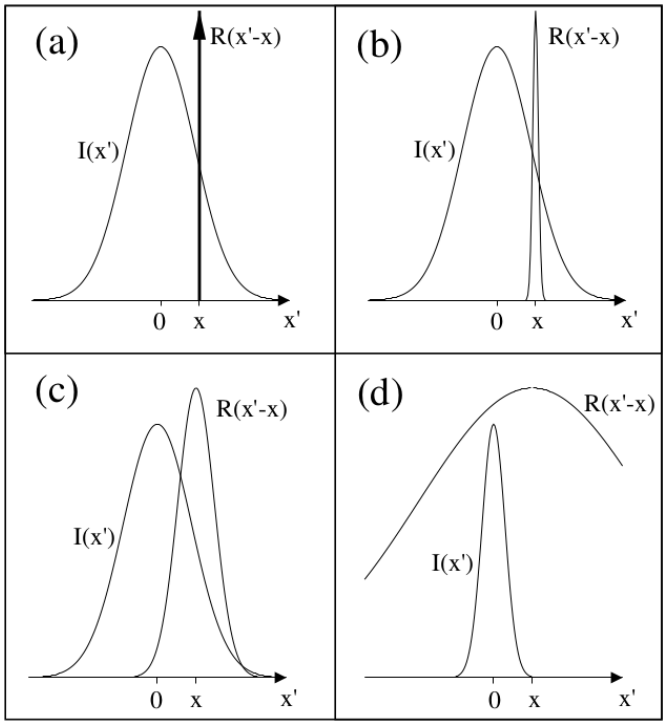

Figure 1.12: Different degrees of nonlocality, as given by the width of the response function $R(x)$ and the intensity profile $I(x)$. Shown is the local (a), the weakly nonlocal (b), the general (c), and the strongly nonlocal (d) response [83].

In the limit of a singular response, $R(x) = \delta(x)$ [see Figure 1. 12(a)], the nonlinearity is a local function of the intensity. For weak nonlocality [see Figure 1. 12(b)], the width of $R(x)$ is finite, but still small compared to the width of $I(x,z)$. In the limit of strong nonlocal response, $R(x)$ is much broader than the intensity profile [see Figure 1. 12(d)].

The weak nonlocal limit has attracted much of our attention in this work. In the following section, we will see the spatially nonlocal nonlinear response in the case of the weak regime.

1.4.2 Spatially nonlocal nonlinearity

Previous research by Horikis et *al.* [85] extended the existence and elastic collision of ring dark and anti-dark solitons in a nonlocal medium with an exponential nonlocal response function in a weak or strong nonlocal regime. In our study, we investigate the dynamics of spatiotemporal dissipative LBs. In the case of the CCGLE, we find that these spatiotemporal dissipative LBs can be stable in a spatially weakly nonlocal self-defocusing fiber with a Gaussian nonlocal response function.

In general, one-dimensional solitons in optical fibers are stable because the linear and nonlinear effects are well balanced in this case. On the contrary, for two-dimensional solitons, especially spatial ones, we observe instability during their movement inside the optical fiber. They undergo an extreme explosion of intensity, called collapse. This is because the nonlinear phase modulation dominates the diffraction, leading to an extreme increase in amplitude.

Collapse is a well-known phenomenon in the theory of wave propagation in nonlinear focusing media. It refers to the situation when strong self-focusing of a beam leads to a catastrophic increase (blow-up) of its intensity in a finite time or after a finite propagation distance [86].

In this case, with critical power, the pulse will continue to decrease in a radially symmetrical manner, thus maintaining a profile independent of its initial shape. As a result, it is difficult to find solitons over long distances in (2+1)-D. However, we can avoid the collapse effect by introducing perturbation effects such as dissipation and nonlinear saturation. In addition, we can take into account the spatial non-locality of the nonlinear response inherent to the optical fiber.

For example, doping the optical fiber makes it possible to have a dissipative medium where gains and losses can amplify the nonlinearity to compensate for diffraction and thus avoid collapse [87,88]. Moreover, nonlocality acts to spread the effects of localized excitations, and as such can suppress instantaneous modulation instabilities of homogeneous states [89]. Therefore, we can expect to observe stable LBs that are (3+1)-D solitons when we take into account the physical phenomena mentioned above.

Let us therefore consider the general form of refractive index changes we have chosen to work with, for a weak nonlocal nonlinear medium, and extended for two transverse coordinates x and

y [77]:

$$\Delta n[I(r)] = q\int_{-\infty}^{\infty} R(r-r^{'})I(r^{'},z)dr^{'} \tag{1.43}$$

The parameter q accounts for the nonlinear response. When the Kerr nonlinearity is self-focusing, the parameter q in the above Eq. (1.43) is positive ($q>0$). On the contrary, when we are dealing with the self-defocusing Kerr nonlinearity, q is negative ($q<0$).

$R(r-r^{'})$ is the real, localized and symmetric function representing the profile of the nonlocal response of the medium, whose width determines the degree of nonlocality, as we mentioned before.

We do not assume asymmetric response functions, since they do not allow to define a Lagrangian and thus to use the variational approach[80]. Therefore, we only consider symmetric response functions. To allow comparison with the local, Kerr case, the response is normalized so that $\int R(r^{'})dr^{'}=1$. The nonlocal intensity ray $I(r^{'},z)$ can be expanded in a Taylor series around $(\xi-\xi^{'})$ and $(\eta-\eta^{'})$, with $\xi,\eta=x,y$.

Equation (1.45) is reduced to

$$\Delta n(I) = q\left[I+\left(\gamma_{\xi\xi}\frac{\partial^2}{\partial\xi^2}+\gamma_{\eta\eta}\frac{\partial^2}{\partial\eta^2}+\gamma_{\xi\eta}\frac{\partial^2}{\partial\xi\partial\eta}\right)I\right], \tag{1.44}$$

with

$$\gamma_{\xi\xi} = \frac{\int_{-\infty}^{\infty} R(\xi-\xi^{'},\eta-\eta^{'})(\xi-\xi^{'})^2 d\xi^{'}d\eta^{'}}{\int_{-\infty}^{\infty} R(\xi^{'},\eta^{'})d\xi^{'}d\eta^{'}}, \tag{1.45}$$

$$\gamma_{\eta\eta} = \frac{\int_{-\infty}^{\infty} R(\eta-\eta^{'},\xi-\xi^{'})(\eta-\eta^{'})^2 d\eta^{'}d\xi^{'}}{\int_{-\infty}^{\infty} R(\eta^{'},\xi^{'})d\eta^{'}d\xi^{'}}, \tag{1.46}$$

and

$$\gamma_{\xi\eta} = \frac{\int_{-\infty}^{\infty} R(\xi-\xi^{'},\eta-\eta^{'})(\xi-\xi^{'})(\eta-\eta^{'})d\xi^{'}d\eta^{'}}{\int_{-\infty}^{\infty} R(\xi^{'},\eta^{'})d\xi^{'}d\eta^{'}}. \tag{1.47}$$

The term $\gamma_{\xi\eta}$ can be neglected in an appropriately chosen and rotated coordinate system. In fact, it has been shown that for a Gaussian response, $\gamma_{\xi\xi}$=$w_{R\xi}^2/2$, with $w_{_R}=0.1\sigma/\sqrt{2}$. We recall that Eqs. (1.44)-(1.47) are justified when the nonlocality becomes weak, that is, $\gamma_{\xi\xi}\ll 1$ [18].

To recover the refractive index as a local function of the light intensity, i.e. $\Delta n(I)=qI(x,y,z)$, we simply have to reduce the nonlocal response function to a local function $R(x,y)=\delta(x,y)$. In this case, the refractive index at a given point is determined solely by the light intensity at that

point.

While working in a nonlocal nonlinear medium such as an optical fiber, recent works have shown that for weak nonlocality, a bright spatial soliton solution for self-focusing nonlinearity ($q > 0$) as well as a dark soliton for self-defocusing nonlinearity ($q < 0$) have been found and the stability of both the bright soliton and the dark soliton has been demonstrated [75]. Furthermore, some works have shown that a weak nonlocal contribution stops the catastrophic self-focusing of high-power optical beams, called collapse, and leads to the formation of stable 2D solitons (diffracting in two transverse dimensions) [75].

In previous work, such as that of Skupin et *al.* [90], it was shown that nonlocality promotes MI in self-defocusing media, while collapse is suppressed in self-focusing media. Furthermore, Hong Li et *al.* [91] state that nonlocality is thus a feature of a large number of nonlinear systems, leading to novel phenomena of a generic nature, and may promote MI in self-defocusing media and suppress wave collapse of multidimensional beams in self-focusing media. However, in our PhD thesis we show that even in self-defocusing nonlinear nonlocal media, collapse can be suppressed by combining dopant with weak nonlocality. As a consequence, three-dimensional dissipative solitons can propagate in a self-defocusing medium when the nonlinearity is weakly nonlocal.

1.4.3 Light bullets under the effect of a spatially nonlocal nonlinear response in a doped optical fiber

To the best of our knowledge, this concept has not yet been studied in depth. We can mathematically model such spatiotemporal LBs with the following (3+1)-D NLSE [2].

$$i\frac{\partial\phi}{\partial z} + \frac{1}{\beta_0}\left(\frac{\partial^2\phi}{\partial x^2} + \frac{\partial^2\phi}{\partial y^2}\right) - \frac{\beta_2}{2}\frac{\partial\phi}{\partial\tau} + q|\phi|^2\phi(x,y,z,\tau) = 0, \tag{1.48}$$

with the reduced time $\tau = t - \beta_1 z$. Physically, β_0 is the propagation constant, β_2 is the GVD parameter. The nonlinear parameter $q = (2\pi/\lambda)n_2$ accounts for the SPM. The two parameters β_2 and q, depending on the way they behave, either normal or anomalous GVD for β_2, or self-focusing vs. self-defocusing for q, are sometimes considered as positive or negative parameters. This depends on the nature of the nonlinear medium. The term $\phi(x,y,z,\tau)$ is the slowly varying envelope that accounts for the transverse coordinates (x,y) and the longitudinal coordinates τ.

It should be noted that, in the case of dissipative LBs propagating in a nonlocal optical fiber, Eq.

(1.48) has a different form, since we are no longer in a conservative system as is the case for the NLSE. In the cubic context, this process allows us to have the description given by the nonlocal CCGLE (see the reference [1] in the "List of publications" section).

$$i\frac{\partial\Phi}{\partial Z}+\zeta_1\left(\frac{\partial^2\Phi}{\partial X^2}+\frac{\partial^2\Phi}{\partial Y^2}\right)+\zeta_2\frac{\partial^2\Phi}{\partial\tau^2}+\zeta_3\Phi+\zeta_4|\Phi|^2\Phi+\zeta_5\frac{\partial^2}{\partial X^2}(|\Phi|^2)\Phi + \zeta_6\frac{\partial^2}{\partial Y^2}(|\Phi|^2)\Phi=Q, \quad (1.49)$$

The left side of Eq. (1.49) is the conservative part, which contains the slowly varying complex envelope $\Phi(X,Y,\tau,Z)$. The coefficient ζ_1 is related to linear diffraction. The second order dispersion term ζ_2. The parameter ζ_4 takes into account the cubic nonlinearity, the spatially nonlocal cubic nonlinear response coefficients ζ_5 and ζ_6. The coefficients ζ_5 and ζ_6 are also in the conservative part, because nonlocality is an inherent effect of the fiber that is generally negligible. The parameter ζ_3 represents the attenuation. The parameter Q contains dissipative terms. You can get some details about the derivation of this equation in chapter two. We show that Eq. (1.49) provides a good description of LBs in nonlocal doped optical fiber for a cubic context.

1.5 Conclusion

This chapter has covered the history, classification, and properties of optical fibers. We have seen that doping an optical fiber, particularly with erbium ions (Er^{3+}), creates a dissipative medium where balanced gains and losses can amplify and counteract nonlinearities, dispersion, attenuation and diffraction effects, ensuring stable propagation of light bullets (LBs). This double balance–between linear and nonlinear effects, as well as between gains and losses–plays a crucial role in the design of optical amplifiers, particularly in erbium-doped fiber amplifiers (EDFAs).

We also discussed the concept of nonlocality, which spreads the effects of localized excitations. This property can help suppress instantaneous modulation instabilities of homogeneous states, enabling the stable observation of LBs. The remaining work involves demonstrating that these LBs can propagate stably in (3+1)-D and without collapsing when the double equilibrium is coupled to a weak, spatially nonlocal nonlinear response.

Chapter II

Models and Methods

2.1 Introduction

Considering the theory of electromagnetic waves from Maxwell's equations, we present an extended (3+1)-D CCGLE and CQCGLE describing the dynamics of dissipative LBs in optical fiber amplifiers under the interplay of a doping effect and a spatially nonlocal nonlinear response.

The governing model equations include the effects of fiber dispersion, linear gain, nonlinear loss, fiber nonlinearity, atomic detuning, linear and nonlinear diffractive transverse effects, and nonlocal nonlinear response. Our primary focus is on the localized Gaussian solution in the form of three-dimensional traveling waves.

We assess the role played by a weak spatial nonlocality term in the shape formation of dissipative LBs. A system of eight coupled first-order differential equations of the LB parameters of interest, for each case, the (3+1)-D CCGLE case and the (3+1)-D CQCGLE case, is derived based on variational equations resulting from the Euler-Lagrange equations. The LB parameters of interest are the amplitude, the temporal and spatial pulse widths, the position of the pulse maximum, the unequal wavefront curvatures, the chirp parameters, and the phase shift.

2.2 Derivation of the (3+1)-D cubic complex Ginzburg-Landau equation from the Maxwell's Equations

2.2.1 Maxwell's equations

We analyze the propagation of optical fields in the framework of Maxwell's equations, written in differential form as follows:

$$\vec{\nabla} \wedge \vec{E} = -\frac{\partial \vec{B}}{\partial t} : (Maxwell - Faraday). \tag{2.1}$$

$$\vec{\nabla} \wedge \vec{H} = \vec{J} + \frac{\partial \vec{D}}{\partial t} : (Maxwell - Ampere). \tag{2.2}$$

$$\vec{\nabla}.\vec{D} = \rho : (Maxwell - Gauss). \tag{2.3}$$

$$\vec{\nabla}.\vec{B} = 0 : (Maxwell - flux), \tag{2.4}$$

where $\vec{E}$ and $\vec{H}$ are the electric and magnetic field vectors, respectively. The quantities $\vec{D}$ and $\vec{B}$ are the electric and magnetic flux densities, respectively. The term $\vec{D}$ is also called the electric displacement and $\vec{B}$ the magnetic induction. The quantities ρ and $\vec{J}$ are the volume charge density and the electric current density (charge flux) of any external charges. The charge and current densities ρ, $\vec{J}$ can be thought of as the sources of the electromagnetic fields in a material medium. The induced polarization $\vec{P}$ and the magnetization $\vec{M}$ can be made explicit in Maxwell's equations by using the constitutive relations:

$$\vec{D} = \epsilon_0 \vec{E} + \vec{P}, \tag{2.5}$$

and

$$\vec{B} = \mu_0(\vec{H} + \vec{M}), \tag{2.6}$$

where ϵ_0 and μ_0 are the permittivity and permeability of the vacuum, respectively. The optical fiber is a dielectric medium free of charge and current. This implies,

$$\vec{J} = \vec{0}, \tag{2.7}$$

$$\rho = 0, \tag{2.8}$$

$$\vec{M} = \vec{0}. \tag{2.9}$$

Thus Maxwell's equations become:

$$\vec{\nabla} \wedge \vec{E} = -\frac{\partial \vec{B}}{\partial t}, \tag{2.10}$$

$$\vec{\nabla} \wedge \vec{B} = \mu_0 \frac{\partial \vec{D}}{\partial t}, \tag{2.11}$$

$$\vec{\nabla}.\vec{D} = 0, \tag{2.12}$$

$$\vec{\nabla}.\vec{B} = 0. \tag{2.13}$$

By taking the curl of both sides of Eq. (2.10) and using the divergence equations together with the vector identity:

$$\vec{\nabla} \wedge \vec{\nabla} \wedge \vec{E} = \vec{\nabla}(\vec{\nabla} \cdot \vec{E}) - \vec{\nabla}^2 \vec{E}, \tag{2.14}$$

we get,

$$\vec{\nabla}(\vec{\nabla} \cdot \vec{E}) - \vec{\nabla}^2 \vec{E} = \frac{\partial}{\partial t}(\vec{\nabla} \wedge \vec{B}). \tag{2.15}$$

Substituting Eq. (2.11) into Eq. (2.15) results in

$$-\vec{\nabla}^2 \vec{E} + \vec{\nabla}(\vec{\nabla} \cdot \vec{E}) = \frac{\partial}{\partial t}\left(-\mu_0 \frac{\partial \vec{\vec{D}}}{\partial t}\right). \tag{2.16}$$

Since

$$\vec{\nabla} \cdot \vec{E} = 0, \tag{2.17}$$

therefore

$$\vec{\nabla}^2\vec{E} - \mu_0\frac{\partial^2\vec{\vec{D}}}{\partial t^2} = 0. \tag{2.18}$$

2.2.2 The extended (3+1)-D cubic complex Ginzburg-Landau equation

Let us recall that for the dielectric material we have in the time domain

$$\vec{D} = \epsilon_0\vec{E} + \vec{P}. \tag{2.19}$$

The vector polarization $\vec{P}$ is given as:

$$\vec{P} = \vec{P}_l + \vec{P}_{Nl}, \tag{2.20}$$

where P_l is the linear polarization and P_{Nl} is the cubic nonlinear polarization.

We have the following for the linear part:

$$\vec{P}_l = \epsilon_0\chi^{(1)}\vec{E}. \tag{2.21}$$

For the cubic nonlinear part, we have:

$$\vec{P}_{Nl} = \epsilon_0\chi^{(3)} : \vec{E}\vec{E}\vec{E}. \tag{2.22}$$

The expression $\chi^{(3)}$:$\vec{E}\vec{E}\vec{E}$ represents the tensor contraction of the rank-4 susceptibility tensor with the outer product of three electric field vectors.

Eq. (2.22) can also be written in a different form:

$$\vec{P}_{Nl} = \epsilon_0\frac{3}{8n_0}\chi^{(3)}|\vec{E}|^2\vec{E}, \tag{2.23}$$

The cubic nonlinear dielectric constant is:

$$\epsilon_{Nl} = \frac{3}{8n_0}\chi^3|\vec{E}|^2. \tag{2.24}$$

Therefore,

$$\vec{P}_{Nl} = \epsilon_0 \epsilon_{Nl} \vec{E}. \tag{2.25}$$

Then, Eq. (2.19) becomes:

$$\vec{D} = \epsilon_0 \vec{E} + \epsilon_0 \chi^{(1)} \vec{E} + \epsilon_0 \epsilon_{Nl} \vec{E}, \tag{2.26}$$

which results in

$$\vec{D} = \epsilon_0 (1 + \chi^{(1)} + \epsilon_{Nl}) \vec{E}. \tag{2.27}$$

Equation (2.27) can also be written as:

$$\vec{D} = \epsilon_0 \epsilon(\omega) \vec{E}, \tag{2.28}$$

where $\epsilon(\omega)$ is the total dielectric constant, including the linear and cubic nonlinear contributions:

$$\epsilon(\omega) = 1 + \chi^{(1)} + \epsilon_{Nl}. \tag{2.29}$$

We will have in the frequency domain:

$$\vec{D} = \epsilon_0 \epsilon(\omega) \tilde{E}(r, \omega). \tag{2.30}$$

It should also be remembered that in the frequency domain

$$\frac{\partial}{\partial t} \rightarrow i\omega \tag{2.31}$$

$$\frac{\partial^2}{\partial t^2} \rightarrow -\omega^2. \tag{2.32}$$

Taking all these considerations into account, the Eq. (2.18) becomes:

$$\vec{\nabla}^2\tilde{E}(r,\omega) + \mu_0\epsilon_0\epsilon(\omega)\omega^2\tilde{E}(r,\omega) = 0. \tag{2.33}$$

Since $\epsilon_0\mu_0 = \frac{1}{c^2}$, the Eq. (2.33) can be reduced to:

$$\vec{\nabla}^2\tilde{E}(r,\omega) + \frac{\omega^2}{c^2}\epsilon(\omega)\tilde{E}(r,\omega) = 0. \tag{2.34}$$

Given that,

$$\beta^2(\omega) = \frac{\omega^2}{c^2}\epsilon(\omega), \tag{2.35}$$

and that,

$$\beta(\omega) = \frac{\omega}{c}\sqrt{\epsilon(\omega)}. \tag{2.36}$$

we have:

$$\left[\vec{\nabla}^2 + \beta^2(\omega)\right]\tilde{E}(r,\omega) = 0. \tag{2.37}$$

The Laplacian operator $\vec{\nabla}^2$ is given in the following way:

$$\vec{\nabla}^2 = \frac{\partial^2}{\partial x^2} + \frac{\partial^2}{\partial y^2} + \frac{\partial^2}{\partial z^2}. \tag{2.38}$$

In the frequency domain, the electric field $\tilde{E}$ is given by the expression:

$$\tilde{E}(r,\omega) = \int_{-\infty}^{+\infty}\vec{E}(r,t)exp(i\beta_0 z - i\omega_0 t)exp(i\omega t)dt + cc. \tag{2.39}$$

Eq. (2.39) can also be written as:

$$\tilde{E}(r,\omega) = \int_{-\infty}^{+\infty}\vec{E}(r,t)exp\left[i\beta_0 z + i(\omega-\omega_0)t\right]dt + cc, \tag{2.40}$$

where $\vec{E}(r,t)$ is the electric field in the time domain, which is given by

$$\vec{E}(r,t) = \frac{1}{2}\vec{e}\phi(r,t)exp\left[i\beta_0 z + i(\omega-\omega_0)t\right] + cc. \tag{2.41}$$

Here, $\phi(x,y,z,t)$ is the slowly varying envelope function that represents the light pulse carrying the information, *c.c.* is the complex conjugate, ω_0 is the carrier frequency, β_0 is the propagation constant at the carrier frequency ω_0, and $\vec{e}$ is the polarization unit vector. The optical fiber has a cylindrical shape with axis (oz), so the radius r is defined as $r = \sqrt{x^2+y^2}$.

Using Eqs (2.38), (2.40) and (2.41), Eq (2.37) becomes:

$$\left(\frac{\partial^2\phi}{\partial x^2} + \frac{\partial^2\phi}{\partial y^2}\right) + \frac{\partial^2\phi}{\partial z^2} + 2i\beta_0\frac{\partial\phi}{\partial z} + \left[\beta^2(\omega) - \beta_0^2(\omega)\right]\phi = 0. \tag{2.42}$$

For optical beams, the paraxial and quasimonochromatic approximations correspond to neglecting the $\frac{\partial^2}{\partial z^2}$ derivatives of the slowly varying amplitude on the grounds that $|\frac{\partial^2\phi}{\partial z^2}| \ll \beta_0|\frac{\partial\phi}{\partial z}|$. This will result in:

$$2i\beta_0\frac{\partial\phi}{\partial z} + \left(\frac{\partial^2\phi}{\partial x^2} + \frac{\partial^2\phi}{\partial y^2}\right) + \left[\beta^2(\omega) - \beta_0^2(\omega)\right]\phi = 0. \tag{2.43}$$

We divide the whole equation (2.43) by $2\beta_0$:

$$i\frac{\partial\phi}{\partial z} + \frac{1}{\beta_0}\left(\frac{\partial^2\phi}{\partial x^2} + \frac{\partial^2\phi}{\partial y^2}\right) + \left[\frac{\beta^2(\omega) - \beta_0^2(\omega)}{2\beta_0(\omega)}\right]\phi = 0. \tag{2.44}$$

The expression $\left[\frac{\beta^2(\omega)-\beta_0^2(\omega)}{2\beta_0(\omega)}\right]$ describes the dispersion of the envelope and,

$$\frac{\beta^2(\omega) - \beta_0^2(\omega)}{2\beta_0(\omega)} = \left[\beta(\omega) - \beta_0(\omega)\right]\left[1 + \frac{\beta(\omega) - \beta_0(\omega)}{2\beta_0(\omega)}\right] \backsimeq \left[\beta(\omega) - \beta_0(\omega)\right]. \tag{2.45}$$

Recall Eq. (2.36), where $\epsilon(\omega)$ is a complex dielectric constant given in Eq. (2.29) and which can also be written as:

$$\epsilon(\omega) = n_f^2 + 2in_f.\frac{\alpha_f}{k_0} + \chi_a(\omega). \tag{2.46}$$

As a result, Eq. (2.36) has the following form (see also Appendix A):

$$\beta(\omega) = \frac{\omega}{c}\sqrt{n_f^2 + 2in_f.\frac{\alpha_f}{k_0} + \chi_a(\omega)}, \tag{2.47}$$

where α_f is the fiber loss defined by:

$$\alpha_f = \frac{10}{L}\log\frac{P_{out}}{P_{in}}, (dB/km) \tag{2.48}$$

where, P_{in} is the input light pulse power, P_{out} is the output light pulse power and L, the length of the optical fiber. k_0 is the wavenumber given by:

$$k_0 = \frac{\omega}{c}, \tag{2.49}$$

with c, the light celerity, and ω, the optical frequency. $\chi_a(\omega)$ is the atomic susceptibility governing the response of the dopant in the optical fiber, which is determined by [18]:

$$\chi_a(\omega) = \frac{g_p}{k_0}\frac{(\omega-\omega_a)T_2 - i}{1+(\omega-\omega_a)^2T_2^2}, \tag{2.50}$$

with the peak gain $g_p = \sigma(N_2 - N_1)$. The parameter σ is a transition cross section, while N_1 and N_2 are the atomic densities for the lower and upper energy levels of the two-level system. ω_a is the atomic resonance frequency, and T_2 is the relaxation time. Moreover, one can expand the function $\chi_a(\omega)$ in Taylor series up to the second order in the vicinity of the carrier frequency ω_0 and find [18]:

$$\chi_a(\omega) = \frac{g_p}{k_0}\left[\frac{\delta - i}{1+\delta^2} + \frac{1-\delta^2+2i\delta}{(1+\delta^2)^2}(\omega-\omega_0)T_2 + \frac{\delta(\delta^2-3)+i(1-3\delta^2)}{(1+\delta^2)^3}(\omega-\omega_0)^2T_2^2\right], \tag{2.51}$$

where $\delta = (\omega_0 - \omega_a)T_2$ is the detuning parameter. n_f, in Eqs. (2.44) and (2.45), is the refractive index of the fiber including linear, nonlinear, doping, and spatial nonlocality phenomena. The given expression of n_f is [92]:

$$n_f = n_0(\omega) + n_2\frac{\int_{-\infty}^{\infty} R(x-x',y-y')I(x',y')dx'dy'}{\int_{-\infty}^{\infty} R(x-x',y-y')dx'dy'}. \tag{2.52}$$

Here, n_2 represents the cubic nonlinear change in the refractive index, $R(x-x',y-y')$ is the nonlocal response function which determines the spatial extent of nonlocality. $I(x',y')$ is the nonlocal intensity which acts not only on the local points *(x,y)*, but also in the neighboring points, and can be evaluated as [92]:

$$I(x',y') = I(x,y) + \frac{1}{2}\frac{\partial^2}{\partial x^2}I(x,y)(x-x')^2 + \frac{1}{2}\frac{\partial^2}{\partial y^2}I(x,y)(y-y')^2 + \frac{\partial^2}{\partial x\partial y}I(x,y)(x-x')(y-y'), \tag{2.53}$$

where $I(x,y)$ is the external action of the intensity on the points *(x,y)*, ($I = |E|^2$). Using this assumption, Eq. (2.52) is rewritten as:

$$n_f = n_0(\omega) + n_2|\vec{E}|^2 + \frac{n_2\gamma_{xx}}{2}\frac{\partial^2}{\partial x^2}(|\vec{E}|^2) + \frac{n_2\gamma_{yy}}{2}\frac{\partial^2}{\partial y^2}(|\vec{E}|^2) + \frac{n_2\gamma_{xy}}{2}\frac{\partial^2}{\partial x\partial y}(|\vec{E}|^2). \quad (2.54)$$

In Eq. (2.54), $\vec{E}$ is the electric-field vector defined in Eq. (2.39). The coefficients γ_{xx}, γ_{yy} and γ_{xy} represent the measures of weak nonlocality degree in the transverse coordinates x and y, respectively. These nonlocality degree coefficients are determined by the relations:

$$\gamma_{\xi\xi} = \frac{\int_{-\infty}^{\infty} R(\xi-\xi^{'},\eta-\eta^{'})(\xi-\xi^{'})^2 d\xi^{'}d\eta^{'}}{\int_{-\infty}^{\infty} R(\xi^{'},\eta^{'})d\xi^{'}d\eta^{'}},$$
$$\gamma_{\eta\eta} = \frac{\int_{-\infty}^{\infty} R(\eta-\eta^{'},\xi-\xi^{'})(\eta-\eta^{'})^2 d\eta^{'}d\xi^{'}}{\int_{-\infty}^{\infty} R(\eta^{'},\xi^{'})d\eta^{'}d\xi^{'}}, \quad (2.55)$$

and

$$\gamma_{\xi\eta} = \frac{\int_{-\infty}^{\infty} R(\xi-\xi^{'},\eta-\eta^{'})(\xi-\xi^{'})(\eta-\eta^{'})d\xi^{'}d\eta^{'}}{\int_{-\infty}^{\infty} R(\xi^{'},\eta^{'})d\xi^{'}d\eta^{'}}, \quad (2.56)$$

for $\xi,\eta = x,y$. The term $\gamma_{\xi\eta}$ can be neglected in a suitably chosen and rotated coordinate system.

Therefore,

$$n_f = n_0(\omega) + n_2|\vec{E}|^2 + \frac{n_2\gamma_{xx}}{2}\frac{\partial^2}{\partial x^2}(|\vec{E}|^2) + \frac{n_2\gamma_{yy}}{2}\frac{\partial^2}{\partial y^2}(|\vec{E}|^2). \quad (2.57)$$

Taking all these considerations into account, Eq (2.47) then becomes (see also the procedure used in Appendix A):

$$\begin{aligned}\beta(\omega) = \beta_0(\omega) &+ i\beta_1\frac{\partial}{\partial t} - \frac{\beta_2}{2}\frac{\partial^2}{\partial t^2} + \left(\frac{\partial\beta_f}{\partial(|\phi|^2)}\right)_0(|\phi|^2) + \frac{\omega}{c}n_2|\phi|^2 + \frac{\omega}{c}\frac{n_2\gamma_{xx}}{2}\frac{\partial^2}{\partial x^2}(|\phi|^2)\\ &+ \frac{\omega}{c}\frac{n_2\gamma_{yy}}{2}\frac{\partial^2}{\partial y^2}(|\phi|^2) + i\alpha_f + i\alpha_f\frac{n_2}{n_0}|\phi|^2 + i\alpha_f\frac{n_2}{n_0}\frac{\gamma_{xx}}{2}\frac{\partial^2}{\partial x^2}(|\phi|^2) + i\alpha_f\frac{n_2}{n_0}\frac{\gamma_{yy}}{2}\frac{\partial^2}{\partial y^2}(|\phi|^2)\\ &+ \frac{g_p}{2n_0}\left[\frac{\delta-i}{1+\delta^2} + \frac{1-\delta^2+2i\delta}{(1+\delta^2)^2}\left(i\frac{\partial}{\partial t}\right)T_2 + \frac{\delta(\delta^2-3)+i(1-3\delta^2)}{(1+\delta^2)^3}\left(-\frac{\partial^2}{\partial t^2}\right)T_2^2\right]. \quad (2.58)\end{aligned}$$

Substituting Eq. (2.56) into Eq. (2.42) gives:

$$i\frac{\partial\phi}{\partial z}+(\beta_{reff}+i\beta_{ieff})\frac{\partial\phi}{\partial t}+\frac{1}{\beta_0}\left(\frac{\partial^2\phi}{\partial x^2}+\frac{\partial^2\phi}{\partial y^2}\right)+(p_r+ip_i)\frac{\partial^2\phi}{\partial t^2}+(\gamma_r+i\gamma_i)\phi$$
$$+(q_r+iq_i)|\phi|^2\phi+(\gamma_{xx,r}+i\gamma_{xx,i})\frac{\partial^2}{\partial x^2}(|\phi|^2)\phi+(\gamma_{yy,r}+i\gamma_{yy,i})\frac{\partial^2}{\partial y^2}(|\phi|^2)\phi=0. \quad (2.59)$$

In the above Eq. (2.59), $\frac{\partial\phi}{\partial z}$ represents the displacement of the light pulse over the propagation distance z. The expression $\left(\frac{\partial^2\phi}{\partial x^2}+\frac{\partial^2\phi}{\partial y^2}\right)$ corresponds to the linear diffraction of the light pulse in the transverse coordinates x and y. The terms $\frac{\partial^2}{\partial x^2}(|\phi|^2)\phi$ and $\frac{\partial^2}{\partial y^2}(|\phi|^2)\phi$ correspond to the nonlinear diffraction related to spatial nonlocality. This nonlinear diffraction is associated with the linear diffraction in order to influence the self-focusing and avoid the collapse [30]. The parameters $\beta_{reff} = -\frac{g_p}{2n_0}\frac{2\delta T_2}{(1+\delta^2)^2}$ and $\beta_{ieff}=\beta_1+\frac{g_p}{2n_0}\frac{(1-\delta^2)T_2}{(1+\delta^2)^2}$, are the real and imaginary parts of the inverse of the group velocity dispersion, respectively. The coefficient $p_r=-\frac{\beta_2}{2}-\frac{g_p}{2n_0}\frac{\delta(\delta^2-3)T_2^2}{(1+\delta^2)^3}$, measures the wave dispersion, and $p_i=-\frac{g_p}{2n_0}\frac{(1-3\delta^2)T_2^2}{(1+\delta^2)^3}$, is the spectral filtering. The term $\gamma_r=\frac{g_p}{2n_0}\frac{\delta}{(1+\delta^2)}$ is the linear loss, and $\gamma_i=\alpha_f-\frac{g_p}{2n_0}\frac{1}{(1+\delta^2)}$ is the frequency shift. The parameter $q_r=n_2\frac{\omega}{c}+\left(\frac{\partial\beta_f}{\partial(|\phi|^2)}\right)_0$, represents the nonlinear coefficient and $q_i=n_2\frac{\alpha_f}{n_0}$, is the nonlinear gain-absorption coefficient. Expressions $\gamma_{\xi\xi,r}=\frac{1}{2}\frac{n_2\omega}{c}\gamma_{\xi\xi}$ and $\gamma_{\xi\xi,i}=\frac{1}{2}\frac{n_2\alpha_f}{n_0}\gamma_{\xi\xi}$, represent the real and imaginary parts of the nonlocality degrees along the transverse coordinates x and y, respectively.

Let us look at Eq. (2.59). If we first substitute p_r, γ_r, q_r, $\gamma_{xx,r}$ and $\gamma_{yy,r}$ into the factor, we get:

$$i\frac{\partial\phi}{\partial z}+(\beta_{reff}+i\beta_{ieff})\frac{\partial\phi}{\partial t}+\frac{1}{\beta_0}\left(\frac{\partial^2\phi}{\partial x^2}+\frac{\partial^2\phi}{\partial y^2}\right)+p_r\left(1+ia_1\right)\frac{\partial^2\phi}{\partial t^2}+\gamma_r\left(1+ic_0\right)\phi$$
$$+q_r\left(1+ib_1\right)|\phi|^2\phi+\gamma_{xx,r}\left(1+ic_{1,xx}\right)\frac{\partial^2}{\partial x^2}(|\phi|^2)\phi+\gamma_{yy,r}\left(1+ic_{2,yy}\right)\frac{\partial^2}{\partial y^2}(|\phi|^2)\phi=0, \quad (2.60)$$

where, $a_1=\frac{p_i}{p_r}$; $c_0=\frac{\gamma_i}{\gamma_r}$; $b_1=\frac{q_i}{q_r}$; $c_{1,xx}=\frac{\gamma_{xx,i}}{\gamma_{xx,r}}$; $c_{2,yy}=\frac{\gamma_{yy,i}}{\gamma_{yy,r}}$.

To scale Eq. (2.60), we introduce the following physical parameters, namely the diffraction length or Rayleigh length in the homogeneous medium: $L_{Diff}=\beta_0 r_0^2$, where r_0 is the beam radius. The dispersion length is $L_{Disp}=\frac{T_0^2}{|p_r|}$. The parameter T_0 is the typical initial pulse width. The effective length, which characterizes the influence of the nonlinearity, is $L_{NL}=\frac{1}{q_r P_0}$. The transverse coordinate scales are $X=\frac{x}{r_0}$ and $Y=\frac{y}{r_0}$. The longitudinal coordinate scale is $Z=\frac{z}{L_{Disp}}$ and the temporal coordinate scale is $\tau=\frac{T}{T_0}$. Here $T=t-\frac{z}{v_g}$ is the time in the moving coordinate

system. The normalized field amplitude is $\Phi(X,Y,Z,\tau) = \sqrt{P_0}N\phi(x,y,z,t)$, where $N^2 = \frac{L_{Disp}}{L_{NL}}$ and $N = \sqrt{\frac{q_r P_0 T_0^2}{|p_r|}}$. Typical optical pulse parameters used in fiber communication systems are [28], the wavelength $\lambda = 1.55\mu m$, the linear refractive index $n_0 = 1.45$, the nonlinear refractive index $n_2 = 2.7 \times 10^{-13} cm^2/W$, the group velocity dispersion $p_r = 50ps^2/km = \beta_2$, the nonlinear gain $g_p = 6.8W^{-1}km^{-1}$, the pulse width $1.763T_0 = 400fs$, the peak power of the incident pulse $P_0 = 9.43MW$. We also set $a_1 = \frac{p_i}{p_r}$, $b_1 = \frac{q_i}{q_r}$, $c_0 = \frac{\gamma_i}{\gamma_r}$, $c_{_{1,XX}} = \frac{\gamma_{XX,i}}{\gamma_{XX,r}}$, and $c_{_{2,YY}} = \frac{\gamma_{YY,i}}{\gamma_{YY,r}}$.
Taking into account these scaling transformations (see Appendix B), Eq. (2.60) then takes the form:

$$i\frac{\partial\Phi}{\partial Z} + \zeta_1\left(\frac{\partial^2\Phi}{\partial X^2} + \frac{\partial^2\Phi}{\partial Y^2}\right) + (1+ia_1)\,\zeta_2\frac{\partial^2\Phi}{\partial\tau^2} + (1+ib_1)\,\zeta_3\Phi + (1+ic_0)\,\zeta_4|\Phi|^2\Phi + \left(1+ic_{_{1,XX}}\right)\zeta_5\frac{\partial^2}{\partial X^2}(|\Phi|^2)\Phi + \left(1+ic_{_{2,YY}}\right)\zeta_6\frac{\partial^2}{\partial Y^2}(|\Phi|^2)\Phi = 0, \quad (2.61)$$

where,

$\zeta_1 = \frac{L_{Disp}}{\beta_0 r_0^2}$, $\zeta_2 = \frac{p_r L_{Disp}}{T_0^2 N\sqrt{P_0}}$, $\zeta_3 = \gamma_r L_{Disp}$, $\zeta_4 = \frac{q_r L_{NL}}{P_0}$, $\zeta_5 = \frac{\gamma_{XX} L_{NL}}{P_0 r_0^2}$, and $\zeta_6 = \frac{\gamma_{YY} L_{NL}}{P_0 r_0^2}$.
The coefficient ζ_1 is related to linear diffraction. The second order dispersion term is ζ_2 and ζ_3 corresponds to the linear losses. The parameter ζ_4 takes into account the cubic nonlinearity, the spatially nonlocal cubic nonlinear response coefficients are ζ_5 and ζ_6. The coefficients ζ_5 and ζ_6 are also in the conservative part, because nonlocality is an inherent effect of the fiber that is generally negligible.

Considering Eq. (2.61), for $a_1 = b_1 = c_0 = c_{_{1,XX}} = c_{_{2,YY}}$, we recover the (2+1)-D nonlocal NLSE equation that was derived by Bezuhanov et *al.* [92] in the limit of weak nonlocality. The conditions for breathing soliton formation in one and two transverse dimensions were established for this equation.
Furthermore, it was shown that the interplay between nonlinear diffraction and self-focusing is found to result in an increase of the power needed to form nonlocal spatial solitons. Indeed, the nonlocal 2D NLS equation has been also derived by Skupin et *al.* [90] in the highly nonlocal limit. Due to the mixture of local and nonlocal types of nonlinearity (Gaussian model of nonlocality, thermal nonlinearity, and the model of a dipolar Bose-Einstein condensate), a variety of solutions, such as rotating and nonrotating azimuthons, accessible solitons can be stabilized. Moreover, the

stabilization of 2D ring dark solitons and ring anti-dark solitons was demonstrated in nonlocal media [73].

2.3 The extended (3+1)-D cubic-quintic complex Ginzburg-Landau equation

As we saw in Section 2.1 that the nonlocal CCGLE is derived from Maxwell's equations. Similarly, the nonlocal CQCGLE is derived from Maxwell's equations. Therefore, in this section, we will start from the following well-defined equation rather than Maxwell's equations:

$$i\frac{\partial\phi}{\partial z}+\frac{1}{\beta_0}\left(\frac{\partial^2\phi}{\partial x^2}+\frac{\partial^2\phi}{\partial y^2}\right)+\left[\beta(\omega)-\beta_0(\omega)\right]\phi=0, \tag{2.62}$$

with the propagation constant $\beta(\omega)$ around the frequency ω given by:

$$\beta(\omega)=\frac{\omega}{c}\sqrt{n_f^2+2in_f.\frac{\alpha_f}{k_0}+\chi_a(\omega)}. \tag{2.63}$$

As we have said, $\chi_a(\omega)$ is the atomic susceptibility that governs the response of the dopant in the optical fiber. To derive the CQCGLE, we expand this atomic susceptibility in Taylor series up to the fourth order in the vicinity of the carrier frequency ω_0:

$$\begin{aligned}\chi_a(\omega)=\frac{g_p}{k_0}\Bigg[&\frac{\delta-i}{1+\delta^2}+\frac{1-\delta^2+2i\delta}{(1+\delta^2)^2}(\omega-\omega_0)T_2+\frac{\delta(\delta^2-3)+i(1-3\delta^2)}{(1+\delta^2)^3}(\omega-\omega_0)^2T_2^2\\&+\frac{6\delta^2-\delta^4-1+i(4\delta^3-4\delta)}{(1+\delta^2)^4}(\omega-\omega_0)^3T_2^3\\&+\frac{\delta^5-10\delta^3+5\delta-i(5\delta^4-10\delta^2+1)}{(1+\delta^2)^5}(\omega-\omega_0)^4T_2^4\Bigg],\end{aligned} \tag{2.64}$$

The refractive index of the fiber, including the linear, nonlinear, doping, and spatial nonlocality phenomena, in the cubic-quintic case is given by :

$$\begin{aligned}n_f=n_0(\omega)+n_2(|E|^2)+\frac{1}{2}n_2\gamma_{xx}\frac{\partial^2(|E|^2)}{\partial x^2}+\frac{1}{2}n_2\gamma_{yy}\frac{\partial^2(|E|^2)}{\partial y^2}+\frac{1}{2}n_2\gamma_{xy}\frac{\partial^2(|E|^2)}{\partial x\partial y}\\+n_4|E|^4+\frac{1}{2}n_4\gamma_{xx}\frac{\partial^2(|E|^4)}{\partial x^2}+\frac{1}{2}n_4\gamma_{yy}\frac{\partial^2(|E|^4)}{\partial y^2}+\frac{1}{2}n_4\gamma_{xy}\frac{\partial^2(|E|^4)}{\partial x\partial y},\end{aligned} \tag{2.65}$$

where n_2 and n_4 represent the cubic and quintic nonlinear refractive index changes, respectively. The nonlocality degree coefficients $\gamma_{\xi\xi}$, $\gamma_{\eta\eta}$ and $\gamma_{\xi\eta}$ are determined as in Eqs. (2.55) and (2.56), for $\xi, \eta = x, y$. The term $\gamma_{\xi\eta}$ can be neglected.

Substituting Eq. (2.65) into Eq. (2.63), we obtain:

$$\begin{aligned}\beta(\omega) = \frac{\omega}{c}n_0(\omega) + \frac{1}{2}\frac{\omega n_2^2|E|^4}{n_0 c} + \frac{\omega n_2|E|^2}{c} + \frac{\omega n_4|E|^4}{c} \\ + \frac{1}{2}\frac{\omega n_2}{c}\left(\gamma_{xx}\frac{\partial^2(|E|^2)}{\partial x^2} + \gamma_{yy}\frac{\partial^2(|E|^2)}{\partial y^2}\right) + \frac{1}{2}\frac{\omega n_4}{c}\left(\gamma_{xx}\frac{\partial^2(|E|^4)}{\partial x^2} + \gamma_{yy}\frac{\partial^2(|E|^4)}{\partial y^2}\right) \\ + \frac{1}{2}\frac{\omega n_2^2}{n_0 c}\left(\gamma_{xx}\frac{\partial^2(|E|^4)}{\partial x^2} + \gamma_{yy}\frac{\partial^2(|E|^4)}{\partial y^2}\right) + \frac{1}{2}\frac{\omega n_2^2}{n_0 c}\left(\gamma_{xx}^2\frac{\partial^4(|E|^4)}{\partial x^4} + \gamma_{yy}^2\frac{\partial^4(|E|^4)}{\partial y^4}\right) \\ + i\alpha_f + i\frac{\alpha_f n_2}{n_0}|E|^2 + i\frac{1}{2}\frac{\alpha_f n_2}{n_0}\left(\gamma_{xx}\frac{\partial^2(|E|^2)}{\partial x^2} + \gamma_{yy}\frac{\partial^2(|E|^2)}{\partial y^2}\right) \\ + i\frac{\alpha_f n_4}{n_0}|E|^4 + i\frac{1}{2}\frac{\alpha_f n_4}{n_0}\left(\gamma_{xx}\frac{\partial^2(|E|^4)}{\partial x^2} + \gamma_{yy}\frac{\partial^2 E^4}{\partial y^2}\right) + \frac{1}{2}\frac{\omega}{n_0 c}\chi_a(\omega). \quad (2.66)\end{aligned}$$

The first expression $\frac{\omega}{c}n_0(\omega)$ is the undoped propagation constant denoted $\beta_f(\omega)$ and given by:

$$\begin{aligned}\beta_f(\omega) = \frac{\omega}{c}n_0(\omega) = \beta_0 + \left(\frac{\partial}{\partial\omega}\beta_f\right)(\omega-\omega_0) + \frac{1}{2}\left(\frac{\partial^2}{\partial\omega^2}\beta_f\right)(\omega-\omega_0)^2 \\ + \frac{1}{6}\left(\frac{\partial^3}{\partial\omega^3}\beta_f\right)(\omega-\omega_0)^3 + \frac{1}{24}\left(\frac{\partial^4}{\partial\omega^4}\beta_f\right)(\omega-\omega_0)^4 + \left(\frac{\partial}{\partial(|E|^2)}\beta_f\right)_0|E|^2 \\ + \left(\frac{\partial^2}{\partial\omega\partial(|E|^2)}\beta_f\right)_0(\omega-\omega_0)|E|^2 + \left(\frac{\partial}{\partial(|E|^2)_t}\beta_f\right)_0(|E|^2)_t + \frac{1}{2}\left(\frac{\partial^2}{\partial(|E|^2)^2}\beta_f\right)_0|E|^4, \quad (2.67)\end{aligned}$$

where $(|E|^2)_t = (|E|^2)\left(\frac{\partial}{\partial t}\right)$.

In Eqs. (2.64) and (2.67), the expression $(\omega-\omega_0)^n = (i)^n(\frac{\partial^n}{\partial t^n})$, with $n = 1...4$. And for Eqs. (2.65), (2.66), and (2.67), $\vec{E}$ is the field vector defined by Eq. (2.41).

By substituting Eqs. (2.64), (2.66) and (2.67) into Eqs. (2.62), we get:

$$
\begin{aligned}
i\frac{\partial\phi}{\partial z}+\frac{1}{\beta_0}\left(\frac{\partial^2\phi}{\partial x^2}+\frac{\partial^2\phi}{\partial y^2}\right)+\left(\gamma_r+i\gamma_i\right)\phi+\left(\beta_{_{eff,r}}+i\beta_{_{eff,i}}\right)\left(\frac{\partial\phi}{\partial t}\right)\\
+\left(p_r+ip_i\right)\left(\frac{\partial^2\phi}{\partial t^2}\right)+\left(d_{3r}+id_{3i}\right)\left(\frac{\partial^3\phi}{\partial t^3}\right)+\left(d_{4r}+id_{4i}\right)\left(\frac{\partial^4\phi}{\partial t^4}\right)\\
+\left(q_r+iq_i\right)|\phi|^2\phi+\left(c_r+ic_i\right)|\phi|^4\phi+\left(m_r\left(\frac{\partial}{\partial\tau}(|\phi|^2)\right)\phi+i\left(n_i\frac{\partial}{\partial\tau}(|\phi|^2\phi)\right)\right)\\
+\left(\gamma_{xx,n_{_{2r}}}+i\gamma_{xx,n_{_{2i}}}\right)\left(\frac{\partial^2}{\partial x^2}|\phi|^2\phi\right)+\left(\gamma_{yy,n_{_{2r}}}+i\gamma_{yy,n_{_{2i}}}\right)\left(\frac{\partial^2}{\partial y^2}|\phi|^2\phi\right)\\
+\left(\gamma_{xx,n_{_{4r}}}+i\gamma_{xx,n_{_{4i}}}\right)\left(\frac{\partial^2}{\partial x^2}|\phi|^4\phi\right)+\left(\gamma_{yy,n_{_{4r}}}+i\gamma_{yy,n_{_{4i}}}\right)\left(\frac{\partial^2}{\partial y^2}|\phi|^4\phi\right)\\
+\left(\gamma_{xx,n_{_{2r}}^2}\left(\frac{\partial^2}{\partial x^2}(|\phi|^4\phi)\right)+\gamma^2_{xx,n_{_{2r}}^2}\left(\frac{\partial^4}{\partial x^4}(|\phi|^4\phi)\right)\right)\\
+\left(\gamma_{yy,n_{_{2r}}^2}\left(\frac{\partial^2}{\partial y^2}(|\phi|^4\phi)\right)+\gamma^2_{yy,n_{_{2r}}^2}\left(\frac{\partial^4}{\partial y^4}(|\phi|^4\phi)\right)\right)=0. \quad (2.68)
\end{aligned}
$$

Equation (2.68) has more terms than Eq. (2.59). This is due to the fact that we are no longer in the cubic case, but in the cubic-quintic case, where correction coefficients are added. The additional terms are: $d_{3r}=\frac{g_pT_2{}^3}{2n_0}\frac{(4\delta^2-4\delta)}{(\delta^2+1)^4}$ and $d_{3\,i}=-\frac{1}{6}\beta_3-\frac{g_pT_2{}^3}{2n_0}\frac{\left(-\delta^4+6\,\delta^2-1\right)}{(\delta^2+1)^4}$. They take into account for the third-order dispersion. $d_{4r}=\frac{1}{24}\beta_4+\frac{g_pT_2^4}{6n_0}\frac{(-2\delta^5+10\delta)}{(\delta^5+1)^5}$ and $d_{4i}=\frac{g_pT_2^4}{6n_0}\frac{(5\delta^4+10\delta^2-3)}{(\delta^5+1)^5}$, account for the fourth-order dispersion. The parameters $c_r=\frac{1}{2}\left(\frac{\partial^2\beta_f}{\partial(|\phi|^2)^2}\right)+\frac{1}{2}\frac{n_2^2\omega}{n_0c}+\frac{\omega n_4}{c}$ and $c_i=\frac{\alpha_f n_4}{n_0}$ stand for the saturation of the nonlinear-gain absorption (if negative), respectively. $m_r=\left(\frac{\partial}{\partial(|\phi|^2)_t}\beta_f\right)_0$ is the nonlinear gradient term responsible for the self-frequency shift and results from the tiequationmeretarded induced by Raman process.

The term $n_i=\left(\frac{\partial^2\beta_f}{\partial\omega\partial(|\phi|^2)}\right)_0$ represents the nonlinear dispersion and is responsible for the self-steepening (Kerr dispersion).

Expressions $\gamma_{\xi\xi,n_{_{2r}}}=\frac{1}{2}\frac{\omega\,n_2}{c}\gamma_{\xi\xi}$ and $\gamma_{\xi\xi,n_{_{2i}}}=\frac{1}{2}\frac{\alpha_f n_2}{n_0}\gamma_{\xi\xi}$, represent the real and imaginary parts of the nonlocality degrees associated with the cubic Kerr nonlinearity, along the transverse coordinates x and y, respectively. Expressions $\gamma_{\xi\xi,n_{_{4r}}}=\frac{1}{2}\frac{\omega\,n_4}{c}\gamma_{\xi\xi}$ and $\gamma_{\xi\xi,n_{_{4i}}}=\frac{1}{2}\frac{\alpha_f n_4}{n_0}\gamma_{\xi\xi}$, correspond to the real and imaginary parts of the nonlocality degrees related to the quintic Kerr nonlinearity, along the transverse coordinates x and y, respectively. Other expressions related to the degree of nonlocality are: $\gamma^2_{xx,n_{_{2r}}^2}=\frac{1}{2}\frac{\omega n_2^2}{n_0c}\gamma^2_{xx}$ and $\gamma_{xx,n_{_{2r}}^2}=\frac{1}{2}\frac{\omega n_2^2}{n_0c}\gamma_{xx}$.

As for Eq. (2.60), in order to scale Eq. (2.68), we need to introduce the following physical parameters: The diffraction length, or Rayleigh length in a homogeneous medium given by $L_{Diff}=$

$\beta_0 r_0^2$, where r_0 is the beam radius. The dispersion length expressed as $L_{Disp} = \frac{T_0^2}{|p_r|}$. The parameter T_0, which is the typical initial pulse width. The effective length, which characterizes the influence of the nonlinearity, is $L_{NL} = \frac{1}{q_r P_0}$. The transverse coordinate scale is $X = \frac{x}{r_0}$ and $Y = \frac{y}{r_0}$. The longitudinal coordinate scales are $Z = \frac{z}{L_{Disp}}$ and the temporal coordinate scale is $\tau = \frac{T}{T_0}$. Here $T = t - \frac{z}{v_g}$ is the time in the moving coordinate system. The normalized field amplitude is $\Phi(X, Y, Z, \tau) = \sqrt{P_0} N \phi(x, y, z, t)$, where $N^2 = \frac{L_{Disp}}{L_{NL}}$ and $N = \sqrt{\frac{q_r P_0 T_0^2}{|p_r|}}$.

Typical optical pulse parameters used in fiber communication systems are [28], the wavelength $\lambda = 1.55\mu m$, the linear refractive index $n_0 = 1.45$, higher-order nonlinear refractive indexes $n_2 = 2.7 \times 10^{-13} cm^2/W$, $n_4 = -7.8 \times 10^{-23} cm^4/W$ the group velocity dispersion $p_r = 50 ps^2/km = \beta_2$, the nonlinear gain $g_p = 6.8 W^{-1} km^{-1}$, the pulse width $1.763 T_0 = 400 fs$, the peak power of the incident pulse $P_0 = 9.43 MW$. We also set $a_1 = \frac{p_{ei}}{p_r}$, $a_3 = \frac{d_{3\,i}}{d_{3\,r}}$, $a_4 = \frac{d_{4\,i}}{d_{4\,r}}$, $b_1 = \frac{\gamma_i}{\gamma_r}$, $c_0 = \frac{q_i}{q_r}$, $d_0 = \frac{c_i}{c_r}$, $f_0 = \frac{n_i}{m_r}$, $c_{1,XX} = \frac{\gamma_{XX,n_{2i}}}{\gamma_{XX,n_{2r}}}$, $c_{2,YY} = \frac{\gamma_{YY,n_{2i}}}{\gamma_{YY,n_{2r}}}$, $c_{3,XX} = \frac{\gamma_{XX,n_{4i}}}{\gamma_{XX,n_{4r}}}$, $c_{4,YY} = \frac{\gamma_{YY,n_{4i}}}{\gamma_{YY,n_{4r}}}$, $c_{5,XX} = \gamma_{XX,n_{2r}^2}$, and $c_{6,YY} = \gamma_{YY,n_{2r}^2}$.

Considering the scaling transformations (see Appendix B as in the case of Eq. (2.60)), the form of Eq. (2.68) becomes:

$$
\begin{aligned}
i\frac{\partial \Phi}{\partial Z} + \zeta_1 \left(\frac{\partial^2 \Phi}{\partial X^2} + \frac{\partial^2 \Phi}{\partial Y^2}\right) + \zeta_{2p_r}(1 + ia_1)\left(\frac{\partial^2 \Phi}{\partial \tau^2}\right) + \zeta_{2d_{3r}}(1 + ia_3)\left(\frac{\partial^3 \Phi}{\partial \tau^3}\right) \\
+ \zeta_{2d_{4r}}(1 + ia_4)\left(\frac{\partial^4 \Phi}{\partial \tau^4}\right) + \zeta_3(1 + ib_1)\Phi + \zeta_{4q_r}(1 + ic_0)|\Phi|^2\Phi \\
+ \zeta_{4c_r}(1 + id_0)|\Phi|^4\Phi + \left[\zeta_{4m_r}\left(\frac{\partial}{\partial \tau}(|\Phi|^2)\right)\Phi + i\left(\zeta_{4f_0}\frac{\partial}{\partial \tau}(|\Phi|^2\Phi)\right)\right] \\
+ \zeta_{5,XX}\left(1 + ic_{1,XX}\right)\left(\frac{\partial^2}{\partial X^2}|\Phi|^2\Phi\right) + \zeta_{6,YY}\left(1 + ic_{2,YY}\right)\left(\frac{\partial^2}{\partial Y^2}|\Phi|^2\Phi\right) \\
+ \zeta_{7,XX}\left(1 + ic_{3,XX}\right)\left(\frac{\partial^2}{\partial X^2}|\Phi|^4\Phi\right) + \zeta_{8,YY}\left(1 + ic_{4,YY}\right)\left(\frac{\partial^2}{\partial Y^2}|\Phi|^4\Phi\right) \\
+ \left[\zeta_{9,XX}\left(\frac{\partial^2}{\partial X^2}|\Phi|^4\Phi\right) + \zeta_{11,XX}\left(c_{5,XX}\frac{\partial^4}{\partial X^4}|\Phi|^4\Phi\right)\right] \\
+ \left[\zeta_{10,YY}\left(\frac{\partial^2}{\partial Y^2}|\Phi|^4\Phi\right) + \zeta_{12,YY}\left(c_{6,YY}\frac{\partial^4}{\partial Y^4}|\Phi|^4\Phi\right)\right] = 0, \quad (2.69)
\end{aligned}
$$

where $\zeta_1 = \frac{L_{Disp}}{2\beta_0 r_0^2}$ refers to linear diffraction. The coefficients $\zeta_{2p_r} = \frac{p_r L_{Disp}}{T_0^2}$, $\zeta_{2d_{3r}} = \frac{d_{3r} L_{Disp}}{T_0^3}$ and $\zeta_{2d_{4r}} = \frac{d_{4r} L_{Disp}}{T_0^4}$, are related to the second, third and fourth order dispersions, respectively. $\zeta_3 = \gamma_r L_{Disp}$ corresponds to the linear losses. The parameter $\zeta_{4q_r} = \frac{q_r L_{NL}}{P_0}$ accounts for the cubic Kerr nonlinearity, while $\zeta_{4c_r} = \frac{c_r L_{NL}}{P_0^2 N^2}$ is associated with the quintic Kerr nonlinearity. $\zeta_{4m_r} = \frac{m_r L_{NL}}{T_0 P_0}$ is the nonlinear gradient term. $\zeta_{4f_0} = \frac{f_0 L_{NL}}{T_0 P_0}$ is the nonlinear dispersion term. $\zeta_{5,XX} = \frac{\gamma_{XX,n_{2r}} L_{NL}}{P_0 r_0^2}$ and $\zeta_{6,YY} = \frac{\gamma_{YY,n_{2r}} L_{NL}}{P_0 r_0^2}$, are the spatially nonlocal cubic nonlinear response coefficients following the transversal coordinates (x, y), respectively. $\zeta_{7,XX} = \frac{\gamma_{XX,n_{4r}} L_{NL}}{P_0^2 r_0^2 N^2}$ and $\zeta_{8,YY} = \frac{\gamma_{YY,n_{4r}} L_{NL}}{P_0^2 r_0^2 N^2}$, are the spatially nonlocal quintic nonlinear response coefficients. These are additional terms related to the spatially nonlocal cubic nonlinear response coefficients: $\zeta_{9,XX} = \frac{\gamma_{XX,n_{2r}^2} L_{NL}}{P_0^2 r_0^2 N^2}$, $\zeta_{10,YY} = \frac{\gamma_{YY,n_{2r}^2} L_{NL}}{P_0^2 r_0^2 N^2}$, $\zeta_{9,XX} = \frac{\gamma_{XX,n_{2r}^2} L_{NL}}{P_0^2 r_0^4 N^2}$, and $\zeta_{12,YY} = \frac{\gamma_{YY,n_{2r}^2} L_{NL}}{P_0^2 r_0^4 N^2}$.

2.4 Variational analysis of the extended (3+1)-D cubic and cubic-quintic complex Ginzburg-Landau models

In this section, we use the variational approach based on Euler-Lagrange equations, to search for approximate solutions to Eqs. (2.61) and (2.69), in order to gain physical insight into some relevant parameters, which will then be implemented in numerical simulations to qualitatively confirm the analytical predictions.

In order to describe the dynamics of pulse evolution, various treatments have been developed to extract approximated soliton solutions to integrable and non-integrable nonlinear partial differential equations and have received many different names depending on the field of application, namely the method of moments [92], method of collective coordinates [91, 21, 27], time-dependent variational method [32], effective-particle method [75, 93] , averaged Lagrangian description [33, 94] , etc. Lagrangian methods have become widely accepted as the preferred approach to account for the dynamics of the light pulses in optical fibers.

2.4.1 Variational analysis of the extended (3+1)-D CCGLE model

In order to use variational approach, the (3+1)-D nonlocal CCGLE given in Eq. (2.61) could be rewritten as:

$$i\frac{\partial\Phi}{\partial Z}+\zeta_1\left(\frac{\partial^2\Phi}{\partial X^2}+\frac{\partial^2\Phi}{\partial Y^2}\right)+\zeta_2\frac{\partial^2\Phi}{\partial\tau^2}+\zeta_3\Phi+\zeta_4|\Phi|^2\Phi+\zeta_5\frac{\partial^2}{\partial X^2}(|\Phi|^2)\Phi + \zeta_6\frac{\partial^2}{\partial Y^2}(|\Phi|^2)\Phi=Q, \quad (2.70)$$

where the right-hand side of Eq. (2.69) contains dissipatives terms:

$$Q = -ia_1\zeta_2\frac{\partial^2\Phi}{\partial\tau^2}-ib_1\zeta_3\Phi-ic_0\zeta_4|\Phi|^2\Phi-ic_{_{1,XX}}\zeta_5\frac{\partial^2}{\partial X^2}(|\Phi|^2)\Phi-ic_{_{2,YY}}\zeta_6\frac{\partial^2}{\partial Y^2}(|\Phi|^2)\Phi. \quad (2.71)$$

It should be noted that defining an appropriate ansatz function is essential for the use of the variational approach. Let us then consider the trial function of Gaussian shape:

$$\Phi(X,Y,Z,\tau)=A(Z)\exp(-\frac{X^2}{\sigma_{_X}^2(Z)}-\frac{Y^2}{\sigma_{_Y}^2(Z)}-\frac{\tau^2}{\sigma_\tau^2(Z)}+\frac{ik_0}{2}(\vartheta_{_X}(Z)X^2+\vartheta_{_Y}(Z)Y^2 + \vartheta_\tau(Z)\tau^2)+i\psi(Z)), \quad (2.72)$$

where $A(Z)$ is the amplitude, $\sigma_{_X}(Z)$ and $\sigma_{_Y}(Z)$ are the beamwidths in the transverse coordinates (X, Y), $\sigma_\tau(Z)$ is the temporal beamwidth, $\vartheta_{_X}(Z)$ and $\vartheta_{_Y}(Z)$ are the wave-front curvatures along the transverse coordinates (X, Y), $\vartheta_\tau(Z)$ is the temporal wave-front curvature, $\psi(Z)$ is the phase, and k_0 is the wave number. Variables $A(Z)$, $\sigma_{_X}(Z)$, $\sigma_{_Y}(Z)$, $\sigma_\tau(Z)$, $\vartheta_{_X}(Z)$, $\vartheta_{_Y}(Z)$, $\vartheta_\tau(Z)$ and $\psi(Z)$ are all the parameters of the light pulse. Then, we obtain the first-order differential equations (FODEs) of these parameters, which describe the evolution of the light pulse in the optical fiber. The variational approach used in this study is based on the Euler-Lagrange equation [74]

$$\frac{d}{dZ}\left(\frac{\partial\langle L_c\rangle}{\partial q'}\right)-\frac{\partial\langle L_c\rangle}{\partial q}=2Re\int_{-\infty}^{\infty}\int_{-\infty}^{\infty}\int_0^{\infty}dXdYd\tau Q\frac{\partial\Phi^*}{\partial q}, \quad (2.73)$$

where, Φ^* is the complex conjugate of the ansatz function Φ; Re denotes the real part and q is the variable which corresponds to all the parameters of the light pulse ($A(Z)$, $\sigma_{_X}(Z)$, $\sigma_{_Y}(Z)$, $\sigma_\tau(Z)$, $\vartheta_{_X}(Z)$, $\vartheta_{_Y}(Z)$, $\vartheta_\tau(Z)$, $\psi(Z)$), with ($q'=\frac{dq}{dZ}$). The left-hand side of Eq. (27), represents the conservative Lagrangian and is noted L_c:

$$L_c=i\frac{\partial\Phi}{\partial Z}+\zeta_1\left(\frac{\partial^2\Phi}{\partial X^2}+\frac{\partial^2\Phi}{\partial Y^2}\right)+\zeta_2\frac{\partial^2\Phi}{\partial\tau^2}+\zeta_3\Phi+\zeta_4|\Phi|^2\Phi+\zeta_5\frac{\partial^2}{\partial X^2}(|\Phi|^2)\Phi+\zeta_6\frac{\partial^2}{\partial Y^2}(|\Phi|^2)\Phi. \quad (2.74)$$

When we normalize L_c, we get the normalized conservative Lagrangian,

$$L_{nc} = \frac{i}{2}\left(\Phi\frac{\partial\Phi^*}{\partial Z} - \Phi^*\frac{\partial\Phi}{\partial Z}\right) + \zeta_1\left(\left|\frac{\partial\Phi}{\partial X}\right|^2 + \left|\frac{\partial\Phi}{\partial Y}\right|^2\right) + \zeta_2\left|\frac{\partial\Phi}{\partial\tau}\right|^2 + \zeta_3|\Phi|^2 + \zeta_4|\Phi|^4 + \zeta_5\left|\frac{\partial}{\partial X}|\Phi|^2\right|^2 + \zeta_6\left|\frac{\partial}{\partial Y}|\Phi|^2\right|^2. \quad (2.75)$$

$\langle L_c\rangle$ is the Lagrangian density given by:

$$\langle L_c\rangle = \int_{-\infty}^{\infty}\int_{-\infty}^{\infty}\int_{0}^{\infty} L_{nc}dXdYd\tau, \quad (2.76)$$

and the right-hand side Q is the dissipative term. Using Eqs. (2.7)-(2.76), we get a set of eight coupled first-order differential equations (FODEs) resulting from the variation with respect to the light pulse parameters:

$$\frac{dA}{dZ} = -A\zeta_1 k_0\vartheta_{_X} - A\zeta_1 k_0\vartheta_{_Y} - A\zeta_2\vartheta_\tau - \frac{7}{2}Ab_1\zeta_3 - \frac{77}{16}A^3\sqrt{2}c_0\zeta_4 + \frac{1}{8}Aa_1\zeta_2\left(35k_0^2\vartheta_\tau^2\sigma_\tau^2 + \frac{156}{\sigma^2}\right) + \frac{1}{128}A^3\sqrt{2}c_{_{1,XX}}\zeta_5\left(75k_0^2\vartheta_{_X}^2\sigma_{_X}^2 + \frac{996}{\sigma_{_X}^2}\right) + \frac{1}{128}A^3\sqrt{2}c_{_{2,YY}}\zeta_6\left(75k_0^2\vartheta_{_Y}^2\sigma_{_Y}^2 + \frac{996}{\sigma_{_Y}^2}\right), \quad (2.77)$$

$$\frac{d\sigma_{_X}}{dZ} = 2\zeta_1 k_0\vartheta_{_X}\sigma_{_X} + b_1\zeta_3\sigma_{_X} + \frac{15}{8}A^2\sqrt{2}c_0\zeta_4\sigma_{_X} + \frac{1}{4}a_1\zeta_2\left(-7k_0^2\vartheta_\tau^2\sigma_\tau^2 - \frac{28}{\sigma_\tau^2}\right)\sigma_{_X} + \frac{1}{64}A^2\sqrt{2}c_{_{1,XX}}\zeta_5\left(13k_0^2\vartheta_{_X}^2\sigma_{_X}^2 - \frac{252}{\sigma_{_X}^2}\right)\sigma_{_X} + \frac{15}{64}A^2\sqrt{2}c_{_{2,YY}}\zeta_6\left(-k_0^2\vartheta_{_Y}^2\sigma_{_Y}^2 - \frac{12}{\sigma_{_Y}^2}\right)\sigma_{_X}, \quad (2.78)$$

$$\frac{d\sigma_{_Y}}{dZ} = 2\zeta_1 k_0 \vartheta_{_Y} \sigma_{_Y} + b_1 \zeta_3 \sigma_{_Y} + \frac{15}{8} A^2 \sqrt{2} c_0 \zeta_4 \sigma_{_Y} + \frac{1}{4} a_1 \zeta_2 \left(-7 k_0^2 \vartheta_\tau^2 \sigma_\tau^2 - \frac{28}{\sigma_\tau^2} \right) \sigma_{_Y} + \frac{15}{64} A^2 \sqrt{2} c_{_{1,XX}} \zeta_5 \left(-k_0^2 \vartheta_{_X}^2 \sigma_{_X}^2 - \frac{12}{\sigma_{_X}^2} \right) \sigma_{_Y} + \frac{1}{64} A^2 \sqrt{2} c_{_{2,YY}} \zeta_6 \left(13 k_0^2 \vartheta_{_Y}^2 \sigma_{_Y}^2 - \frac{252}{\sigma_{_Y}^2} \right) \sigma_{_Y}, \quad (2.79)$$

$$\frac{d\sigma_\tau}{dZ} = 2\zeta_2 \vartheta_\tau \sigma_\tau + b_1 \zeta_3 \sigma_\tau + \frac{15}{8} A^2 \sqrt{2} c_0 \zeta_4 \sigma_\tau + \frac{1}{4} a_1 \zeta_2 \left(-5 k_0^2 \vartheta_\tau^2 \sigma_\tau^2 - \frac{36}{\sigma_\tau^2} \right) \sigma_\tau + \frac{15}{64} A^2 \sqrt{2} c_{_{1,XX}} \zeta_5 \left(-k_0^2 \vartheta_{_X}^2 \sigma_{_X}^2 - \frac{12}{\sigma_{_X}^2} \right) \sigma_\tau + \frac{15}{64} A^2 \sqrt{2} c_{_{2,YY}} \zeta_6 \left(-k_0^2 \vartheta_{_Y}^2 \sigma_{_Y}^2 - \frac{12}{\sigma_{_Y}^2} \right) \sigma_\tau, \quad (2.80)$$

$$\frac{d\vartheta_{_X}}{dZ} = A^2 \sqrt{2} \zeta_4 \frac{1}{k_0 \sigma_{_X}^2} + 8\zeta_1 \frac{1}{\sigma_{_X}^4} - 2\zeta_1 k_0 \vartheta_{_X}^2 + \frac{1}{36} \frac{A^2 \sqrt{2} c_{_{1,XX}} \zeta_5}{k_0 \sigma_{_X}^2} \left(\frac{216}{\sigma_{_X}^2} + 127 k_0 \vartheta_{_X} \right) + \frac{1}{36} \frac{A^2 \sqrt{2} c_{_{2,YY}} \zeta_6}{k_0 \sigma_{_X}^2} \left(\frac{72}{\sigma_{_Y}^2} + 73 k_0 \vartheta_{_Y} \right), \quad (2.81)$$

$$\frac{d\vartheta_{_Y}}{dZ} = A^2 \sqrt{2} \zeta_4 \frac{1}{k_0 \sigma_{_Y}^2} + 8\zeta_1 \frac{1}{\sigma_{_Y}^4} - 2\zeta_1 k_0 \vartheta_{_Y}^2 + \frac{1}{36} \frac{A^2 \sqrt{2} c_{_{1,XX}} \zeta_5}{k_0 \sigma_{_Y}^2} \left(\frac{72}{\sigma_{_X}^2} + 73 k_0 \vartheta_{_X} \right) + \frac{1}{36} \frac{A^2 \sqrt{2} c_{_{2,YY}} \zeta_6}{k_0 \sigma_{_Y}^2} \left(\frac{216}{\sigma_{_Y}^2} + 127 k_0 \vartheta_{_Y} \right), \quad (2.82)$$

$$\frac{d\vartheta_\tau}{dZ} = A^2\sqrt{2}\zeta_4\frac{1}{k_0\sigma_\tau^2} + 8a_1\zeta_2\frac{\vartheta_\tau}{\sigma_\tau^2} - 8\zeta_2\frac{1}{k_0\sigma_\tau^4} - 2\zeta_2 k_0\vartheta_\tau^2 + \frac{1}{36}\frac{A^2\sqrt{2}c_{_{1,XX}}\zeta_5}{k_0\sigma_\tau^2}\left(\frac{72}{\sigma_{_X}^2} + 73k_0\vartheta_{_X}\right) + \frac{1}{36}\frac{A^2\sqrt{2}c_{_{2,YY}}\zeta_6}{k_0\sigma_\tau^2}\left(\frac{72}{\sigma_{_Y}^2} + 73k_0\vartheta_{_Y}\right), \quad (2.83)$$

$$\frac{d\psi}{dZ} = -2\frac{\zeta_1}{\sigma_{_X}^2} - 2\frac{\zeta_1}{\sigma_{_Y}^2} - 2\frac{\zeta_2}{\sigma_\tau^2} - \frac{7}{8}A^2\sqrt{2}\zeta_4 - \zeta_3 - a_1\zeta_2 k_0\vartheta_\tau + \frac{1}{288}A^2\sqrt{2}c_{_{1,XX}}\zeta_5\left(-\frac{648}{\sigma_{_X}^2} - 401k_0\vartheta_{_X}\right) + \frac{1}{288}A^2\sqrt{2}c_{_{2,YY}}\zeta_6\left(-\frac{648}{\sigma_{_Y}^2} - 401k_0\vartheta_{_Y}\right). \quad (2.84)$$

2.4.2 Variational analysis of the extended (3+1)-D CQCGLE model

In order to apply the variational approach on the (3+1)-D nonlocal CQCGLE given in Eq. (2.69), we split it into two parts:

$$
\begin{aligned}
i\frac{\partial\Phi}{\partial Z}+\zeta_1\left(\frac{\partial^2\Phi}{\partial X^2}+\frac{\partial^2\Phi}{\partial Y^2}\right)+\zeta_{2p_r}\left(\frac{\partial^2\Phi}{\partial\tau^2}\right)+\zeta_{2d_{3r}}\left(\frac{\partial^3\Phi}{\partial\tau^3}\right)\\
+\zeta_{2d_{4r}}\left(\frac{\partial^4\Phi}{\partial\tau^4}\right)+\zeta_3\Phi+\zeta_{4q_r}|\Phi|^2\Phi+\zeta_{4c_r}|\Phi|^4\Phi+\left(\zeta_{4m_r}(|\Phi|^2)_t\Phi\right)\\
+\zeta_{5,XX}\left(\frac{\partial^2}{\partial X^2}|\Phi|^2\Phi\right)+\zeta_{6,YY}\left(\frac{\partial^2}{\partial Y^2}|\Phi|^2\Phi\right)\\
+\zeta_{7,XX}\left(\frac{\partial^2}{\partial X^2}|\Phi|^4\Phi\right)+\zeta_{8,YY}\left(\frac{\partial^2}{\partial Y^2}|\Phi|^4\Phi\right)\\
+\left[\zeta_{9,XX}\left(\frac{\partial^2}{\partial X^2}|\Phi|^4\Phi\right)+\zeta_{11,XX}\left(c_{5,XX}\frac{\partial^4}{\partial X^4}|\Phi|^4\Phi\right)\right]\\
+\left[\zeta_{10,YY}\left(\frac{\partial^2}{\partial Y^2}|\Phi|^4\Phi\right)+\zeta_{12,YY}\left(c_{6,YY}\frac{\partial^4}{\partial Y^4}|\Phi|^4\Phi\right)\right]=Q_{cq}, \quad (2.85)
\end{aligned}
$$

where the conservative part L_{Ccq} is given as:

$$
\begin{aligned}
L_{Ccq}=i\frac{\partial\Phi}{\partial Z}+\zeta_1\left(\frac{\partial^2\Phi}{\partial X^2}+\frac{\partial^2\Phi}{\partial Y^2}\right)+\zeta_{2p_r}\left(\frac{\partial^2\Phi}{\partial\tau^2}\right)+\zeta_{2d_{3r}}\left(\frac{\partial^3\Phi}{\partial\tau^3}\right)\\
+\zeta_{2d_{4r}}\left(\frac{\partial^4\Phi}{\partial\tau^4}\right)+\zeta_3\Phi+\zeta_{4q_r}|\Phi|^2\Phi+\zeta_{4c_r}|\Phi|^4\Phi+\left(\zeta_{4m_r}(|\Phi|^2)_t\Phi\right)\\
+\zeta_{5,XX}\left(\frac{\partial^2}{\partial X^2}|\Phi|^2\Phi\right)+\zeta_{6,YY}\left(\frac{\partial^2}{\partial Y^2}|\Phi|^2\Phi\right)\\
+\zeta_{7,XX}\left(\frac{\partial^2}{\partial X^2}|\Phi|^4\Phi\right)+\zeta_{8,YY}\left(\frac{\partial^2}{\partial Y^2}|\Phi|^4\Phi\right)\\
+\left[\zeta_{9,XX}\left(\frac{\partial^2}{\partial X^2}|\Phi|^4\Phi\right)+\zeta_{11,XX}\left(c_{5,XX}\frac{\partial^4}{\partial X^4}|\Phi|^4\Phi\right)\right]\\
+\left[\zeta_{10,YY}\left(\frac{\partial^2}{\partial Y^2}|\Phi|^4\Phi\right)+\zeta_{12,YY}\left(c_{6,YY}\frac{\partial^4}{\partial Y^4}|\Phi|^4\Phi\right)\right], \quad (2.86)
\end{aligned}
$$

and the dissipative part Q_{cq} is:

$$\begin{aligned} Q_{cq} = &-ia_1\zeta_{2p_r}\left(\frac{\partial^2\Phi}{\partial\tau^2}\right) - ia_3\zeta_{2d_{3r}}\left(\frac{\partial^3\Phi}{\partial\tau^3}\right) \\ &- ia_4\zeta_{2d_{4r}}\left(\frac{\partial^4\Phi}{\partial\tau^4}\right) - ib_1\zeta_3\Phi - ic_0\zeta_{4q_r}|\Phi|^2\Phi - id_0\zeta_{4c_r}|\Phi|^4\Phi - i\left(\zeta_{4f_0}(|\Phi|^2\Phi)_t\right) \\ &- ic_{_{1,XX}}\zeta_{_{5,XX}}\left(\frac{\partial^2}{\partial X^2}|\Phi|^2\Phi\right) - ic_{_{2,YY}}\zeta_{_{6,YY}}\left(\frac{\partial^2}{\partial Y^2}|\Phi|^2\Phi\right) \\ &- ic_{_{3,XX}}\zeta_{_{7,XX}}\left(\frac{\partial^2}{\partial X^2}|\Phi|^4\Phi\right) - ic_{_{4,YY}}\zeta_{_{8,YY}}\left(\frac{\partial^2}{\partial Y^2}|\Phi|^4\Phi\right). \quad (2.87) \end{aligned}$$

We define a trial function of Gaussian shape as our ansatz function, the same as in the case of the CCGLE for the use of the variational approach:

$$\begin{aligned} \Phi(X,Y,Z,\tau) = A(Z)\exp(-\frac{X^2}{\sigma_{_X}^2(Z)} - \frac{Y^2}{\sigma_{_Y}^2(Z)} - \frac{\tau^2}{\sigma_\tau^2(Z)} + \frac{ik_0}{2}(\vartheta_{_X}(Z)X^2 + \vartheta_{_Y}(Z)Y^2 \\ + \vartheta_\tau(Z)\tau^2) + i\psi(Z)), \quad (2.88) \end{aligned}$$

The Euler-Lagrange equation is given as:

$$\frac{d}{dZ}\left(\frac{\partial\langle L_{Ccq}\rangle}{\partial q'}\right) - \frac{\partial\langle L_{Ccq}\rangle}{\partial q} = 2Re\int_{-\infty}^{\infty}\int_{-\infty}^{\infty}\int_{0}^{\infty} dXdYd\tau Q_{cq}\frac{\partial\Phi^*}{\partial q}, \quad (2.89)$$

where, $\langle L_c\rangle$ is the Lagrangian density given by:

$$\langle L_{Ccq}\rangle = \int_{-\infty}^{\infty}\int_{-\infty}^{\infty}\int_{0}^{\infty} L_{nCcq}dXdYd\tau. \quad (2.90)$$

The term L_{nCcq} is the normalized conservative Lagrangian.

Using Eqs. (2.86)-(2.90), we get a set of eight coupled FODEs resulting from the variation with respect to the light pulse parameters:

$$\begin{aligned}\frac{dA}{dZ} = &-k_0\zeta_1\vartheta_{_X}A - k_0\zeta_1\vartheta_{_Y}A - k_0\zeta_{2\,pr}\vartheta_\tau A + \frac{1}{2}a_1\zeta_{2p_r}A\left(-\frac{41}{\sigma_\tau^2} - \frac{45}{4}k_0^2\vartheta_\tau^2\sigma_{\tau^2}\right)\\
&+ \frac{1}{2}\zeta_{2d_{3r}}A^2\sqrt{2}\left(-\frac{16}{9}\frac{k_0\vartheta_\tau}{\sigma_\tau\sqrt{\pi}} - \frac{4}{9}\frac{k_0^3\vartheta_\tau^3\sigma_\tau^3}{\sqrt{\pi}}\right) + \frac{1}{2}a_3\zeta_{2d_{3r}}A\sqrt{2}\left(\frac{172}{\sigma_\tau^3\sqrt{\pi}} + \frac{3k_0^2\vartheta_\tau^2\sigma_\tau}{\sqrt{\pi}}\right)\\
&+ \frac{1}{2}\zeta_{2d_{4r}}A^3\left(-\frac{12k_0\vartheta_\tau}{\sigma_\tau^2} - 3k_0^3\vartheta_\tau^3\sigma_\tau^2\right) + \frac{1}{2}a_4\zeta_{2d_{4r}}A\left(-\frac{227}{\sigma_\tau^4} + \frac{301}{2}k_0^2\vartheta_\tau^2 + \frac{141}{16}k_0^4\vartheta_\tau^4\sigma_\tau^4\right)\\
&+ \frac{43}{2}b_1\zeta_3 A - \frac{21}{2}\frac{\zeta_{4f_0}A^3\sqrt{2}}{\sigma_\tau\sqrt{\pi}} + \frac{83}{16}c_0\zeta_{4q_r}A^3\sqrt{2} + \frac{41}{36}d_0\zeta_{4c_r}A^5\sqrt{2}\sqrt{6}\\
&+ \frac{1}{2}c_{1,XX}\zeta_{5,XX}A^3\sqrt{2}\left(-\frac{231}{16\sigma_{_X}^2} - \frac{85}{64}k_0^2\vartheta_{_X}^2\sigma_{_X}^2\right) + \frac{1}{2}c_{2,YY}\zeta_{6,YY}A^3\sqrt{2}\left(-\frac{231}{16\sigma_{_Y}^2} - \frac{85}{64}k_0^2\vartheta_{_Y}^2\sigma_{_Y}^2\right)\\
&+ \frac{1}{2}c_{3,XX}\zeta_{7,XX}A^5\sqrt{2}\sqrt{6}\left(-\frac{565}{162\sigma_{_X}^2} - \frac{125}{648}k_0^2\vartheta_{_X}^2\sigma_{_X}^2\right)\\
&+ \frac{1}{2}c_{4,YY}\zeta_{8,YY}A^5\sqrt{2}\sqrt{6}\left(-\frac{565}{162\sigma_{_Y}^2} - \frac{125}{648}k_0^2\vartheta_{_Y}^2\sigma_{_Y}^2\right) \quad (2.91)\end{aligned}$$

$$\begin{aligned}\frac{d\sigma_{_X}}{dZ} = &\,2k_0\zeta_1\vartheta_{_X}\sigma_{_X} + a_1\zeta_{2p_r}\left(\frac{9}{\sigma_\tau^2} + \frac{9}{4}k_0^2\vartheta_\tau^2\sigma_\tau^2\right)\sigma_{_X}\\
&- \frac{36a_3\zeta_{2d_{3r}}\sqrt{2}\sigma_{_X}}{\sigma_\tau^2\sqrt{\pi}} + a_4\zeta_{2d_{4r}}\sigma_{_X}\left(\frac{45}{\sigma_\tau^4} - \frac{63}{2}k_0^2\vartheta_\tau^2 - \frac{27}{16}k_0^4\vartheta_\tau^4\sigma_\tau^4\right)\\
&- 9b_1\zeta_3\sigma_{_X} + \frac{17}{4}\frac{\zeta_{4f_0}A^2\sqrt{2}\sigma_{_X}}{\sigma_\tau\sqrt{\pi}} - \frac{17}{8}c_0\zeta_{4q_r}A^2\sqrt{2}\sigma_{_X} - \frac{25}{54}d_0\zeta_{4c_r}A^4\sqrt{2}\sqrt{6}\sigma_{_X}\\
&+ c_{1,XX}\zeta_{5,XX}A^2\sqrt{2}\left(\frac{33}{16\sigma_{_X}^2} + \frac{19}{64}k_0^2\vartheta_{_X}^2\sigma_{_X}^2\right)\sigma_{_X} + c_{2,YY}\zeta_{6,YY}A^2\sqrt{2}\left(\frac{51}{16\sigma_{_Y}^2} + \frac{17}{64}k_0^2\vartheta_{_Y}^2\sigma_{_Y}^2\right)\sigma_{_X}\\
&+ c_{3,XX}\zeta_{7,XX}A^4\sqrt{2}\sqrt{6}\left(\frac{25}{54\sigma_{_X}^2} + \frac{1}{24}k_0^2\vartheta_{_X}^2\sigma_{_X}^2\right)\sigma_{_X}\\
&+ c_{4,YY}\zeta_{8,YY}A^4\sqrt{2}\sqrt{6}\left(\frac{125}{162\sigma_{_Y}^2} + \frac{25}{648}k_0^2\vartheta_{_Y}^2\sigma_{_Y}^2\right)\sigma_{_X} \quad (2.92)\end{aligned}$$

$$\begin{aligned}\frac{d\sigma_{_Y}}{dZ} &= 2k_0\zeta_1\vartheta_{_Y}\sigma_{_Y} + a_1\zeta_{2p_r}\left(\frac{9}{\sigma_\tau^2}+\frac{9}{4}k_0^2\vartheta_\tau^2\sigma_\tau^2\right)\sigma_{_Y}\\ &\quad - \frac{36a_3\zeta_{2d_{3r}}\sqrt{2}\sigma_{_Y}}{\sigma_\tau^2\sqrt{\pi}} + a_4\zeta_{2d_{4r}}\sigma_{_Y}\left(\frac{45}{\sigma_\tau^4}-\frac{63}{2}k_0^2\vartheta_\tau^2-\frac{27}{16}k_0^4\vartheta_\tau^4\sigma_\tau^4\right)\\ &\quad - 9b_1\zeta_3\sigma_{_Y} + \frac{17}{4}\frac{\zeta_{4f_0}A^2\sqrt{2}\sigma_{_Y}}{\sigma_\tau\sqrt{\pi}} - \frac{17}{8}c_0\zeta_{4q_r}A^2\sqrt{2}\sigma_{_Y} - \frac{25}{54}d_0\zeta_{4c_r}A^4\sqrt{2}\sqrt{6}\sigma_{_Y}\\ &\quad + c_{1,XX}\zeta_{5,XX}A^2\sqrt{2}\left(\frac{51}{16\sigma_{_Y}^2}+\frac{17}{64}k_0^2\vartheta_{_Y}^2\sigma_{_Y}^2\right)\sigma_{_Y} + c_{2,YY}\zeta_{6,YY}A^2\sqrt{2}\left(\frac{33}{16\sigma_{_Y}^2}+\frac{19}{64}k_0^2\vartheta_{_Y}^2\sigma_{_Y}^2\right)\sigma_{_Y}\\ &\quad + c_{3,XX}\zeta_{7,XX}A^4\sqrt{2}\sqrt{6}\left(\frac{125}{162\sigma_{_Y}^2}+\frac{25}{648}k_0^2\vartheta_{_Y}^2\sigma_{_Y}^2\right)\sigma_{_Y}\\ &\quad + c_{4,YY}\zeta_{8,YY}A^4\sqrt{2}\sqrt{6}\left(\frac{25}{54\sigma_{_Y}^2}+\frac{1}{24}k_0^2\vartheta_{_Y}^2\sigma_{_Y}^2\right)\sigma_{_Y}\end{aligned} \tag{2.93}$$

$$\begin{aligned}\frac{d\sigma_\tau}{dZ} &= 2k_0\zeta_{2p_r}\vartheta_\tau\sigma_\tau + a_1\zeta_{2p_r}\left(\frac{7}{\sigma_\tau^2}+\frac{11}{4}k_0^2\vartheta_\tau^2\sigma_\tau^2\right)\sigma_\tau\\ &\quad + \zeta_{2d_{3r}}A\sqrt{2}\left(\frac{16}{9}\frac{k_0\vartheta_\tau}{\sigma_\tau\sqrt{\pi}}+\frac{4}{9}\frac{k_0^3\vartheta_\tau^3\sigma_\tau^3}{\sqrt{\pi}}\right)\sigma_\tau\\ &\quad + a_3\zeta_{2d_{3r}}\sqrt{2}\left(-\frac{36}{\sigma_\tau^3\sqrt{\pi}}-\frac{3k_0^2\vartheta_\tau^2\sigma_\tau}{\sqrt{\pi}}\right)\sigma_\tau\\ &\quad + a_4\zeta_{2d_{4r}}\left(\frac{57}{\sigma_\tau^4}-\frac{63}{2}k_0^2\vartheta_\tau^2\sigma_\tau^2-\frac{39}{16}k_0^4\vartheta_\tau^4\sigma_\tau^4\right)\sigma_\tau\\ &\quad + \zeta_{2d_{4r}}A^2\left(\frac{12k_0\vartheta_\tau}{\sigma_\tau^2}+3k_0^3\vartheta_\tau^3\sigma_\tau^2\right)\sigma_\tau\\ &\quad - 9b_1\zeta_3\sigma_\tau + \frac{9}{2}\frac{\zeta_{4f_0}A^2\sqrt{2}}{\sqrt{\pi}} - \frac{17}{8}c_0\zeta_{4q_r}A^2\sqrt{2}\sigma_\tau - \frac{25}{54}d_0\zeta_{4c_r}A^4\sqrt{2}\sqrt{6}\sigma_\tau\\ &\quad + c_{1,XX}\zeta_{5,XX}A^2\sqrt{2}\left(\frac{51}{16\sigma_{_X}^2}+\frac{17}{64}k_0^2\vartheta_{_X}^2\sigma_{_X}^2\right)\sigma_\tau + c_{2,YY}\zeta_{6,YY}A^2\sqrt{2}\left(\frac{51}{16\sigma_{_Y}^2}+\frac{17}{64}k_0^2\vartheta_{_Y}^2\sigma_{_Y}^2\right)\sigma_\tau\\ &\quad + c_{3,XX}\zeta_{7,XX}A^4\sqrt{2}\sqrt{6}\left(\frac{125}{162\sigma_{_X}^2}+\frac{25}{648}k_0^2\vartheta_{_X}^2\sigma_{_X}^2\right)\sigma_\tau\\ &\quad + c_{4,YY}\zeta_{8,YY}A^4\sqrt{2}\sqrt{6}\left(\frac{125}{162\sigma_{_Y}^2}+\frac{25}{648}k_0^2\vartheta_{_Y}^2\sigma_{_Y}^2\right)\sigma_\tau\end{aligned} \tag{2.94}$$

$$\begin{aligned}\frac{d\vartheta_{_X}}{dZ} = {} & \frac{8\zeta_1}{k_0\sigma_{_X}^4} - 2\zeta_1 k_0\vartheta_{_X}^2 + \frac{\zeta_{4m_r}A^2}{k_0\sigma_{_X}^2}\left(\frac{4\sqrt{2}}{\sigma_\tau\sqrt{\pi}}\right) \\ & + \frac{8\zeta_{2d_{3r}}A\sqrt{2}}{k_0\sigma_{_X}^2}\left(\frac{4}{27}\frac{1}{\sigma_\tau^3\sqrt{\pi}} + \frac{1}{18}\frac{k_0^2\vartheta_\tau^2}{\sqrt{\pi}} + \frac{1}{144}\frac{k_0^4\vartheta_\tau^4\sigma_\tau^5}{\sqrt{\pi}}\right) \\ & + \frac{8\zeta_{2d_{4r}}A^2}{k_0\sigma_{_X}^2}\left(\frac{3}{2}\frac{1}{\sigma_\tau^4} + \frac{3}{4}k_0^2\vartheta_\tau^2 + \frac{3}{32}k_0^4\vartheta_\tau^4\sigma_\tau^4\right) + \frac{\zeta_{4q_r}A^2\sqrt{2}}{k_0\sigma_{_X}^2} + \frac{4}{9}\frac{\zeta_{4c_r}A^4\sqrt{2}\sqrt{6}}{k_0\sigma_{_X}^2} \\ & + \frac{8\zeta_{5,XX}A^2\sqrt{2}}{k_0\sigma_{_X}^2}\left(\frac{3}{4}\frac{1}{\sigma_{_X}^2} + \frac{5}{32}c_{1,XX}k_0\vartheta_{_X}\right) + \frac{8\zeta_{6,YY}A^2\sqrt{2}}{k_0\sigma_{_X}^2}\left(\frac{1}{4\sigma_{_Y}^2} - \frac{1}{32}c_{2,YY}k_0\vartheta_{_Y}\right) \\ & + \frac{8\zeta_{7,XX}A^4\sqrt{2}\sqrt{6}}{k_0\sigma_{_X}^2}\left(-\frac{1}{3\sigma_{_X}^2} + \frac{1}{54}c_{3,XX}k_0\vartheta_{_X}\right) + \frac{8\zeta_{8,YY}A^4\sqrt{2}\sqrt{6}}{k_0\sigma_{_X}^2}\left(-\frac{1}{6\sigma_{_Y}^2} - \frac{1}{81}c_{4,YY}k_0\vartheta_{_Y}\right) \\ & + \frac{8A^4\sqrt{2}\sqrt{6}}{k_0\sigma_{_X}^2}\left(-\frac{\zeta_{9,XX}}{3\sigma_{_X}^2} - \frac{9}{32}\frac{c_{5,XX}\zeta_{11,XX}}{\sigma_{_X}^4}\right) + \frac{8A^4\sqrt{2}\sqrt{6}}{k_0\sigma_{_X}^2}\left(-\frac{\zeta_{10,YY}}{6\sigma_{_Y}^2} - \frac{3}{32}\frac{c_{6,YY}\zeta_{12,YY}}{\sigma_{_Y}^4}\right) \end{aligned} \quad (2.95)$$

$$\begin{aligned}\frac{d\vartheta_{_Y}}{dZ} = {} & \frac{8\zeta_1}{k_0\sigma_{_Y}^4} - 2\zeta_1 k_0\vartheta_{_Y}^2 + \frac{\zeta_{4m_r}A^2}{k_0\sigma_{_Y}^2}\left(\frac{4\sqrt{2}}{\sigma_\tau\sqrt{\pi}}\right) \\ & + \frac{8\zeta_{2d_{3r}}A\sqrt{2}}{k_0\sigma_{_Y}^2}\left(\frac{4}{27}\frac{1}{\sigma_\tau^3\sqrt{\pi}} + \frac{1}{18}\frac{k_0^2\vartheta_\tau^2}{\sqrt{\pi}} + \frac{1}{144}\frac{k_0^4\vartheta_\tau^4\sigma_\tau^5}{\sqrt{\pi}}\right) \\ & + \frac{8\zeta_{2d_{4r}}A^2}{k_0\sigma_{_Y}^2}\left(\frac{3}{2}\frac{1}{\sigma_\tau^4} + \frac{3}{4}k_0^2\vartheta_\tau^2 + \frac{3}{32}k_0^4\vartheta_\tau^4\sigma_\tau^4\right) + \frac{\zeta_{4q_r}A^2\sqrt{2}}{k_0\sigma_{_Y}^2} + \frac{4}{9}\frac{\zeta_{4c_r}A^4\sqrt{2}\sqrt{6}}{k_0\sigma_{_Y}^2} \\ & + \frac{8\zeta_{5,XX}A^2\sqrt{2}}{k_0\sigma_{_Y}^2}\left(\frac{1}{4\sigma_{_X}^2} - \frac{1}{32}c_{1,XX}k_0\vartheta_{_X}\right) + \frac{8\zeta_{6,YY}A^2\sqrt{2}}{k_0\sigma_{_Y}^2}\left(\frac{3}{4}\frac{1}{\sigma_{_Y}^2} + \frac{5}{32}c_{2,YY}k_0\vartheta_{_Y}\right) \\ & + \frac{8\zeta_{7,XX}A^4\sqrt{2}\sqrt{6}}{k_0\sigma_{_Y}^2}\left(-\frac{1}{6\sigma_{_X}^2} - \frac{1}{81}c_{3,XX}k_0\vartheta_{_X}\right) + \frac{8\zeta_{8,YY}A^4\sqrt{2}\sqrt{6}}{k_0\sigma_{_Y}^2}\left(-\frac{1}{3\sigma_{_Y}^2} + \frac{1}{54}c_{4,YY}k_0\vartheta_{_Y}\right) \\ & + \frac{8A^4\sqrt{2}\sqrt{6}}{k_0\sigma_{_Y}^2}\left(-\frac{\zeta_{9,XX}}{6\sigma_{_X}^2} - \frac{3}{32}\frac{c_{5,XX}\zeta_{11,XX}}{\sigma_{_X}^4}\right) + \frac{8A^4\sqrt{2}\sqrt{6}}{k_0\sigma_{_Y}^2}\left(-\frac{\zeta_{10,YY}}{3\sigma_{_Y}^2} - \frac{9}{32}\frac{c_{6,YY}\zeta_{12,YY}}{\sigma_{_Y}^4}\right) \end{aligned} \quad (2.96)$$

$$\begin{aligned}\frac{d\vartheta_\tau}{dZ} = {} & \frac{8\zeta_{2p_r}}{k_0\sigma_\tau^2}\left(\frac{1}{\sigma_\tau^2}-\frac{1}{4}k_0^2\vartheta_\tau^2\sigma_\tau^2\right)+\frac{8a_1\zeta_{2p_r}\vartheta_\tau}{\sigma_\tau^2}+\frac{\zeta_{4m_r}A^2}{k_0\sigma_\tau^2}\left(\frac{8\sqrt{2}}{\sigma_\tau\sqrt{\pi}}\right)\\ & +\frac{8\zeta_{2d_{3r}}A\sqrt{2}}{k_0\sigma_\tau^2}\left(\frac{28}{27}\frac{1}{\sigma_\tau^3\sqrt{\pi}}-\frac{1}{18}\frac{k_0^2\vartheta_\tau^2}{\sqrt{\pi}}-\frac{1}{16}\frac{k_0^4\vartheta_\tau^4\sigma_\tau^5}{\sqrt{\pi}}\right)\\ & +\frac{8a_3\zeta_{2d_{3r}}\sqrt{2}}{k_0\sigma_\tau^2}\left(-\frac{3}{2}\frac{k_0\vartheta_\tau}{\sigma_\tau\sqrt{\pi}}+\frac{3}{8}\frac{k_0^3\vartheta_\tau^3\sigma_\tau^3}{\sqrt{\pi}}\right)\\ & +\frac{8\zeta_{2d_{4r}}A^2}{k_0\sigma_\tau^2}\left(\frac{15}{2}\frac{1}{\sigma_\tau^4}+\frac{3}{4}k_0^2\vartheta_\tau^2-\frac{9}{32}k_0^4\vartheta_\tau^4\sigma_\tau^4\right)\\ & +\frac{8a_4\zeta_{2d_{4r}}}{k_0\sigma_\tau^2}\left(-\frac{6k_0\vartheta_\tau}{\sigma_\tau^2}-\frac{3}{2}k_0^3\vartheta_\tau^3\sigma_\tau^2\right)\\ & +\frac{\zeta_{4q_r}A^2\sqrt{2}}{k_0\sigma_\tau^2}+\frac{4}{9}\frac{\zeta_{4c_r}A^4\sqrt{2}\sqrt{6}}{k_0\sigma_\tau^2}\\ & +\frac{8\zeta_{5,XX}A^2\sqrt{2}}{k_0\sigma_\tau^2}\left(\frac{1}{4\sigma_X^2}-\frac{1}{32}c_{1,XX}k_0\vartheta_X\right)+\frac{8\zeta_{6,YY}A^2\sqrt{2}}{k_0\sigma_\tau^2}\left(\frac{3}{4}\frac{1}{\sigma_Y^2}+\frac{5}{32}c_{2,YY}k_0\vartheta_Y\right)\\ & +\frac{8\zeta_{7,XX}A^4\sqrt{2}\sqrt{6}}{k_0\sigma_\tau^2}\left(-\frac{1}{6\sigma_X^2}-\frac{1}{81}c_{3,XX}k_0\vartheta_X\right)+\frac{8\zeta_{8,YY}A^4\sqrt{2}\sqrt{6}}{k_0\sigma_\tau^2}\left(-\frac{1}{3\sigma_Y^2}+\frac{1}{54}c_{4,YY}k_0\vartheta_Y\right)\\ & +\frac{8A^4\sqrt{2}\sqrt{6}}{k_0\sigma_\tau^2}\left(-\frac{\zeta_{9,XX}}{6\sigma_X^2}-\frac{3}{32}\frac{c_{5,XX}\zeta_{11,XX}}{\sigma_X^4}\right)+\frac{8A^4\sqrt{2}\sqrt{6}}{k_0\sigma_\tau^2}\left(-\frac{\zeta_{10,YY}}{3\sigma_Y^2}-\frac{9}{32}\frac{c_{6,YY}\zeta_{12,YY}}{\sigma_Y^4}\right)\end{aligned} \tag{2.97}$$

$$\begin{aligned}\frac{d\psi}{dZ} & -\frac{2\zeta_{2p_r}}{\sigma_\tau^2}-\frac{2\zeta_1}{\sigma_X^2}-\frac{2\zeta_1}{\sigma_Y^2}-a_1\zeta_{2p_r}k_0\vartheta_\tau-\zeta_3+\zeta_{4m_r}A^2\sqrt{2}\left(-\frac{4}{\sigma_\tau\sqrt{\pi}}\right)\\ & +\zeta_{2d_{3r}}A\sqrt{2}\left(-\frac{20}{9}\frac{1}{\sigma_\tau^3\sqrt{\pi}}-\frac{7}{18}\frac{k_0^2\vartheta_\tau^2\sigma_\tau}{\sqrt{\pi}}+\frac{1}{144}\frac{k_0^4\vartheta_\tau^4\sigma_\tau^5}{\sqrt{\pi}}\right)+a_3\zeta_{2d_{3r}}\sqrt{2}\left(\frac{9}{2}\frac{k_0}{\sigma_\tau}-\frac{1}{8}\frac{k_0^3\vartheta_\tau^3\sigma_\tau^3}{\sqrt{\pi}}\right)\\ & +\zeta_{2d_{4r}}A^2\left(-\frac{33}{2}\frac{1}{\sigma_\tau^4}-\frac{21}{4}k_0^2\vartheta_\tau^2-\frac{9}{32}k_0^4\vartheta_\tau^4\sigma_\tau^4\right)+a_4\zeta_{2d_{4r}}\left(-\frac{2k_0\vartheta_\tau}{\sigma_\tau^2}+\frac{3}{2}k_0^3\vartheta_\tau^3\sigma_\tau^2\right)\\ & -\frac{7}{8}\zeta_{4q_r}A^2\sqrt{2}-\frac{1}{3}\zeta_{4c_r}A^4\sqrt{2}\sqrt{6}\\ & +\zeta_{\cdot 5,XX}A^2\sqrt{2}\left(-\frac{9}{4}\frac{1}{\sigma_X^2}+\frac{1}{32}c_{1,XX}k_0\vartheta_X\right)+\zeta_{6,YY}A^2\sqrt{2}\left(-\frac{9}{4}\frac{1}{\sigma_Y^2}+\frac{1}{32}c_{2,YY}k_0\vartheta_Y\right)\\ & +\zeta_{7,XX}A^4\sqrt{2}\sqrt{6}\left(\frac{7}{6}\frac{1}{\sigma_X^2}+\frac{7}{162}c_{3,XX}k_0\vartheta_X\right)+\zeta_{8,YY}A^4\sqrt{2}\sqrt{6}\left(\frac{7}{6}\frac{1}{\sigma_Y^2}+\frac{7}{162}c_{4,YY}k_0\vartheta_Y\right)\\ & +A^4\sqrt{2}\sqrt{6}\left(\frac{7}{6}\frac{\zeta_{9,XX}}{\sigma_X^2}+\frac{3}{4}\frac{c_{5,XX}\zeta_{11,XX}}{\sigma_X^4}\right)+A^4\sqrt{2}\sqrt{6}\left(\frac{7}{6}\frac{\zeta_{10,YY}}{\sigma_Y^2}+\frac{3}{4}\frac{c_{6,YY}\zeta_{12,YY}}{\sigma_Y^4}\right)\end{aligned} \tag{2.98}$$

2.5 Conclusion

We have successfully derived the nonlocal CCGLE and CQCGLE by considering the electromagnetic wave theory based on Maxwell's equations. Scaling transformations related to the practical use of optical fibers have been applied to the CCGLE and CQCGLE to tailor them for a good description of LB propagation in doped nonlocal optical fibers. We found that the nonlocal CQCGLE has more terms compared to the nonlocal CCGLE, namely the third and fourth-order dispersion, the saturation of the nonlinear gain absorption (if negative), the nonlinear gradient term responsible for the self-frequency shift and the nonlinear dispersion responsible for the self-steepening.

We used the variational approach based on the Euler-Lagrange equations to find approximate solutions to the nonlocal CCGLE and CQCGLE to gain physical insight into some relevant parameters. To qualitatively validate our analytical predictions, we implement these solutions in numerical simulations in the following chapter.

Chapter III

Results and Discussion

3.1 Introduction

Previously, we derived the nonlocal CCGLE and the CQCGLE from Maxwell's equations. We have shown that the CCGLE and the CQCGLE each give rise to a system of eight coupled first-order differential equations, obtained using the variational approach based on the Euler-Lagrange equations.

The next step is to confirm these analytical results by performing numerical simulations based on the Runge-Kutta and split-step Fourier methods. Before proceeding, we need to determine the stability regions of the LB characteristic parameters. These parameters include the amplitude, the temporal and spatial pulse widths and the position of the pulse maximum, the unequal wavefront curvatures, the chirp parameters, and the phase shift. The Routh-Hurwitz stability criterion will be employed for the determination of the stability regions from which the initial values for the simulations are taken.

3.2 Stability criterion for steady-state solutions in a cubic context

We have chosen the Routh-Hurwitz stability criterion, described as a necessary and sufficient condition for reaching the stability zone. Applying this stability criterion requires that we construct a Jacoby determinant. From the Jacoby determinant, we obtain the polynomial characteristic equation. We can then verify the necessary and sufficient conditions of the Routh-Hurwitz stability criterion.

In the following, we introduce the notations: $F_A \equiv \frac{dA}{dZ}$, $F_\sigma \equiv \frac{d\sigma}{dZ}$, $F_\vartheta \equiv \frac{d\vartheta}{dZ}$, $F_{\sigma_\tau} \equiv \frac{d\sigma_\tau}{dZ}$, and $F_{\vartheta_\tau} \equiv \frac{d\vartheta_\tau}{dZ}$, resulting from Eqs. (2.77)-(2.84). Recall that in the case of a symmetric input, the set

of Eqs. (2.77)-(2.84) is reduced to only five equations: (2.77), (2.78), (2.80), (2.81) and (2.83). The Jacoby determinant is constructed from the derivatives of these terms F_A, F_σ, F_ϑ, F_{σ_τ}, and F_{ϑ_τ}, with respect to amplitude, spatial and temporal widths, spatial and temporal curvatures taken in steady, i.e., equilibrium state:

$$det(J - \lambda I) = \begin{vmatrix} \frac{\partial F_A}{\partial A} - \lambda & \frac{\partial F_A}{\partial \sigma} & \frac{\partial F_A}{\partial \vartheta} & \frac{\partial F_A}{\partial \sigma_\tau} & \frac{\partial F_A}{\partial \vartheta_\tau} \\ \frac{\partial F_\sigma}{\partial A} & \frac{\partial F_\sigma}{\partial \sigma} - \lambda & \frac{\partial F_\sigma}{\partial \vartheta} & \frac{\partial F_\sigma}{\partial \sigma_\tau} & \frac{\partial F_\sigma}{\partial \vartheta_\tau} \\ \frac{\partial F_\vartheta}{\partial A} & \frac{\partial F_\vartheta}{\partial \sigma} & \frac{\partial F_\vartheta}{\partial \vartheta} - \lambda & \frac{\partial F_\vartheta}{\partial \sigma_\tau} & \frac{\partial F_\vartheta}{\partial \vartheta_\tau} \\ \frac{\partial F_{\sigma_\tau}}{\partial A} & \frac{\partial F_{\sigma_\tau}}{\partial \sigma} & \frac{\partial F_{\sigma_\tau}}{\partial \vartheta} & \frac{\partial F_{\sigma_\tau}}{\partial \sigma_\tau} - \lambda & \frac{\partial F_{\sigma_\tau}}{\partial \vartheta_\tau} \\ \frac{\partial F_{\vartheta_\tau}}{\partial A} & \frac{\partial F_{\vartheta_\tau}}{\partial \sigma} & \frac{\partial F_{\vartheta_\tau}}{\partial \vartheta} & \frac{\partial F_{\vartheta_\tau}}{\partial F_{\sigma_\tau}} & \frac{\partial F_{\vartheta_\tau}}{\partial \vartheta_\tau} - \lambda \end{vmatrix} = 0. \quad (3.1)$$

The fifth-order characteristic polynomial equation obtained from the Jacoby determinant is as follows:

$$\lambda^5 + a_1\lambda^4 + a_2\lambda^3 + a_3\lambda^2 + a_4\lambda + a_5 = 0. \quad (3.2)$$

The coefficients $a_1, ..., a_5$, depend on the partial derivatives of the functions F_A, F_σ, F_ϑ, F_{σ_τ}, and F_{ϑ_τ}. However, these analytical expressions could not be presented due to their length. The partial derivatives of the functions are provided in Appendix C.

For the stability to be reached, the necessary condition implies that all the roots of the characteristic Eq. (3.2) should have negative real parts i.e., $R(\lambda_i) < 0$, with $i = 1$,...,5.

The sufficient condition based on the Routh-Hurwitz criterion is that the coefficients $a_1, ..., a_5$ should be positive [38, 48]:

$$a_i > 0, \text{with } i = 1, ..., 5, \quad (3.3)$$

as well as their combinations:

$$b_1 = \frac{a_1 a_2 - a_3}{a_1} > 0, \tag{3.4}$$

$$b_3 = \frac{a_1 a_4 - a_5}{a_1} > 0, \tag{3.5}$$

$$c_1 = \frac{b_1 a_3 - a_1 b_2}{b_1} > 0, \tag{3.6}$$

$$d_1 = \frac{c_1 b_3 - b_1 c_2}{c_1} > 0, \tag{3.7}$$

have to be positive.

In Figure 3.1, we represent the double solutions A_+ and A_- of the steady-state amplitudes versus q_i and $\gamma_{X=Y}$, where the dissipative parameter q_i represents the nonlinear loss related to the self-defocusing Kerr nonlinearity ($q_r < 0$), and the parameter $\gamma_{X=Y}$ denotes the symmetric nonlocality degree along the transverse directions. By using the normalized coefficient $N_r = 2^{1/2}(4/3)^{3/4}$, assuming a linear gain γ_r under anomalous dispersion, the following parameter values have been used for illustration: $p_r = 0.579/N_r$, $p_i = 0.201/N_r$, $q_r = -110/N_r$, $\gamma_r = 150/N_r$, $\gamma_i = -530/N_r$, $k_0 = 2\pi/1.55$.

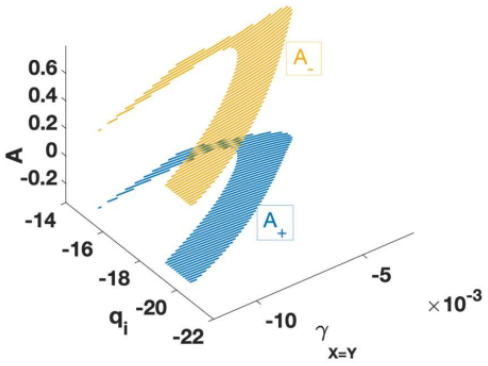

Figure 3.1: Double solutions A_+ and A_- of the steady-state amplitudes versus (q_i, $\gamma_{X=Y}$). The solution A_- (yellow sheet) is stable. The solution A_+ (blue sheet) is rather unstable. The following parameter values have been used: $N_r = 2^{1/2}(4/3)^{3/4}$ (the normalized coefficient), $p_r = 0.579/N_r$ (the anomalous dispersion), $p_i = 0.201/N_r$ (the spectral filtering), $q_r = -110/N_r$ (the self-defocusing Kerr nonlinearity), $\gamma_r = 150/N_r$ (the linear gain), $\gamma_i = -530/N_r$ (the frequency shift), and $k_0 = 2\pi/1.55$ (the wave number).

As stated before [74], the stability of the solution A_- is only a prerequisite to obtaining optical LBs after a spatiotemporal self-organized evolution. It can clearly be seen in Figure 3.1 that when the spatial nonlocal self-defocusing Kerr nonlinearity response ($\gamma_{X=Y}$) and the nonlinear loss (q_i) increase, the stability zone (yellow area representing A_-) gets expanded.

Hence, the nonlocality and the nonlinear loss enhance optical LBs localization in this regime. On the other hand, the lower blue sheet of Figure 3.1 shows that the solution A_+ is everywhere unstable. Therefore, it will be beneficial to pay more attention to the stable solution A_- as it remains the only prerequisite for the formation of stable LBs during the propagation of an input pulse.

So doing, in Figure 3.2(a) and (b), the stability zones (hatched areas) are shown for the spatial width versus q_i and $\gamma_{X=Y}$, respectively, while the same procedure is repeated for the temporal width σ_τ in Figure 3.2(c) and 3.2(d) for the stable solution A_- under anomalous dispersion. The set of spatial and temporal widths values derived from these diagrams will be chosen from this stability range for the numerical simulations of the input spatiotemporal pulses.

Zones of stability for the spatial and temporal chirps, $\vartheta_{X=Y}$ and ϑ_τ, respectively, versus q_i and $\gamma_{X=Y}$, for the stable solution A_- and the anomalous dispersion are depicted in Figure 3.3. The set of spatial and temporal chirps derived from these curves will be chosen from this stability range for the numerical simulations of the input spatiotemporal pulses.

The stability zones for the phase ψ are depicted in Figure 3.4(a) and (b) versus q_i and $\gamma_{X=Y}$, respectively, for the stable solution A_- under the anomalous dispersion. The set of phase values obtained from these diagrams will be chosen from this stability range for the numerical implementation of the input spatiotemporal pulses.

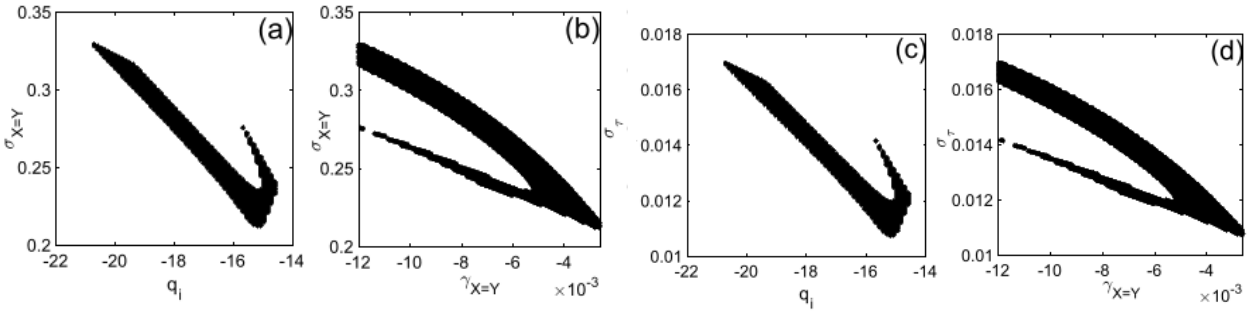

Figure 3.2: Diagrams of stability in the (q_i, $\sigma_{X=Y}$)-plane [panel (a)], the ($\gamma_{X=Y}$, $\sigma_{X=Y}$)-plane [panel (b)], the (q_i, σ_τ)-plane [panel(c)] and the ($\gamma_{X=Y}$, σ_τ)-plane [panel(d)], where the dark zone stands for the stable solution A_- under anomalous dispersion. The parameter values used are the same as in Figure 3.1.

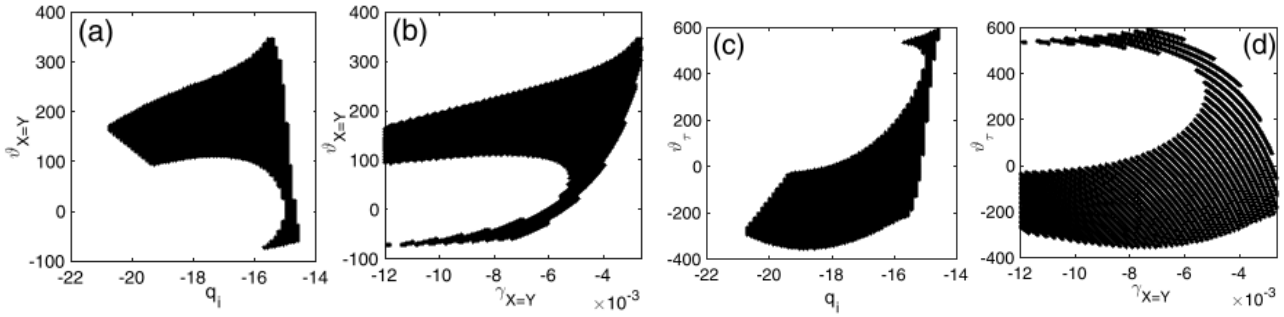

Figure 3.3: Diagrams of stability in the (q_i, $\vartheta_{X=Y}$)-plane [panel (a)], the ($\gamma_{X=Y}$, $\vartheta_{X=Y}$)-plane [panel (b)], the (q_i, ϑ_τ)-plane [panel(c)] and the ($\gamma_{X=Y}$, ϑ_τ)-plane [panel(d)], where the dark zone stands for the stable solution A_- under anomalous dispersion. The parameter values used are the same as in Figure 3.1.

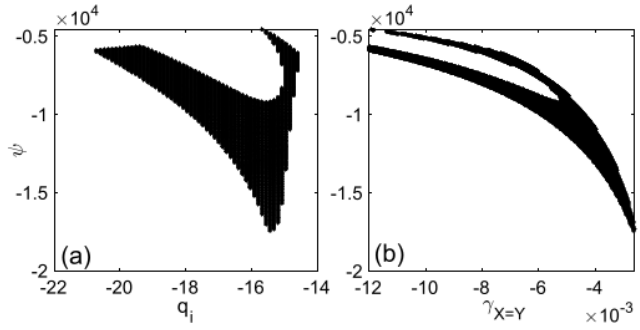

Figure 3.4: Panel (a) shows the stability zone (dark area) for the solution A_- in the (q_i, ψ)-plane, while panel (b) displays the stability zone in the (q_i, $\gamma_{X=Y}$)-plane, under anomalous dispersion. Parameter values are those used in Figure 3.1.

3.3 Stability criterion for steady-state solutions in the CQ case

3.3.1 The first set of parameters for steady-state solutions in the CQ case.

In Figure (3.5), we represent the double solutions A_+ and A_- of the steady-state amplitudes versus c_i and $\gamma_{X=Y}$, where the dissipative parameter c_i represents the saturation nonlinear loss/gain ($c_i < 0/c_i > 0$) related to the quintic self-focusing Kerr nonlinearity ($c_r > 0$), and the parameter $\gamma_{X=Y}$ denotes the symmetric nonlocality degree along the transverse directions. By using the normalized coefficient $N_r = 2^{1/2}(4/3)^{3/4}$, assuming a linear loss (γ_r<0) under normal dispersion, the following parameter values have been used for illustration: $p_r = -150.579/N_r$, $p_i = 0.000201/N_r$, $q_r = -60.8/N_r$, $q_i = 6/N_r$, $\gamma_r = -150/N_r$, $\gamma_i = 330/N_r$, $d_{3r} = 0.579/N_r$, $d_{3i} = -0.08/N_r$, $d_{4r} = -60.8/N_r$, $d_{4i} = 0.002/N_r$, $c_r = 0.00342/N_r$, $n_i = 0.025/N_r$, $m_r = -0.5/N_r$, $k_0 = 2\pi/1.55$.

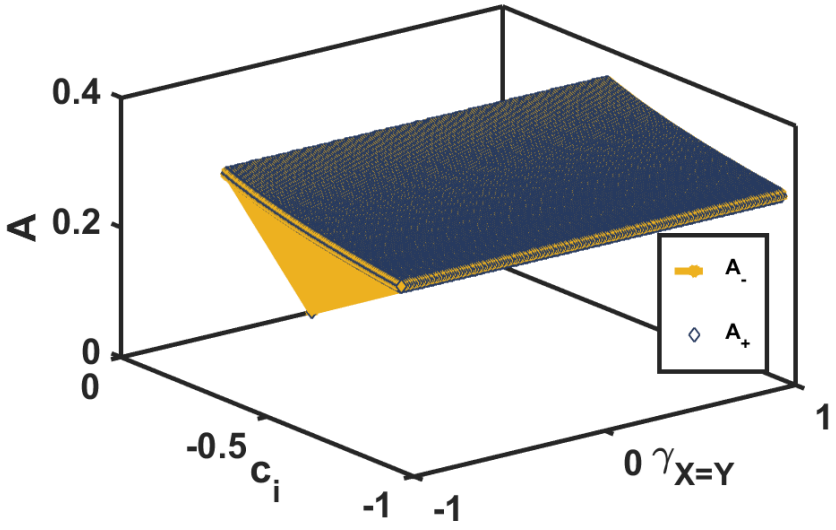

Figure 3.5: Double solutions A_+ and A_- of the steady-state amplitudes versus (c_i, $\gamma_{X=Y}$). The solutions A_- (yellow sheet) and A_+ (blue sheet) are stable. The following parameter values have been used: $N_r = 2^{1/2}(4/3)^{3/4}$ (the normalized coefficient), $p_r = -150.579/N_r$ (normal dispersion), $p_i = 0.000201/N_r$ (the spectral filtering), $q_r = -60.8/N_r$ (the self-defocusing cubic Kerr nonlinearity), $q_i = 6/N_r$ (dissipative cubic nonlinear gain), $\gamma_r = -150/N_r$ (the linear gain), $\gamma_i = 330/N_r$ (the frequency shift), $d_{3r} = 0.0006/N_r$ (the third order linear dispersion), $d_{3i} = -0.08/N_r$ (the dissipative third order linear dispersion), $d_{4r} = 0.002/N_r$ (the fourth order linear dispersion), $d_{4i} = -0.04/N_r$ (the dissipative fourth order linear dispersion), $c_r = 0.00342/N_r$ (the quintic self-focusing Kerr nonlinearity), $n_i = 0.025/N_r$ (the nonlinear dispersion term), $m_r = -0.5/N_r$ (the nonlinear gradient), $k_0 = 2\pi/1.55$.

Figure 3.5 shows that we have succeeded in producing amplitudes A_- and A_+ in a positive

value zone, unlike the cubic case where only amplitude A_- was stable, and amplitude A_+ corresponded only to negative numerical values and was always unstable. The two amplitudes blend seamlessly, as shown by the blue star representing amplitude A_+ positioned underneath the yellow sheet (amplitude A_-). By incorporating additional effects, such as quintic correction terms, into the initial cubic medium, we find that the A_- solution is no longer the only prerequisite for obtaining LBs after self-organized spatiotemporal evolution. As the nonlocal spatial response of the Kerr nonlinearity ($\gamma_{X=Y}$) and the saturation of nonlinear loss/gain ($c_i < 0/c_i > 0$) increase, we observe that the stability zones (yellow sheet representing A_- and blue sheet representing A_+) expand, hence, nonlocality and nonlinear loss/gain improve the localization of optical LBs in this regime. Thus, it is appropriate to state that the stability diagrams for the other characteristic LB parameters can be obtained by selecting either A_- or A_+ as the stable solution.

So doing, in Figure 3.6, the stability zones (green areas) are shown for the spatial width versus c_i and $\gamma_{X=Y}$, respectively, while the same procedure is repeated for the temporal width σ_τ in Figure 3.8 for the stable solution A_+ under normal dispersion. The set of spatial and temporal widths values derived from these diagrams will be chosen from this stability range for the numerical simulations of the input spatiotemporal pulses in the subsection (3.7.1).

Zones of stability for the spatial and temporal chirps, $\vartheta_{X=Y}$ and ϑ_τ, respectively, versus c_i and $\gamma_{X=Y}$, for the stable solution A_+ and the normal dispersion are depicted in Figs. 3.7 and 3.9. The set of spatial and temporal chirps derived from these curves will be chosen from this stability range for the numerical simulations of the input spatiotemporal pulses in the subsection (3.7.1). The stability zones for the phase ψ are depicted in Figure 3.10 versus c_i and $\gamma_{X=Y}$, respectively, for the stable solution A_+ under the normal dispersion. The set of phase values obtained from these diagrams will be chosen from this stability range for the numerical implementation of the input spatiotemporal pulses in the subsection (3.7.1).

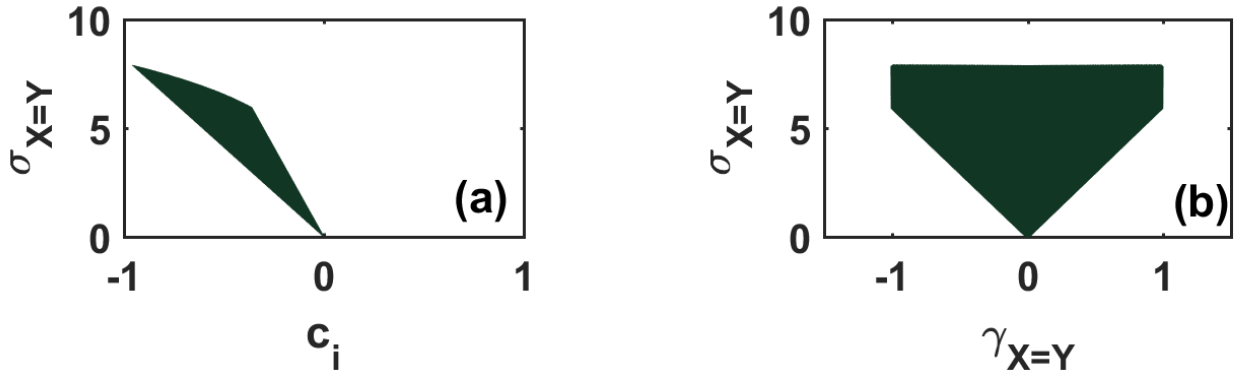

Figure 3.6: Stability diagrams in the (c_i, $\sigma_{_{X=Y}}$)-plane, from left to right, the (c_i, $\sigma_{_{X=Y}}$)-plane and the ($\gamma_{_{X=Y}}$, $\sigma_{_{X=Y}}$)-plane, respectively. The green area stands for the stable solution A_+ under normal dispersion. The parameter values used are the same as in Figure 3.5.

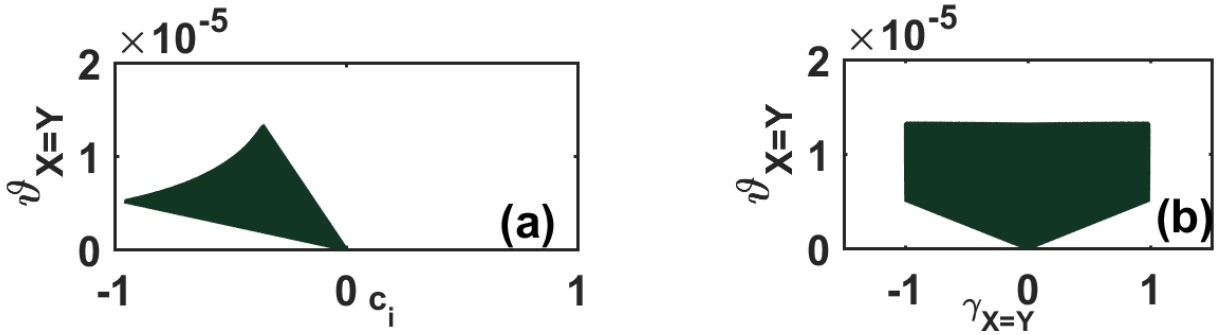

Figure 3.7: Diagrams of stability in the (c_i, $\vartheta_{_{X=Y}}$)-plane, from left to right, the (c_i, $\vartheta_{_{X=Y}}$)-plane and the ($\gamma_{_{X=Y}}$, $\vartheta_{_{X=Y}}$)-plane, respectively. The green area stands for the stable solution A_+ under normal dispersion. The parameter values used are the same as in Figure 3.5.

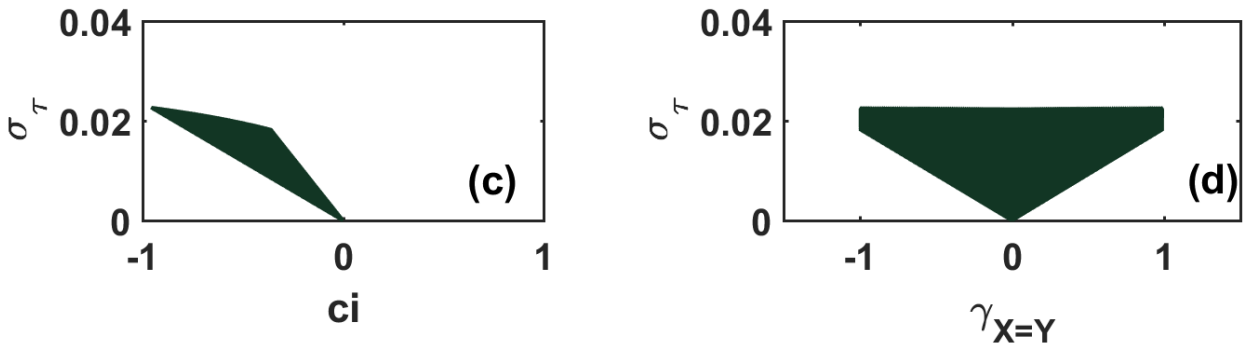

Figure 3.8: Diagrams of stability in the (c_i, σ_τ)-plane, from left right, the (c_i, σ_τ)-plane and the ($\gamma_{_{X=Y}}$, σ_τ)-plane, respectively. The green area stands for the stable solution A_+ under normal dispersion. The parameter values used are the same as in Figure 3.5.

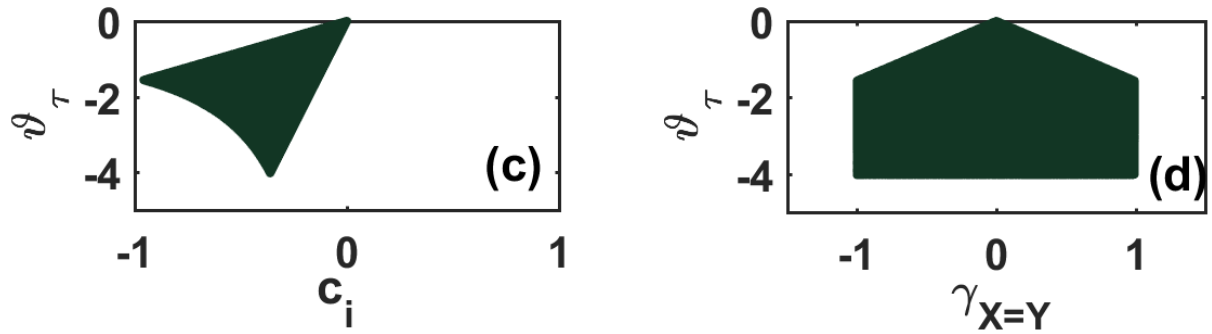

Figure 3.9: Diagrams of stability in the (c_i, ϑ_τ)-plane, from left to right, the (c_i, ϑ_τ)-plane and the ($\gamma_{X=Y}$, ϑ_τ)-plane, respectively. The green area stands for the stable solution A_+ under normal dispersion. The parameter values used are the same as in Figure 3.5.

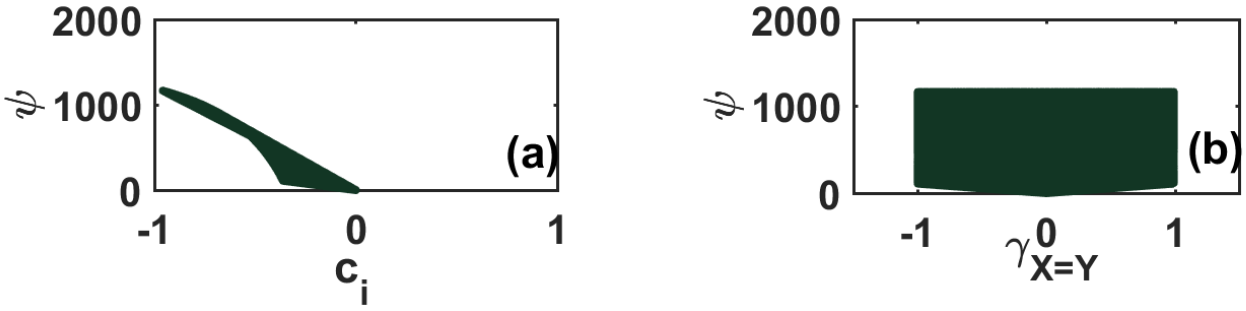

Figure 3.10: Diagrams of stability in the (c_i, ψ)-plane, from left to right, the (c_i, ψ)-plane and the ($\gamma_{X=Y}$, ψ)-plane, respectively. The green area stands for the stable solution A_+ under normal dispersion. The parameter values used are the same as in Figure 3.5.

3.3.2 The second set of parameters for steady-state solutions in the CQ case.

In Figure 3.11, we represent the double solutions A_+ and A_- of the steady-state amplitudes versus c_i and $\gamma_{X=Y}$, where the dissipative parameter c_i represents the saturation nonlinear gain ($c_i > 0$) related to the quintic self-focusing Kerr nonlinearity ($c_r > 0$), and the parameter $\gamma_{X=Y}$ denotes the symmetric nonlocality degree along the transverse directions. By using the normalized coefficient $N_r = 2^{1/2}(4/3)^{3/4}$, assuming a linear loss ($\gamma_r<0$) under anomalous dispersion, the following parameter values have been used for illustration: $p_r = 2/N_r$, $p_i = 0.00201/N_r$, $q_r =$

$-105/N_r$, $q_i = -5/N_r$, $\gamma_r = -150/N_r$, $\gamma_i = 390/N_r$, $d_{3r} = 0.0006/N_r$, $d_{3i} = -0.083/N_r$, $d_{4r} = -0.4/N_r$, $d_{4i} = 0.002/N_r$, $c_r = 0.0342/N_r$, $n_i = 0.025/N_r$, $m_r = -0.5/N_r$, $k_0 = 2\pi/1.55$.

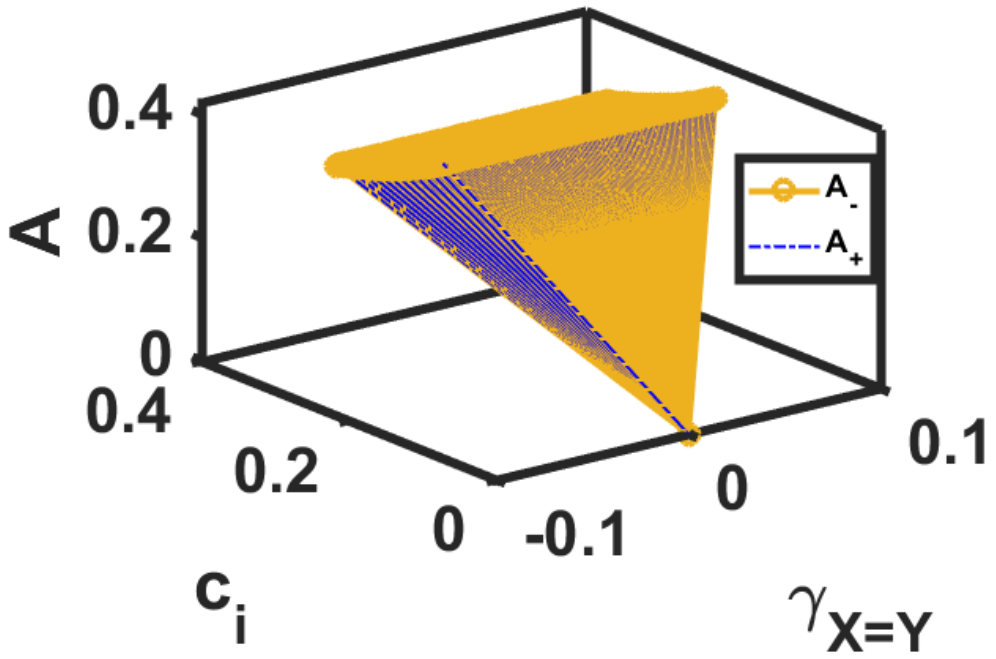

Figure 3.11: Double solutions A_+ and A_- of the steady-state amplitudes versus $(c_i, \gamma_{X=Y})$. The solutions A_- (yellow sheet) and A_+ (blue sheet) are stable. The following parameter values have been used: $N_r = 2^{1/2}(4/3)^{3/4}$, $p_r = 2/N_r$ anomalous dispersion, $p_i = 0.00201/N_r$, $q_r = -105/N_r$, $q_i = -5/N_r$, $\gamma_r = -150/N_r$, $\gamma_i = 390/N_r$, $d_{3r} = 0.0006/N_r$, $d_{3i} = -0.083/N_r$, $d_{4r} = -0.4/N_r$, $d_{4i} = 0.002/N_r$, $c_r = 0.0342/N_r$ (the quintic self-focusing Kerr nonlinearity), $n_i = 0.025/N_r$, $m_r = -0.5/N_r$, $k_0 = 2\pi/1.55$.

As in Figure 3.5, Figure 3.11 shows that we have succeeded in producing amplitudes A_- and A_+ in a positive value zone, unlike the cubic case where only amplitude A_- was stable, and amplitude A_+ corresponded only to negative numerical values and was always unstable. The two amplitudes blend seamlessly. By incorporating additional effects, such as quintic correction terms, into the initial cubic medium, we find that the A_- solution is no longer the only prerequisite for obtaining LBs after self-organized spatiotemporal evolution. As the nonlocal spatial response of the Kerr nonlinearity $(\gamma_{X=Y})$ and the saturation of nonlinear gain $(c_i > 0)$ increase, we observe that the stability zones (yellow sheet representing A_- and blue sheet representing A_+) expand, hence, nonlocality and nonlinear gain improve the localization of optical LBs in this regime. Thus, it is appropriate to state that the stability diagrams for the other characteristic LB parameters

can be obtained by selecting either A_- or A_+ as the stable solution.

So doing, in Figure 3.12, the stability zones (green areas) are shown for the spatial width versus c_i and $\gamma_{X=Y}$, respectively, while the same procedure is repeated for the temporal width σ_τ in Figure 3.14 for the stable solution A_- under anomalous dispersion. The set of spatial and temporal widths values derived from these diagrams will be chosen from this stability range for the numerical simulations of the input spatiotemporal pulses in the subsection (3.7.2). Zones of stability for the spatial and temporal chirps, $\vartheta_{X=Y}$ and ϑ_τ, respectively, versus c_i and $\gamma_{X=Y}$, for the stable solution A_- and the anomalous dispersion are depicted in Figs. 3.13 and 3.15. The set of spatial and temporal chirps derived from these curves will be chosen from this stability range for the numerical simulations of the input spatiotemporal pulses in the subsection (3.7.2).
The stability zones for the phase ψ are depicted in Figure 3.16 versus c_i and $\gamma_{X=Y}$, respectively, for the stable solution A_- under the anomalous dispersion. The set of phase values obtained from these diagrams will be chosen from this stability range for the numerical implementation of the input spatiotemporal pulses in the subsection (3.7.2).

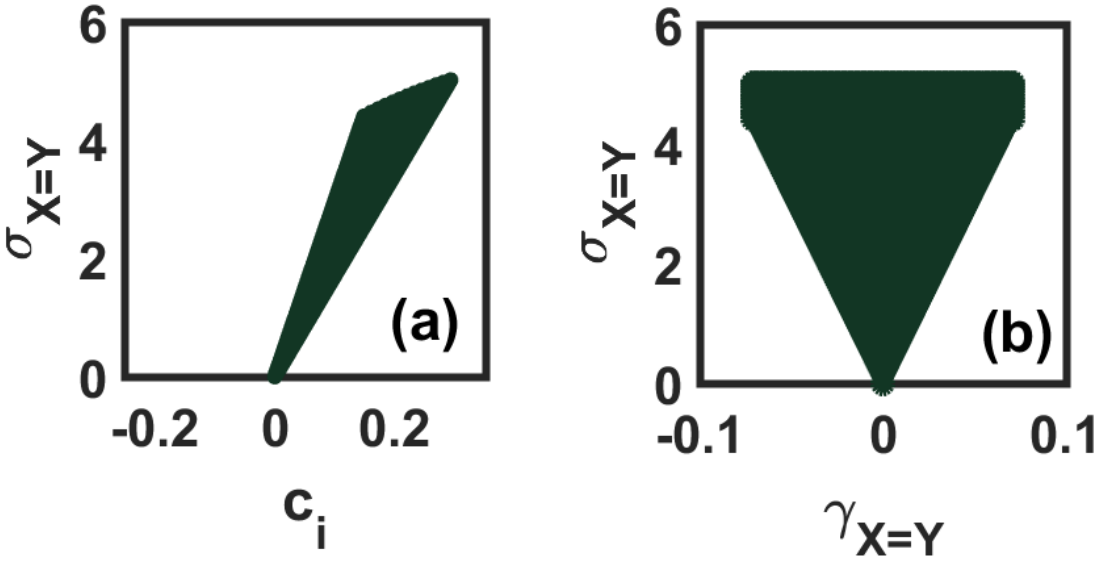

Figure 3.12: Diagrams of stability in the (c_i, $\sigma_{X=Y}$)-plane, from left to right, the (c_i, $\sigma_{X=Y}$)-plane and the ($\gamma_{X=Y}$, $\sigma_{X=Y}$)-plane, respectively. The green area stands for the stable solution A_- under anomalous dispersion. The parameter values used are the same as in Figure 3.11.

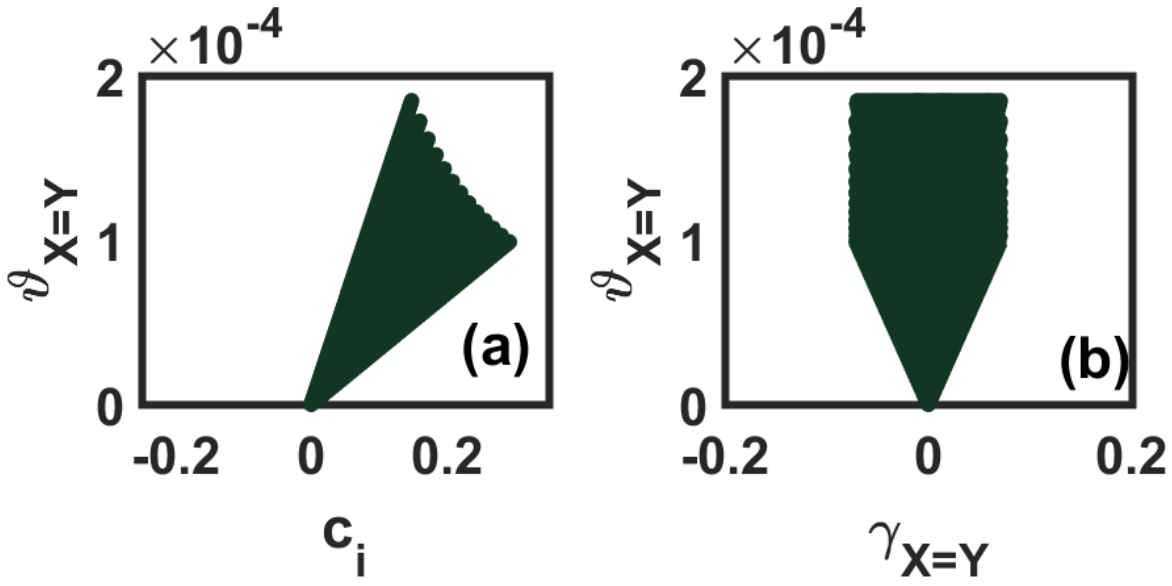

Figure 3.13: Diagrams of stability in the (c_i, $\vartheta_{X=Y}$)-plane, from left to right, the (c_i, $\vartheta_{X=Y}$)-plane and the ($\gamma_{X=Y}$, $\vartheta_{X=Y}$)-plane, respectively. The green area stands for the stable solution A_- under anomalous dispersion. The parameter values used are the same as in Figure 3.11.

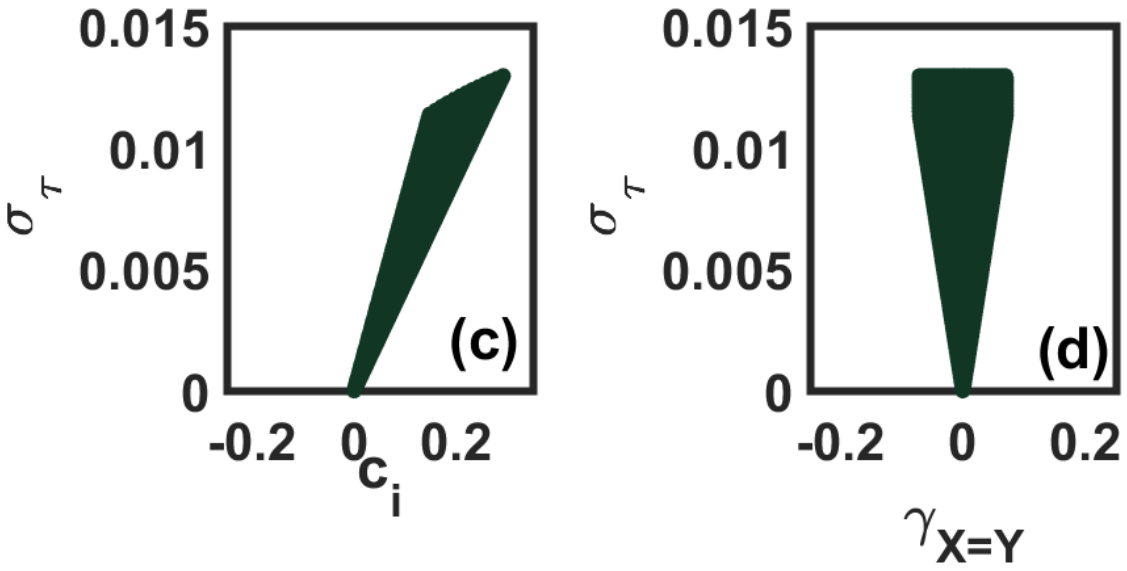

Figure 3.14: Diagrams of stability in the (c_i, σ_τ)-plane, from left to right, the (c_i, σ_τ)-plane and the ($\gamma_{X=Y}$, σ_τ)-plane, respectively. The green area stands for the stable solution A_- under anomalous dispersion. The parameter values used are the same as in Figure 3.11.

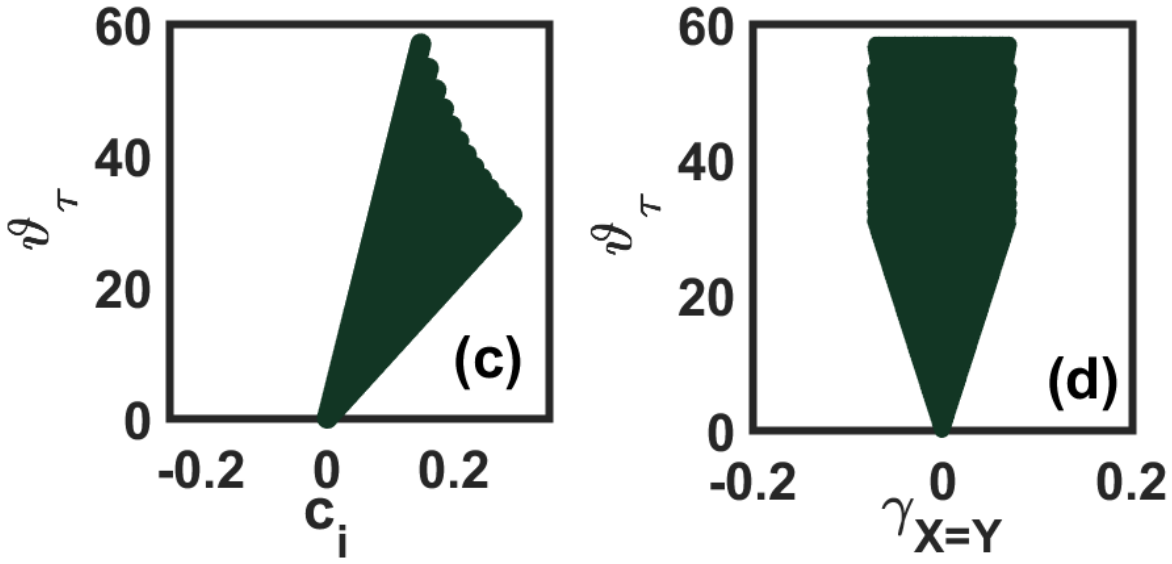

Figure 3.15: Diagrams of stability in the (c_i, ϑ_τ)-plane, from left to right, the (c_i, ϑ_τ)-plane and the ($\gamma_{_{X=Y}}$, ϑ_τ)-plane, respectively. The green area stands for the stable solution A_- under anomalous dispersion. The parameter values used are the same as in Figure 3.11.

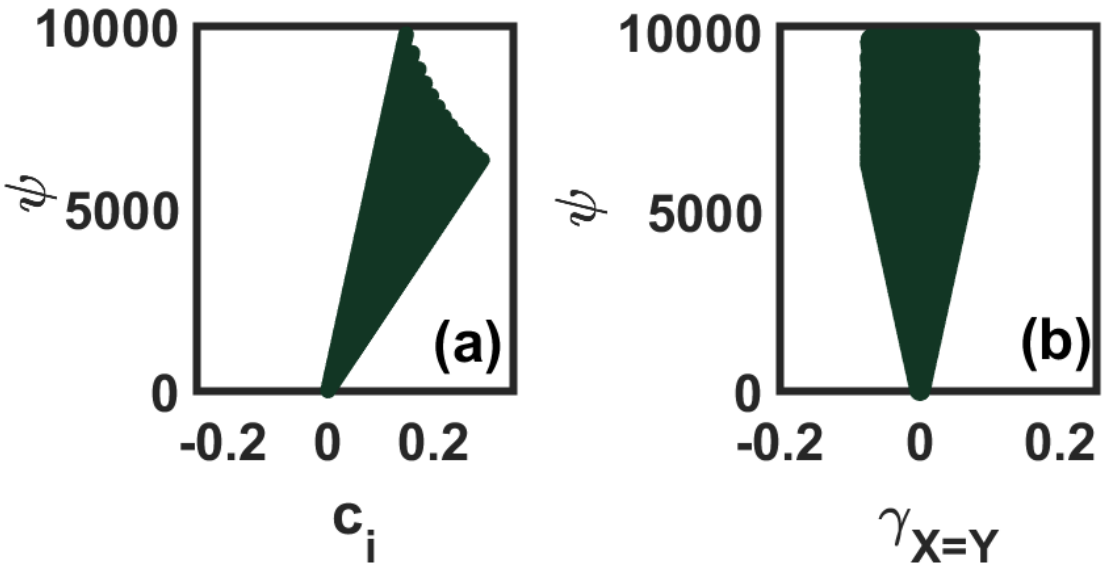

Figure 3.16: Diagrams of stability in the (c_i, $\gamma_{_{X=Y}}$)-plane, from left to right, the (c_i, ψ)-plane, the ($\gamma_{_{X=Y}}$, ψ)-plane, respectively. The green area stands for the stable solution A_- under anomalous dispersion. The parameter values used are the same as in Figure 3.11.

3.3.3 The third set of parameters for steady-state solutions in the CQ case.

In Figure (3.17), we represent the double solutions A_+ and A_- of the steady-state amplitudes versus c_i and $\gamma_{X=Y}$, where the dissipative parameter c_i represents the saturation nonlinear gain ($c_i > 0$) related to the quintic self-focusing Kerr nonlinearity ($c_r > 0$), and the parameter $\gamma_{X=Y}$ denotes the symmetric nonlocality degree along the transverse directions. By using the normalized coefficient $N_r = 2^{1/2}(4/3)^{3/4}$, assuming a linear gain ($\gamma_r<0$) under normal dispersion, the following parameter values have been used for illustration: $p_r = -5/N_r$, $p_i = 0.0201/N_r$, $q_r = -700/N_r$, $q_i = 26.8/N_r$, $\gamma_r = 1050/N_r$, $\gamma_i = -990/N_r$, $d_{3r} = 0.03/N_r$, $d_{3i} = -0.06/N_r$, $d_{4r} = -0.04/N_r$, $d_{4i} = 0.002/N_r$, $c_r = 0.00342/N_r$, $n_i = 0.025/N_r$, $m_r = -0.5/N_r$, $k_0 = 2\pi/1.55$.

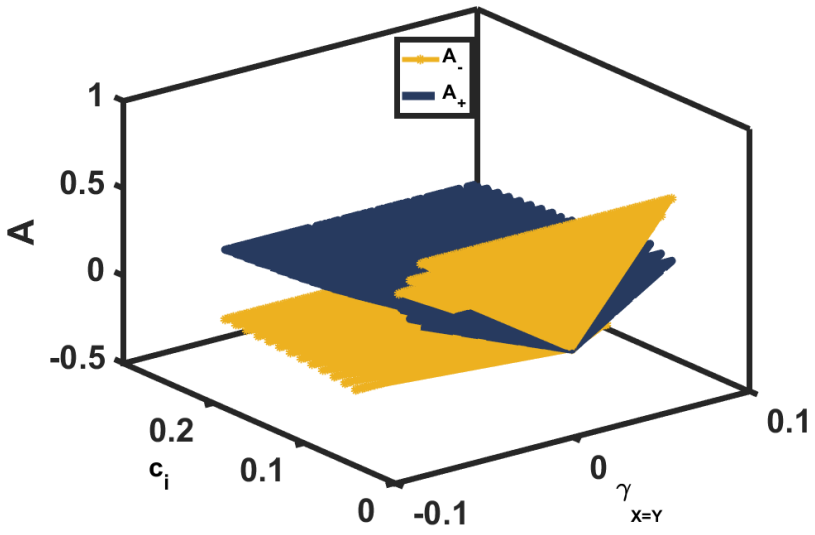

Figure 3.17: Double solutions A_+ and A_- of the steady-state amplitudes versus $(c_i, \gamma_{X=Y})$. The solution A_- (yellow sheet) is stable. The following parameter values have been used: $N_r = 2^{1/2}(4/3)^{3/4}$ (the normalized coefficient), $p_r = -5/N_r$ (normal dispersion), $p_i = 0.0201/N_r$, $q_r = -700/N_r$, $q_i = 26.8/N_r$, $\gamma_r = 1050/N_r$, $\gamma_i = -990/N_r$, $d_{3r} = 0.03/N_r$, $d_{3i} = -0.06/N_r$, $d_{4r} = -0.04/N_r$, $d_{4i} = 0.002/N_r$, $c_r = 0.00342/N_r$ (the quintic self-focusing Kerr nonlinearity), $n_i = 0.025/N_r$, $m_r = -0.5/N_r$, $k_0 = 2\pi/1.55$.

Figure 3.17 highlights that the representations amplitudes A_- and A_+ are distinctly separate, while both remain in the positive value zone. The nonlocal spatial response of the Kerr nonlinearity ($\gamma_{X=Y}$) and the saturation of the nonlinear gain ($c_i > 0$) increase and lead to an expansion of the stability zone A_- (yellow sheet) and the stability zone A_- (blue sheet). The nonlocality and the nonlinear gain are well-suited for the localization of optical LBs in this cubic-quintic regime. In

the following, the amplitude A_{-} is the stable solution used when plotting other LB characteristic parameters.

So doing, in Figure 3.18, the stability zones (green areas) are shown for the spatial width versus c_i and $\gamma_{_{X=Y}}$, respectively, while the same procedure is repeated for the temporal width σ_τ in Figure 3.20 for the stable solution A_{-} under normal dispersion. The set of spatial and temporal widths values derived from these diagrams will be chosen from this stability range for the numerical simulations of the input spatiotemporal pulses in the subsection (3.7.3). Zones of stability for the spatial and temporal chirps, $\vartheta_{X=Y}$ and ϑ_τ, respectively, versus c_i and $\gamma_{_{X=Y}}$, for the stable solution A_{-} and the normal dispersion are depicted in Figs. 3.19 and 3.21. The set of spatial and temporal chirps derived from these curves will be chosen from this stability range for the numerical simulations of the input spatiotemporal pulses in the subsection (3.7.3).

The stability zones for the phase ψ are depicted in Figure 3.22 versus c_i and $\gamma_{_{X=Y}}$, respectively, for the stable solution A_{-} under the normal dispersion. The set of phase values obtained from these diagrams will be chosen from this stability range for the numerical implementation of the input spatiotemporal pulses in the subsection (3.7.3).

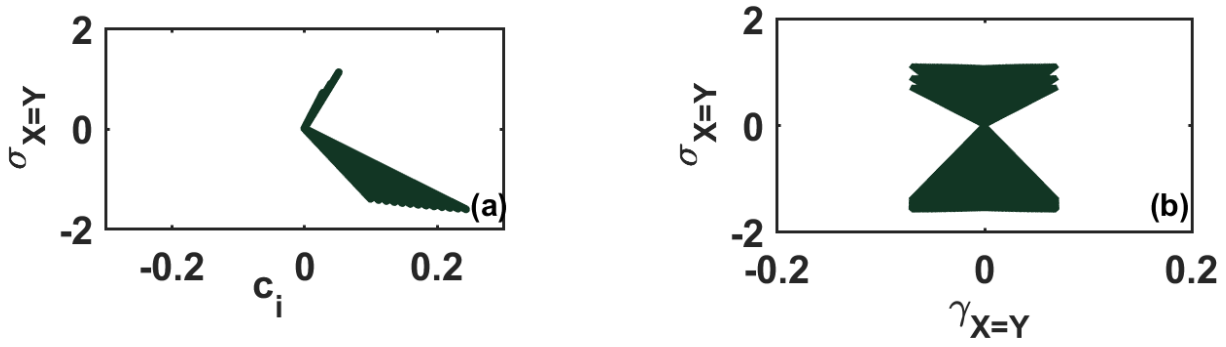

Figure 3.18: Diagrams of stability in the (c_i, $\sigma_{_{X=Y}}$), from left to right, the (c_i, $\sigma_{_{X=Y}}$)-plane and the ($\gamma_{_{X=Y}}$, $\sigma_{_{X=Y}}$)-plane,, respectively. The green area stands for the stable solution A_{-} under normal dispersion. The parameter values used are the same as in Figure 3.17.

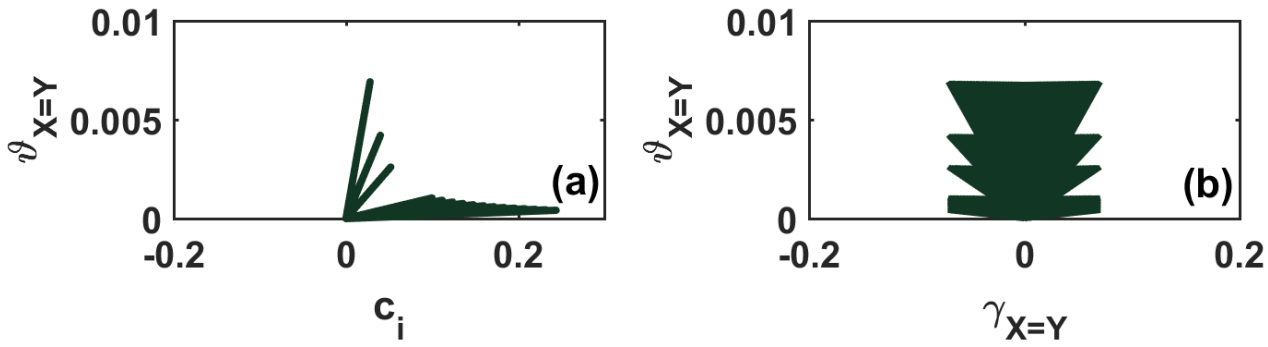

Figure 3.19: Diagrams of stability in the (c_i, $\vartheta_{_{X=Y}}$)-plane, from left to right, the (c_i, $\vartheta_{_{X=Y}}$)-plane and the ($\gamma_{_{X=Y}}$, $\vartheta_{_{X=Y}}$)-plane,, respectively. The green area stands for the stable solution A_{-} under normal dispersion. The parameter values used are the same as in Figure 3.17.

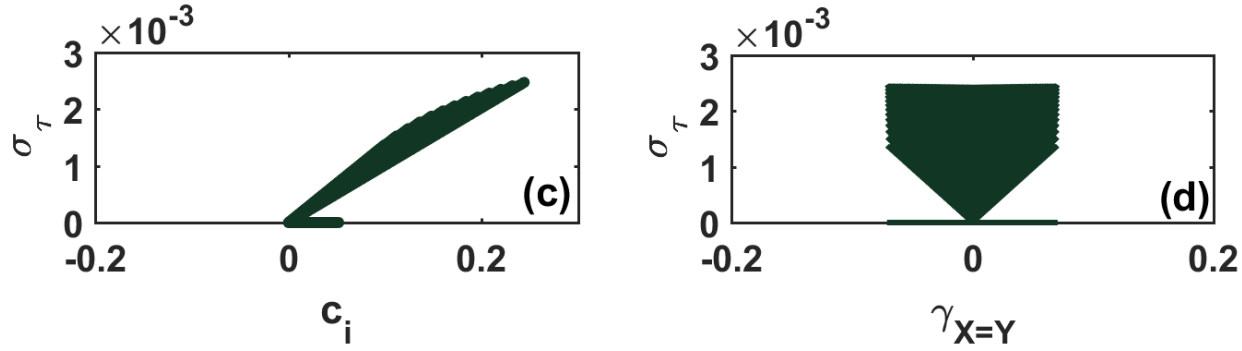

Figure 3.20: Diagrams of stability in the (c_i, σ_τ)-plane, from left to right, the (c_i, σ_τ)-plane and the ($\gamma_{_{X=Y}}$, σ_τ)-plane, respectively. The green area stands for the stable solution A_{-} under normal dispersion. The parameter values used are the same as in Figure 3.17.

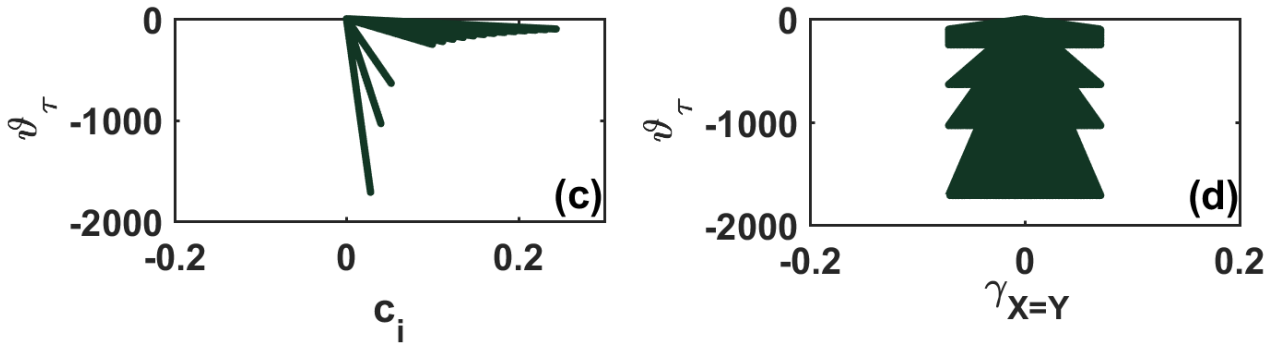

Figure 3.21: Diagrams of stability in the (c_i, ϑ_τ)-plane, from left to right, the (c_i, ϑ_τ)-plane and the ($\gamma_{_{X=Y}}$, ϑ_τ)-plane, respectively. The green area stands for the stable solution A_{-} under normal dispersion. The parameter values used are the same as in Figure 3.17.

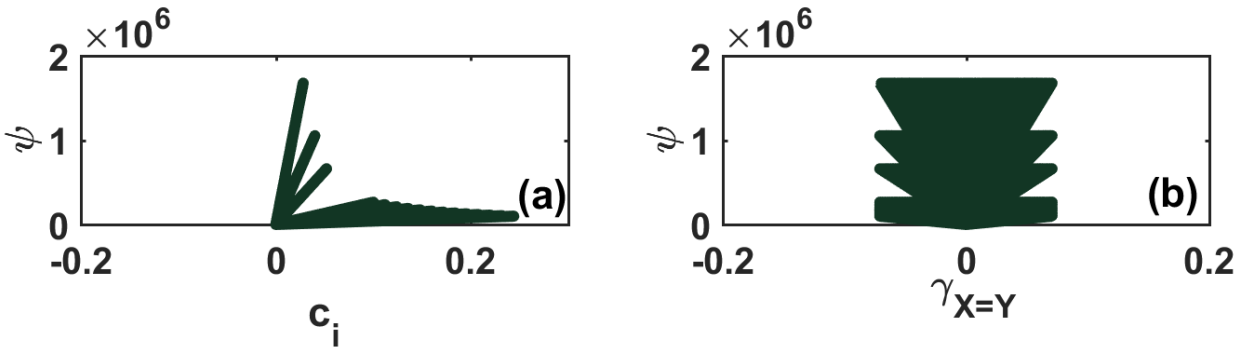

Figure 3.22: Diagrams of stability in the (c_i, $\gamma_{X=Y}$)-plane, from left to right, the (c_i, ψ)-plane and the ($\gamma_{X=Y}$, ψ)-plane, respectively. The green area stands for the stable solution A_- under normal dispersion. The parameter values used are the same as in Figure 3.17.

3.4 Numerical experiments for the nonlocal CCGLE

This section aims to confirm the analytical results obtained previously by carrying out numerical simulations based on the Runge-Kutta and the Split-Step Fourier Method.

3.4.1 Runge-Kutta Method

The Runge-Kutta method is a numerical integration technique highlighting higher accuracy and efficiency in approximating solutions at specified points. This method coordinates with the solution of Taylor's series up to the term in hr, where r varies from method to method and represents the order of that method.

Consider an ordinary differential equation of $dy/dx = f(x, y)$ with initial condition $y(x_0) = y_0$. For this, we can define the formulas for Runge-Kutta methods as follows.

(a) First Order Runge-Kutta method:

$$y_1 = y_0 + hf(x_0, y_0) = y_0 + hy_0^{'}, \text{ since y' = f(x, y).} \tag{3.8}$$

(b) Second Order Runge-Kutta method:

$$y_1 = y_0 + \frac{1}{2}(k_1 + k_2), \tag{3.9}$$

where

$$k_1 = hf(x_0, y_0) \tag{3.10}$$

$$k_2 = hf(x_0 + h, y_0 + k_1). \tag{3.11}$$

(c) Third Order Runge-Kutta method:

$$y_1 = y_0 + \frac{1}{6}(k_1 + 4k_2 + k_3), \tag{3.12}$$

where

$$k_1 = hf(x_0, y_0) \tag{3.13}$$

$$k_2 = hf\left(x_0 + \frac{1}{2}h, y_0 + \frac{1}{2}k_1\right) \tag{3.14}$$

$$k_3 = hf(x_0 + h, y_0 + k_1) \text{ such that } k_1 = hf(x_0 + h, y_0 + k_1). \tag{3.15}$$

(d) Fourth Runge-Kutta method:

$$y_1 = y_0 + \frac{1}{6}(k_1 + 2k_2 + 2k_3 + k_4), \tag{3.16}$$

where

$$k_1 = hf(x_0, y_0) \tag{3.17}$$

$$k_2 = hf\left(x_0 + \frac{1}{6}h, y_0 + \frac{1}{2}k_1\right) \tag{3.18}$$

$$k_3 = hf\left(x_0 + \frac{1}{2}h, y_0 + \frac{1}{2}k_2\right) \tag{3.19}$$

$$k_4 = hf(x_0 + h, y_0 + k_3). \tag{3.20}$$

(e) Fourth Runge-Kutta method (RK4) applied to our model

We consider the system of eight coupled FODEs, Eqs. (2.77-2.84). We set them as follows,

$$\frac{d\sigma_\tau}{dZ} = F_1(\sigma_\tau, \sigma_X, \sigma_Y, \vartheta_\tau, \vartheta_X, \vartheta_Y, \psi,), \tag{3.21}$$
$$\frac{d\sigma_X}{dZ} = F_2(\sigma_\tau, \sigma_X, \sigma_Y, \vartheta_\tau, \vartheta_X, \vartheta_Y, \psi,), \tag{3.22}$$
$$\frac{d\sigma_Y}{dZ} = F_3(\sigma_\tau, \sigma_X, \sigma_Y, \vartheta_\tau, \vartheta_X, \vartheta_Y, \psi,), \tag{3.23}$$
$$\frac{d\vartheta_\tau}{dZ} = F_4(\sigma_\tau, \sigma_X, \sigma_Y, \vartheta_\tau, \vartheta_X, \vartheta_Y, \psi,), \tag{3.24}$$
$$\frac{d\vartheta_X}{dZ} = F_5(\sigma_\tau, \sigma_X, \sigma_Y, \vartheta_\tau, \vartheta_X, \vartheta_Y, \psi,), \tag{3.25}$$
$$\frac{d\vartheta_Y}{dZ} = F_6(\sigma_\tau, \sigma_X, \sigma_Y, \vartheta_\tau, \vartheta_X, \vartheta_Y, \psi,), \tag{3.26}$$
$$\frac{d\psi}{dZ} = F_7(\sigma_\tau, \sigma_X, \sigma_Y, \vartheta_\tau, \vartheta_X, \vartheta_Y, \psi,), \tag{3.27}$$
$$\frac{dA}{dZ} = F_8(\sigma_\tau, \sigma_X, \sigma_Y, \vartheta_\tau, \vartheta_X, \vartheta_Y, \psi,), \tag{3.28}$$

with

$$\begin{aligned} F_1 = {} & 2\zeta_2\vartheta_\tau\sigma_\tau + b_1\zeta_3\sigma_\tau \\ & + \frac{15}{8}A^2\sqrt{2}c_0\zeta_4\sigma_\tau + \frac{1}{4}a_1\zeta_2\left(-5k_0^2\vartheta_\tau^2\sigma_\tau^2 - \frac{36}{\sigma_\tau^2}\right)\sigma_\tau \\ & + \frac{15}{64}A^2\sqrt{2}c_{_{1,XX}}\zeta_5\left(-k_0^2\vartheta_{_X}^2\sigma_{_X}^2 - \frac{12}{\sigma_{_X}^2}\right)\sigma_\tau \\ & + \frac{15}{64}A^2\sqrt{2}c_{_{2,YY}}\zeta_6\left(-k_0^2\vartheta_{_Y}^2\sigma_{_Y}^2 - \frac{12}{\sigma_{_Y}^2}\right)\sigma_\tau, \end{aligned} \tag{3.29}$$

$$\begin{aligned} F_2 = {} & 2\zeta_1 k_0\vartheta_{_X}\sigma_{_X} + b_1\zeta_3\sigma_{_X} \\ & + \frac{15}{8}A^2\sqrt{2}c_0\zeta_4\sigma_{_X} + \frac{1}{4}a_1\zeta_2\left(-7k_0^2\vartheta_\tau^2\sigma_\tau^2 - \frac{28}{\sigma_\tau^2}\right)\sigma_{_X} \\ & + \frac{1}{64}A^2\sqrt{2}c_{_{1,XX}}\zeta_5\left(13k_0^2\vartheta_{_X}^2\sigma_{_X}^2 - \frac{252}{\sigma_{_X}^2}\right)\sigma_{_X} \\ & + \frac{15}{64}A^2\sqrt{2}c_{_{2,YY}}\zeta_6\left(-k_0^2\vartheta_{_Y}^2\sigma_{_Y}^2 - \frac{12}{\sigma_{_Y}^2}\right)\sigma_{_X}, \end{aligned} \tag{3.30}$$

$$F_3 = 2\zeta_1 k_0 \vartheta_{_Y} \sigma_{_Y} + b_1 \zeta_3 \sigma_{_Y} + \frac{15}{8} A^2 \sqrt{2} c_0 \zeta_4 \sigma_{_Y} + \frac{1}{4} a_1 \zeta_2 \left(-7 k_0^2 \vartheta_\tau^2 \sigma_\tau^2 - \frac{28}{\sigma_\tau^2} \right) \sigma_{_Y} + \frac{15}{64} A^2 \sqrt{2} c_{_{1,XX}} \zeta_5 \left(-k_0^2 \vartheta_{_X}^2 \sigma_{_X}^2 - \frac{12}{\sigma_{_X}^2} \right) \sigma_{_Y} + \frac{1}{64} A^2 \sqrt{2} c_{_{2,YY}} \zeta_6 \left(13 k_0^2 \vartheta_{_Y}^2 \sigma_{_Y}^2 - \frac{252}{\sigma_{_Y}^2} \right) \sigma_{_Y}, \quad (3.31)$$

$$F_4 = A^2 \sqrt{2} \zeta_4 \frac{1}{k_0 \sigma_\tau^2} + 8 a_1 \zeta_2 \frac{\vartheta_\tau}{\sigma_\tau^2} - 8 \zeta_2 \frac{1}{k_0 \sigma_\tau^4} - 2 \zeta_2 k_0 \vartheta_\tau^2 + \frac{1}{36} \frac{A^2 \sqrt{2} c_{_{1,XX}} \zeta_5}{k_0 \sigma_\tau^2} \left(\frac{72}{\sigma_{_X}^2} + 73 k_0 \vartheta_{_X} \right) + \frac{1}{36} \frac{A^2 \sqrt{2} c_{_{2,YY}} \zeta_6}{k_0 \sigma_\tau^2} \left(\frac{72}{\sigma_{_Y}^2} + 73 k_0 \vartheta_{_Y} \right), \quad (3.32)$$

$$F_5 = A^2 \sqrt{2} \zeta_4 \frac{1}{k_0 \sigma_{_X}^2} + 8 \zeta_1 \frac{1}{\sigma_{_X}^4} - 2 \zeta_1 k_0 \vartheta_{_X}^2 + \frac{1}{36} \frac{A^2 \sqrt{2} c_{_{1,XX}} \zeta_5}{k_0 \sigma_{_X}^2} \left(\frac{216}{\sigma_{_X}^2} + 127 k_0 \vartheta_{_X} \right) + \frac{1}{36} \frac{A^2 \sqrt{2} c_{_{2,YY}} \zeta_6}{k_0 \sigma_{_X}^2} \left(\frac{72}{\sigma_{_Y}^2} + 73 k_0 \vartheta_{_Y} \right), \quad (3.33)$$

$$F_6 = A^2 \sqrt{2} \zeta_4 \frac{1}{k_0 \sigma_{_Y}^2} + 8 \zeta_1 \frac{1}{\sigma_{_Y}^4} - 2 \zeta_1 k_0 \vartheta_{_Y}^2 + \frac{1}{36} \frac{A^2 \sqrt{2} c_{_{1,XX}} \zeta_5}{k_0 \sigma_{_Y}^2} \left(\frac{72}{\sigma_{_X}^2} + 73 k_0 \vartheta_{_X} \right) + \frac{1}{36} \frac{A^2 \sqrt{2} c_{_{2,YY}} \zeta_6}{k_0 \sigma_{_Y}^2} \left(\frac{216}{\sigma_{_Y}^2} + 127 k_0 \vartheta_{_Y} \right), \quad (3.34)$$

$$F_7 = -2\frac{\zeta_1}{\sigma_X^2} - 2\frac{\zeta_1}{\sigma_Y^2} - 2\frac{\zeta_2}{\sigma_\tau^2} - \frac{7}{8}A^2\sqrt{2}\zeta_4 - \zeta_3 - a_1\zeta_2 k_0\vartheta_\tau + \frac{1}{288}A^2\sqrt{2}c_{_{1,XX}}\zeta_5\left(-\frac{648}{\sigma_X^2} - 401k_0\vartheta_{_X}\right) + \frac{1}{288}A^2\sqrt{2}c_{_{2,YY}}\zeta_6\left(-\frac{648}{\sigma_Y^2} - 401k_0\vartheta_{_Y}\right). \quad (3.35)$$

$$F_8 = -A\zeta_1 k_0\vartheta_{_X} - A\zeta_1 k_0\vartheta_{_Y} - A\zeta_2\vartheta_\tau - \frac{7}{2}Ab_1\zeta_3 - \frac{77}{16}A^3\sqrt{2}c_0\zeta_4 + \frac{1}{8}Aa_1\zeta_2\left(35k_0^2\vartheta_\tau^2\sigma_\tau^2 + \frac{156}{\sigma^2}\right) + \frac{1}{128}A^3\sqrt{2}c_{_{1,XX}}\zeta_5\left(75k_0^2\vartheta_{_X}^2\sigma_{_X}^2 + \frac{996}{\sigma_{_X}^2}\right) + \frac{1}{128}A^3\sqrt{2}c_{_{2,YY}}\zeta_6\left(75k_0^2\vartheta_{_Y}^2\sigma_{_Y}^2 + \frac{996}{\sigma_{_Y}^2}\right). \quad (3.36)$$

We calculate the first iteration.

- **First itteration**

$$d\sigma_{\tau 1} = hF_1(\sigma_\tau(j), \sigma_{_X}(j), \sigma_{_Y}(j), \vartheta_\tau(j), \vartheta_{_X}(j), \vartheta_{_Y}(j), A(j));$$
$$d\sigma_{_X 1} = hF2(\sigma_\tau(j), \sigma_{_X}(j), \sigma_{_Y}(j), \vartheta_\tau(j), \vartheta_{_X}(j), \vartheta_{_Y}(j), A(j));$$
$$d\sigma_{_Y 1} = hF3(\sigma_\tau(j), \sigma_{_X}(j), \sigma_{_Y}(j), \vartheta_\tau(j), \vartheta_{_X}(j), \vartheta_{_Y}(j), A(j));$$
$$d\vartheta_{\tau 1} = hF4(\sigma_\tau(j), \sigma_{_X}(j), \sigma_{_Y}(j), \vartheta_\tau(j), \vartheta_{_X}(j), \vartheta_{_Y}(j), A(j));$$
$$d\vartheta_{_{X1}} = hF5(\sigma_{_X}(j), \sigma_{_Y}(j), \vartheta_{_X}(j), \vartheta_{_Y}(j), A(j));$$
$$d\vartheta_{_Y 1} = hF6(\sigma_{_X}(j), \sigma_{_Y}(j), \vartheta_{_X}(j), \vartheta_{_Y}(j), A(j));$$
$$d\psi_1 = hF7(\sigma_\tau(j), \sigma_{_X}(j), \sigma_{_Y}(j), \vartheta_\tau(j), \vartheta_{_X}(j), \vartheta_{_Y}(j), A(j));$$
$$dA_1 = hF8(\sigma_\tau(j), \sigma_{_X}(j), \sigma_{_Y}(j), \vartheta_\tau(j), \vartheta_{_X}(j), \vartheta_{_Y}(j), A(j)); \quad (3.37)$$

The second, third and fourth iterations are also calculated.

3.4.2 Split-Step Fourier Method

The Split-Step Fourier Method (SSFM) consists of splitting the equation into two parts, the nonlinear and the linear part.

We consider Eq. (2.61) in the cubic context. Applying the SSFM to Eq.(2.61) implies writing it in the form

$$\frac{\partial \Phi}{\partial Z} = \underbrace{\left[-i\zeta_1\left(\frac{\partial^2}{\partial X^2}+\frac{\partial^2}{\partial Y^2}\right) - i\left(1+ia_1\right)\zeta_2\frac{\partial^2}{\partial \tau^2} - i\left(1+ib_1\right)\zeta_3\right]}_{\mathcal{D}}\Phi$$
$$+ i\underbrace{\left[-\left(1+ic_0\right)\zeta_4|\Phi|^2 - \left(1+ic_{_{1,XX}}\right)\zeta_5\frac{\partial^2}{\partial X^2}(|\Phi|^2) - \left(1+ic_{_{2,YY}}\right)\zeta_6\frac{\partial^2}{\partial Y^2}(|\Phi|^2)\right]}_{\mathcal{N}}\Phi, \quad (3.38)$$

where $\mathcal{D}(\Phi)$ is the operator of all linear terms in Φ and with $\mathcal{N}(\Phi)$ the operator of all nonlinearities terms in Φ. Using these definitions, we write Eq. (3.38) in short as

$$\frac{\partial \Phi}{\partial Z} = \left(\mathcal{D}+\mathcal{N}\right)\Phi. \quad (3.39)$$

The SSMF approximates a solution by assuming that linear and nonlinear effects act independently when propagating the optical field over a small distance h. More specifically, propagation from Z to $Z+h$ is carried out in two steps. In the first step, the nonlinearity acts alone, and $\mathcal{D}=0$. In the second step, linearity acts alone, and $\mathcal{N}=0$, in Eq. (3.39).

$\mathcal{D}=0$, then Eq. (3.39) reduces to

$$\frac{\partial \Phi}{\partial Z} = \left(\mathcal{N}\right)\Phi. \quad (3.40)$$

The integration of Eq. (3.40) gives

$$\Phi(Z+h,\tau) = \exp(h\mathcal{N})\Phi(Z,\tau). \quad (3.41)$$

$\mathcal{N}=0$, then Eq. (3.39) reduces to

$$\frac{\partial \Phi}{\partial Z} = \left(\mathcal{D}\right)\Phi. \quad (3.42)$$

The integration of Eq. (3.42) gives

$$\Phi(Z+h,\tau) = \exp(\frac{h}{2}\mathcal{D}))\exp(\frac{h}{2}\mathcal{D})\Phi(Z,\tau). \quad (3.43)$$

The exponential $\exp(\frac{h}{2}\mathcal{D})$ can be evaluated in the Fourier domain using the prescription:

$$\exp(\frac{h}{2}\mathcal{D})\Phi(Z,\tau) = \mathcal{F}^{-1}\left\{\left[-i\zeta_1\left(\frac{\partial^2}{\partial X^2}+\frac{\partial^2}{\partial Y^2}\right) - i\left(1+ia_1\right)\zeta_2\frac{\partial^2}{\partial \tau^2} - i\left(1+ib_1\right)\zeta_3\right]\right\}\mathcal{F}\Phi(Z,\tau), \tag{3.44}$$

where $\mathcal{F}$ and $\mathcal{F}^{-1}$ denote Fourier and inverse Fourier transformation, respectively.

3.4.3 Numerical simulations

Numerical studies of the evolution of the dissipative LBs along a doped and weakly nonlocal optical fiber are performed using the RK4 computational method and the SSFM. We examine the accuracy of numerical experiments by testing different time and space steps. The variables X, Y and Z are in the units of time (for Z) and space (for X, Y). The mesh sizes are chosen equal to ΔX=ΔY=0.002 and $\Delta\tau$=0.003.

Then, we solve the original (3+1)-D nonlocal CCGLE given in Eq. (2.69) via the SSFM with the longitudinal step size ΔZ=0.063×10^{-6}, over a total distance $Z = 200$. The following typical optical pulse parameters used in fiber-optic communication systems are adopted [18, 28], the wavelength $\lambda = 1.55\ \mu m$, the linear refractive index $n_0 = 1.45\ cm^2/W$, the nonlinear refractive index $n_2 = 2.7 \times 10^{-13}\ cm^2/W$, the group velocity dispersion $\beta_2 = 50\ ps^2/km$, the nonlinear gain $g_p = 6.8\ W^{-1}km^{-1}$, the pulse width $1.763T_0 = 400fs$, the peak power of the incident pulse $P_0 = 9.43\ MW$.

To start, the analytically generated variational bifurcation branches for A_- and A_+ are compared to numerically obtained branches in Figure 3.23. Precision should, however, be made that values of parameters used to generate the numerical branches have been chosen from the stable zones of Figs. (3.1)-(3.4), as indicated earlier. The obtained analytical features corresponding to the steady-state solutions of the amplitudes A_- and A_+ as functions of the spatial nonlocality parameter $\gamma_{_{X=Y}}$, respectively, are a good approximation of the numerically obtained curves. Along the same line, the analytical and numerical solutions of the steady-state A_- highlight the upper stable branches. On the contrary, the curves describing the analytical and numerical solutions of the steady-state A_+ are on the lower unstable branches. For the stable evolution of the self-organized dissipative LBs represented in numerical simulations, we choose the stable solution A_- as an input spatiotemporal pulse.

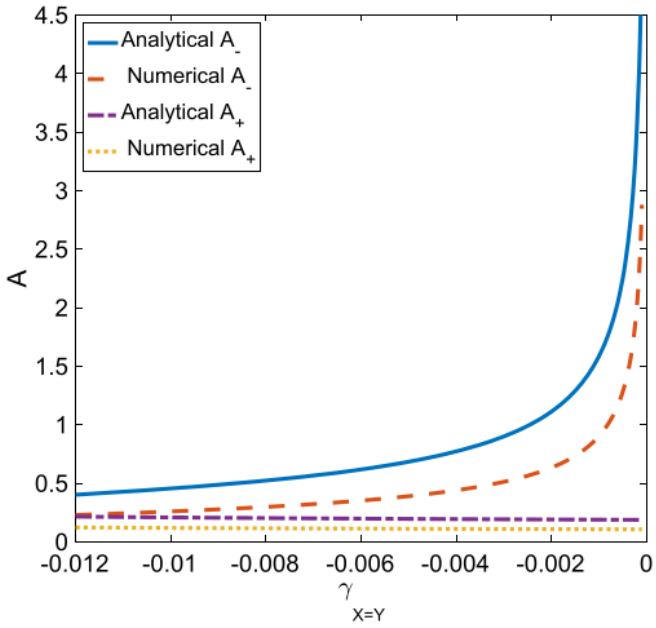

Figure 3.23: Analytical and numerical bifurcation curves of the steady-state solutions A_+ and A_- for anomalous dispersion, respectively, $p_r = 0.579/N_r$ and for the following parameter values: $N_r = 2^{1/2}(4/3)^{3/4}$, $p_i = 0.201/N_r$, $q_r = -110/N_r$, $q_i = -14.7/N_r$, $\gamma_r = 150/N_r$, $\gamma_i = -530/N_r$, and $k_0 = 2\pi/1.55$.

Figure 3.24 shows clearly that the light pulse remains practically constant during its evolution in the spatial domain. We can then notice that the anomalous dispersion, the linear diffraction, the linear gain and the nonlinear diffraction, the spatial nonlocal self-defocusing Kerr nonlinearity response, and the nonlinear loss are well balanced.

In Figure 3.25, the temporal input and output are identical, showing that no loss has been observed. In the same way, we can notice that the anomalous dispersion, the linear diffraction, the linear gain and the nonlinear diffraction, the spatial nonlocal self-defocusing Kerr nonlinearity response, and the nonlinear loss are also well balanced. From the dynamical behaviors depicted in Figure 3.26, we show the evolution of the temporal field profile of the dissipative LB intensity distribution in the propagation regime of anomalous dispersion, where the input and output pulses are similar, further confirming our stability predictions, under well-balanced competition from the various involved effects in addition to nonlocality.

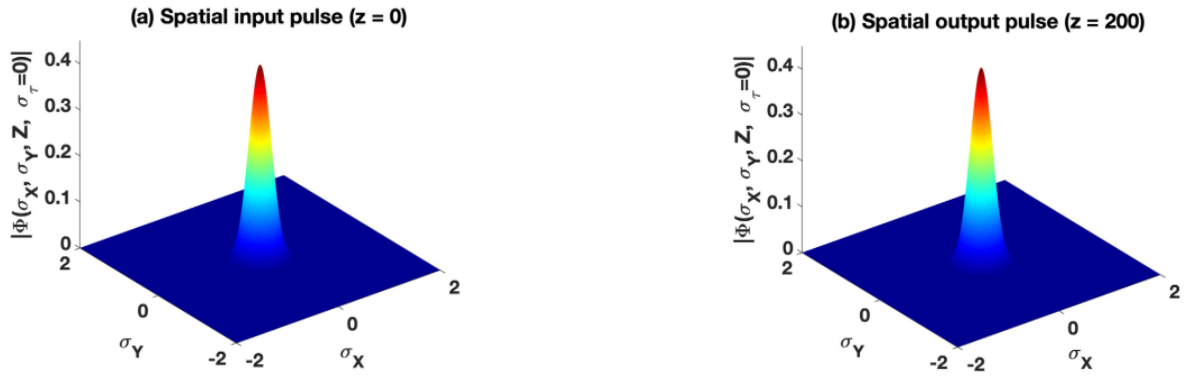

Figure 3.24: Profiles of the spatial input [panel (a)] and output pulse [panel (b)] for the stable steady-state solution A_- under anomalous dispersion. The following parameters have been used: $\gamma_{X=Y} = -0.007$, $\sigma_{X0} = \sigma_{Y0} = 0.2439$, $\vartheta_{X0} = \vartheta_{Y0} = 56.03$, $A_0 = 0.4225$, $p_r = 0.579/N_r$, $q_i = -14.7/N_r$, $p_i = 0.201/N_r$, $q_r = -110/N_r$, $q_i = -14.7/N_r$, $\gamma_r = 150/N_r$, $\gamma_i = -530/N_r$, $k_0 = 2\pi/1.55$, and $N_r = 2^{1/2}(4/3)^{3/4}$.

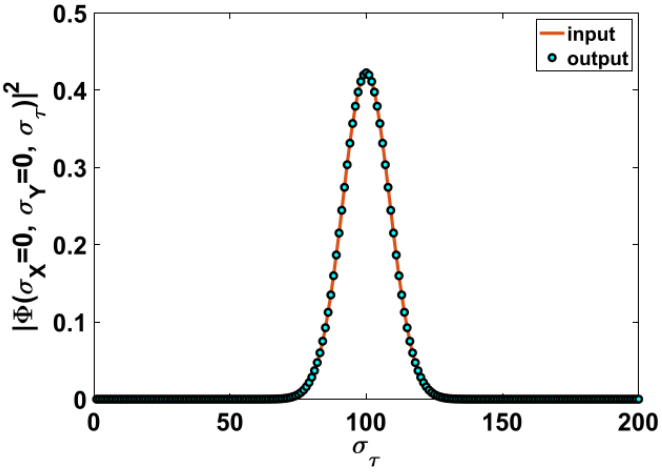

Figure 3.25: Profiles of the temporal input and output pulse for the stable steady-state solution A_- and for anomalous dispersion. The following parameters have been used: $\gamma_{X=Y} = -0.007$, $\sigma_{\tau 0} = 0.01217$, $\vartheta_{\tau 0} = 572.8$,$A_0 = 0.4225$, $p_r = 0.579/N_r$, $q_i = -14.7/N_r$, $p_i = 0.201/N_r$, $q_r = -110/N_r$, $q_i = -14.7/N_r$, $\gamma_r = 150/N_r$, $\gamma_i = -530/N_r$, $k_0 = 2\pi/1.55$, and $N_r = 2^{1/2}(4/3)^{3/4}$.

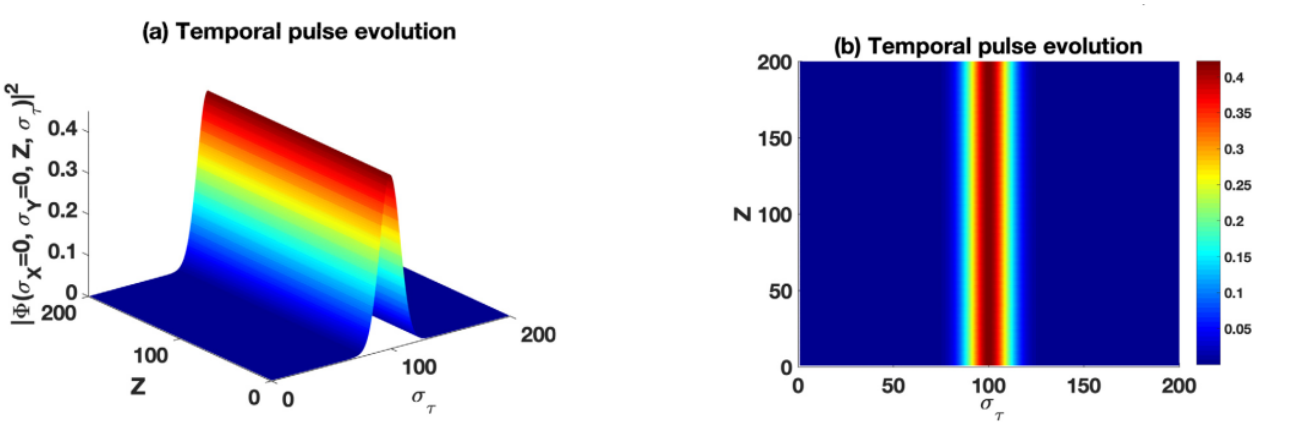

Figure 3.26: Profile of the temporal pulse evolution [panel (a)] and its corresponding density plot [panel(b)] for the stable steady-state solution under anomalous dispersion. Keeping the rest of parameters as in Figure 3.6, the following parameters have been used: $\gamma_{_{X=Y}} = -0.007$, $\sigma_{\tau 0} = 0.01217$, $\vartheta_{\tau 0} = 572.8$, $A_{0\_} = 0.4225$, $p_r = 0.579/N_r$, $q_i = -14.7/N_r$, $p_i = 0.201/N_r$, $q_r = -110/N_r$, $q_i = -14.7/N_r$, $\gamma_r = 150/N_r$, $\gamma_i = -530/N_r$, $k_0 = 2\pi/1.55$, and $N_r = 2^{1/2}(4/3)^{3/4}$.

For consistency, we consider the unstable region of Figure 3.27(a) and attribute the value $\sigma_{\tau 0} = 0.221$ to the initial temporal parameter. We then obtain the pulse evolution and its density representation in Figure 3.27(b). Under such a particular but noticeable change of temporal parameter, one observes a propagation of the initial pulse that collapses after a short propagation distance. Clearly, the obtained results confirm our predictions since the value of the temporal parameter chosen from the unstable region produces a pulse whose evolution differs from what unstable, and collapse have been of great concern since understanding such a phenomenon is crucial for applications in optical communication, where solitons are used to transmit information over long distances without distortion.

In our study, such a process involves the proposed nonlocal CGL equation that can be exploited under some conditions, taking advantage of suitable parameter values. In that direction, it is widely known that pulses in optical fibers with phase-sensitive amplifiers are stable over a wide range of parameter values, ensuring effective propagation of information in soliton-based optical communication systems, especially when higher-order effects are considered [54].

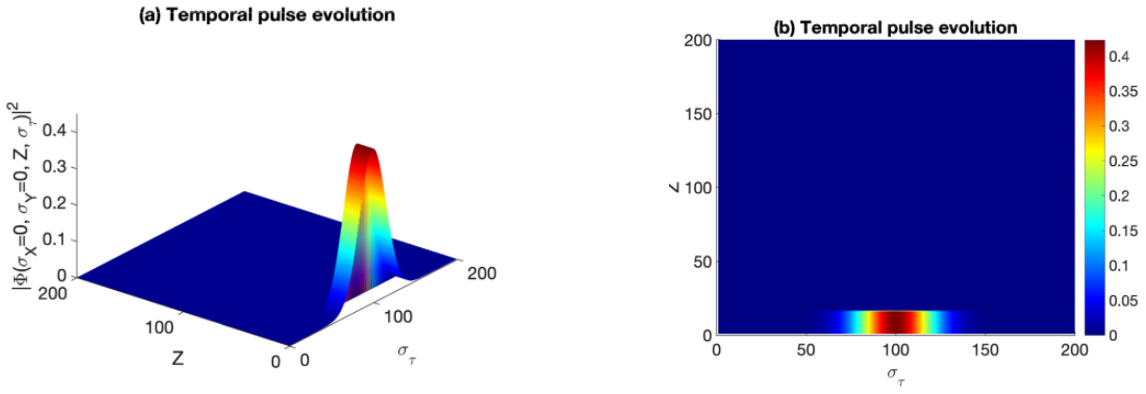

Figure 3.27: Profile of the unstable temporal pulse evolution [panel (a)] and its corresponding density plot [panel(b)] for the unstable steady-state solution under anomalous dispersion. We have used the same parameter values as in Figure 3.8, except for spatial and temporal widths: $\sigma_{X_0} = \sigma_{Y_0} = 0.20$ and $\sigma_{\tau 0} = 0.221$, respectively.

3.5 Numerical experiments for the nonlocal CQCGLE

Numerical studies of the evolution of the dissipative LBs along a doped and weakly nonlocal optical fiber are performed using the fourth-order Runge-Kutta computational method and the split-step Fourier method. We examine the accuracy of numerical experiments by testing different time and space steps. The variables X, Y and Z are in the units of time (for Z) and space (for X, Y). The mesh sizes are chosen equal to ΔX=ΔY=0.002 and $\Delta\tau$=0.003.

Then, we solve the original (3+1)-D nonlocal CCGLE given in Eq. (2.69) via the split-step Fourier method with the longitudinal step size ΔZ=0.063×10^{-6}, over a total distance $Z = 200$. The following typical optical pulse parameters used in fiber-optic communication systems are adopted [18, 28], the wavelength $\lambda = 1.55\ \mu m$, the linear refractive index $n_0 = 1.45\ cm^2/W$, the cubic and quintic nonlinear refractive indices $n_2 = 2.7 \times 10^{-13}\ cm^2/W$ and $n_4 = -7.8 \times 10^{-23}$, the group velocity dispersion $\beta_2 = 50\ ps^2/km$, the nonlinear gain $g_p = 6.8\ W^{-1}km^{-1}$, the pulse width $1.763T_0 = 400fs$, the peak power of the incident pulse $P_0 = 9.43\ MW$.

We chose three different sets of cubic-quintic parameters within the stability zones in order to demonstrate that our results are not tied to a single isolated point. By selecting multiple representative values inside the stable domain, we ensure that the observed behaviors are generic and robust within the CQ context, and not an artifact of one particular parameter choice. The three parameter sets do not give identical results, but they reveal different behaviors inside the CQ

stability zones. That is actually a strength, because we can state that:

• The CQ context allows multiple stable dynamics.

• Different parameter choices emphasize different balances between the nonlinear terms and dissipative effects.

• The differences observed (temporal gap, agreement, pulse narrowing) show how sensitive the propagation can be within stability.

3.5.1 Numerical simulations for the first set of CQ parameters

The analytically generated variational bifurcation branches for A_- and A_+ are compared with the numerically obtained branches in Figure 3.28. It should be noted, however, that the values of the parameters used to generate the numerical branches were chosen from the stable regions of Figs. (3.5)-(3.10), as indicated earlier.

The analytical features obtained, corresponding to the steady-state solutions of the amplitudes A_- and A_+ as functions of the spatial nonlocality parameter $\gamma_{X=Y}$, respectively, are a good approximation to the numerically obtained curves. Similarly, the analytical and numerical solutions of the steady states A_- and A_+ highlight the upper stable branches.

For the stable evolution of the self-organized dissipative LBs represented in the numerical simulations, we have chosen the stable solution A_+ as the input spatiotemporal pulse. From left to right, we can see that we obtained unstable curves for negative nonlocality and stable curves for positive nonlocality, which is different from the result obtained for the cubic case.

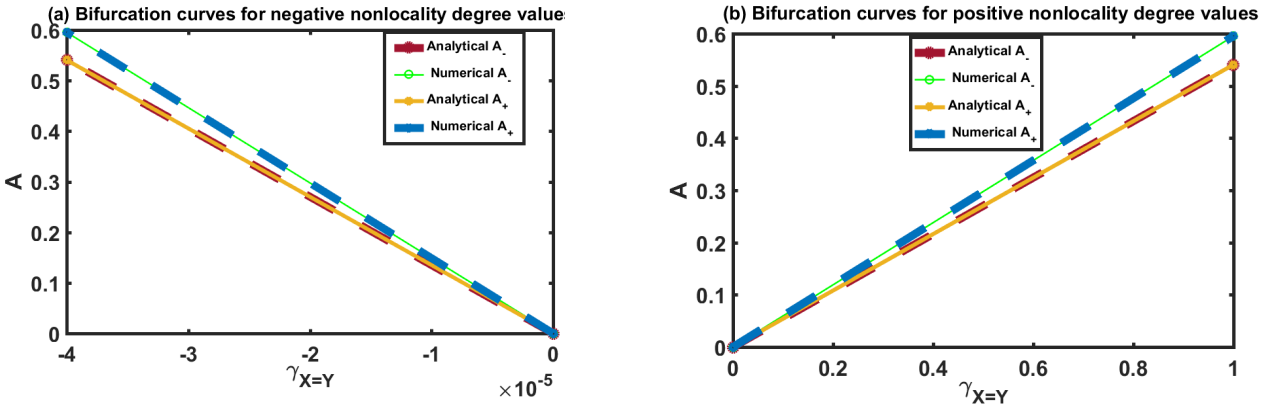

Figure 3.28: Analytical and numerical bifurcation curves of the steady-state solutions A_+ and A_- for normal dispersion, respectively, $p_r = -150.579/N_r$ and for the following parameter values have been used: $N_r = 2^{1/2}(4/3)^{3/4}$, $p_i = 0.000201/N_r$, $q_r = -60.8/N_r$, $q_i = 6/N_r$, $\gamma_r = -150/N_r$, $\gamma_i = 330/N_r$, $d_{3r} = 0.0006/N_r$, $d_{3i} = -0.08/N_r$, $d_{4r} = 0.002/N_r$, $c_i = -0.64/N_r$ the saturation of the nonlinear absorption(negative ci), $c_r = 0.00342/N_r$ (the quintic self-focusing Kerr nonlinearity), $n_i = 0.025/N_r$, $m_r = -0.5/N_r$, $k_0 = 2\pi/1.55$.

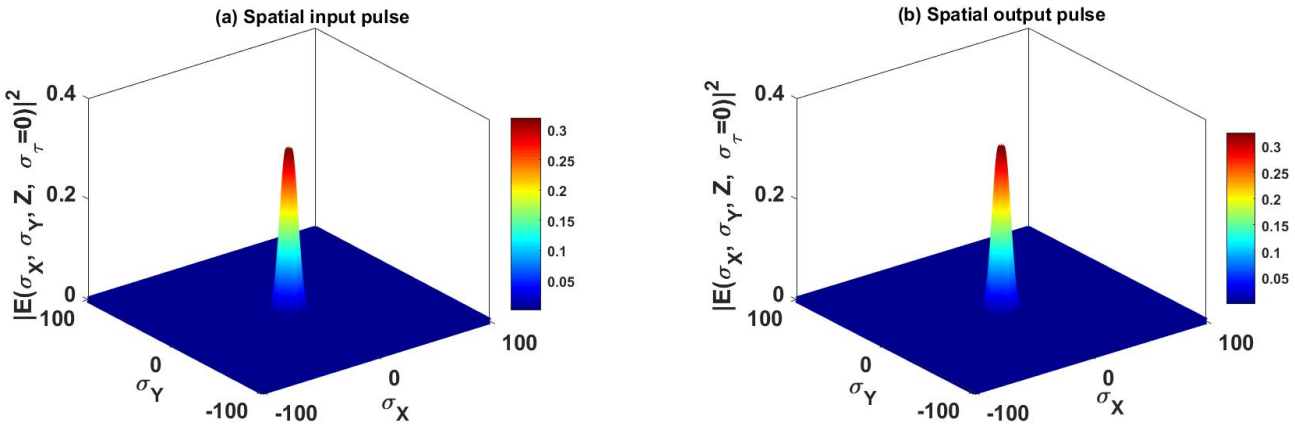

Figure 3.29: Profiles of the spatial input and output pulse, from left to right, for the stable steady-state solution A_+ under normal dispersion. The following parameters have been used: $\gamma_{X=Y} = 0.8$, $\sigma_{X0} = \sigma_{Y0} = 6.071$, $\vartheta_{X0} = \vartheta_{Y0} =$ -0.1258, $A_0 = 0.3201$, $p_r = -150.579/N_r$, $p_i = 0.000201/N_r$, $q_r = -60.8/N_r$, $q_i = 6/N_r$, $\gamma_r = -150/N_r$, $\gamma_i = 330/N_r$, $d_{3r} = 0.0006/N_r$, $d_{3i} = -0.08/N_r$, $d_{4r} = 0.002/N_r$, $d_{4i} = -0.04/N_r$, $c_r = 0.00342/N_r$, $n_i = 0.025/N_r$, $m_r = -0.5/N_r$, $k_0 = 2\pi/1.55$, $k_0 = 2\pi/1.55$, and $N_r = 2^{1/2}(4/3)^{3/4}$.

Figure 3.29 clearly demonstrates that the light pulse remains nearly constant throughout its propagation in the spatial domain. This indicates a well-balanced interplay among normal dispersion, linear diffraction, linear gain, nonlinear diffraction, the spatially nonlocal CQ self-focusing Kerr nonlinearity, and nonlinear loss.

Figure 3.30 presents the evolution of all characteristic parameters of the LB along the propagation axis OZ. Notably, all parameters exhibit similar dynamic behavior except for the temporal chirp, which may account for the observed discrepancy between the temporal input and output profiles shown inFigure 3.31.

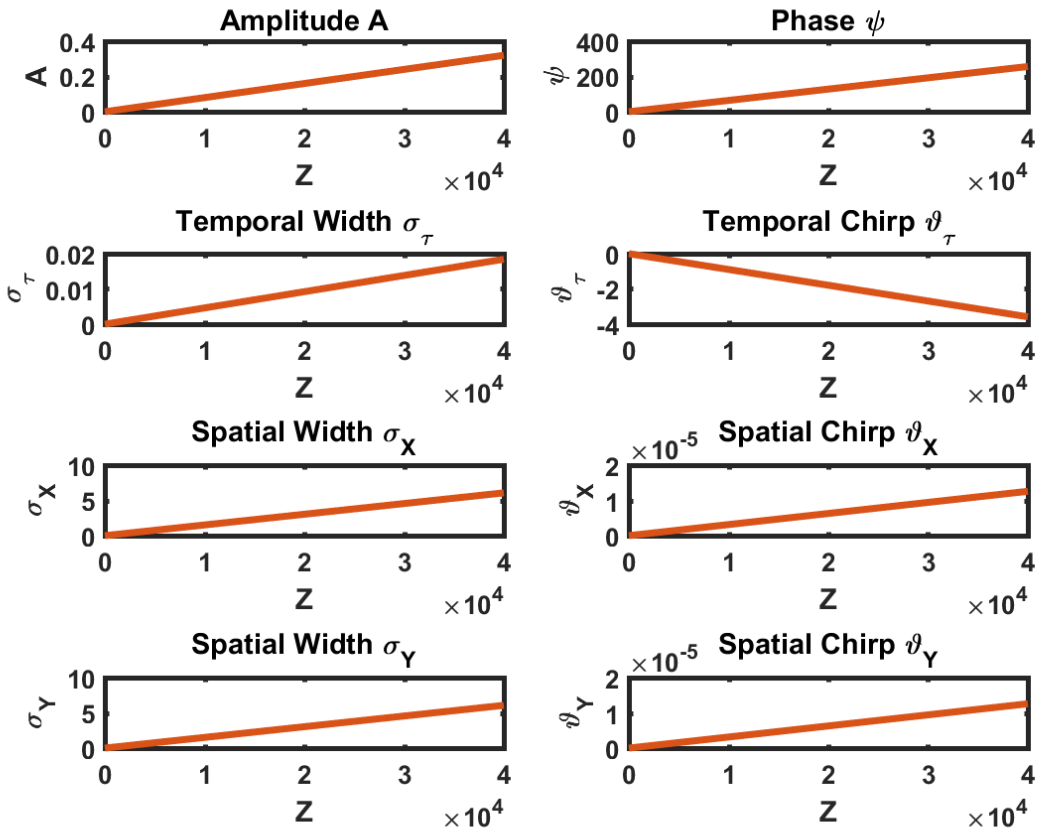

Figure 3.30: LB characteristic parameters profiles for the stable steady-state solution A_+ and for normal dispersion. The following parameters have been used: $\gamma_{X=Y} = 0.8$, $\sigma_{X0} = \sigma_{Y0} = 6.071$, $\vartheta_{X0} = \vartheta_{Y0}$ = -0.1258, $\sigma_{\tau 0} = 0.01843$, $\vartheta_{\tau 0}$ = -3.583, $A_0 = 0.3201$, $p_r = -150.579/N_r$, $p_i = 0.000201/N_r$, $q_r = -60.8/N_r$, $q_i = 6/N_r$, $\gamma_r = -150/N_r$, $\gamma_i = 330/N_r$, $d_{3r} = 0.0006/N_r$, $d_{3i} = -0.08/N_r$, $d_{4r} = 0.002/N_r$, $d_{4i} = -0.04/N_r$, $c_r = 0.00342/N_r$, $n_i = 0.025/N_r$, $m_r = -0.5/N_r$, $k_0 = 2\pi/1.55$, $k_0 = 2\pi/1.55$, and $N_r = 2^{1/2}(4/3)^{3/4}$.

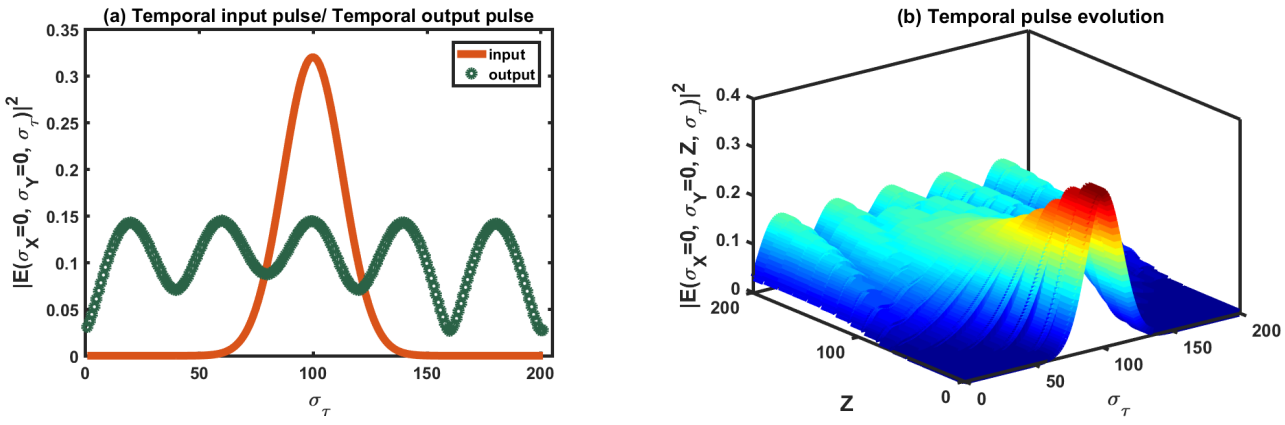

Figure 3.31: Profiles of the temporal input and output pulses and profile of the temporal pulse evolution, from left to right, for the stable steady-state solution A_+ and for normal dispersion. The following parameters have been used: $\gamma_{X=Y} = 0.8$, $\sigma_{\tau 0} = 0.01843$, $\vartheta_{\tau 0} =$ -3.583, $A_0 = 0.3201$, $p_r = -150.579/N_r$, $p_i = 0.000201/N_r$, $q_r = -60.8/N_r$, $q_i = 6/N_r$, $\gamma_r = -150/N_r$, $\gamma_i = 330/N_r$, $d_{3r} = 0.0006/N_r$, $d_{3i} = -0.08/N_r$, $d_{4r} = 0.002/N_r$, $d_{4i} = -0.04/N_r$, $c_r = 0.00342/N_r$, $n_i = 0.025/N_r$, $m_r = -0.5/N_r$, $k_0 = 2\pi/1.55$, $k_0 = 2\pi/1.55$, and $N_r = 2^{1/2}(4/3)^{3/4}$.

Unlike the stable spatial evolution illustrated in Figure 3.29, the temporal input and output profiles shown in Figure 3.31 display notable differences, although the signal remains detectable. This implies that attenuation has occurred to a degree that is only partially compensated, without fully extinguishing the pulse.

This discrepancy between the temporal input and output is likely caused by the unstable behavior of a crucial LB parameter, namely the temporal chirp in Figure 3.30. This reveals the intricate and fluctuating nature of the temporal chirp parameter, which appears to undermine the temporal consistency of the pulse during propagation.

Within the normal dispersion regime, the temporal field evolves such that the input and output pulses differ substantially. With the current CQ parameter set, the predicted stability cannot be fully validated. This suggests that, despite selecting parameters from the stable zones identified in Figures (3.5) through (3.10), they do not adequately balance the various competing effects, including spatial nonlocality, required for stable and robust spatiotemporal pulse evolution.

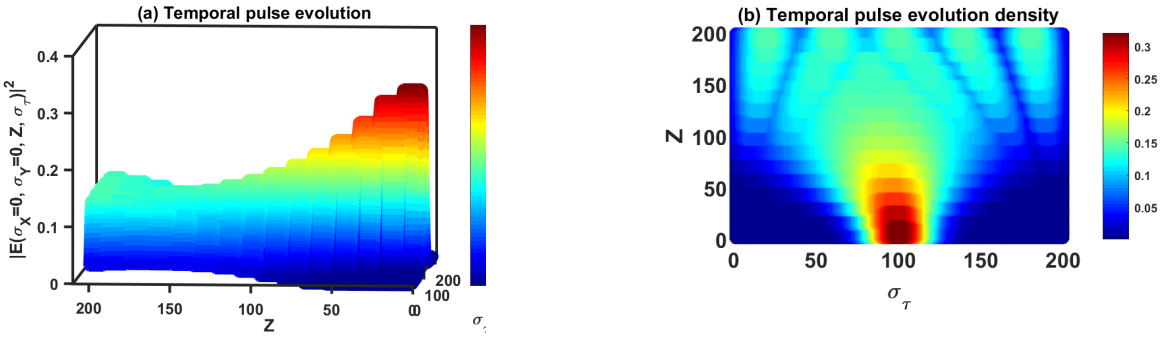

Figure 3.32: The corresponding density plot of Figure (3.31) for the stable steady-state solution under normal dispersion for the stable steady-state solution A_+.

3.5.2 Numerical simulations for the second set of CQ parameters

The analytically generated variational bifurcation branches for A_- and A_+ are compared to numerically obtained branches in Figure 3.33. Precision should, however, be made that values of parameters used to generate the numerical branches have been chosen from the stable zones of Figs. (3.11)-(3.16), as indicated earlier. The obtained analytical features corresponding to the steady-state solutions of the amplitudes A_- and A_+ as functions of the spatial nonlocality parameter $\gamma_{X=Y}$, respectively, are a good approximation of the numerically obtained curves.
Both analytical and numerical solutions emphasize the upper stable branches. For simulating the stable evolution of self-organized dissipative LBs, the stable solution A_- and A_+ was used as the initial spatiotemporal pulse. from top to bottom, unstable branches appear for negative nonlocality, while stable branches correspond to positive nonlocality, behavior that differs from the purely cubic case.

For the second set of CQ parameters, Figure 3.34 clearly shows that the light pulse maintains a constant profile during spatial propagation. This indicates a well-balanced interplay among anomalous dispersion, linear diffraction, linear gain, nonlinear diffraction, the spatially nonlocal cubic?quintic self-focusing Kerr nonlinearity, and nonlinear loss.

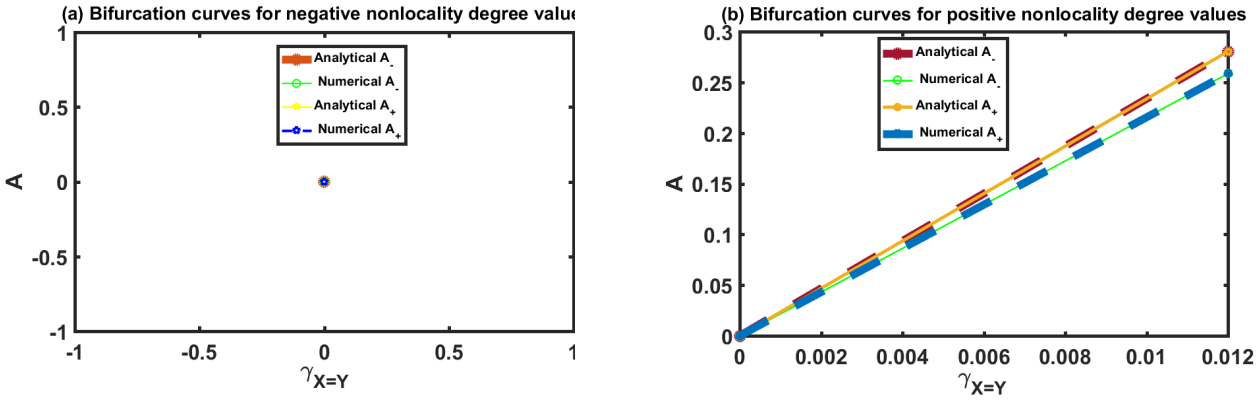

Figure 3.33: Analytical and numerical bifurcation curves of the steady-state solutions A_+ and A_- for anomalous dispersion, respectively, $p_r = 2/N_r$ and for the following parameter values have been used: $N_r = 2^{1/2}(4/3)^{3/4}$, $p_i = 0.00201/N_r$, $q_r = -105/N_r$, $q_i = -5/N_r$, $\gamma_r = -150/N_r$, $\gamma_i = 390/N_r$, $d_{3r} = 0.0006/N_r$, $d_{3i} = -0.083/N_r$, $d_{4r} = -0.4/N_r$, $d_{4i} = 0.002/N_r$, $c_i = 0.148/N_r$ the saturation of the nonlinear gain (positive ci), $c_r = 0.0342/N_r$ (the quintic self-focusing Kerr nonlinearity), $n_i = 0.025/N_r$, $m_r = -0.5/N_r$, $k_0 = 2\pi/1.55$.

Figure 3.35 illustrates the evolution of all characteristic LB parameters along the propagation axis OZ. These parameters exhibit similar dynamic behavior, resulting in the stable temporal pulse propagation shown in Figure 3.36, where the input and output temporal profiles closely match.

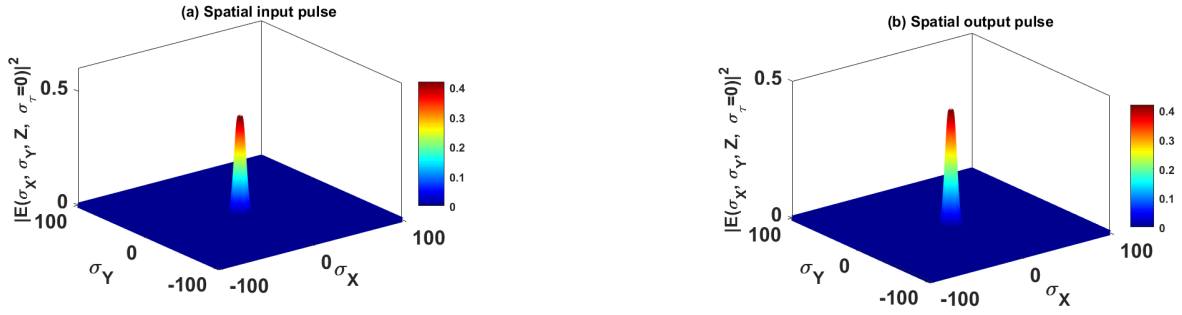

Figure 3.34: Profiles of the spatial input and output pulse, from the left to the right, for the stable steady-state solution A_- under anomalous dispersion. The following parameters have been used: $\gamma_{X=Y} = 0.07068$, $\sigma_{X0} = \sigma_{Y0} = 4.402$, $\vartheta_{X0} = \vartheta_{Y0} = 0.0001847$, $A_0 = 0.4198$, $p_r = 2/N_r$, $p_i = 0.00201/N_r$, $q_r = -105/N_r$, $q_i = -5/N_r$, $\gamma_r = -150/N_r$, $\gamma_i = 390/N_r$, $d_{3r} = 0.0006/N_r$, $d_{3i} = -0.083/N_r$, $d_{4r} = -0.4/N_r$, $d_{4i} = 0.002/N_r$, $c_r = 0.0342/N_r$, $n_i = 0.025/N_r$, $m_r = -0.5/N_r$, $k_0 = 2\pi/1.55$.

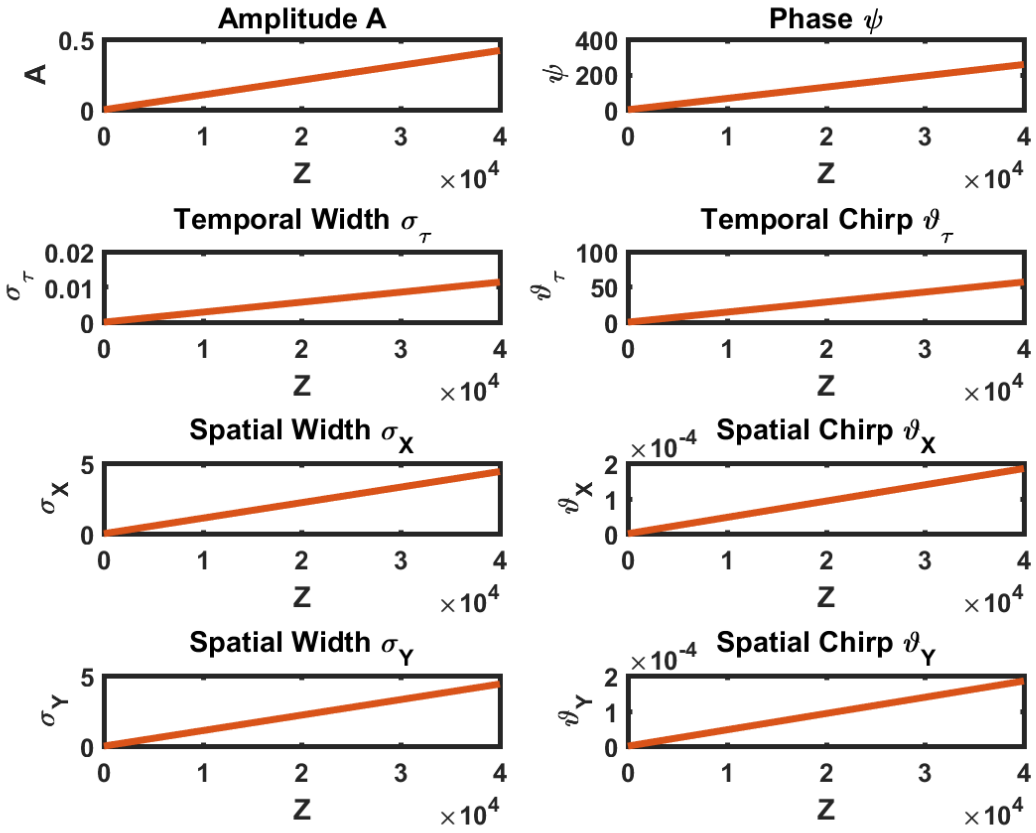

Figure 3.35: Light bullet characteristic parameters profiles for the stable steady-state solution A_{-} and for anomalous dispersion. The following parameters have been used: $\gamma_{X=Y} = 0.07068$, $\sigma_{X0} = \sigma_{Y0} = 4.402$, $\vartheta_{X0} = \vartheta_{Y0} = 0.0001847$, $\vartheta_{\tau 0} = 56.94$, $\sigma_{\tau 0} = 0.01136$, $A_0 = 0.4198$, $p_r = 2/N_r$, $p_i = 0.00201/N_r$, $q_r = -105/N_r$, $q_i = -5/N_r$, $\gamma_r = -150/N_r$, $\gamma_i = 390/N_r$, $d_{3r} = 0.0006/N_r$, $d_{3i} = -0.083/N_r$, $d_{4r} = -0.4/N_r$, $d_{4i} = 0.002/N_r$, $c_r = 0.0342/N_r$, $n_i = 0.025/N_r$, $m_r = -0.5/N_r$, $k_0 = 2\pi/1.55$.

Both the spatial evolution Figure 3.34 and the temporal evolution Figure 3.36 confirm stable pulse propagation. This suggests that the second set of CQ parameters, selected from the stable regions identified Figs. (3.11)-(3.16), effectively balances the competing effects, including spatial nonlocality, necessary for achieving stable spatiotemporal evolution.

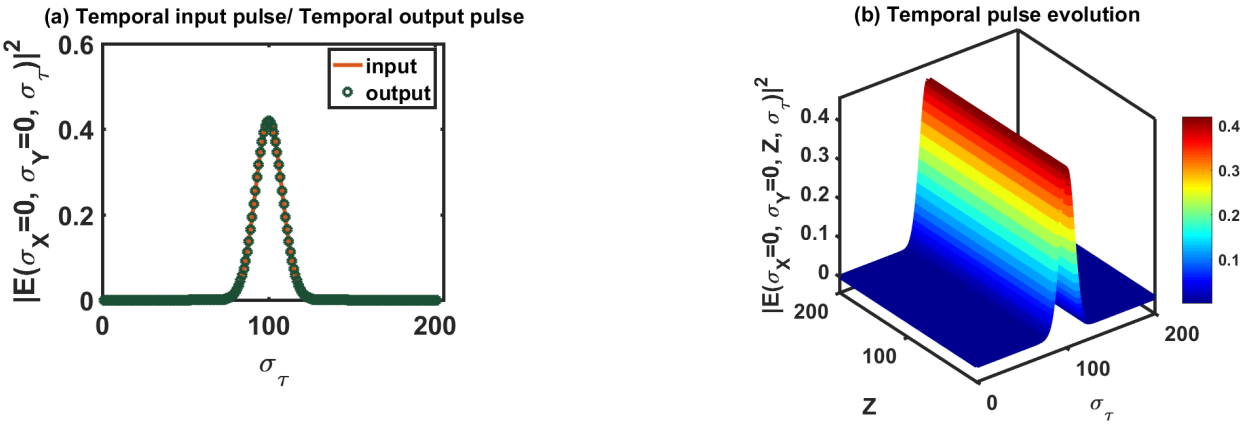

Figure 3.36: Profiles of the temporal input and output pulses and profile of the temporal pulse evolution, from left to right, for the stable steady-state solution A_- under anomalous dispersion. The following parameters have been used: $\gamma_{X=Y} = 0.07068$, $\vartheta_{\tau 0} = 56.94$, $\sigma_{\tau 0} = 0.01136$, $A_0 = 0.4198$, $p_r = 2/N_r$, $p_i = 0.00201/N_r$, $q_r = -105/N_r$, $q_i = -5/N_r$, $\gamma_r = -150/N_r$, $\gamma_i = 390/N_r$, $d_{3r} = 0.0006/N_r$, $d_{3i} = -0.083/N_r$, $d_{4r} = -0.4/N_r$, $d_{4i} = 0.002/N_r$, $c_r = 0.0342/N_r$, $n_i = 0.025/N_r$, $m_r = -0.5/N_r$, $k_0 = 2\pi/1.55$.

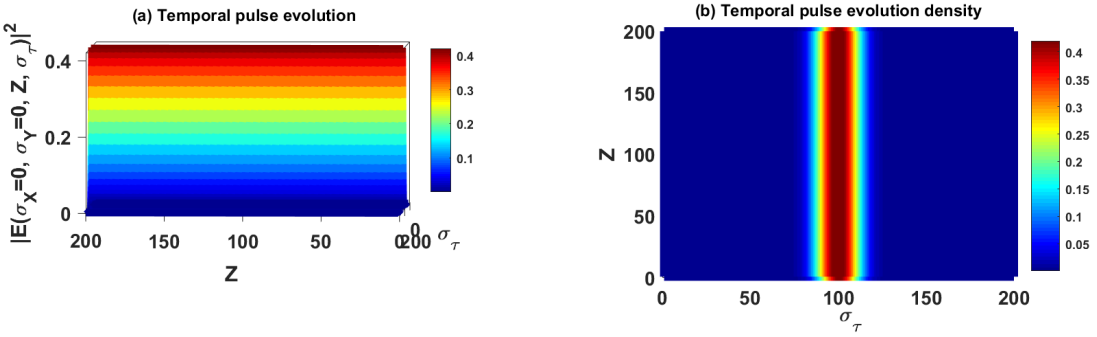

Figure 3.37: The corresponding density plot of Figure (3.36) for the stable steady-state solution under normal dispersion for the stable steady-state solution A_-.

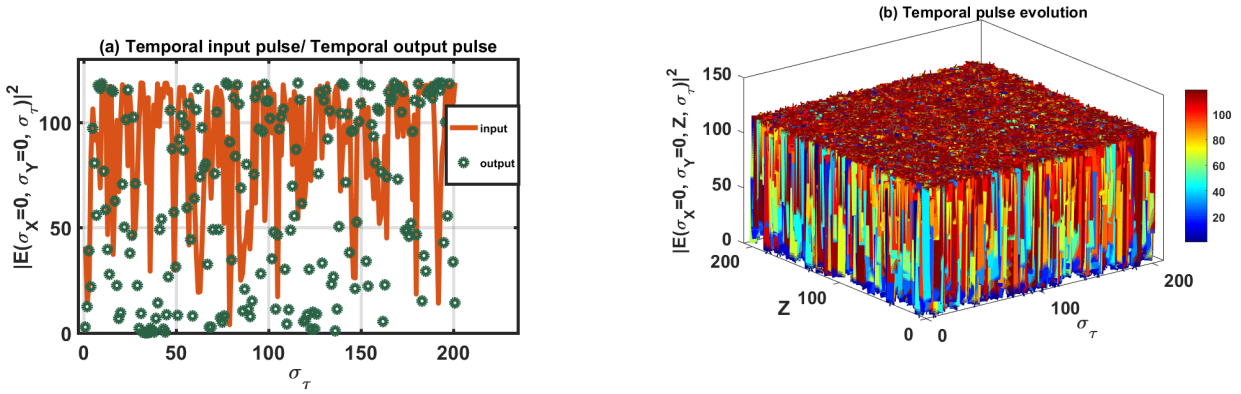

Figure 3.38: Profiles of the unstable temporal input and output pulse and the temporal pulse evolution, from left to right, under anomalous dispersion. We have used the same parameter values as in Figure 3.36, except for the temporal width $\sigma_{\tau 0} = 0.71136$.

3.5.3 Numerical simulations for the third set of CQ parameters

To start, the analytically generated variational bifurcation branches for A_- and A_+ are compared to numerically obtained branches in Figure 3.5. Precision should, however, be made that values of parameters used to generate the numerical branches have been chosen from the stable zones of Figs. (3.22)-(3.27), as indicated earlier. The obtained analytical features corresponding to the steady-state solutions of the amplitudes A_- and A_+ as functions of the spatial nonlocality parameter $\gamma_{X=Y}$, respectively, are a good approximation of the numerically obtained curves. Along the same line, the analytical and numerical solutions of the steady-state A_- and A_+ highlight the upper stable branches.

For the stable evolution of the self-organized dissipative LBs represented in numerical simulations, we choose the stable solution A_- as an input spatiotemporal pulse. We see that for negative nonlocality, nothing happens, and that for positive nonlocality, stable curves are observed.

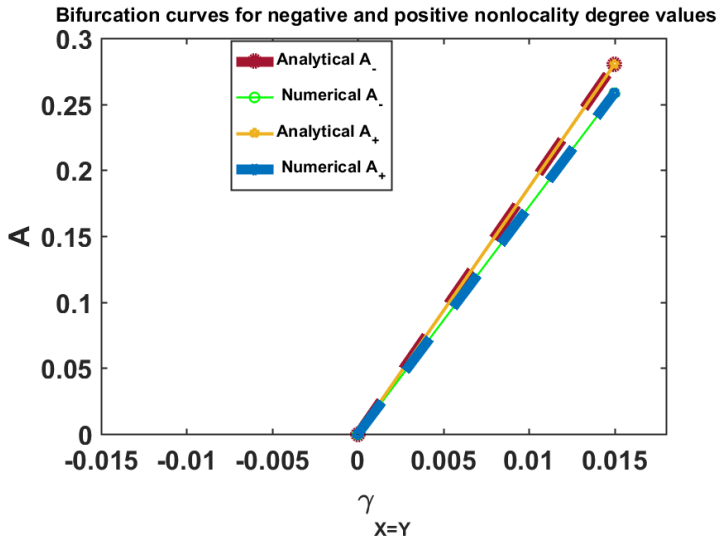

Figure 3.39: Analytical and numerical bifurcation curves of the steady-state solutions A_+ and A_- for normal dispersion, respectively, $p_r = -5/N_r$ and for the following parameter values have been used: $N_r = 2^{1/2}(4/3)^{3/4}$, $p_i = 0.0201/N_r$, $q_r = -700/N_r$, $q_i = 26.8/N_r$, $\gamma_r = 1050/N_r$, $\gamma_i = -990/N_r$, $d_{3r} = 0.03/N_r$, $d_{3i} = -0.06/N_r$, $d_{4r} = -0.04/N_r$, $d_{4i} = 0.002/N_r$, $c_i = 0.2/N_r$ the saturation of the nonlinear gain ($c_i > 0$), $c_r = 0.00342/N_r$ (the quintic self-focusing Kerr nonlinearity), $n_i = 0.025/N_r$, $m_r = -0.5/N_r$, $k_0 = 2\pi/1.55$.

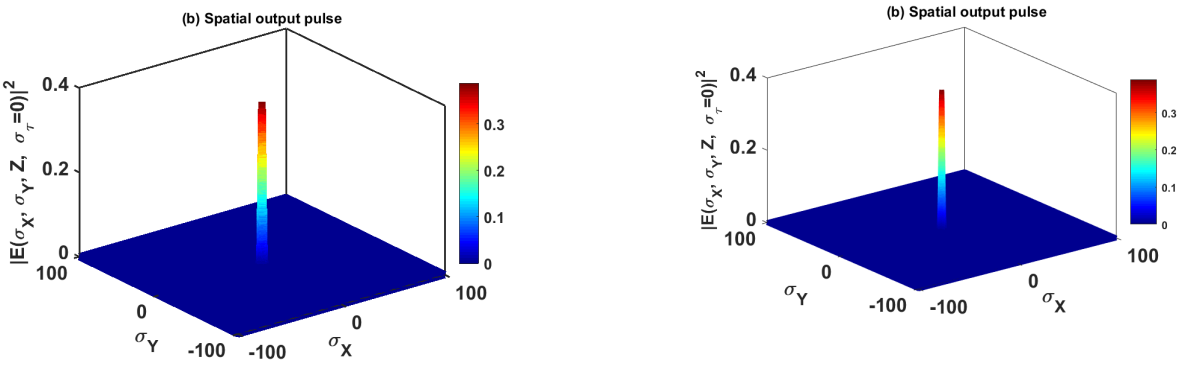

Figure 3.40: Profiles of the spatial input and output pulses, from left to right, for the stable steady-state solution A_- under normal dispersion. The following parameters have been used: $\gamma_{X=Y} = 0.06732$, $\sigma_{X0} = \sigma_{Y0} = 1.124$, $\vartheta_{X0} = \vartheta_{Y0} = 0.0006976$, $A_0 = 0.3882$, $N_r = 2^{1/2}(4/3)^{3/4}$, $p_r = -5/N_r$, $p_i = 0.0201/N_r$, $q_r = -700/N_r$, $q_i = 26.8/N_r$, $\gamma_r = 1050/N_r$, $\gamma_i = -990/N_r$, $d_{3r} = 0.03/N_r$, $d_{3i} = -0.06/N_r$, $d_{4r} = -0.04/N_r$, $d_{4i} = 0.002/N_r$, $c_r = 0.00342/N_r$, $c_i = 0.2/N_r$, $n_i = 0.025/N_r$, $m_r = -0.5/N_r$, $k_0 = 2\pi/1.55$.

Figure 3.41 shows all the LB characteristic parameters and their evolution along the optical axis Z. All LB parameters evolve similarly except the temporal chirp, which could explain the shrinking of the pulses in Figure 3.42.

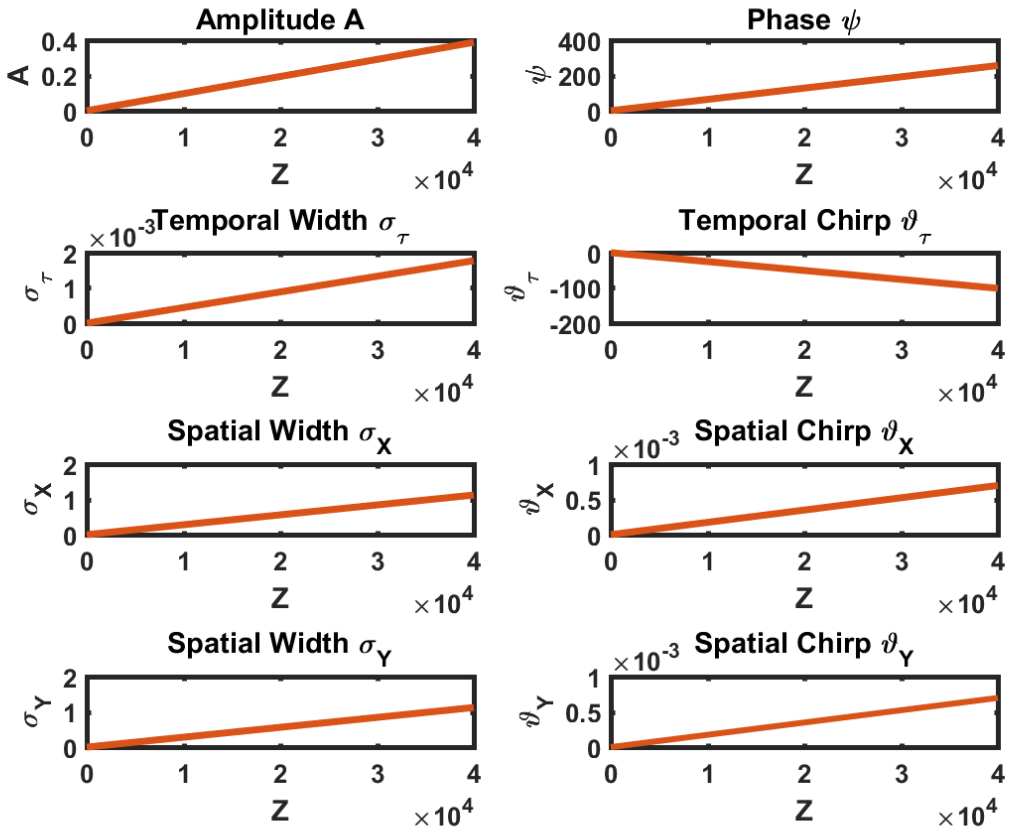

Figure 3.41: Light bullet characteristic parameters profiles for the stable steady-state solution A_{-} and for normal dispersion. The following parameters have been used: $\gamma_{X=Y} = 0.06732$, $\sigma_{X0} = \sigma_{Y0} = 1.124$, $\vartheta_{X0} = \vartheta_{Y0} = 0.0006976$, $\vartheta_{\tau 0}$ = -101.1, $\sigma_{\tau 0}$ = 0.001774, $A_0 = 0.3882$, $N_r = 2^{1/2}(4/3)^{3/4}$, $p_r = -5/N_r$, $p_i = 0.0201/N_r$, $q_r = -700/N_r$, $q_i = 26.8/N_r$, $\gamma_r = 1050/N_r$, $\gamma_i = -990/N_r$, $d_{3r} = 0.03/N_r$, $d_{3i} = -0.06/N_r$, $d_{4r} = -0.04/N_r$, $d_{4i} = 0.002/N_r$, $c_r = 0.00342/N_r$, $c_i = 0.2/N_r$, $n_i = 0.025/N_r$, $m_r = -0.5/N_r$, $k_0 = 2\pi/1.55$.

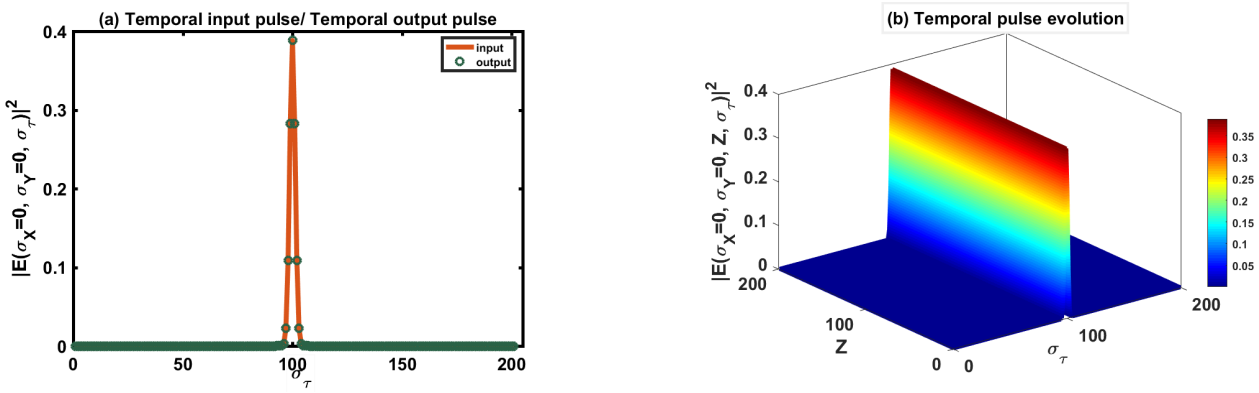

Figure 3.42: Profiles of the temporal input and output pulse and profile of the temporal pulse evolution from the left to the right, for the stable steady-state solution A_- under normal dispersion. The following parameters have been used: $\gamma_{X=Y}$ = 0.06732, $\vartheta_{\tau 0}$ = -101.1, $\sigma_{\tau 0}$ = 0.001774, A_0 = 0.3882, $N_r = 2^{1/2}(4/3)^{3/4}$, $p_r = -5/N_r$, $p_i = 0.0201/N_r$, $q_r = -700/N_r$, $q_i = 26.8/N_r$, $\gamma_r = 1050/N_r$, $\gamma_i = -990/N_r$, $d_{3r} = 0.03/N_r$, $d_{3i} = -0.06/N_r$, $d_{4r} = -0.04/N_r$, $d_{4i} = 0.002/N_r$, $c_r = 0.00342/N_r$, $c_i = 0.2/N_r$, $n_i = 0.025/N_r$, $m_r = -0.5/N_r$, $k_0 = 2\pi/1.55$.

3.6 Conclusion

To confirm the previous analytical results, we first identified the stability zones of the characteristic LB parameters, including the amplitude, temporal, and spatial pulse widths and position of the pulse maximum, unequal wavefront curvatures, chirp parameters, and phase shift. We used the Routh-Hurwitz stability criterion, which requires the construction of a Jacoby determinant from the derivatives of the system of eight coupled first-order differential equations, taken with respect to each of the LB parameters in a steady, i.e. equilibrium, state. From the Jacoby determinant, we derived the characteristic polynomial equation, enabling us to verify the necessary and sufficient conditions for stability to be reached.

Numerical studies were then conducted on nonlocal CCGLE and CQCGLE illustrating the spatial and temporal evolution of dissipative solitons (LBs) within a doped and weakly nonlocal optical fiber. For the spatial evolution, we used the fourth-order Runge-Kutta method, while for the temporal evolution, we employed the Split-Step Fourier method.

Regarding the CCGLE, our study of each evolution revealed that the light pulse remained consistent throughout its progression when we used the initial values of the LB characteristic

parameters within the stability regions. We noted that the dissipative parameter coefficient q_i, representing the nonlinear loss, was effectively balanced with the term representing the spatially nonlocal self-defocusing Kerr nonlinearity response. This balance enhanced the optical localization of the LBs.

Furthermore, we found a good balance among the effects of anomalous dispersion, linear diffraction, linear gain, and nonlinear diffraction. Notably, we demonstrated that even in cubic self-defocusing nonlocal nonlinear media, it is possible to suppress collapse by combining the doping effect with weak spatial nonlocality. As a result, three-dimensional dissipative optical solitons or LBs can propagate stably without collapsing in self-defocusing nonlocal nonlinear media under anomalous dispersion.

Conversely, we have shown that instability can arise in the evolution of the temporal pulse when parameter values are chosen outside the stability zone.
Concerning the CQCGLE, we have succeeded in producing amplitudes A_- and A_+ in a positive value zone, unlike the cubic case where only amplitude A_- was stable, and amplitude A_+ corresponded only to negative numerical values and was always unstable. For the first and second sets of cubic-quintic parameter cases, we observed that the two amplitudes merged seamlessly. The third case shows rather two amplitudes separated as in the cubic case, but all with positive values. Still, in the cubic-quintic case, the numerical experiments on the spatial evolution revealed that the light pulse remained consistent throughout its progression when we used the initial values of the LB characteristic parameters within the stability regions. We found that the dissipative parameter coefficient c_i, representing the saturation of the nonlinear loss/gain ($c_i < 0/c_i > 0$), was effectively balanced with the term representing the spatially nonlocal self-defocusing/self-focusing Kerr nonlinearity response. This balance enhanced the optical localization of the LBs.

The temporal evolution for the first set of cubic-quintic parameters reveals a gap between the input and output pulses. In contrast, the second and third sets of cubic-quintic parameters showed a good agreement between the input and the output pulses. So, by including additional effects, such as quintic correction terms, into the initial cubic medium, the A_- solution is no longer the

only prerequisite for obtaining LBs after self-organized spatiotemporal evolution. The nonlocal spatial response of the Kerr nonlinearity ($\gamma_{_{X=Y}}$) and the saturation of the nonlinear loss/gain ($c_i < 0/c_i > 0$) under normal and anomalous dispersion were in good agreement to allow the existence of LBs in a cubic-quintic medium, thus nonlocality and nonlinear loss/gain improve the localization of optical LBs in this regime.

General Conclusion

• Summary and Contributions

In this PhD study, we started by giving the history, classification, and properties of optical fibers. We have seen that doping an optical fiber, particularly with erbium ions (Er^{3+}), creates a dissipative medium where balanced gains and losses can amplify and counteract nonlinearities, dispersion, attenuation and diffraction effects, ensuring stable propagation of light bullets (LBs). This double balance–between linear and nonlinear effects, as well as between gains and losses–plays a crucial role in the design of optical amplifiers, particularly in erbium-doped fiber amplifiers (EDFAs).

We also discussed the concept of nonlocality, which spreads the effects of localized excitations. We have seen that, this property can help suppress instantaneous modulation instabilities of homogeneous states, enabling the stable observation of LBs.

Next, we successfully derived the nonlocal CCGLE and CQCGLE by considering the electromagnetic wave theory based on Maxwell's equations. Scaling transformations related to the practical use of optical fibers have been applied to the CCGLE and CQCGLE to tailor them for a good description of LBs propagation in doped nonlocal optical fibers. We found that the nonlocal CQCGLE has more terms compared to the nonlocal CCGLE, namely the third and fourth-order dispersion, the saturation of the nonlinear gain absorption (if negative), the nonlinear gradient term responsible for the self-frequency shift and the nonlinear dispersion responsible for the self-steepening. We used the variational approach based on the Euler-Lagrange equations to find approximate solutions to the nonlocal CCGLE and CQCGLE in order to gain physical insight into some relevant parameters.

Additionally, to qualitatively validate our analytical predictions, we subsequently implemented these solutions in numerical simulations. We first identified the stability zones of the characteristic LB parameters, including the amplitude, temporal, and spatial pulse widths and position of the pulse maximum, unequal wavefront curvatures, chirp parameters, and phase shift. We used the Routh-Hurwitz stability criterion, which requires the construction of a Jacoby determinant from the derivatives of the system of eight coupled first-order differential equations, taken with respect to each of the LB parameters in a steady, i.e. equilibrium, state. From the Jacoby determinant, we derived the characteristic polynomial equation, enabling us to verify the necessary and sufficient conditions for stability to be reached. Numerical studies were then conducted, illustrating the spatial and temporal evolution of dissipative solitons (LBs) within a doped and weakly nonlocal optical fiber. For the spatial evolution, we used the fourth-order Runge-Kutta method, while for the temporal evolution, we employed the split-step Fourier method.

Regarding the CCGLE, our study of each evolution revealed that the light pulse remained consistent throughout its progression when we used the initial values of the LB characteristic parameters within the stability regions. We noted that the dissipative parameter coefficient q_i, representing the nonlinear loss, was effectively balanced with the term representing the spatially nonlocal self-defocusing Kerr nonlinearity response. This balance enhanced the optical localization of the LBs.

Furthermore, we found a good balance among the effects of anomalous dispersion, linear diffraction, linear gain, and nonlinear diffraction. Notably, we demonstrated that in cubic self-defocusing nonlocal nonlinear media, it is possible to suppress collapse by combining the doping effect with weak spatial nonlocality. As a result, three-dimensional dissipative optical solitons or LBs can propagate stably without collapsing in self-defocusing nonlocal nonlinear media under anomalous dispersion. Conversely, we have shown that instability can arise in the evolution of the temporal pulse when parameter values are chosen outside the stability zone.

Concerning the CQCGLE, we have succeeded in producing amplitudes A_- and A_+ in a positive value zone, unlike the cubic case where only amplitude A_- was stable, and amplitude A_+ corresponded only to negative numerical values and was always unstable. For the first and second sets of cubic-quintic parameter cases, we observed that the two amplitudes merged seamlessly. The third case shows rather two amplitudes separated as in the cubic case, but all with positive

values. Still, in the cubic-quintic case, the numerical experiments on the spatial evolution revealed that the light pulse remained consistent throughout its progression when we used the initial values of the LB characteristic parameters within the stability regions. We found that the dissipative parameter coefficient c_i, representing the saturation of the nonlinear loss/gain ($c_i < 0/c_i > 0$), was effectively balanced with the term representing the spatially nonlocal self-defocusing/self-focusing Kerr nonlinearity response. This balance enhanced the optical localization of the LBs.

The temporal evolution for the first set of cubic-quintic parameters reveals a gap between the input and output pulses. In contrast, the second and third sets of cubic-quintic parameters showed a good agreement between the input and the output pulses. So, by including additional effects, such as quintic correction terms, into the initial cubic medium, the A_{-} solution is no longer the only prerequisite for obtaining LBs after self-organized spatiotemporal evolution. The nonlocal spatial response of the Kerr nonlinearity ($\gamma_{_{X=Y}}$) and the saturation of the nonlinear loss/gain ($c_i < 0/c_i > 0$) under normal and anomalous dispersion were in good agreement to allow the existence of LBs in a cubic-quintic medium, thus nonlocality and nonlinear loss/gain improve the localization of optical LBs in this regime.

In summary, we have predicted the dissipative LBs in optical fiber amplifiers for several reasons:
(i) we have rigorously derived a (3+1)-D nonlocal CCGLE and CQCGLE valid for the dynamics of the dissipative LBs in optical fiber amplifiers under the effects fiber dispersion, linear gain, nonlinear loss, fiber nonlinearity, atomic detuning, linear and nonlinear diffractive transverse effects, and nonlocal nonlinear response.
(ii) We have also derived eight coupled first-order differential equations of motion of the dissipative LB parameters for the nonlocal (3+1)-D Cnonlocal CCGLE and CQCGLE under the interplay between dopants and a spatially weakly nonlocal nonlinear response, with the help of the variational technique using the Gaussian Ansatz function.
(iii) We established the Routh-Hurwitz stability criterion for dissipative spatiotemporal LBs, where a domain of dissipative parameters for stable steady-state solutions has been found.
(iv) We carried out the direct integration of the proposed nonlocal evolution equation, which allowed us to investigate the evolution of the Gaussian beam along a doped nonlocal optical fiber, showing stable self-organized dissipative spatiotemporal LBs.

We have notably demonstrated that in cubic self-defocusing and in cubic-quintic self-

focusing/self-defocusing nonlocal nonlinear doped optical fiber, it is possible to counteract the attenuation issue and prevent collapse by combining the doping effects with weak spatial nonlocality. In essence, when introducing a weak spatial nonlocality, alongside achieving the double balance between linear and nonlinear effects, as well as between gains and losses, three-dimensional dissipative optical solitons or LBs can propagate stably without collapsing within an optical fiber. Our results indicate that it is possible to simultaneously control the doping parameters and the spatial nonlocality coefficient in fiber-optic propagations to counteract attenuation and avoid collapse. There are several reasons why this work can be considered revolutionary in comparison to current solutions.

Our approach is fundamentally different in that it acts within the fiber, rather than around it. It demonstrates that we can modify the behaviour of the doped fibre itself by introducing impurities during the design phase to increase nonlocality, which acts as an integrated noise filter for each amplification.

We present nonlocality as a natural noise filter, demonstrating that by reinforcing the nonlocality of the optical medium, a self-stabilising physical mechanism is introduced. Nonlocality can smooth out fluctuations and noise instability in doped optical fibres.

We show that it is possible to counteract attenuation with amplification and, in the same way, avoid the collapse of the light signal by introducing nonlocality, which acts as a filter and suppresses parasitic noise components at each amplification stage.

We present the concept of an intelligent, self-regulating fiber amplifier that improves transmission stability. This concept could lead to optical fibers that 'self-clean' of noise at each amplification stage, resulting in less complex electronic processing, longer distances without critical signal loss, simpler architecture, and reduced operating costs.

• Perspectives

This research opens several promising directions for future investigations and technological development:

1) **Towards a new generation of 'nonlocal Erbium-Doped Fiber Amplifiers (EDFAs)**'. The key insight of this work will be the initiation of a new generation of EDFAs, referred to as 'nonlocal' doped EDFAs, which combine amplification and natural noise filtering.

This solution will not rely on electronic components, but rather on a physical property of the amplifier material itself.

It will enable networks over long distances without the need for costly intermediate correction amplifiers. Rather than compensating for noise with external technological layers, this approach acts at the source: the doped fiber itself becomes smarter thanks to induced nonlocality, which naturally filters out optical noise. The concept of nonlocality in doped fiber represents a new philosophy of optical amplification that is more integrated, efficient, and sustainable.

Therefore, experimental validation in collaboration with **international optical laboratories** seems to be an obvious step for the future, as evidenced by the publication of an article. The aim is to identify specific impurities that could enhance the weak nonlocality of doped fibers and enable spatial nonlocality to be controlled during fiber design.

2)**Stability versus instability**

In this study, our role as technological surgeons was to determine how to evaluate a set of parameters in order to obtain a stable environment. Although our research focused on how nonlocality brings stability to the medium by combining cubic and cubic-quintic terms, our work could pave the way for further research into the converse: whether nonlocality can also cause instability when the light bullet's characteristic parameters are chosen outside the stability zones.

Such results could be highly valuable for researchers working on instability modulation in nonlinear optical systems. As demonstrated in the case of the temporal evolution profile, instability can be deliberately induced by operating outside the stability region. A similar principle could be applied to spatial dynamics, providing new ways to control or exploit optical turbulence.

3)**Bifurcation dynamics and parameter interplay**

Another promising direction would be to study how bifurcations evolve as system parameters vary, in order to map the transition between different propagation regimes. Investigating the interplay between cubic and quintic nonlinear terms could provide deeper insight into how nonlinearities cooperate or compete to influence stability collapse, and soliton formation.

4) **Extension towards quantum and ultrafast optics**

A fascinating question is whether the framework developed here could be extended to quantum optics, where nonlocality manifests in the temporal domain. Establishing this connection could open perspectives for quantum communication, noise-resilient quantum amplifiers, and the design

of quantum analogues of dissipative solitons.

5) **Cross-disciplinary applications: photonics, biology, and medicine**

Beyond photonics, this work could inspire **biophysical** and **medical imaging** models, where 'dissipative solitons' are already used to describe self-organized living systems.

In such contexts, solitons are not merely optical structures but entities that exchange energy and matter with their surroundings, behaving almost like living organisms.

Understanding how nonlocality influences their stability could shed light on **biological pattern formation**, **homeostasis**, or **energy regulation** in complex systems.

In summary, this research establishes the theoretical foundation for a new conceptual and technological paradigm in nonlinear optics, in which doping, nonlocality, and nonlinearity coexist as complementary mechanisms.

Beyond its immediate implications for telecommunications, this opens the door to a wide spectrum of interdisciplinary studies, from advanced fiber technologies to quantum and biological systems.

Appendices

APPENDIX A: Expression of the constant propagation

The propagation constant around the frequency ω is given as follows

$$\beta(\omega) = \frac{\omega}{c}\sqrt{\epsilon(\omega)}, \tag{45}$$

where $\epsilon(\omega)$ is a complex dielectric constant given by

$$\epsilon(\omega) = n_f^2 + 2in_f.\frac{\alpha_f}{k_0} + \chi_a(\omega). \tag{46}$$

Therefore

$$\beta(\omega) = \frac{\omega}{c}\sqrt{n_f^2 + 2in_f.\frac{\alpha_f}{k_0} + \chi_a(\omega)}. \tag{47}$$

The given expression of n_f is

$$n_f = n_0(\omega) + n_2|\vec{E}|^2 + \frac{n_2\gamma_{xx}}{2}\frac{\partial^2}{\partial x^2}(|\vec{E}|^2) + \frac{n_2\gamma_{yy}}{2}\frac{\partial^2}{\partial y^2}(|\vec{E}|^2), \tag{48}$$

and

$$n_f^2 = \left[n_0^2(\omega) + 2n_0n_2|\vec{E}|^2 + 2\left\{\frac{n_0n_2\gamma_{xx}}{2}\frac{\partial^2}{\partial x^2}(|\vec{E}|)^2 + \frac{n_0n_2\gamma_{yy}}{2}\frac{\partial^2}{\partial y^2}(|\vec{E}|^2)\right\}\right]. \tag{49}$$

Replacing n_f and n_f^2 by their expressions lead to:

$$\beta(\omega) = \frac{\omega}{c}\,[\, n_0^2(\omega) + 2n_0 n_2|\vec{E}|^2 + \{\, \frac{n_0 n_2 \gamma_{xx}}{2}\frac{\partial^2}{\partial x^2}(|\vec{E}|)^2 + \frac{n_0 n_2 \gamma_{yy}}{2}\frac{\partial^2}{\partial y^2}(|\vec{E}|^2)\,\} + 2i\left\{ n_0(\omega) + n_2|\vec{E}|^2 + \frac{n_2\gamma_{xx}}{2}\frac{\partial^2}{\partial x^2}(|\vec{E}|^2) + \frac{n_2\gamma_{yy}}{2}\frac{\partial^2}{\partial y^2}(|\vec{E}|^2)\right\}\frac{\alpha_f}{k_0} + \chi_a(\omega)\,]^{1/2}. \quad (50)$$

Putting n_0 out of the square root gives:

$$\beta(\omega) = \frac{\omega n_0(\omega)}{c}\left[1 + \frac{2n_0 n_2|\vec{E}|^2}{n_0^2(\omega)} + \left\{\frac{n_0 n_2\gamma_{xx}}{2n_0^2(\omega)}\frac{\partial^2}{\partial x^2}(|\vec{E}|)^2 + \frac{n_0 n_2\gamma_{yy}}{2n_0^2(\omega)}\frac{\partial^2}{\partial y^2}(|\vec{E}|^2)\right\} \frac{2i}{n_0^2(\omega)}\left\{ n_0(\omega) + n_2|\vec{E}|^2 + \frac{n_2\gamma_{xx}}{2}\frac{\partial^2}{\partial x^2}(|\vec{E}|^2) + \frac{n_2\gamma_{yy}}{2}\frac{\partial^2}{\partial y^2}(|\vec{E}|^2)\right\}\frac{\alpha_f}{k_0} + \frac{1}{n_0^2(\omega)}\chi_a(\omega)\right]^{1/2}. \quad (51)$$

We consider the approximation

$$\sqrt{1+X} = (1+X)^{1/2} \approx \left(1 + \frac{1}{2}X\right), \quad (52)$$

then we have

$$\beta(\omega) = \frac{\omega n_0(\omega)}{c} + \left(\frac{\omega n_0(\omega)}{c}\frac{2n_0 n_2|\vec{E}|^2}{2n_0^2(\omega)}\right) + \frac{1}{2n_0^2(\omega)}\frac{\omega n_0(\omega)}{c}\chi_a(\omega) + \frac{1}{2}\frac{\omega n_0(\omega)}{c}\left\{\frac{n_0 n_2\gamma_{xx}}{2n_0^2(\omega)}\frac{\partial^2}{\partial x^2}(|\vec{E}|)^2 + \frac{n_0 n_2\gamma_{yy}}{2n_0^2(\omega)}\frac{\partial^2}{\partial y^2}(|\vec{E}|^2)\right\} \frac{2i\omega n_0(\omega)}{2cn_0^2(\omega)}\left\{ n_0(\omega) + n_2|\vec{E}|^2 + \frac{n_2\gamma_{xx}}{2}\frac{\partial^2}{\partial x^2}(|\vec{E}|^2) + \frac{n_2\gamma_{yy}}{2}\frac{\partial^2}{\partial y^2}(|\vec{E}|^2)\right\}\frac{\alpha_f}{k_0}, \quad (53)$$

which gives

$$\beta(\omega) = \frac{\omega n_0(\omega)}{c} + \frac{\omega}{c}n_2|E|^2 + \frac{1}{2n_0}\frac{\omega}{c}\chi_a(\omega) + \left\{\frac{\omega}{c}\frac{n_2\gamma_{xx}}{2}\frac{\partial^2}{\partial x^2}(|E|^2) + \frac{\omega}{c}\frac{n_2\gamma_{yy}}{2}\frac{\partial^2}{\partial y^2}(|E|^2)\right\} + \left\{ i\alpha_f + i\alpha_f\frac{n_2}{n_0}|E|^2 + i\alpha_f\frac{n_2}{n_0}\frac{\gamma_{xx}}{2}\frac{\partial^2}{\partial x^2}(|E|^2) + i\alpha_f\frac{n_2}{n_0}\frac{\gamma_{yy}}{2}\frac{\partial^2}{\partial y^2}(|E|^2)\right\}. \quad (54)$$

The first expression $\frac{\omega}{c}n_0(\omega)$ is the undoped propagation constant anointed $\beta_f(\omega)$ and given by:

$$\beta_f(\omega) \;=\; \beta_0 \;+\; \left(\frac{\partial}{\partial\omega}\beta_f\right)(\omega \;-\; \omega_0) \;+\; \frac{1}{2}\left(\frac{\partial^2}{\partial\omega^2}\beta_f\right)(\omega \;-\; \omega_0)^2 \;+\; \left(\frac{\partial}{\partial(|E|^2)}\beta_f\right)_0 |E|^2, \quad (55)$$

and $\chi_a(\omega)$, the atomic susceptibility governing the response of the dopant in the optical fiber extended in Taaylor series up to the second order is given as:

$$\chi_a(\omega) = \frac{g_p}{k_0}\left[\frac{\delta - i}{1+\delta^2} + \frac{1-\delta^2+2i\delta}{(1+\delta^2)^2}(\omega-\omega_0)T_2 + \frac{\delta(\delta^2-3)+i(1-3\delta^2)}{(1+\delta^2)^3}(\omega-\omega_0)^2T_2^2\right]. \quad (56)$$

We recall that the expression $(\omega-\omega_0)^n = (i)^n(\frac{\partial^n}{\partial t^n})$, with $n = 1...4$.

Hence,

$$\begin{aligned}\beta(\omega) = \beta_0(\omega) + i\beta_1\frac{\partial}{\partial t} - \frac{\beta_2}{2}\frac{\partial^2}{\partial t^2} + \left(\frac{\partial\beta_f}{\partial(|E|^2)}\right)_0(|E|^2) + \frac{\omega}{c}n_2|E|^2 + \frac{\omega}{c}\frac{n_2\gamma_{xx}}{2}\frac{\partial^2}{\partial x^2}(|E|^2) \\ + \frac{\omega}{c}\frac{n_2\gamma_{yy}}{2}\frac{\partial^2}{\partial y^2}(|E|^2) + i\alpha_f + i\alpha_f\frac{n_2}{n_0}|E|^2 + i\alpha_f\frac{n_2}{n_0}\frac{\gamma_{xx}}{2}\frac{\partial^2}{\partial x^2}(|E|^2) + i\alpha_f\frac{n_2}{n_0}\frac{\gamma_{yy}}{2}\frac{\partial^2}{\partial y^2}(|E|^2) \\ + \frac{g_p}{2n_0}\left[\frac{\delta-i}{1+\delta^2} + \frac{1-\delta^2+2i\delta}{(1+\delta^2)^2}\left(i\frac{\partial}{\partial t}\right)T_2 + \frac{\delta(\delta^2-3)+i(1-3\delta^2)}{(1+\delta^2)^3}\left(-\frac{\partial^2}{\partial t^2}\right)T_2^2\right]. \quad (57)\end{aligned}$$

APPENDIX B: Computations for adimensionment

(B1)Computations of $\frac{\partial^2\phi}{\partial x^2}$ and $\frac{\partial\phi^2}{\partial y^2}$

Let's recall that

$$X = \frac{x}{r_0}\sqrt{\frac{L_{diff}}{L_{disp}}} \quad (58)$$

$$Y = \frac{y}{r_0}\sqrt{\frac{L_{diff}}{L_{disp}}}. \quad (59)$$

Then,

$$\frac{\partial X}{\partial x} = \frac{1}{r_0}\sqrt{\frac{L_{diff}}{L_{disp}}} \quad (60)$$

$$\frac{\partial Y}{\partial y} = \frac{1}{r_0}\sqrt{\frac{L_{diff}}{L_{disp}}}. \quad (61)$$

We can therefore write

$$\frac{\partial \phi}{\partial x} = \frac{\partial \phi}{\partial X}\frac{\partial X}{\partial x} \tag{62}$$

$$= \frac{1}{r_0}\sqrt{\frac{L_{diff}}{L_{disp}}}\frac{\partial \phi}{\partial X}, \tag{63}$$

and

$$\frac{\partial \phi}{\partial y} = \frac{\partial \phi}{\partial Y}\frac{\partial Y}{\partial y} \tag{64}$$

$$= \frac{1}{r_0}\sqrt{\frac{L_{diff}}{L_{disp}}}\frac{\partial \phi}{\partial Y}. \tag{65}$$

The second derivative is given as

$$\frac{\partial^2 \phi}{\partial x^2} = \frac{\partial \phi}{\partial x}\left[\frac{\partial \phi}{\partial x}\right] \tag{66}$$

$$= \frac{\partial \phi}{\partial x}\left[\frac{1}{r_0}\sqrt{\frac{L_{diff}}{L_{disp}}}\right]\frac{\partial \phi}{\partial X} \tag{67}$$

$$= \frac{1}{r_0}\sqrt{\frac{L_{diff}}{L_{disp}}}\frac{\partial \phi}{\partial X}\left[\frac{\partial \phi}{\partial x}\right] \tag{68}$$

$$= \frac{1}{r_0}\sqrt{\frac{L_{diff}}{L_{disp}}}\frac{\partial \phi}{\partial X}\left[\frac{1}{r_0}\sqrt{\frac{L_{diff}}{L_{disp}}}\frac{\partial \phi}{\partial X}\right] \tag{69}$$

$$= \frac{1}{r_0^2}\frac{L_{diff}}{L_{disp}}\frac{\partial \phi^2}{\partial X^2}. \tag{70}$$

Since

$$\Phi(X, Y, Z, \tau) = \sqrt{P_0}N\phi(x, y, z, t), \tag{71}$$

then,

$$\phi(x, y, z, t) = \frac{1}{\sqrt{P_0}N}\Phi(X, Y, Z, \tau), \tag{72}$$

and

$$\frac{\partial \phi}{\partial X} = \frac{1}{\sqrt{P_0}N}\frac{\partial \Phi}{\partial X}. \tag{73}$$

This lead to,

$$\frac{\partial \phi^2}{\partial X^2} = \frac{1}{\sqrt{P_0}N}\frac{\partial \Phi^2}{\partial X^2}, \tag{74}$$

and

$$\frac{\partial^2 \phi}{\partial x^2} = \frac{1}{r_0^2}\frac{L_{diff}}{L_{disp}}\frac{1}{\sqrt{P_0}N}\frac{\partial \Phi^2}{\partial X^2}. \tag{75}$$

In the same way,

$$\frac{\partial \phi^2}{\partial Y^2} = \frac{1}{\sqrt{P_0}N}\frac{\partial \Phi^2}{\partial Y^2}, \tag{76}$$

and

$$\frac{\partial^2 \phi}{\partial y^2} = \frac{1}{r_0^2}\frac{L_{diff}}{L_{disp}}\frac{1}{\sqrt{P_0}N}\frac{\partial \Phi^2}{\partial Y^2}. \tag{77}$$

(B2) Computations of $\frac{\partial}{\partial t}$ and $\frac{\partial}{\partial z}$

We consider the functions $f(t, z)$ and $f(t, \tau)$ which depend on two old (t,z) and two new variables (τ, Z). We compute the exact total differential of f in both cases and equalize the partial derivatives

$$df(t, z) = \frac{\partial f}{\partial t}dt + \frac{\partial f}{\partial z}dz, \tag{78}$$

$$df(\tau, Z) = \frac{\partial f}{\partial \tau}d\tau + \frac{\partial f}{\partial Z}dZ. \tag{79}$$

Since $\tau = \frac{T}{T_0}$ and $Z = \frac{z}{Ldisp}$, we can write

$$df(\tau, Z) = \frac{\partial f}{\partial \tau}d\left(\frac{T}{T_0}\right) + \frac{\partial f}{\partial Z}d\left(\frac{z}{Ldisp}\right), \tag{80}$$

and

$$df(\tau, Z) = \left(\frac{1}{T_0}\right)\frac{\partial f}{\partial \tau}dT + \left(\frac{z}{Ldisp}\right)\frac{\partial f}{\partial Z}dz. \tag{81}$$

Since

$$T = t - \frac{z}{v_g} = \tag{82}$$

$$t - \beta_{eff}z, \tag{83}$$

with

$$\beta_{eff} = \frac{1}{v_g} \tag{84}$$

$$= \beta_{reff} + i\beta_{ieff}, \tag{85}$$

then

$$df(\tau, Z) = \left(\frac{1}{T_0}\right)\frac{\partial f}{\partial \tau}d\left(t - \beta_{eff}z\right) + \left(\frac{z}{Ldisp}\right)\frac{\partial f}{\partial Z}dz. \tag{86}$$

Hence

$$df(\tau, Z) = \left(\frac{1}{T_0}\right)\frac{\partial f}{\partial \tau}dt - \left(\frac{1}{T_0}\right)\beta_{eff}\frac{\partial f}{\partial \tau}dz + \left(\frac{z}{Ldisp}\right)\frac{\partial f}{\partial Z}dz, \tag{87}$$

and

$$df(\tau, Z) = \left(\frac{1}{T_0}\right)\frac{\partial f}{\partial \tau}dt\left(-\left(\frac{1}{T_0}\right)\beta_{eff}\frac{\partial f}{\partial \tau}dz + \left(\frac{z}{Ldisp}\right)\frac{\partial f}{\partial Z}\right)dz. \tag{88}$$

Comaparing Eq. (68) and Eq. (69) we get

$$\frac{\partial}{\partial t} = \frac{1}{T_0}\frac{\partial f}{\partial z}, \tag{89}$$

and

$$\frac{\partial}{\partial z} = \left(-\left(\frac{1}{T_0}\right)\beta_{eff}\frac{\partial f}{\partial \tau}dz + \left(\frac{z}{Ldisp}\right)\frac{\partial f}{\partial Z}\right). \tag{90}$$

(B3) Computations of $|\phi|^2$

Given that

$$\Phi(X,Y,Z,\tau) = \sqrt{P_0}N\phi(x,y,z,t), \tag{91}$$

then,

$$\phi(x,y,z,t) = \frac{1}{\sqrt{P_0}N}\Phi(X,Y,Z,\tau), \tag{92}$$

and

$$\begin{aligned} |\phi|^2 =& \phi\phi^* && (93)\\ =& \frac{1}{\sqrt{P_0}N}\Phi\frac{1}{\sqrt{P_0}N}\Phi^* && (94)\\ =& \frac{1}{P_0N^2}|\Phi|^2 && (95) \end{aligned}$$

(B4) Computations of $|\phi|^2\phi$

$$\begin{aligned} |\phi|^2\phi =& \frac{1}{P_0N^2}|\Phi|^2\frac{1}{\sqrt{P_0}N}\Phi && (96)\\ =& \frac{1}{P_0\sqrt{P_0}N^3}|\Phi|^2\Phi && (97) \end{aligned}$$

(B5) Computations of $\frac{\partial}{\partial x^2}(|\phi|^2)\phi$ and $\frac{\partial}{\partial y^2}(|\phi|^2)\phi$

$$\begin{aligned} \frac{\partial^2}{\partial x^2}(|\phi|^2) =& \frac{\partial}{\partial x^2}\left(\frac{1}{P_0N^2}|\Phi|^2\right) && (98)\\ =& \frac{1}{P_0N^2}\frac{\partial}{\partial x^2}\left(|\Phi|^2\right) && (99)\\ =& \frac{1}{P_0N^2r_0^2}\frac{Ldiff}{Ldisp}\frac{\partial}{\partial X^2}\left(|\Phi|^2,\right) && (100) \end{aligned}$$

thus

$$\frac{\partial^2}{\partial x^2}(|\phi|^2)\phi = \frac{\partial}{\partial x^2}\left(\frac{1}{P_0N^2}|\Phi|^2\right)\frac{1}{\sqrt{P_0}N}\Phi \tag{101}$$

$$= \frac{1}{P_0\sqrt{P_0}N^3}\frac{\partial}{\partial x^2}\left(|\Phi|^2\right) \tag{102}$$

$$= \frac{1}{P_0\sqrt{P_0}N^3r_0^2}\frac{Ldiff}{Ldisp}\frac{\partial}{\partial X^2}\left(|\Phi|^2\right). \tag{103}$$

In the same way

$$\frac{\partial^2}{\partial y^2}(|\phi|^2)\phi = \frac{\partial}{\partial y^2}\left(\frac{1}{P_0N^2}|\Phi|^2\right)\frac{1}{\sqrt{P_0}N}\Phi \tag{104}$$

$$= \frac{1}{P_0\sqrt{P_0}N^3}\frac{\partial}{\partial y^2}\left(|\Phi|^2\right) \tag{105}$$

$$= \frac{1}{P_0\sqrt{P_0}N^3r_0^2}\frac{Ldiff}{Ldisp}\frac{\partial}{\partial Y^2}\left(|\Phi|^2\right). \tag{106}$$

(B6) Computations of $\frac{\partial\phi^2}{\partial t^2}$

$$\frac{\partial}{\partial t} \to \frac{1}{T_0}\frac{\partial}{\partial \tau}, \tag{107}$$

then

$$\frac{\partial\phi}{\partial t} = \frac{1}{T_0}\frac{\partial\phi}{\partial\tau} \tag{108}$$

$$= \frac{1}{T_0}\frac{\partial}{\partial\tau}\left(\frac{1}{\sqrt{P_0}N}\Phi\right). \tag{109}$$

Given that

$$\phi(x,y,z,t) = \frac{1}{\sqrt{P_0}N}\Phi(X,Y,Z,\tau), \tag{110}$$

we have

$$\frac{\partial\phi}{\partial t} = \frac{1}{T_0}\frac{\partial\phi}{\partial\tau} \tag{111}$$

$$= \frac{1}{T_0}\frac{1}{\sqrt{P_0}N}\frac{\partial\Phi}{\partial\tau}. \tag{112}$$

Therefore

$$\frac{\partial \phi^2}{\partial t^2} = \frac{\partial}{\partial t}\left(\frac{\partial \phi}{\partial t}\right) \tag{113}$$

$$= \frac{\partial}{\partial t}\left(\frac{1}{T_0}\frac{1}{\sqrt{P_0}N}\frac{\partial \Phi}{\partial \tau}\right) \tag{114}$$

$$= \frac{\partial}{\partial t}\left(\frac{1}{T_0}\frac{1}{\sqrt{P_0}N}\frac{\partial \Phi}{\partial \tau}\right) \tag{115}$$

$$= \frac{1}{T_0}\frac{\partial}{\partial \tau}\left(\frac{1}{T_0}\frac{1}{\sqrt{P_0}N}\frac{\partial \Phi}{\partial \tau}\right) \tag{116}$$

$$= \frac{1}{T_0^2}\frac{1}{\sqrt{P_0}N}\frac{\partial \Phi^2}{\partial \tau^2}, \tag{117}$$

with

$$\frac{\partial}{\partial t} \rightarrow \frac{1}{T_0}\frac{\partial}{\partial \tau}. \tag{118}$$

(B7) Computation of $\frac{\partial \phi}{\partial z}$

$$\frac{\partial}{\partial z} \rightarrow \left(-\left(\frac{1}{T_0}\right)\beta_{eff}\frac{\partial f}{\partial \tau}dz + \left(\frac{z}{Ldisp}\right)\frac{\partial f}{\partial Z}\right) \tag{119}$$

$$\frac{\partial \phi}{\partial z} = \left(-\left(\frac{1}{T_0}\right)\beta_{eff}\frac{\partial f}{\partial \tau} + \left(\frac{z}{Ldisp}\right)\frac{\partial f}{\partial Z}\right)\phi \tag{120}$$

$$= \left(-\left(\frac{1}{T_0}\right)\beta_{eff}\frac{\partial}{\partial \tau} + \left(\frac{z}{Ldisp}\right)\frac{\partial}{\partial Z}\right)\frac{1}{\sqrt{P_0}N}\Phi \tag{121}$$

$$= -\frac{1}{\sqrt{P_0}N}\frac{1}{T_0}\beta_{eff}\frac{\partial \Phi}{\partial \tau} + \frac{1}{\sqrt{P_0}N}\frac{z}{Ldisp}\frac{\partial \Phi}{\partial Z} \tag{122}$$

APPENDIX C: Partial derivatives of the functions F_A, F_σ, F_ϑ, F_{σ_τ}, F_{ϑ_τ}

$$\frac{\partial F_A}{\partial A} = -\zeta_1 k_0\vartheta - \zeta_1 k_0\vartheta - \zeta_2\vartheta_\tau - (7\zeta_3 b_1)/2 - (231A^2\sqrt{2}c_0\zeta_4)/16 + a_1\zeta_2(35k_0^2\vartheta_\tau^2\sigma_\tau^2 + 156/\sigma_\tau^2)/8 + (3A^2 c_{X=Y}\zeta_{X=Y}\sqrt{2}(75k_0^2\vartheta^2\sigma^2 + 996/\sigma^2))/128 + (3A^2 c_{X=Y}\zeta_{X=Y}\sqrt{2}(75k_0^2\vartheta^2\sigma^2 + 996/\sigma^2))/12, \quad (123)$$

$$\frac{\partial F_\sigma}{\partial A} = (15A\sqrt{2}c_0\zeta_4\sigma)/4 + (A\sqrt{2}c_{X=Y}\zeta_{X=Y}(13k_0^2\vartheta^2\sigma^2 - 252/\sigma^2)\sigma)/32 + (15A\sqrt{2}c_{X=Y}\zeta_{X=Y}(-k_0^2\vartheta^2\sigma^2 - 12/\sigma^2)\sigma)/32, \quad (124)$$

$$\frac{\partial F_{\sigma_\tau}}{\partial A} = (15A\sqrt{2}c_0\zeta_4\sigma_\tau)/4 + (15A\sqrt{2}c_{X=Y}\zeta_{X=Y}(-k_0^2\vartheta^2\sigma^2 - 12/\sigma^2)\sigma_\tau)/32 + (15A\sqrt{2}c_{X=Y}\zeta_{X=Y}(-k_0^2\vartheta^2\sigma^2 - 12/\sigma^2)\sigma_\tau)/32, \quad (125)$$

$$\frac{\partial F_\vartheta}{\partial A} = 2A\sqrt{2}\zeta_4/(k_0\sigma^2) + (A\sqrt{2}c_{X=Y}\zeta_{X=Y})(24/\sigma^2 + 5k_0\vartheta)/(2k_0\sigma^2) + (A\sqrt{2}c_{X=Y}\zeta_{X=Y})(8/\sigma^2 - k_0\vartheta)/(2k_0\sigma^2), \quad (126)$$

$$\frac{\partial F_{\vartheta_\tau}}{\partial A} = 2A\sqrt{2}\zeta_4/(k_0\sigma_\tau^2) + (A\sqrt{2}c_{X=Y}\zeta_{X=Y})(8/\sigma^2 - k_0\vartheta)/(2k_0\sigma_\tau^2) + (A\sqrt{2}c_{X=Y}\zeta_{X=Y})(8/\sigma^2 - k_0\vartheta)/(2k_0\sigma_\tau^2), \quad (127)$$

$$\frac{\partial F_A}{\partial \sigma} = A^3 c_{X=Y}\zeta_{X=Y}\sqrt{2}(150k_0^2\vartheta^2\sigma - 1992/\sigma^3)/128, \quad (128)$$

$$\frac{\partial F_\sigma}{\partial \sigma} = 2\zeta_1 k_0\vartheta + \zeta_3 b_1 + (15A^2\sqrt{2}c_0\zeta_4)/8 + a_1\zeta_2(-7k_0^2\vartheta_\tau^2\sigma_\tau^2 - 28/\sigma_\tau^2)/4 + A^2\sqrt{2}c_{X=Y}\zeta_{X=Y}(26k_0^2\vartheta^2\sigma + 504/\sigma^3)\sigma/64 + A^2\sqrt{2}c_{X=Y}\zeta_{X=Y}(13k_0^2\vartheta^2\sigma^2 - 252/\sigma^2)/64 + (15A^2\sqrt{2}c_{X=Y}\zeta_{X=Y}(-k_0^2\vartheta^2\sigma^2 - 12/\sigma^2))/64, \quad (129)$$

$$\frac{\partial F_{\sigma_\tau}}{\partial \sigma} = (15A^2\sqrt{2}c_{_{X=Y}}\zeta_{_{X=Y}}(-2k_0^2\vartheta^2\sigma + 24/\sigma^3)\sigma_\tau)/64, \tag{130}$$

$$\frac{\partial F_{\vartheta}}{\partial \sigma} = -2A^2\sqrt{2}\zeta_4/(k_0\sigma^3) - 32\zeta_1/(k_0\sigma^5) - c_{_{X=Y}}\zeta_{_{X=Y}}A^2\sqrt{2}(24/\sigma^2 + 5k_0\vartheta)/(2k_0\sigma^3)$$
$$- 12c_{_{X=Y}}\zeta_{_{X=Y}}A^2\sqrt{2}/(k_0\sigma^5) - A^2\sqrt{2}c_{_{X=Y}}\zeta_{_{X=Y}}(8/\sigma^2 - k_0\vartheta)/(2k_0\sigma^3), \tag{131}$$

$$\frac{\partial F_{\vartheta_\tau}}{\partial \sigma} = -4c_{_{X=Y}}\zeta_{_{X=Y}}A^2\sqrt{2}/(\sigma^3 k_0\sigma_\tau^2), \tag{132}$$

$$\frac{\partial F_{A}}{\partial \sigma_\tau} = Aa_1\zeta_2(70k_0^2\vartheta_\tau^2\sigma_\tau. - 312/\sigma_\tau^3)/8, \tag{133}$$

$$\frac{\partial F_{\sigma}}{\partial \sigma_\tau} = a_1\zeta_2\sigma(-14k_0^2\vartheta_\tau^2\sigma_\tau + 56/\sigma_\tau^3)/4, \tag{134}$$

$$\frac{\partial F_{\sigma_\tau}}{\partial \sigma_\tau} = 2\zeta_2\vartheta_\tau + (15A^2\sqrt{2}c_0\zeta_4)/8 + \zeta_3 b_1 + a_1\zeta_2(-5k_0^2\vartheta_\tau^2\sigma_\tau^2 - 36/\sigma_\tau^2)/4$$
$$+ a_1\zeta_2\sigma_\tau(10k_0^2\vartheta_\tau^2\sigma_\tau + 72/\sigma_\tau^3)/4 + (15A^2\sqrt{2}c_{_{X=Y}}\zeta_{_{X=Y}}(-k_0^2\vartheta^2\sigma^2 - 12/\sigma^2))/32, \tag{135}$$

$$\frac{\partial F_{\vartheta}}{\partial \sigma_\tau} = 0, \tag{136}$$

$$\frac{\partial F_{\vartheta_\tau}}{\partial \sigma_\tau} = -2A^2\sqrt{2}\zeta_4/(k_0\sigma_\tau^3) - 16\zeta_2 a_1\vartheta_\tau/\sigma_\tau^3 + 32\zeta_2/(k_0\sigma_\tau^5)$$
$$- \zeta_{_{X=Y}}c_{_{X=Y}}A^2\sqrt{2}(8/\sigma^2 - k_0\vartheta)/(k_0\sigma_\tau^3), \tag{137}$$

$$\frac{\partial F_{A}}{\partial \vartheta} = -A\zeta_1 k_0 + (75A^3 c_{_{X=Y}}\zeta_{_{X=Y}}\sqrt{2}k_0^2\vartheta\sigma^2)/64, \tag{138}$$

$$\frac{\partial F_{\sigma}}{\partial \vartheta} = 2\zeta_1 k_0 \sigma + (13 c_{_{X=Y}} \zeta_{_{X=Y}} A^2 \sqrt{2} k_0^2 \vartheta \sigma^3)/32, \tag{139}$$

$$\frac{\partial F_{\sigma_\tau}}{\partial \vartheta} = -(15 A^2 \sqrt{2} c_{_{X=Y}} \zeta_{_{X=Y}} k_0^2 \vartheta \sigma^2 \sigma_\tau)/32, \tag{140}$$

$$\frac{\partial F_{\vartheta}}{\partial \vartheta} = -4\zeta_1 k_0 \vartheta + (50 \zeta_{_{X=Y}} c_{_{X=Y}} A^2 \sqrt{2})/(9\sigma^2), \tag{141}$$

$$\frac{\partial F_{\vartheta_\tau}}{\partial \vartheta} = -(\zeta_{_{X=Y}} c_{_{X=Y}} A^2 \sqrt{2})/(4\sigma_\tau^2), \tag{142}$$

$$\frac{\partial F_A}{\partial \vartheta_\tau} = A\zeta_2 + (35/4) A a_1 \zeta_2 k_0^2 \vartheta_\tau \sigma_\tau^2, \tag{143}$$

$$\frac{\partial F_{\sigma}}{\partial \vartheta_\tau} = -(7 a_1 \zeta_2 \sigma k_0^2 \vartheta_\tau \sigma_\tau^2)/2, \tag{144}$$

$$\frac{\partial F_{\sigma_\tau}}{\partial \vartheta_\tau} = 2\zeta_2 \sigma_\tau - 5/2 a_1 \zeta_2 \sigma_\tau^3 k_0^2 \vartheta_\tau, \tag{145}$$

$$\frac{\partial F_{\vartheta}}{\partial \vartheta_\tau} = 0, \tag{146}$$

$$\frac{\partial F_{\vartheta_\tau}}{\partial \vartheta_\tau} = 8\zeta_2 a_1/\sigma_\tau^2 - 4\zeta_2 k_0 \vartheta_\tau. \tag{147}$$

Bibliography

[1] B. A. Malomed, D. Mihalache, F. W. Wise, and L. Torner, *J. Opt. B: Quantum Semiclass. Opt.* **7**, R53 (2005).

[2] Y. Kivshar, G.P. Agrawal, Optical Solitons: From Fibers to Photonic Crystals, Academic Press, San Diego, 2003.

[3] D. Suter and T. Blasberg, *Phys. Rev. A* **48**, 4583 (1993).

[4] C. Rotschild, O. Cohen, O. Manela, M. Segev, and T. Carmon, *Phys. Rev. Lett.* **95**, 213904 (2005).

[5] W. Krolikowski, O. Bang, N. I. Nikolov, D. Neshev, J. Wyller, J.J. Rasmussen, and D. Edmundson, *J. Opt. B* **6**, S288 (2004).

[6] H. Tagwo, A. Mohamadou, C. G. Latchio Tiofack, and T. C. Kofane, *Optik* **144** , 246 (2017).

[7] O. Bang, W. Krolikowski, J. Wyller, and J. J. Rasmussen, *Phys. Rev. E* **66**, 046619 (2002).

[8] M. Peccianti, K. A. Brzdakiewicz, and G. Assanto, *Opt. Lett.* **27**, 1460 (2002).

[9] N. I. Nikolov, D. Neshev, W. Krolikowski, O. Bang, J. J. Rasmussen, and P. L. Christiansen, *Opt. Lett.* **29**, 286 (2004).

[10] Z. Xu, Y. V. Kartashov, and L. Torner, *Opt. Lett.* **30**, 3171 (2005).

[11] A. S. Desyatnikov, Yu. S. Kivshar, and L. Torner, *Prog. Opt.* **47**, 291 (2005).

[12] A. I. Yakimenko, Yu. A. Zaliznyak, and Yu. S. Kivshar, *Phys. Rev. E* **71**, 065603 (2005).

[13] D. Briedis, D. E. Petersen, D. Edmundson, W. Krolikowski, and O. Bang, *Opt. Express* **13**, 435 (2005).

[14] A. S. Desyatnikov and Yu. S. Kivshar, *Phys. Rev. Lett.* **88**, 053901 (2002).

[15] A. S. Desyatnikov, A. A. Sukhorukov, and Yu. S. Kivshar, *Phys. Rev. Lett.* **95**, 203904 (2005).

[16] E. Desurvire, J. R. Simpson, and P. C. Becker, *Opt. Lett.* **12**, 888 (1987).

[17] G. P. Agrawal, Lightwave technology: telecommunication systems, John Wiley & Sons, 2005.

[18] G. P. Agrawal, *Phys. Rev. A* **44**, 7493 (1991).

[19] M. Manousakis, S. Droulias, P. Papagiannis, and K. Hizanidis, *Opt. Commun.* **213**, 293 (2002).

[20] S. I. Fewo and T. C. Kofane, *Opt. Commun.* **281**, 2893 (2008).

[21] S. I. Fewo, C. M. Ngabireng, and T. C. Kofane, *J. Phys. Soc. Jpn.* **77**, 074401 (2008).

[22] C. G. Latchio Tiofack, A. Mohamadou, T. C. Kofane, and A. B. Moubissi, *Phys. Rev. E* **80**, 066604 (2009).

[23] M. Soljacic and M. Segev, *Phys. Rev. Lett.* **86**, 420 (2001).

[24] I. Towers, and B. A. Malomed, *J. Opt. Soc. Am. B* **19**, 537 (2002).

[25] M. Matuszewski, M. Trippenbach, B. A. Malomed, E. Infeld, and A. A. Skorupski, *Phys. Rev. E* **70**, 016603 (2004).

[26] Y. J. He, H. H. Fan, J. W. Dong, and H. Z. Wang, *Phys. Rev. E* **74**, 016611 (2006).

.

[27] A. Kamagate, P. Grelu, P. Tchofo-Dinda, J. M. Soto- Crespo, and N. Akhmediev, *Phys. Rev. E* **79**, 026609 (2009).

[28] M. Djoko and T. C. Kofane, *Opt. Commun.* **416**, 190201 (2018).

[29] B. Malomed, L. Torner, F. Wise, and D. Mihalache, *J. Phys. B: At. Mol. Opt. Phys.* **49**, 170502 (2016).

[30] D. Zanga, S. I. Fewo, C. B. Tabi, and T. C. Kofane, *Commun. Nonl. Sci. Num. Simul.* **80**, 104993 (2020).

[31] C. B. Tabi, H. Tagwo, C. G. L. Tiofack, and T. C. Kofane, *Opt. Lett.* **47**, 5557-5560 (2022).

[32] C.G. Tiofack Latchio, C.B. Tabi, H. Tagwo, T.C. Kofane, *J. Opt.* **25**, 054001 (2023).

[33] C. B. Tabi, H. Tagwo, and T. C. Kofane, *Phys. Rev. E* **106**, 054201 (2022).

[34] E. Conway, Optical fiber communications principles and practice, Scientific e-Resources, 2019.

[35] A. G. Bell, *Science.* **11**, 130-134 (1880).

[36] J. Hecht, City of light: the story of fiber optics, Oxford University Press, USA, 2004.

[37] J. D. Montgomery and C. DeCusatis, History of fiber optics, Fiber optic data communication: technological trends and advances, 2002.

[38] J. D. Montgomery, Communication through the Ages, Fiber Optic Data Communication: Technology Advances and Futures, 2002.

[39] Y. Koike and K. Koike, Optical Fibers, Polymer Science: A Comprehensive Reference, 10 Volume Set, Elsevier, 2012.

[40] G. P. Agrawal, Nonlinear fiber optics, In Nonlinear Science at the Dawn of the 21st Century, Springer, 2000.

[41] T. E. Stern, G. Ellinas, and K. Bala, Multiwavelength optical networks: architectures, design, and control, Cambridge University Press, 2009.

[42] L. F. Mollenauer, R. H. Stolen, and J. P. Gordon, *Phys. Rev. Lett.* **45**, 1095 (1980).

[43] H. Nakatsuka, D. Grischkowsky, and A. C. Balant, *Phys. Rev. Lett.* **45**, 910 (1981).

[44] J. M. Senior, and M. Y. Jamro, Optical fiber communications: principles and practice, Pearson Education, 2009.

[45] G. P. Agrawal, Fiber-optic communication systems, John Wiley & Sons, 2012.

[46] P. L. Christiansen, M. P. Sorensen, and A. C. Scott, Nonlinear Science at the Dawn of the 21st Century, Springer Science & Business Media, 2000.

[47] J. A. Buck, Nonlinear effects in optical fibers, Fiber Optics Handbook, 2002.

[48] P. R. Trischitta, and W. C. Marra, *IEEE Communications Magazine* **36**, 62-66 (1998).

[49] T. Li, *Proceedings of the IEEE* **81**, 1568-1579 (1993).

[50] T. E. Stern, G. Ellinas, and K. Bala, Multiwavelength optical networks: architectures, design, and control, Cambridge University Press, 2009.

[51] Y. Kimura, K. Suzuki, and M. Nakazawa, *Electron. Lett.* **24**, 1656-1657 (1989).

[52] B. Pedersen, A. Bjarklev, J. H. Povlsen, K. Dybdal, and C. C. Larsen, *J. Light. Technol.* **9**, 1105-1112. (1991).

[53] E. Desuryire, C. R. Giles, J. R. Simpson, and J. L. Zyskind, *Opt. Lett.* **14**, 1266 (1989).

[54] C. R. Giles, E. Desurvire, J. R. Talman, J. R. Simpson, and P. C. Becker, *J. Light. Technol.* **7**, 651 (1989).

[55] G. P. Agrawal, *Phys. Rev. E* **48**, 2316 (1993).

[56] J. S. Russell, Report on waves, Fourteenth meeting of the British Association for the Advancement of Science, London: John Murray, 1844.

[57] A. Hasegawa, and F. Tappert, *Appl. Phys. Lett.* **23**, 142-144 (1973).

[58] A. Hasegawa, and F. Tappert, *Appl. Phys. Lett.* **23**, 171-173. (1973).

[59] Y Silberberg, *Opt. Lett.* **15**, 1282-1284. (1990).

[60] F. Mollenauer, R. H. Stolen, and J. P. Gordon, *Phys. Rev. Lett.* **45**, 1095. (1980).

[61] S. Trillo, and W. Torruellas, Spatial solitons, Berlin, Springer-Verlag, 2001.

[62] G. Assanto, Nematicons: Spatial optical solitons in nematic liquid crystals, New York, John Wiley & Sons, 2012.

[63] M. Peccianti, and G. Assanto, *Phys. Rep.* **516**, 147-208. (2012).

[64] Q. Guo, D. Lu, and D. Deng, Nonlocal spatial optical solitons, Advances in Nonlinear Optics, 2015.

[65] P. L. Kelley, *Phys. Rev. Lett.* **15**, 1005-1008.. (1965).

[66] L. Bergé, *Phys. Rep.* **303**, 259-370. (1998).

[67] J. H. Marburger and E. Dawes, *Phys. Rev. Lett.* **21**, 556. (1968).

[68] E. L. Dawes, and J. H. Marburger, *Phys. Rev.* **179**, 862-868. (1969).

[69] O. Bang, W. Królikowski, J. Wyller, and J. J. Rasmussen, *Phys. Rev. E* **66**, 0466198. (2002).

[70] N. I. Nikolov, D. Neshev and O. Bang, *Phys. Rev. E* **68**, 036614. (2003).

[71] A.W. Snyder, and D.J. Mitchell, *Science.* **276**, 1538-1541. (1997).

[72] B. A Malomed, D. Mihalache, F. Wise, and L. Torner, *J. Opt. B: Quantum Semiclass. Opt.* **7**, R53. (2005).

[73] P. Grelu, and J. M. Soto-Crespo, Dissipative Solitons: From optics to biology and medicine, Lecture Notes in Physics (Springer, 2008), 2008.

[74] V. Skarka and N. B. Aleksi´c, *Phys. Rev. Lett.* **96**, 013903. (2006); N. B. Aleksi´c, V. Skarka, D. V. Timotijevi´c, and D. Gauthier, *Phys. Rev. A* **75**, 061802(R). (2007); V. Skarka, D. V. Timotijevi´c, and N. B. Aleksi´c, *J. Opt. A: Pure Appl. Opt.* **10**, 075102. (2008).

[75] W. Chen, Q. Wang, S. J. hi, Q. Kong, Y. Chen, and M. Shen, *J. Phys. B At. Mol. Opt. Phys.* **50**, 135401 (2017).

[76] W. Królikowski, O. Bang, N. I. Nikolov, D. Neshev, J. Wyller, J. J. Rasmussen, and D. Edmundson, *J. Opt. B.* **6**, 288-294 (2004).

[77] C. Sun, C. Barsi, and J. W. Fleischer, *Opt. Express.* **16**, 20676-20686 (2008).

[78] W. Chen, Q. Wang, J. Shi, M.Shen, and J. Wyller, *Opt. Commun.* **403**, 22-26 (2017).

[79] T.P. Horikis, D.J. Frantzeskakis, *Opt. Lett.* **41** 583-586 (2016).

[80] W. Królikowski, O. Bang, J. J. Rasmussen, and J. Wyller, *Phys. Rev. A* **82**, 013826 (2010).

[81] L. Chen, Q. Wang, M. Shen, H. Zhao, Y. Y. Lin, C. C. Jeng, R. K. Lee, and W. Krolikowski, *Opt. Lett.* **38**, 13-15 (2013).

[82] M. Shen, D. Wu, H. Zhao and B. Li, *J. Phys. B* **47**, 155401 (2014).

[83] W. Królikowski, O. Bang, J. J. Rasmussen, and J. Wyller, *Phys. Rev. E* **64**, 016612-016619 (2001).

[84] Qi. Guo, Nonlocal spatial solitons and their interactions, In Optical Transmission, Switching, and Subsystems, SPIE, 2004.

[85] T. P. Horikis, and D. J. Frantzeskakis, *Opt. Lett.* **41**, 583-586 (2016).

[86] W. Krolikowski, O. Bang, D. Briedis, A. Dreischuh, D. Edmundson, B. Luther-Davies, D. Neshev, N. Nikolov, D. E. Petersen, J. J. Rasmussen, and J. Wyller, Nonlocal solitons, In Nonlinear Optics Applications, SPIE, 2005.

[87] J. T. Manassah, *Opt. Lett.* **17**, 1259-1261 (1992).

[88] N. N. Rosanov, Spatial hysteresis and optical patterns, Springer Science and Business Media, 2002.

[89] C. Rotschild, O. Cohen, O. Manela, M. Segev, and T. Carmon, *Phys. Rev. Lett.* **95**, 213904 (2005).

[90] S. Skupin, O. Bang, D. Edmundson, and W. Królikowski, *Phys. Rev. E* **73**, 066603 (2006).

[91] H. Li, *Waves in Random Media* **24**, 191-202 (2014).

[92] K. S. Bezuhanov, A. A. Dreischuh, W. Krolikowski, *Phys. Rev. A* **77** 033825 (2008).

[93] D.J. Kaup, B.A. Malomed, *Physica D* **87** 155 (1995).

[94] A. Ankiewicz, N. Akhmediev, N. Devine, *Opt. Fiber Technol.* **13** 91 (2007).

[95] P. Grelu, N. Akhmediev, *Nat. Photonics* **6** 84 (2012).

[96] A. Djazet, S.I. Fewo, C.B. Tabi, T.C. Kofané, *Appl. Phys. B* **127** 151 (2021).

[97] T. Mayteevarunyoo, B.A. Malomed, D.V. Skryabin, *Opt. Express* **26** 8849 (2018).

[98] M. Abemgnigni Njifon, C.B. Tabi, T.C. Kofané, *J. Opt. Soc. Am. B* **37** A331 (2020).

[99] L. Megne Tiam, C.B. Tabi, T.C. Kofané, *Phys. Rev. E* **102** 042207 (2020).

[100] L. Tiam Megne, C.B. Tabi, J.A. Ambassa Otsobo, C.M. Muiva, T.C. Kofané, *Nonlinear Dyn.* **111** 20289 (2023).

[101] P. Otlaadisa, C.B. Tabi, T.C. Kofané, *Phys. Rev. E* **103** 052206 (2021).

[102] C.B. Tabi, P. Otlaadisa, T.C. Kofané, *Phys. Lett. A* **449** 128334 (2022).

[103] P. Legoya, A.S. Etémé, C.B. Tabi, A. Mohamadou, T.C. Kofané, *Chaos Solitons Fractals* **146** 112599 (2022).

[104] C.D. Bansi Kamdem, P.A. Ndjawa Yomi, C.B. Tabi, A. Mohamadou, *Eur. Phys. J. Plus* **138** 176 (2023).

[105] B.P. Edouma Biloa, C.B. Tabi, H.P. Ekobena Fouda, T.C. Kofané, *Phys. Scr.* **98** 115230 (2023) .

[106] C.D. Bansi, C.B. Tabi, A. Mohamadou, *Chaos Solitons Fractals* **109** 170 (2018).

[107] C.B. Tabi, A.S. Etémé, A. Mohamadou, *Physica A* **474** 186 (2017).

[108] G.P. Agrawal, Nonlinear Fiber Optics, 5th edn, Academic Press, San Diego, 2013.

[109] Y. Kuramoto, *Prog. Theor. Phys.* **94** 321 (1995).

[110] D. Tanaka, Y. Kuramoto, *Phys. Rev. E* **68** 026219 (2003).

[111] Y. Kuramoto, D. Battogtokh, H. Nakao, *Phys. Rev. Lett.* **81** 3543 (1998).

[112] D.M. Abrams, S.H. Strogatz, *Phys. Rev. Lett.* **93** 174102 (2004).

[113] V. Garcia-Morales, K. Krischer, *Phys. Rev. Lett.* **100** 054101 (2008).

[114] H. Varela, C. Beta, A. Bonnefont, K. Krischer, *Phys. Rev. Lett.* **94** 174104 (2005).

[115] V. Garcia-Morales, R.W. Holzel, K. Krischer, *Phys. Rev. E* **78** 026215 (2008).

List of publications

[1] Ghislaine Flore Kabadiang Ngon, Conrad B. Tabi and Timoléon C. Kofané, "*Dissipative light bullets in a doped and weakly nonlocal optical fiber*", Phys. Lett. A. **494**, 129291 (2024).

Physics Letters A 494 (2024) 129291

Contents lists available at ScienceDirect

Physics Letters A

journal homepage: www.elsevier.com/locate/pla

Letter

Dissipative light bullets in a doped and weakly nonlocal optical fiber

Ghislaine Flore Kabadiang Ngon [a], Conrad Bertrand Tabi [b,*], Timoléon Crépin Kofané [b,a]

[a] Laboratory of Mechanics, Department of Physics, Faculty of Science, University of Yaoundé I, P.O. Box 812, Yaoundé, Cameroon
[b] Department of Physics and Astronomy, Botswana International University of Science and Technology, Private Mail Bag 16 Palapye, Botswana

ARTICLE INFO

Communicated by B. Malomed

Keywords:
Dissipative light bullet
Nonlocal complex Ginzburg-Landau equation
Optical fiber amplifiers

ABSTRACT

The letter introduces an extended (3+1)-dimensional [(3+1)D] nonlocal cubic complex Ginzburg-Landau equation describing the dynamics of dissipative light bullets in optical fiber amplifiers under the interplay between dopants and a spatially nonlocal nonlinear response. The model equation includes the effects of fiber dispersion, linear gain, nonlinear loss, fiber nonlinearity, atomic detuning, linear and nonlinear diffractive transverse effects, and nonlocal nonlinear response. A system of coupled ordinary differential equations for the amplitude, temporal, and spatial pulse widths and position of the pulse maximum, unequal wavefront curvatures, chirp parameters, and phase shift is derived using the variational technique. A stability criterion is established, where a domain of dissipative parameters for stable steady-state solutions is found. Direct integration of the proposed nonlocal evolution equation is performed, which allows us to investigate the evolution of the Gaussian beam along a doped nonlocal optical fiber, showing stable self-organized dissipative spatiotemporal light bullets.

1. Introduction

Optical solitons have promising potential to become principal information carriers in telecommunication due to their capability to propagate long-distance signals without attenuation and change their shapes. One of the major goals in the field of soliton physics is the production of light fields that are localized in all three dimensions of space and time, which we will refer to as 3D spatiotemporal solitons or light bullets. This results from the simultaneous balance of diffraction and the group velocity dispersion (GVD) by the transverse self-focusing and nonlinear phase modulation in the longitudinal direction, respectively [1].

Considerable attention is being paid to theoretically and experimentally analyzing spatial optical solitons' dynamics in material with local nonlinear and nonlocal responses [2–4]. Local nonlinearity of optical media is usually approximated by a local function of the light intensity assuming the refractive index change at a given spatial location depends solely on the light intensity at the same location, while nonlocality means that the change of the refractive index in a particular point is determined by the light intensity not only in the same point but also in its vicinity. Recently, it has been revealed that nonlocality can provide new effects such as strong modification of modulational instability [5,6], suppression of beam collapse [7], dramatic change of the soliton interaction [8,9], formation of multi-soliton bound states [10], stabilization of spatially localized vortex solitons [11], symmetry breaking azimuthal instability [12,13] as well as stabilization of different nonlinear structures such as ringlike clusters of many solitons [14] and modulated localized vortex beams or azimuthons [15].

In long-distance soliton propagation, the energy of the soliton decreases because of fiber losses. This would produce soliton broadening because a reduced peak power weakens the self-phase modulation (SPM) effect necessary to counteract the effect of GVD. Therefore, soliton must be amplified periodically using either the lumped or the distributed amplification scheme to overcome the effect of fiber losses. It was demonstrated that by doping the optical fiber with rare earth ions, such as Neodymium, Erbium, Praseodymium, and Ytterbium ions, just to name a few, energy gains were made in addition to the optical fiber. Thus, the light signal could be amplified each time it weakened, and the loss of information could be avoided [16]. On the other hand, there are interesting studies on the pulse propagation problem in doped fiber amplifiers within the rate equation approximation, the governing equation being the cubic complex Ginzburg-Landau (CGL) equation and its variants [17–22]. Dissipative solitons can be propagated in such active fiber over long distances. In some previous studies [23–29], multidimensional spatiotemporal optical solitons, i.e., both (2+1)-dimensional [(2+1)D] and (3+1)-dimensional [(3+1)D] dissipative optical bullets were considered taking the (2+1)D and (3+1)D family of CGL equations. Stable spatiotemporal dissipative solitons have been reported.

* Corresponding author.
E-mail addresses: ngonghislaine@yahoo.fr (G.F. Kabadiang Ngon), tabic@biust.ac.bw (C.B. Tabi), tckofane@gmail.com (T.C. Kofané).

https://doi.org/10.1016/j.physleta.2023.129291
Received 14 April 2023; Received in revised form 6 December 2023; Accepted 19 December 2023
Available online 27 December 2023

Among them are stationary stable and pulsating solutions, double, quadruple, sixfold, eightfold, and tenfold bullet complexes, self-trapped necklace-ring, ring-vortex solitons, uniform ring beams, spherical and rhombic distributions of light bullets, fundamental and cluster solitons, respectively. Recently, the stability diagram obtained from the Lenz transformation and the linear stability analysis has revealed that higher values of the quintic nonlocality contribute to reducing the modulational instability (MI) in weakly cubic-quintic nonlocal nonlinear media [30]. Very recently, it has been shown that instability regions from the pure quartic MI gain in weakly nonlocal birefringent fibers are more expanded due to nonlocality, which was confirmed via direct numerical simulations showing the emergence of Akhmediev breathers [31,32]. For a nonlinear saturable media with competing nonlocal nonlinearity, it was reported that the quenching effect of the nonlocal nonlinearity on the MI is corrected, especially when the saturable index and the nonlocality range are well-balanced [33].

The main purpose of the present work is to investigate (3+1)D dissipative light bullets in fiber amplifiers under the interplay between dopant and a spatially nonlocal nonlinear response which, to the best of our knowledge, has not yet been proposed in the literature. The dopant is modeled as a two-level system whose dynamic response is governed by the population and dipole relaxation times. For incident optical of width such that, in cases of weak nonlocality and in the paraxial wave approximation, the (3+1)D cubic complex Ginzburg-Landau equation is derived, which includes the effects of fiber dispersion, linear gain, nonlinear loss, fiber nonlinearity, atomic detuning, linear and nonlinear diffractive transverse effects, and nonlocal nonlinear response. We mainly focus on the localized Gaussian solution in the form of three-dimensional traveling waves. Our main purpose is to assess the role played by a weak spatial nonlocality term in the shape formation of a dissipative light bullet. A system of eight coupled first-order differential equations of the solution's parameters of interest is derived on the basis of variational equations resulting from the Euler-Lagrange equations.

The remaining part of this paper is organized as follows. In Sec. 2, we derive the (3+1)D nonlocal cubic complex Ginzburg-Landau (CGL) equation governing the dynamics of the dissipative light bullets in a doped and weakly nonlocal nonlinear medium. In Sec. 3, the dynamic characteristics of the dissipative light bullets, such as the amplitude, temporal and spatial pulse widths, the position of the pulse maximum, unequal wavefront curvatures, chirp parameters, and the phase shift in specially designed media, are studied using the variational technique. In Sec. 4, a stability criterion for steady-state solutions of the (3+1)D nonlocal cubic CGL equation is established, fixing a domain of dissipative light bullets parameters. In Sec. 5, the direct integration of the (3+1)D nonlocal cubic CGL equation with the Runge-Kutta and the split-step Fourier methods have been carried out, showing stable self-organized dissipative spatiotemporal light bullets. Some concluding remarks are given in Sec. 6

2. Derivation of the nonlinear evolution equation for electromagnetic pulse propagation in doped and weakly nonlocal nonlinear media

The light pulse propagation problem in doped optical fiber can be solved by defining a complex dielectric constant as follows [17]:

$$\epsilon(\omega) = n_f^2 + 2in_f\frac{\alpha_f}{k_0} + \chi_a(\omega), \tag{1}$$

where ω is the optical frequency, with α_f being the fiber loss defined by:

$$\alpha_f = \frac{10}{L}\log\frac{P_{out}}{P_{in}}(\mathrm{dB/km}), \tag{2}$$

where P_{in} is the input light pulse power, P_{out} is the output light pulse power and L, the length of the optical fiber. k_0 is the wavenumber given by $k_0 = \omega_0/c$, with c being the light speed, and ω_0, the carrier frequency. $\chi_a(\omega)$ is the atomic susceptibility governing the response of the dopant in the optical fiber, which is determined by [17]

$$\chi_a(\omega) = \frac{g_p}{k_0}\frac{(\omega-\omega_a)T_2 - i}{1+(\omega-\omega_a)^2T_2^2}, \tag{3}$$

with the peak gain $g_p = \sigma(N_2 - N_1)$. The parameter σ is a transition cross-section, while N_1 and N_2 are the atomic densities for the two-level system's lower and upper energy levels. ω_a is the atomic resonance frequency, and T_2 is the relaxation time. Moreover, one can expand the function $\chi_a(\omega)$ in Taylor's series up to the second order in the vicinity of the carrier frequency ω_0 and find [17]

$$\chi_a(\omega) = \frac{g_p}{k_0}\left[\frac{\delta - i}{1+\delta^2} + \frac{1-\delta^2+2i\delta}{(1+\delta^2)^2}(\omega-\omega_0)T_2 + \frac{\delta(\delta^2-3)+i(1-3\delta^2)}{(1+\delta^2)^3}(\omega-\omega_0)^2T_2^2\right], \tag{4}$$

where $\delta = (\omega_0 - \omega_a)T_2$ is the detuning parameter. The term n_f, in Eq. (1), is the refractive index of the fiber, including linear, nonlinear, doping, and spatial-nonlocality phenomena. The given expression of n_f is [34]

$$n_f = n_0(\omega) + n_2\frac{\int R(x-x',y-y')I(x',y')dx'dy'}{\int R(x-x',y-y')dx'dy'}. \tag{5}$$

Here, $n_0(\omega)$ is the linear refractive index, n_2 represents the nonlinear change in the refractive index, $R(x-x',y-y')$ is the nonlocal response function which determines the spatial extent of nonlocality. $I(x',y')$ is the nonlocal intensity which acts not only on the local points *(x,y)*, but also in the neighboring points and can be evaluated as [34]

$$I(x',y') = I(x,y) + \frac{1}{2}\frac{\partial^2}{\partial x^2}I(x,y)(x-x')^2 + \frac{1}{2}\frac{\partial^2}{\partial y^2}I(x,y)(y-y')^2 + \frac{\partial^2}{\partial x\partial y}I(x,y)(x-x')(y-y'), \tag{6}$$

where $I(x,y)$ is the external action of the intensity on the points *(x,y)*. Using this assumption, Eq. (5) can be rewritten as

$$n_f = n_0(\omega) + n_2|\vec{E}|^2 + \frac{n_2\gamma_{xx}}{2}\frac{\partial^2}{\partial x^2}(|\vec{E}|^2) + \frac{n_2\gamma_{yy}}{2}\frac{\partial^2}{\partial y^2}(|\vec{E}|^2) + \frac{n_2\gamma_{xy}}{2}\frac{\partial^2}{\partial x\partial y}(|\vec{E}|^2). \tag{7}$$

In Eq. (7), we have considered $I(x,y) = |\vec{E}|^2$, where $\vec{E}$ is the electric-field vector. The coefficients γ_{xx}, γ_{yy} and γ_{xy} represent the measures of weak nonlocality degree in the transverse coordinates x and y, respectively. These nonlocality degree coefficients are determined by the relations

$$\gamma_{\xi\xi} = \frac{\int_{-\infty}^{\infty}R(\xi-\xi',\eta-\eta')(\xi-\xi')^2d\xi'd\eta'}{\int_{-\infty}^{\infty}R(\xi',\eta')d\xi'd\eta'}, \qquad \gamma_{\eta\eta} = \frac{\int_{-\infty}^{\infty}R(\eta-\eta',\xi-\xi')(\eta-\eta')^2d\eta'd\xi'}{\int_{-\infty}^{\infty}R(\eta',\xi')d\eta'd\xi'}, \tag{8}$$

and

$$\gamma_{\xi\eta} = \frac{\int_{-\infty}^{\infty}R(\xi-\xi',\eta-\eta')(\xi-\xi')(\eta-\eta')d\xi'd\eta'}{\int_{-\infty}^{\infty}R(\xi',\eta')d\xi'd\eta'}, \tag{9}$$

for $(\xi,\eta) = (x,y)$. The term $\gamma_{\xi\eta}$ can be neglected in a suitably chosen and rotated coordinate system. Here, we consider the case of the so-called Gaussian nonlocal response functions [35]

$$R(r-r') = \frac{1}{\pi\sigma^2}e^{-\frac{(r-r')}{\sigma^2}}, \tag{10}$$

with a characteristic width σ defining the degree of nonlocality. Indeed, it has been shown that, for a Gaussian response, $\gamma_{\xi\xi} = w_{R\xi}^2/2$, with $w_R = 0.1\sigma/\sqrt{2}$. We recall that Eq. (6) is justified [34] when the nonlocality becomes weak, that is, $\gamma_{\xi\xi} \ll 1$. Another necessary parameter to consider, as much as the dielectric constant, in the propagation of light in a doped optical fiber, is the propagation constant around the frequency ω given as follows [17]

$$\beta(\omega) = \frac{\omega}{c}\sqrt{\epsilon(\omega)}. \tag{11}$$

From Eqs. (1)-(7), we can rewrite the propagation constant expressed in Eq. (11). Given that the term $n_0(\omega)\frac{\omega}{c}$ corresponds to the propagation constant of the undoped fiber denoted $\beta_f(\omega)$, we then obtain the following equation

$$\begin{aligned}\beta(\omega) = \beta_f(\omega) &+ \frac{\omega}{c}n_2|\vec{E}|^2 + \frac{\omega}{c}\frac{n_2\gamma_{xx}}{2}\frac{\partial^2}{\partial x^2}(|\vec{E}|^2)\\ &+ \frac{\omega}{c}\frac{n_2\gamma_{yy}}{2}\frac{\partial^2}{\partial y^2}(|\vec{E}|^2) + i\alpha_f + i\alpha_f\frac{n_2}{n_0}|\vec{E}|^2\\ &+ i\alpha_f\frac{n_2}{n_0}\frac{\gamma_{xx}}{2}\frac{\partial^2}{\partial x^2}(|\vec{E}|^2) + i\alpha_f\frac{n_2}{n_0}\frac{\gamma_{yy}}{2}\frac{\partial^2}{\partial y^2}(|\vec{E}|^2)\\ &+ \frac{1}{2}\frac{\omega}{c}\frac{\chi_a}{n_0}.\end{aligned} \tag{12}$$

In the framework of Maxwell's equations, we analyze the propagation of optical fields, and we get the following wave equation for each component of the field vector $\vec{E}$

$$\Delta\vec{E} - \mu_0\frac{\partial^2\vec{D}}{\partial t^2} = 0. \tag{13}$$

The operator Δ is the Laplacian operator whose expression in cartesian coordinates is $\Delta = \frac{\partial^2}{\partial x^2} + \frac{\partial^2}{\partial y^2} + \frac{\partial^2}{\partial z^2}$. The Fourier transform of the quantity $\vec{D}$, known as the electric displacement vector, is related to that of the electric field via the constitutive relation

$$\tilde{D}(r, \omega-\omega_0) = \epsilon_0\epsilon(\omega)\tilde{E}(r, \omega-\omega_0), \tag{14}$$

where ϵ_0 is the vacuum permittivity and $\tilde{E}$ denotes the Fourier transform of the electric field $\vec{E}$ defined as

$$\tilde{E}(r, \omega-\omega_0) = \int_{-\infty}^{\infty}\vec{E}(r,t)\exp(i(\omega-\omega_0)t)dt. \tag{15}$$

In the frequency domain, Eq. (13) takes the form of the Helmholtz equation

$$\Delta\tilde{E} + \beta^2(\omega)\tilde{E} = 0. \tag{16}$$

The electric field vector $\vec{E}(r,t)$ is written as

$$\vec{E}(r,t) = \frac{1}{2}(\vec{e}\phi(x,y,z,t)\exp[i(\beta_0 z - \omega_0 t)] + c.c.). \tag{17}$$

Here, $\phi(x,y,z,t)$ is the slowly varying envelope function which represents the light pulse carrying the information, $c.c.$ is the complex conjugate, $\beta_0 = n_0(\omega_0)k_0$ is the propagation constant at the carrier frequency ω_0, and $\vec{e}$ is the polarization unit vector. The optical fiber has a cylinder shape with axis (oz), therefore, the radius r is defined as $r = \sqrt{x^2+y^2}$. For optical beams, the paraxial and quasi-monochromatic approximations correspond to neglecting the $\frac{\partial^2}{\partial z^2}$ derivatives of the slowly varying amplitude on the grounds that $\left|\frac{\partial^2\phi}{\partial z^2}\right| \ll \beta_0\left|\frac{\partial\phi}{\partial z}\right|$. This procedure leads to

$$i\frac{\partial\phi}{\partial z} + \frac{1}{2\beta_0}\left(\frac{\partial^2\phi}{\partial x^2} + \frac{\partial^2\phi}{\partial y^2}\right) + (\beta(\omega) - \beta_0(\omega))\phi = 0. \tag{18}$$

Fiber dispersion plays a critical role in the propagation of optical pulses because different spectral components associated with pulse broadening can be detrimental to optical communication systems. Mathematically, the effects due to fiber dispersion are accounted for by expanding the mode-propagation coefficient $\beta_f(\omega)$ in a Taylor series about the carrier frequency ω_0 at which the pulse spectrum is centred [20]

$$\begin{aligned}\beta_f(\omega, |\phi|^2) = \beta_0 &+ i\beta_1\frac{\partial}{\partial t} - \frac{\beta_2}{2}\frac{\partial^2}{\partial t^2}\\ &+ \left(\frac{\partial\beta_f}{\partial(|\phi|^2)}\right)_0|\phi|^2,\end{aligned} \tag{19}$$

where $(...)_0$ denotes the evaluation at $\omega = \omega_0$, $|\phi|^2 = 0$, $\beta_1 = (\frac{\partial\beta}{\partial\omega})_{\omega=\omega_0}$ and $\beta_2 = (\frac{\partial^2\beta}{\partial\omega^2})_{\omega=\omega_0}$. Hence, the propagation constant $\beta(\omega)$ given in Eq. (12) becomes

$$\begin{aligned}\beta(\omega) = \beta_0 &+ i\beta_1\frac{\partial}{\partial t} - \frac{\beta_2}{2}\frac{\partial^2}{\partial t^2} + \left(\frac{\partial\beta_f}{\partial(|\phi|^2)}\right)_0(|\phi|^2)\\ &+ \frac{\omega}{c}n_2|\phi|^2 + \frac{\omega}{c}\frac{n_2\gamma_{xx}}{2}\frac{\partial^2}{\partial x^2}(|\phi|^2) + \frac{\omega}{c}\frac{n_2\gamma_{yy}}{2}\frac{\partial^2}{\partial y^2}(|\phi|^2)\\ &+ i\alpha_f + i\alpha_f\frac{n_2}{n_0}|\phi|^2 + i\alpha_f\frac{n_2}{n_0}\frac{\gamma_{xx}}{2}\frac{\partial^2}{\partial x^2}(|\phi|^2)\\ &+ i\alpha_f\frac{n_2}{n_0}\frac{\gamma_{yy}}{2}\frac{\partial^2}{\partial y^2}(|\phi|^2) + \frac{1}{2}\frac{\omega}{c}\frac{\chi_a}{n_0}.\end{aligned} \tag{20}$$

Using Eq. (20) and substituting χ_a defined in Eq. (4), we derive the following (3+1)D nonlocal cubic CGL equation:

$$\begin{aligned}i\frac{\partial\phi}{\partial z} &+ (\beta_{reff} + i\beta_{ieff})\frac{\partial\phi}{\partial t} + \frac{1}{2\beta_0}\left(\frac{\partial^2\phi}{\partial x^2} + \frac{\partial^2\phi}{\partial y^2}\right)\\ &+ (p_r + ip_i)\frac{\partial^2\phi}{\partial t^2} + (\gamma_r + i\gamma_i)\phi + (q_r + iq_i)|\phi|^2\phi\\ &+ \left(\gamma_{xx,r} + i\gamma_{xx,i}\right)\frac{\partial^2}{\partial x^2}(|\phi|^2)\phi\\ &+ \left(\gamma_{yy,r} + i\gamma_{yy,i}\right)\frac{\partial^2}{\partial y^2}(|\phi|^2)\phi = 0.\end{aligned} \tag{21}$$

In the above, $\frac{\partial\phi}{\partial z}$ represents the displacement of the light pulse over the propagation distance z. The expression $\left(\frac{\partial^2\phi}{\partial x^2} + \frac{\partial^2\phi}{\partial y^2}\right)$ corresponds to the linear diffraction of the light pulse along the transverse directions x and y. The terms $\frac{\partial^2}{\partial x^2}(|\phi|^2)\phi$ and $\frac{\partial^2}{\partial y^2}(|\phi|^2)\phi$ correspond to the nonlinear diffraction related to spatial nonlocality. This nonlinear diffraction is associated with linear diffraction in order to influence self-focusing and avoid collapse [34]. The parameters $\beta_{reff} = -\frac{g_p}{2n_0}\frac{2\delta T_2}{(1+\delta^2)^2}$ and $\beta_{ieff} = \beta_1 + \frac{g_p}{2n_0}\frac{(1-\delta^2)T_2}{(1+\delta^2)^2}$, are the real and imaginary parts of the inverse of the group velocity, respectively. The coefficient $p_r = -\frac{\beta_2}{2} - \frac{g_p}{2n_0}\frac{\delta(\delta^2-3)T_2^2}{(1+\delta^2)^3}$, measures the wave dispersion, and $p_i = -\frac{g_p}{2n_0}\frac{(1-3\delta^2)T_2^2}{(1+\delta^2)^3}$ is the spectral filtering. The term $\gamma_r = \frac{g_p}{2n_0}\frac{\delta}{(1+\delta^2)}$ is the linear loss/gain, and $\gamma_i = \alpha_f - \frac{g_p}{2n_0}\frac{1}{(1+\delta^2)}$ is the frequency shift. The parameter $q_r = n_2\frac{\omega}{c} + \left(\frac{\partial\beta_f}{\partial(|\phi|^2)}\right)_0$ represents the nonlinear coefficient. The case $q_r>0$ corresponds to the self-focusing Kerr nonlinearity, while the case $q_r<0$ corresponds to the self-defocusing Kerr nonlinearity. The parameter $q_i = n_2\frac{\alpha_f}{n_0}$, accounts for nonlinear gain (loss) and/or other amplification (absorption) processes. Expressions $\gamma_{xx,r} = \frac{1}{2}\frac{n_2\omega}{c}\gamma_{xx}$, $\gamma_{yy,r} = \frac{1}{2}\frac{n_2\omega}{c}\gamma_{yy}$, $\gamma_{xx,i} = \frac{1}{2}\frac{n_2\alpha_f}{n_0}\gamma_{xx}$, and $\gamma_{yy,i} = \frac{1}{2}\frac{n_2\alpha_f}{n_0}\gamma_{yy}$, represent the real and imaginary parts of the nonlocality degrees along the transverse coordinates x and y, respectively.

To scale Eq. (21), we introduce the following physical parameters, namely, the diffraction length or Rayleigh length in the homogeneous medium: $L_{Diff} = \beta_0 r_0^2$, where r_0 is the beam radius. The dispersion length $L_{Disp} = \frac{T_0^2}{|p_r|}$, with T_0 representing the typical initial pulse width. The effective length characterizing the influence of the nonlinearity $L_{NL} = \frac{1}{q_r P_0}$, where P_0 is the peak power of the incident

pulse. The transverse coordinates scale are $X = \frac{x}{r_0}$ and $Y = \frac{y}{r_0}$, respectively. The longitudinal coordinate scale $Z = \frac{z}{L_{Disp}}$, and the temporal coordinate scale $\tau = \frac{T}{T_0}$. Here, $T = t - \frac{z}{v_g}$ is the time in the moving coordinate system. The normalized field amplitude is $\Phi(X, Y, Z, \tau) = \sqrt{P_0} N \phi(x, y, z, t)$, where $N^2 = \frac{L_{Disp}}{L_{NL}}$, with $N = \sqrt{\frac{q_r P_0 T_0^2}{|p_r|}}$. We also set $a_1 = \frac{p_i}{p_r}$, $b_1 = \frac{\gamma_i}{\gamma_r}$, $c_0 = \frac{q_i}{q_r}$, $c_{1,XX} = \frac{\gamma_{XX,i}}{\gamma_{XX,r}}$, and $c_{2,YY} = \frac{\gamma_{YY,i}}{\gamma_{YY,r}}$.

Taking into account these scaling transformations, Eq. (21) then takes the form

$$\begin{aligned} i\frac{\partial\Phi}{\partial Z} &+ \zeta_1\left(\frac{\partial^2\Phi}{\partial X^2} + \frac{\partial^2\Phi}{\partial Y^2}\right) + \left(1 + ia_1\right)\zeta_2\frac{\partial^2\Phi}{\partial\tau^2} \\ &+ \left(1 + ib_1\right)\zeta_3\Phi + \left(1 + ic_0\right)\zeta_4|\Phi|^2\Phi \\ &+ \left(1 + ic_{1,XX}\right)\zeta_5\frac{\partial^2}{\partial X^2}(|\Phi|^2)\Phi \\ &+ \left(1 + ic_{2,YY}\right)\zeta_6\frac{\partial^2}{\partial Y^2}(|\Phi|^2)\Phi = 0, \end{aligned} \tag{22}$$

where $\zeta_1 = \frac{L_{Disp}}{\beta_0 r_0^2}$, $\zeta_2 = \frac{p_r L_{Disp}}{T_0^2 N\sqrt{P_0}}$, $\zeta_3 = \gamma_r L_{Disp}$, $\zeta_4 = \frac{q_r L_{NL}}{P_0}$, $\zeta_5 = \frac{\gamma_{XX} L_{NL}}{P_0 r_0^2}$, and $\zeta_6 = \frac{\gamma_{YY} L_{NL}}{P_0 r_0^2}$. Considering Eq. (24), for $a_1 = b_1 = c_0 = c_{1,XX} = c_{2,YY} = 0$, and neglecting the second-order dispersion term $\frac{\partial^2\Phi}{\partial\tau^2}$, we recover the (2+1)D nonlocal nonlinear Schrödinger (NLS) equation that was derived by Bezuhanov et al. [34] in the limit of weak nonlocality. The conditions for breathing soliton formation in one and two transverse dimensions were established for this equation. Furthermore, it was shown that the interplay between nonlinear diffraction and self-focusing is found to result in an increase of the power needed to form nonlocal spatial solitons. Indeed, the nonlocal 2D NLS equation has been also derived by Skupin et al. [35] in the highly nonlocal limit. Due to the mixture of local and nonlocal types of nonlinearity (Gaussian model of nonlocality, thermal nonlinearity, and the model of a dipolar Bose-Einstein condensate), a variety of solutions, such as rotating and nonrotating azimuthons, accessible solitons can be stabilized. Moreover, the stabilization of 2D ring dark solitons and ring anti-dark solitons was demonstrated in nonlocal media [36].

3. Analytical treatment using variational approach

In this section, we employ the variational method [37–39] for dissipative systems to look for approximated solutions to Eq. (22) and obtain physical insight in terms of a few relevant parameters that will be then implemented in numerical simulations to confirm the analytic predictions qualitatively. In order to describe the dynamics of pulse evolution, various treatments have been developed to extract approximated soliton solutions to integrable and non-integrable nonlinear partial differential equations and have received many different names depending on the field of application, namely the method of moments [40], the method of collective coordinates [20,27,41], the time-dependent variational method [38], the effective-particle method [42,43], averaged Lagrangian description [39,44], to name a few. Lagrangian methods have become widely accepted as the preferred approach to account for the dynamics of the light pulse in optical fiber. Thus, in order to use the variational approach, the (3+1)D nonlocal cubic CGL equation can be rewritten in the form

$$\begin{aligned} i\frac{\partial\Phi}{\partial Z} &+ \zeta_1\left(\frac{\partial^2\Phi}{\partial X^2} + \frac{\partial^2\Phi}{\partial Y^2}\right) + \zeta_2\frac{\partial^2\Phi}{\partial\tau^2} + \zeta_3\Phi \\ &+ \zeta_4|\Phi|^2\Phi + \zeta_5\frac{\partial^2}{\partial X^2}(|\Phi|^2)\Phi \\ &+ \zeta_6\frac{\partial^2}{\partial Y^2}(|\Phi|^2)\Phi = \mathcal{Q}, \end{aligned} \tag{23}$$

in which the right-hand side contains dissipative terms

$$\begin{aligned} \mathcal{Q} = &-ia_1\zeta_2\frac{\partial^2\Phi}{\partial\tau^2} - ib_1\zeta_3\Phi - ic_0\zeta_4|\Phi|^2\Phi \\ &- ic_{1,XX}\zeta_5\frac{\partial^2}{\partial X^2}(|\Phi|^2)\Phi - ic_{2,YY}\zeta_6\frac{\partial^2}{\partial Y^2}(|\Phi|^2)\Phi. \end{aligned} \tag{24}$$

It should be noted that defining an appropriate ansatz function is essential for using the variational approach. In doing so, let us consider the trial function of the Gaussian shape

$$\begin{aligned} \Phi(X, Y, Z, \tau) = A(Z)\exp\Big(&-\frac{X^2}{\sigma_X^2(Z)} - \frac{Y^2}{\sigma_Y^2(Z)} \\ &- \frac{\tau^2}{\sigma_\tau^2(Z)} + \frac{ik_0}{2}(\vartheta_X(Z)X^2 \\ &+ \vartheta_Y(Z)Y^2 + \vartheta_\tau(Z)\tau^2) + i\psi(Z)\Big), \end{aligned} \tag{25}$$

where $A(Z)$ is the amplitude, $\sigma_X(Z)$ and $\sigma_Y(Z)$ are the beamwidths in the transverse coordinates (X, Y), $\sigma_\tau(Z)$ is the temporal beamwidth, $\vartheta_X(Z)$ and $\vartheta_Y(Z)$ are the wave-front curvatures along the transverse coordinates (X, Y), $\vartheta_\tau(Z)$ is the temporal wave-front curvature, $\psi(Z)$ is the phase, and k_0 is the wavenumber. Variables $A(Z)$, $\sigma_X(Z)$, $\sigma_Y(Z)$, $\sigma_\tau(Z)$, $\vartheta_X(Z)$, $\vartheta_Y(Z)$, $\vartheta_\tau(Z)$ and $\psi(Z)$ are all the parameters of the light pulse. Then, we obtain the first-order differential equations (FODEs) of these parameters, which describe the evolution of the light pulse in the optical fiber. The variational approach used in this study is based on the Euler-Lagrange equation [45,46]

$$\begin{aligned} \frac{d}{dZ}\left(\frac{\partial\langle L_c\rangle}{\partial q'}\right) - \frac{\partial\langle L_c\rangle}{\partial q} \\ = 2\mathrm{Re}\left\{\iiint dX dY d\tau \mathcal{Q}\frac{\partial\Phi^*}{\partial q}\right\}, \end{aligned} \tag{26}$$

where Φ^* is the complex conjugate of the ansatz function Φ, $\mathrm{Re}\{\cdot\}$ denotes the real part, and q is the variable that corresponds to all the parameters of the light pulse ($A(Z)$, $\sigma_X(Z)$, $\sigma_Y(Z)$, $\sigma_\tau(Z)$, $\vartheta_X(Z)$, $\vartheta_Y(Z)$, $\vartheta_\tau(Z)$, $\psi(Z)$), with ($q' = \frac{dq}{dZ}$). The left-hand side of Eq. (23), represents the conservative Lagrange's equation, with the conservative Lagrangian L_c being given by

$$\begin{aligned} L_c = &i\frac{\partial\Phi}{\partial Z} + \zeta_1\left(\frac{\partial^2\Phi}{\partial X^2} + \frac{\partial^2\Phi}{\partial Y^2}\right) + \zeta_2\frac{\partial^2\Phi}{\partial\tau^2} \\ &+ \zeta_3\Phi + \zeta_4|\Phi|^2\Phi + \zeta_5\frac{\partial^2}{\partial X^2}(|\Phi|^2)\Phi \\ &+ \zeta_6\frac{\partial^2}{\partial Y^2}(|\Phi|^2)\Phi. \end{aligned} \tag{27}$$

Moreover, $\langle L_c\rangle$ is the Lagrangian density written as

$$\langle L_c\rangle = \iiint L_c dX dY d\tau, \tag{28}$$

and the right-hand side $\mathcal{Q}$ of Eq. (23) is the dissipative term. Using Eqs. (24)-(28), we get the following set of coupled first-order differential equations resulting from the variation with respect to the light pulse parameters:

$$\begin{aligned} \frac{dA}{dZ} = &-A\zeta_1 k_0\vartheta_X - A\zeta_1 k_0\vartheta_Y - A\zeta_2\vartheta_\tau - \frac{7}{2}Ab_1\zeta_3 \\ &- \frac{77}{16}A^3\sqrt{2}c_0\zeta_4 + \frac{1}{8}Aa_1\zeta_2\left(35k_0^2\vartheta_\tau^2\sigma_\tau^2 + \frac{156}{\sigma^2}\right) \\ &+ \frac{1}{128}A^3\sqrt{2}c_{1,XX}\zeta_5\left(75k_0^2\vartheta_X^2\sigma_X^2 + \frac{996}{\sigma_X^2}\right) \\ &+ \frac{1}{128}A^3\sqrt{2}c_{2,YY}\zeta_6\left(75k_0^2\vartheta_Y^2\sigma_Y^2 + \frac{996}{\sigma_Y^2}\right), \end{aligned} \tag{29a}$$

$$\frac{d\sigma_X}{dZ} = 2\zeta_1 k_0\vartheta_X\sigma_X + b_1\zeta_3\sigma_X + \frac{15}{8}A^2\sqrt{2}c_0\zeta_4\sigma_X$$

$$+\frac{1}{4}a_1\zeta_2\left(-7k_0^2\vartheta_\tau^2\sigma_\tau^2-\frac{28}{\sigma_\tau^2}\right)\sigma_X$$
$$+\frac{1}{64}A^2\sqrt{2}c_{1,XX}\zeta_5\left(13k_0^2\vartheta_X^2\sigma_X^2-\frac{252}{\sigma_X^2}\right)\sigma_X$$
$$+\frac{15}{64}A^2\sqrt{2}c_{2,YY}\zeta_6\left(-k_0^2\vartheta_Y^2\sigma_Y^2-\frac{12}{\sigma_Y^2}\right)\sigma_X, \tag{29b}$$

$$\frac{d\sigma_Y}{dZ}=2\zeta_1k_0\vartheta_Y\sigma_Y+b_1\zeta_3\sigma_Y+\frac{15}{8}A^2\sqrt{2}c_0\zeta_4\sigma_Y$$
$$+\frac{1}{4}a_1\zeta_2\left(-7k_0^2\vartheta_\tau^2\sigma_\tau^2-\frac{28}{\sigma_\tau^2}\right)\sigma_Y$$
$$+\frac{15}{64}A^2\sqrt{2}c_{1,XX}\zeta_5\left(-k_0^2\vartheta_X^2\sigma_X^2-\frac{12}{\sigma_X^2}\right)\sigma_Y$$
$$+\frac{1}{64}A^2\sqrt{2}c_{2,YY}\zeta_6\left(13k_0^2\vartheta_Y^2\sigma_Y^2-\frac{252}{\sigma_Y^2}\right)\sigma_Y, \tag{29c}$$

$$\frac{d\sigma_\tau}{dZ}=2\zeta_2\vartheta_\tau\sigma_\tau+b_1\zeta_3\sigma_\tau+\frac{15}{8}A^2\sqrt{2}c_0\zeta_4\sigma_\tau$$
$$+\frac{1}{4}a_1\zeta_2\left(-5k_0^2\vartheta_\tau^2\sigma_\tau^2-\frac{36}{\sigma_\tau^2}\right)\sigma_\tau$$
$$+\frac{15}{64}A^2\sqrt{2}c_{1,XX}\zeta_5\left(-k_0^2\vartheta_X^2\sigma_X^2-\frac{12}{\sigma_X^2}\right)\sigma_\tau$$
$$+\frac{15}{64}A^2\sqrt{2}c_{2,YY}\zeta_6\left(-k_0^2\vartheta_Y^2\sigma_Y^2-\frac{12}{\sigma_Y^2}\right)\sigma_\tau, \tag{29d}$$

$$\frac{d\vartheta_X}{dZ}=A^2\sqrt{2}\zeta_4\frac{1}{k_0\sigma_X^2}+8\zeta_1\frac{1}{\sigma_X^4}-2\zeta_1k_0\vartheta_X^2$$
$$+\frac{1}{36}\frac{A^2\sqrt{2}c_{1,XX}\zeta_5}{k_0\sigma_X^2}\left(\frac{216}{\sigma_X^2}+127k_0\vartheta_X\right)$$
$$+\frac{1}{36}\frac{A^2\sqrt{2}c_{2,YY}\zeta_6}{k_0\sigma_X^2}\left(\frac{72}{\sigma_Y^2}+73k_0\vartheta_Y\right), \tag{29e}$$

$$\frac{d\vartheta_Y}{dZ}=A^2\sqrt{2}\zeta_4\frac{1}{k_0\sigma_Y^2}+8\zeta_1\frac{1}{\sigma_Y^4}-2\zeta_1k_0\vartheta_Y^2$$
$$+\frac{1}{36}\frac{A^2\sqrt{2}c_{1,XX}\zeta_5}{k_0\sigma_Y^2}\left(\frac{72}{\sigma_X^2}+73k_0\vartheta_X\right)$$
$$+\frac{1}{36}\frac{A^2\sqrt{2}c_{2,YY}\zeta_6}{k_0\sigma_Y^2}\left(\frac{216}{\sigma_Y^2}+127k_0\vartheta_Y\right), \tag{29f}$$

$$\frac{d\vartheta_\tau}{dZ}=A^2\sqrt{2}\zeta_4\frac{1}{k_0\sigma_\tau^2}+8a_1\zeta_2\frac{\vartheta_\tau}{\sigma_\tau^2}$$
$$-8\zeta_2\frac{1}{k_0\sigma_\tau^4}-2\zeta_2k_0\vartheta_\tau^2$$
$$+\frac{1}{36}\frac{A^2\sqrt{2}c_{1,XX}\zeta_5}{k_0\sigma_\tau^2}\left(\frac{72}{\sigma_X^2}+73k_0\vartheta_X\right)$$
$$+\frac{1}{36}\frac{A^2\sqrt{2}c_{2,YY}\zeta_6}{k_0\sigma_\tau^2}\left(\frac{72}{\sigma_Y^2}+73k_0\vartheta_Y\right), \tag{29g}$$

$$\frac{d\psi}{dZ}=-2\frac{\zeta_1}{\sigma_X^2}-2\frac{\zeta_1}{\sigma_Y^2}-2\frac{\zeta_2}{\sigma_\tau^2}$$
$$-\frac{7}{8}A^2\sqrt{2}\zeta_4-\zeta_3-a_1\zeta_2k_0\vartheta_\tau$$
$$+\frac{1}{288}A^2\sqrt{2}c_{1,XX}\zeta_5\left(-\frac{648}{\sigma_X^2}-401k_0\vartheta_X\right)$$
$$+\frac{1}{288}A^2\sqrt{2}c_{2,YY}\zeta_6\left(-\frac{648}{\sigma_Y^2}-401k_0\vartheta_Y\right). \tag{29h}$$

Eq. (29a)-(29h) constitute a complete set of variable parameters characterizing dissipative light bullets in optical fiber amplifiers under the suitable competition between dopants and a spatially nonlocal nonlinear response. To reach the steady-state solutions of the system of Eqs. (29a)-(29g), we set Z derivatives of the light pulse parameters to zero. The problem of light pulse instabilities that depend on the number of space dimensions and nonlinearity strength has recently attracted considerable attention. In fact, the existence and stability of multidimensional optical dissipative soliton solutions of the cubic-quintic CGL equation were addressed and comprehensively analyzed [39]. In the dissipative case, it was already remarked that the family of solutions reduces to a fixed double solution for a given set of dissipative parameters [47]. Indeed, only symmetric steady-state solutions with equal spatial widths, curvatures, and nonlocality degrees can exist, which means $\sigma_X=\sigma_Y=\sigma_{X=Y}=\sigma$, $\vartheta_X=\vartheta_Y=\vartheta_{X=Y}=\vartheta$, $\gamma_{XX}=\gamma_{YY}=\gamma_{X=Y}$, $\zeta_5=\zeta_6=\zeta_{X=Y}$ and $c_{1,XX}=c_{2,YY}=c_{X=Y}$. Under such conditions, the amplitude as a steady state solution of Eqs. (29a)-(29g) has two discrete values A_+ and A_- given by

$$A_\pm=\sqrt{\frac{-D\pm\sqrt{D^2-4BC}}{2B}}+O(\theta^2), \tag{30}$$

where

$$B=\sqrt{2}\zeta_4\zeta_{X=Y}c_{X=Y}(240a_1-496c_0-249),$$
$$D=-320b_1\zeta_3\zeta_{X=Y}c_{X=Y}+\zeta_1\zeta_4(128a_1-256c_0), \tag{31}$$
$$C=-128\sqrt{2}b_1\zeta_1\zeta_3,$$

and $\theta=\max\left(|a_1\zeta_2|,|b_1\zeta_3|,|c_0\zeta_4|,|c_{X=Y}\zeta_{X=Y}|\right)$. The other relevant stationary solutions are explicitly given by the following four-parameter family of the dissipative light bullets:

(i) The beamwidth in the transverse coordinates

$$\sigma_{X=Y}=\frac{2\sqrt{-\zeta_4\left(2\zeta_{X=Y}c_{X=Y}A^2+\sqrt{2}\zeta_1\right)}}{A\zeta_4}+O(\theta^2), \tag{32}$$

(ii) The temporal beamwidth

$$\sigma_\tau=\frac{2\sqrt{\zeta_4\sqrt{2}\zeta_2}}{A\zeta_4}+O(\theta^2), \tag{33}$$

(iii) The wave-front curvatures along the transverse coordinates

$$\vartheta_{X=Y}=\frac{1}{32k_0\zeta_1\left(2A^2\zeta_{X=Y}c_{X=Y}+\sqrt{2}\zeta_1\right)}$$
$$\times\left(28A^2a_1\zeta_1\zeta_4-60A^2c_0\zeta_1\zeta_4\right.$$
$$\left.-32A^2b_1\zeta_3\zeta_{X=Y}c_{X=Y}-16\sqrt{2}b_1\zeta_1\zeta_3\right)+O(\theta^2), \tag{34}$$

(iv) The temporal wave-front curvature

$$\vartheta_\tau=\frac{\left(9A^2\sqrt{2}a_1\zeta_4-15A^2\sqrt{2}c_0\zeta_4-8b_1\zeta_3\right)}{16\zeta_2}+O(\theta^2). \tag{35}$$

To further proceed, we first need to make a remark about the conservative systems. In this case, the total energy or beam power is conserved. For dissipative systems, the total energy or the beam power $P=(\frac{\pi}{2})^{3/2}A^2\sigma_{X=Y}^2\sigma_\tau$ is no longer conserved contrary to the case of conservative systems, but evolves in the so-called balance equation with nonzero curvatures. Therefore, using steady-state solutions given in Eqs. (32) and (33), the total power corresponding to ansatz (25) for the non-conservative (3+1)D nonlocal cubic CGL equation (23) is given by [47]

$$P = \frac{8\left(2\zeta_{X=Y}c_{X=Y}A^2 + \sqrt{2}\zeta_1\right)\sqrt{\zeta_4\sqrt{2}\zeta_2}}{\left(\frac{\pi}{2}\right)^{-3/2}A\zeta_4^2}. \quad (36)$$

It is also worth mentioning that the simultaneous balance between linear diffraction, dispersion, and nonlinear diffraction is induced by the spatial nonlocality and between gain and loss, depending on fixed steady-state solutions with nonzero spatial and temporal curvatures.

4. Stability criterion for steady-state solutions

In order to picture the stability zone, we use the Routh-Hurwitz stability criterion described by a necessary condition and a sufficient condition. Applying this stability criterion requires that we construct a Jacobi determinant. From the latter, we get the polynomial characteristic equation, and we are then able to verify the necessary and sufficient condition of the Routh-Hurwitz stability criterion. In the following, we introduce the notations: $F_A \equiv \frac{dA}{dZ}$, $F_\sigma \equiv \frac{d\sigma}{dZ}$, $F_\vartheta \equiv \frac{d\vartheta}{dZ}$, $F_{\sigma_\tau} \equiv \frac{d\sigma_\tau}{dZ}$, and $F_{\vartheta_\tau} \equiv \frac{d\vartheta_\tau}{dZ}$, resulting from Eqs. (29a)-(29g). Recall that in the case of a symmetric input, the set of Eqs. (29a)-(29g) is reduced to only five equations: (29a), (29b), (29d), (29e) and (29g). The Jacobi determinant is constructed from the derivatives of these terms F_A, F_σ, F_ϑ, F_{σ_τ}, and F_{ϑ_τ}, with respect to amplitude, spatial and temporal widths, spatial and temporal curvatures taken at the equilibrium state

$$\det(J-\lambda I) = \begin{vmatrix} \frac{\partial F_A}{\partial A}-\lambda & \frac{\partial F_A}{\partial \sigma} & \frac{\partial F_A}{\partial \vartheta} & \frac{\partial F_A}{\partial \sigma_\tau} & \frac{\partial F_A}{\partial \vartheta_\tau} \\ \frac{\partial F_\sigma}{\partial A} & \frac{\partial F_\sigma}{\partial \sigma}-\lambda & \frac{\partial F_\sigma}{\partial \vartheta} & \frac{\partial F_\sigma}{\partial \sigma_\tau} & \frac{\partial F_\sigma}{\partial \vartheta_\tau} \\ \frac{\partial F_\vartheta}{\partial A} & \frac{\partial F_\vartheta}{\partial \sigma} & \frac{\partial F_\vartheta}{\partial \vartheta}-\lambda & \frac{\partial F_\vartheta}{\partial \sigma_\tau} & \frac{\partial F_\vartheta}{\partial \vartheta_\tau} \\ \frac{\partial F_{\sigma_\tau}}{\partial A} & \frac{\partial F_{\sigma_\tau}}{\partial \sigma} & \frac{\partial F_{\sigma_\tau}}{\partial \vartheta} & \frac{\partial F_{\sigma_\tau}}{\partial \sigma_\tau}-\lambda & \frac{\partial F_{\sigma_\tau}}{\partial \vartheta_\tau} \\ \frac{\partial F_{\vartheta_\tau}}{\partial A} & \frac{\partial F_{\vartheta_\tau}}{\partial \sigma} & \frac{\partial F_{\vartheta_\tau}}{\partial \vartheta} & \frac{\partial F_{\vartheta_\tau}}{\partial F_{\sigma_\tau}} & \frac{\partial F_{\vartheta_\tau}}{\partial \vartheta_\tau}-\lambda \end{vmatrix} = 0, \quad (37)$$

where I is the identity matrix. The fifth-order characteristic polynomial obtained from the Jacobi determinant is given by

$$\lambda^5 + a_1\lambda^4 + a_2\lambda^3 + a_3\lambda^2 + a_4\lambda + a_5 = 0. \quad (38)$$

The coefficients $a_1, ..., a_5$, depend on the partial derivatives of the functions F_A, F_σ, F_ϑ, F_{σ_τ}, and F_{ϑ_τ} given in the Appendix. However, the analytical expressions of those coefficients could not be presented due to their complicated expressions. For stability to be reached, the necessary condition implies that all the roots of the characteristic Eq. (38) should have negative real parts, i.e., $\mathrm{Re}(\lambda_i) < 0$, with $i = 1,...,5$. The sufficient condition based on the Routh-Hurwitz criterion is such that the coefficients $a_1, ..., a_5$ and their combinations should be positive [44,48], i.e.,

$$a_i > 0, \text{ with } i = 1, ..., 5, \quad (39)$$

and

$$b_1 = \frac{a_1a_2 - a_3}{a_1}, \quad b_3 = \frac{a_1a_4 - a_5}{a_1}, \quad c_1 = \frac{b_1a_3 - a_1b_2}{b_1}, \quad d_1 = \frac{c_1b_3 - b_1c_2}{c_1}. \quad (40)$$

In Fig. 1, we represent the double solutions A_+ and A_- of the steady state amplitudes versus q_i and $\gamma_{X=Y}$, where the dissipative parameter q_i represents the nonlinear loss related to the self-defocusing Kerr nonlinearity ($q_r < 0$), and the parameter $\gamma_{X=Y}$ denotes the symmetric nonlocality degree along the transverse directions. By using the normalized coefficient $N_r = 2^{1/2}(4/3)^{3/4}$ [49], assuming a linear gain γ_r under anomalous dispersion, the following parameter values have been used for illustration: $p_r = 0.579/N_r$, $p_i = 0.201/N_r$, $q_r = -110/N_r$, $\gamma_r = 150/N_r$, $\gamma_i = -530/N_r$, $k_0 = 2\pi/1.55$. As stated before [47], the stability of the solution A_- is only a prerequisite to obtaining optical light bullets after a spatiotemporal self-organized evolution. It can clearly be seen in Fig. 1 that when the spatial nonlocal self-defocusing Kerr nonlinearity response ($\gamma_{X=Y}$) and the nonlinear loss (q_i) increase, the stability zone (yellow area representing A_-) gets expanded. Hence, the nonlocality and the nonlinear loss enhance optical light bullets localization in this regime. On the other hand, the lower blue sheet of Fig. 1 shows that the solution A_+ is everywhere unstable. Therefore, it will be beneficial to pay more attention to the stable solution A_- as it remains the only prerequisite for the formation of stable light bullets during the propagation of an input pulse. So doing, in Fig. 2(a) and (b), the stability zones (hatched areas) are shown for the spatial width versus q_i and $\gamma_{X=Y}$, respectively, while the same procedure is repeated for the temporal widths $\sigma_{X=Y}$ in Fig. 2(c) and (d) for the stable solution A_- under anomalous dispersion. The set of spatial and temporal widths values derived from these diagrams will be chosen from this stability range for the numerical simulations of the input spatiotemporal pulses.

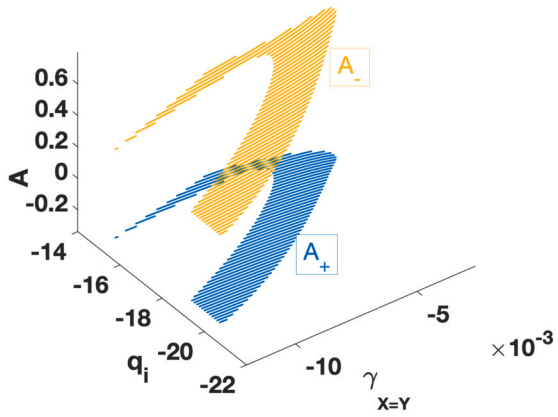

Fig. 1. Double solutions A_+ and A_- of the steady state amplitudes versus q_i and $\gamma_{X=Y}$. The solution A_- (yellow sheet) is stable. The solution A_+ (blue sheet) is rather unstable. The following parameter values have been used: $N_r = 2^{1/2}(4/3)^{3/4}$ (the normalized coefficient), $p_r = 0.579/N_r$ (the anomalous dispersion), $p_i = 0.201/N_r$ (the spectral filtering), $q_r = -110/N_r$ (the self-defocusing Kerr nonlinearity), $\gamma_r = 150/N_r$ (the linear gain), $\gamma_i = -530/N_r$ (the frequency shift), and $k_0 = 2\pi/1.55$ (the wavenumber).

Zones of stability for the spatial and temporal chirps, $\vartheta_{X=Y}$ and ϑ_τ, respectively, versus q_i and $\gamma_{X=Y}$, for the stable solution A_- and the anomalous dispersion are depicted in Fig. 3. The set of spatial and temporal chirps derived from these curves will be chosen from this stability range for the numerical simulations of the input spatiotemporal pulses.

The stability zones for the phase ψ are depicted in Fig. 4(a) and (b) versus q_i and $\gamma_{X=Y}$, respectively, for the stable solution A_- under the anomalous dispersion. The set of phase values obtained from these diagrams will be chosen from this stability range for the numerical implementation of the input spatiotemporal pulses.

5. Numerical experiments

Numerical studies of the evolution of the dissipative light bullet along a doped and weakly nonlocal optical fiber are carried out by means of the fourth-order Runge-Kutta computational method and the split-step Fourier method. The accuracy of numerical experiments is examined by testing different time and space steps. The mesh sizes are chosen as $\Delta X = \Delta Y = 0.002$ and $\Delta\tau = 0.003$. Then, we solve the original (3+1)D nonlocal cubic CGL equation given in Eq. (23) via the split-step Fourier method with the longitudinal step size $\Delta Z = 0.063 \times 10^{-6}$, over a total distance $Z = 200$. The following typical optical pulse parameters used in fiber-optic communication systems are adopted [17,50,68]: the wavelength $\lambda = 1.55$ μm, the linear refractive index $n_0 = 1.45$ cm^2/W, the nonlinear refractive index $n_2 = 2.7 \times 10^{-13}$ cm^2/W, the group veloc-

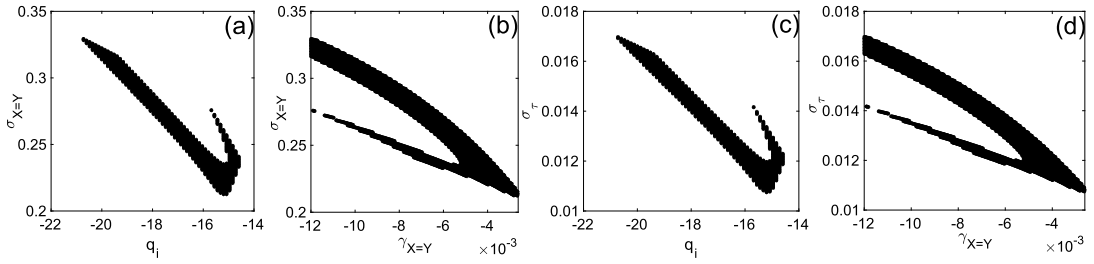

Fig. 2. Diagrams of stability in the $(q_i, \sigma_{X=Y})$-plane [panel (a)], the $(\gamma_{X=Y}, \sigma_{X=Y})$-plane [panel (b)], the (q_i, σ_τ)-plane [panel(c)] and the $(\gamma_{X=Y}, \sigma_\tau)$-plane [panel(d)], where the dark zone stands for the stable solution A_- under anomalous dispersion. The parameter values used are the same as in Fig. 1.

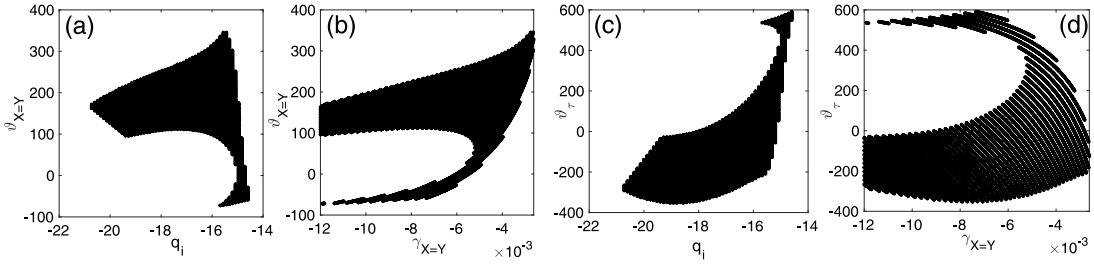

Fig. 3. Diagrams of stability in the $(q_i, \vartheta_{X=Y})$-plane [panel (a)], the $(\gamma_{X=Y}, \vartheta_{X=Y})$-plane [panel (b)], the (q_i, ϑ_τ)-plane [panel(c)] and the $(\gamma_{X=Y}, \vartheta_\tau)$-plane [panel(d)], where the dark zone stands for the stable solution A_- under anomalous dispersion. The parameter values used are the same as in Fig. 1.

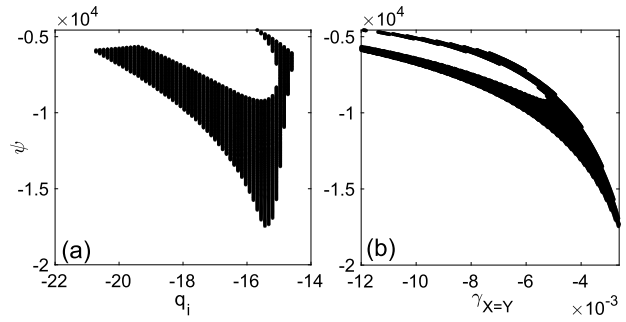

Fig. 4. Panel (a) shows the stability zone (dark area) for the solution A_- in the (q_i, ψ)-plane, while panel (b) displays the stability zone in the $(q_i, \gamma_{X=Y})$-plane, under anomalous dispersion. Parameter values are those used in Fig. 1.

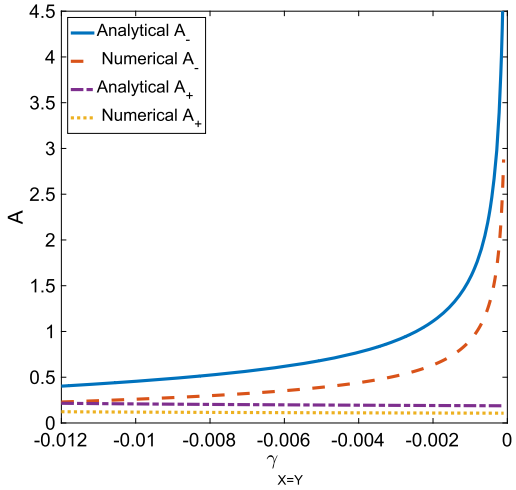

Fig. 5. Analytical and numerical bifurcation curves of the steady state solutions A_- and A_+ for anomalous dispersion, respectively, $p_r = 0.579/N_r$ and for the following parameter values: $N_r = 2^{1/2}(4/3)^{3/4}$, $p_i = 0.201/N_r$, $q_r = -110/N_r$, $q_i = -14.7/N_r$, $\gamma_r = 150/N_r$, $\gamma_i = -530/N_r$, and $k_0 = 2\pi/1.55$.

ity dispersion $\beta_2 = 50$ ps^2/km, the nonlinear gain $g_p = 6.8$ W^{-1}km^{-1}, the pulse width $1.763T_0 = 400$ fs, the peak power of the incident pulse $P_0 = 9.43$ MW, and the nonlinear parameter q_r.

To start, the analytically generated variational bifurcation branches for A_- and A_+ are compared to numerically obtained branches in Fig. 5. Precision should, however, be made that values of parameters used to generate the numerical branches have been chosen from the stable zones of Figs. 1-4, as indicated earlier. The obtained analytical features corresponding to the steady-state solutions of the amplitudes A_- and A_+ as functions of the spatial nonlocality parameter $\gamma_{X=Y}$, respectively, are a good approximation of the numerically obtained curves. Along the same line, the analytical and numerical solutions of the steady-state A_- highlight the upper stable branches. On the contrary, the curves describing the analytical and numerical solutions of the steady-state A_+ are on the lower unstable branches. For the stable evolution of the self-organized dissipative light bullets represented in numerical simulations, we choose the stable solution A_- as an input spatiotemporal pulse.

Fig. 6 shows clearly that the light pulse remains practically constant during its evolution in the spatial domain. We can then notice that the anomalous dispersion, the linear diffraction, the linear gain and the nonlinear diffraction, the spatial nonlocal self-defocusing Kerr nonlinearity response, and the nonlinear loss are well balanced.

In Fig. 7, the temporal input and output are identical, showing that no loss has been observed. In the same way, we can notice that the anomalous dispersion, the linear diffraction, the linear gain and the nonlinear diffraction, the spatial nonlocal self-defocusing Kerr nonlinearity response, and the nonlinear loss are well balanced. From the dynamical behaviors depicted in Fig. 8, we show the evolution of the temporal field profile of the dissipative light bullet intensity distribution in the propagation regime of anomalous dispersion, where the input and output pulses are similar, further confirming our stability predictions, under well-balanced competition from the various involved effects in addition to nonlocality.

For consistency, we consider the unstable region of Fig. 2 and attribute the value $\sigma_{\tau_0} = 0.221$ to the initial temporal parameter. We then obtain the pulse evolution of Fig. 9(a) and its density representation of Fig. 9(b). Under such a particular but noticeable change of temporal parameter, one observes a propagation of the initial pulse that collapses after a short propagation distance. Clearly, the obtained results confirm our predictions since the value of the temporal parameter chosen from the unstable region produces a pulse whose evolution differs from what

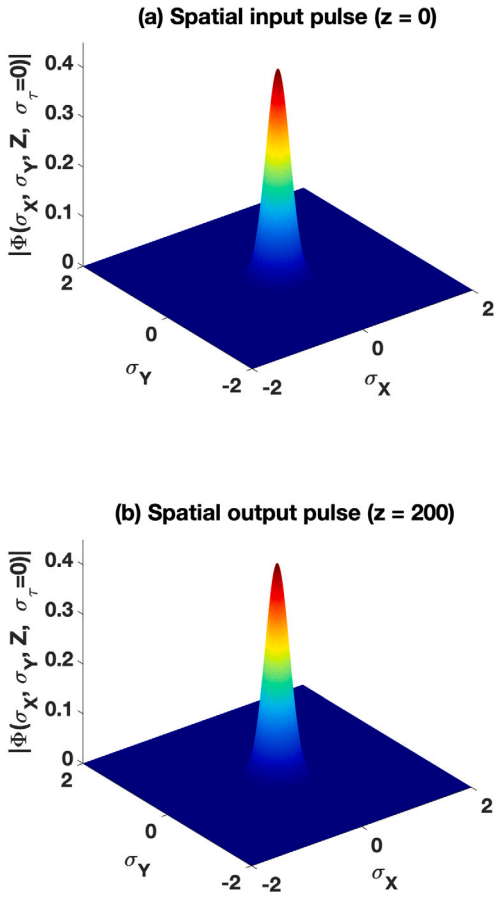

Fig. 6. Profiles of the spatial input [panel (a)] and output pulse [panel (b)] for the stable steady state solution A_- under anomalous dispersion. The following parameters have been used: $\gamma_{X=Y} = -0.007$, $\sigma_{X_0} = \sigma_{Y_0} = 0.2439$, $\vartheta_{X_0} = \vartheta_{Y_0} = -56.03$, $A_{0-} = 0.4225$, $p_r = 0.579/N_r$, $q_i = -14.7/N_r$, $p_i = 0.201/N_r$, $q_r = -110/N_r$, $\gamma_r = 150/N_r$, $\gamma_i = -530/N_r$, $k_0 = 2\pi/1.55$, and $N_r = 2^{1/2}(4/3)^{3/4}$.

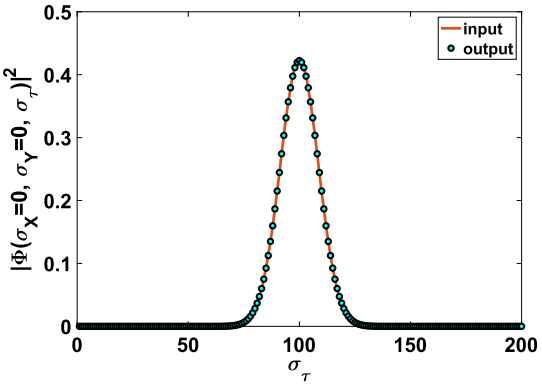

Fig. 7. Profiles of the temporal input and output pulse for the stable steady state solution A_- and for anomalous dispersion. The following parameters have been used: $\gamma_{X=Y} = -0.007$, $\sigma_{\tau_0} = 0.01217$, $\vartheta_{\tau_0} = 572.8$, $A_{0-} = 0.4225$, $p_r = 0.579/N_r$, $q_i = -14.7/N_r$, $p_i = 0.201/N_r$, $q_r = -110/N_r$, $\gamma_r = 150/N_r$, $\gamma_i = -530/N_r$, $k_0 = 2\pi/1.55$, and $N_r = 2^{1/2}(4/3)^{3/4}$.

was reported in Fig. 8. To remind, solitons rely on a balance between dispersion, which tends to spread the wave out, and nonlinearity, which tends to focus the wave. When this balance is disrupted, for instance, due to changes in the medium or external perturbations, the soliton may collapse. Interestingly, the collapse of solitons has been studied in various physical systems, including optics, plasma physics, and condensed matter physics [51–53]. The conditions under which solitons become

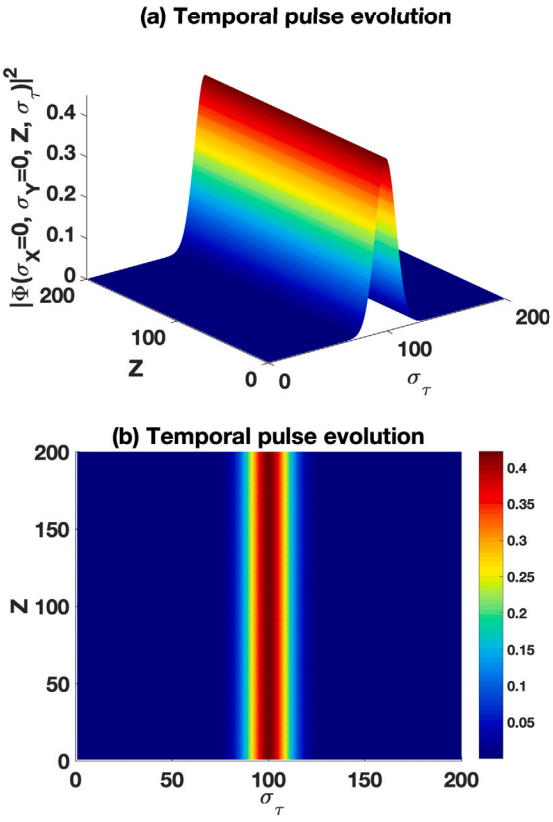

Fig. 8. Profile of the temporal pulse evolution [panel (a)] and its corresponding density plot [panel(b)] for the stable steady state solution under anomalous dispersion. Keeping the rest of parameters as in Fig. 6, the following parameters have been used: $\gamma_{X=Y} = -0.007$, $\sigma_{\tau_0} = 0.01217$, $\vartheta_{\tau_0} = 572.8$, $A_{0-} = 0.4225$, $p_r = 0.579/N_r$, $q_i = -14.7/N_r$, $p_i = 0.201/N_r$, $q_r = -110/N_r$, $\gamma_r = 150/N_r$, $\gamma_i = -530/N_r$, $k_0 = 2\pi/1.55$, and $N_r = 2^{1/2}(4/3)^{3/4}$.

unstable, and collapse have been of great concern since understanding such a phenomenon is crucial for applications in optical communication, where solitons are used to transmit information over long distances without distortion. In our study, such a process involves the proposed nonlocal CGL equation that can be exploited under some conditions, taking advantage of suitable parameter values. In that direction, it is widely known that pulses in optical fibers with phase-sensitive amplifiers are stable over a wide range of parameter values, ensuring effective propagation of information in soliton-based optical communication systems, especially when higher-order effects are considered [54].

6. Concluding remarks

In summary, we have predicted the dissipative light bullets in optical fiber amplifiers for a number of reasons: (i) we have rigorously derived a (3+1)D nonlocal cubic CGL equation valid for the dynamics of the dissipative light bullets in optical fiber amplifiers under the effects fiber dispersion, linear gain, nonlinear loss, fiber nonlinearity, atomic detuning, linear and nonlinear diffractive transverse effects, and nonlocal nonlinear response. (ii) We have also derived eight coupled first-order differential equations of motion of the dissipative light bullet parameters for the nonlocal (3+1)D CGL equation under the interplay between dopants and a spatially weakly nonlocal nonlinear response, with the help of the variational technique using the Gaussian ansatz function. (iii) We have established a Routh-Hurwitz stability criterion for dissipative spatiotemporal light bullets, where a domain of dissipative parameters for stable steady-state solutions has been found. (iv) We have carried out the direct integration of the proposed nonlocal evolution equation, which allowed us to investigate the evolution of

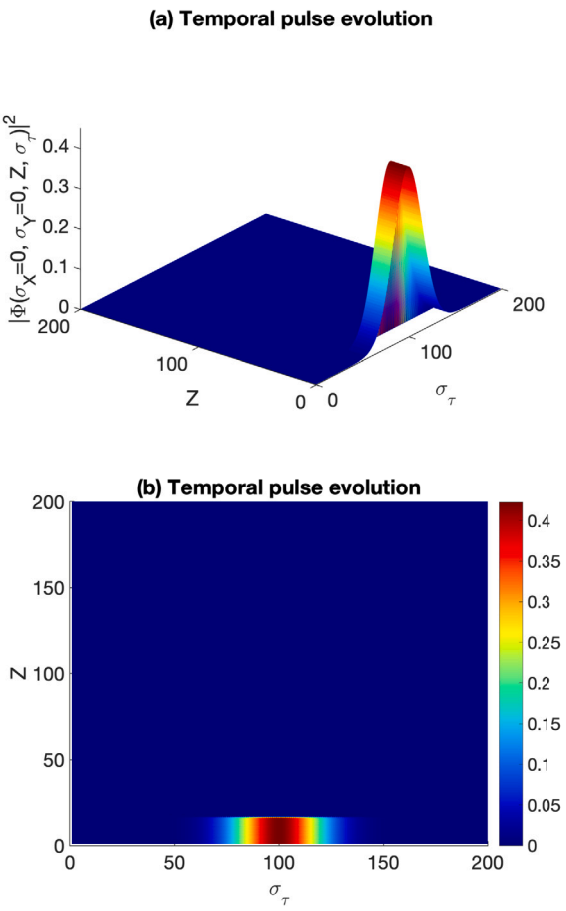

Fig. 9. Profile of the unstable temporal pulse evolution [panel (a)] and its corresponding density plot [panel(b)] for the unstable steady state solution under anomalous dispersion. We have used the same parameter values as in Fig. 8, except for spatial and temporal widths: $\sigma_{\tau_0} = 0.221$.

the Gaussian beam along a doped nonlocal optical fiber, showing stable self-organized dissipative spatiotemporal light bullets.

The CGL equation is a widely used model for describing dissipative systems. It finds applications in various fields such as pulse generation in mode-locked soliton lasers [55–57], signal transmission in all-optical communication lines and metamaterials [58–60], dissipative matter waves in cold atoms [61,62], and pattern formation in several biological systems [63–67]. Depending on the system parameters, the CGL equation has different solutions including solitons, fronts, and pulsating solitons. Considering the nonlocal CGL equation that we have derived, there are undoubtedly systems in other fields to which they would also apply. For example, Kuramoto [69] has proposed the nonlocal CGL equation for populations of biologically oscillating cells secreting substances whose rapid diffusion mediates the cell-cell interaction. It was found that under certain conditions, the correlations and fluctuations obey a power law similar to the one in the fully developed Navier-Stokes turbulence. Also, effective nonlocality in coupling may become relevant when the reaction-diffusion system involves three or more chemical components. Thus, Tanaka and Kuramoto [70] have proposed the nonlocal CGL equation as a reduced form of a universal class of reaction-diffusion systems near the Hopf bifurcation. In this context, novel dynamical states have been predicted, such as multi-affine chemical turbulence [71] and chimera states [72]. In addition, the nonlocal CGL equation has been used extensively to study electrochemical turbulence for electrochemical systems with migration coupling [73,74]. Indeed, oscillatory electrochemical systems can be considered active distributed media and are mathematically described by a set of coupled partial differential equations. They only differ from the reaction-diffusion system in the spatial coupling term of the electric potential drop across the electrode/electrolyte interface. The spatial coupling in electrochemical systems is nonlocal. Some coherent structures have been found in the nonlocal CGL equation in the turbulent regime, which includes standing waves and robust heteroclinic orbits between fixed points or limit cycles [75]. We believe that such studies can be extended to the proposed model by studying their azimuthal manifestation on spherical surfaces, for example. Investigations in that direction are ongoing and will be published elsewhere.

CRediT authorship contribution statement

Ghislaine Flore Kabadiang Ngon: Writing – original draft, Visualization, Formal analysis, Data curation, Conceptualization. **Conrad Bertrand Tabi:** Writing – review & editing, Writing – original draft, Visualization, Validation, Supervision, Project administration, Methodology, Investigation, Funding acquisition, Formal analysis, Data curation, Conceptualization. **Timoléon Crépin Kofané:** Writing – review & editing, Writing – original draft, Formal analysis, Data curation, Conceptualization.

Declaration of competing interest

The authors declare no conflict of interest.

Data availability

Data will be made available on request.

Acknowledgements

The work by CBT is supported by the Botswana International University of Science and Technology under the grant DVC/RDI/2/1/16I (25). CBT thanks the Kavli Institute for Theoretical Physics (KITP), the University of California Santa Barbara (USA), where this work was supported in part by the National Science Foundation Grant no. NSF PHY-1748958, NIH Grant no. R25GM067110, and the Gordon and Betty Moore Foundation Grant no. 2919.01.

Appendix A. Partial derivatives of the functions F_A, F_σ, F_ϑ, F_{σ_τ}, F_{ϑ_τ}

$$\begin{aligned}
\frac{\partial F_A}{\partial A} &= -\zeta_1 k_0 \vartheta - \zeta_1 k_0 \vartheta - \zeta_2 \vartheta_\tau - (7\zeta_3 b_1)/2 \\
&\quad - (231A^2\sqrt{2}c_0\zeta_4)/16 + a_1\zeta_2(35k_0^2\vartheta_\tau^2\sigma_\tau^2 + 156/\sigma_\tau^2)/8 \\
&\quad + (3A^2 c_{X=Y}\zeta_{X=Y}\sqrt{2}(75k_0^2\vartheta^2\sigma^2 + 996/\sigma^2))/128 \\
&\quad + (3A^2 c_{X=Y}\zeta_{X=Y}\sqrt{2}(75k_0^2\vartheta^2\sigma^2 + 996/\sigma^2))/12, \\
\frac{\partial F_\sigma}{\partial A} &= (15A\sqrt{2}c_0\zeta_4\sigma)/4 \\
&\quad + (A\sqrt{2}c_{X=Y}\zeta_{X=Y}(13k_0^2\vartheta^2\sigma^2 - 252/\sigma^2)\sigma)/32 \\
&\quad + (15A\sqrt{2}c_{X=Y}\zeta_{X=Y}(-k_0^2\vartheta^2\sigma^2 - 12/\sigma^2)\sigma)/32, \\
\frac{\partial F_{\sigma_\tau}}{\partial A} &= (15A\sqrt{2}c_0\zeta_4\sigma_\tau)/4 \\
&\quad + (15A\sqrt{2}c_{X=Y}\zeta_{X=Y}(-k_0^2\vartheta^2\sigma^2 - 12/\sigma^2)\sigma_\tau)/32 \\
&\quad + (15A\sqrt{2}c_{X=Y}\zeta_{X=Y}(-k_0^2\vartheta^2\sigma^2 - 12/\sigma^2)\sigma_\tau)/32, \\
\frac{\partial F_\vartheta}{\partial A} &= 2A\sqrt{2}\zeta_4/(k_0\sigma^2) + (A\sqrt{2}c_{X=Y}\zeta_{X=Y})(24/\sigma^2 + 5k_0\vartheta)/(2k_0\sigma^2) \\
&\quad + (A\sqrt{2}c_{X=Y}\zeta_{X=Y})(8/\sigma^2 - k_0\vartheta)/(2k_0\sigma^2), \\
\frac{\partial F_{\vartheta_\tau}}{\partial A} &= 2A\sqrt{2}\zeta_4/(k_0\sigma_\tau^2) + (A\sqrt{2}c_{X=Y}\zeta_{X=Y})(8/\sigma^2 - k_0\vartheta)/(2k_0\sigma_\tau^2)
\end{aligned}$$

$$
\begin{aligned}
&+ (A\sqrt{2}c_{X=Y}\zeta_{X=Y})(8/\sigma^2 - k_0\vartheta)/(2k_0\sigma_\tau^2),\\
\frac{\partial F_A}{\partial\sigma} &= A^3 c_{X=Y}\zeta_{X=Y}\sqrt{2}(150k_0^2\vartheta^2\sigma - 1992/\sigma^3)/128,\\
\frac{\partial F_\sigma}{\partial\sigma} &= 2\zeta_1 k_0\vartheta + \zeta_3 b_1 + (15A^2\sqrt{2}c_0\zeta_4)/8\\
&+ a_1\zeta_2(-7k_0^2\vartheta_\tau^2\sigma_\tau^2 - 28/\sigma_\tau^2)/4\\
&+ A^2\sqrt{2}c_{X=Y}\zeta_{X=Y}(26k_0^2\vartheta^2\sigma + 504/\sigma^3)\sigma/64\\
&+ A^2\sqrt{2}c_{X=Y}\zeta_{X=Y}(13k_0^2\vartheta^2\sigma^2 - 252/\sigma^2)/64\\
&+ (15A^2\sqrt{2}c_{X=Y}\zeta_{X=Y}(-k_0^2\vartheta^2\sigma^2 - 12/\sigma^2))/64,\\
\frac{\partial F_{\sigma_\tau}}{\partial\sigma} &= (15A^2\sqrt{2}c_{X=Y}\zeta_{X=Y}(-2k_0^2\vartheta^2\sigma + 24/\sigma^3)\sigma_\tau)/64,\\
\frac{\partial F_\vartheta}{\partial\sigma} &= -2A^2\sqrt{2}\zeta_4/(k_0\sigma^3) - 32\zeta_1/(k_0\sigma^5) - c_{X=Y}\zeta_{X=Y}A^2\sqrt{2}(24/\sigma^2\\
&+ 5k_0\vartheta)/(2k_0\sigma^3) - 12c_{X=Y}\zeta_{X=Y}A^2\sqrt{2}/(k_0\sigma^5)\\
&- A^2\sqrt{2}c_{X=Y}\zeta_{X=Y}(8/\sigma^2 - k_0\vartheta)/(2k_0\sigma^3),\\
\frac{\partial F_{\vartheta_\tau}}{\partial\sigma} &= -4c_{X=Y}\zeta_{X=Y}A^2\sqrt{2}/(\sigma^3 k_0\sigma_\tau^2),\\
\frac{\partial F_A}{\partial\sigma_\tau} &= Aa_1\zeta_2(70k_0^2\vartheta_\tau^2\sigma_\tau - 312/\sigma_\tau^3)/8,\\
\frac{\partial F_\sigma}{\partial\sigma_\tau} &= a_1\zeta_2\sigma(-14k_0^2\vartheta_\tau^2\sigma_\tau + 56/\sigma_\tau^3)/4,\\
\frac{\partial F_{\sigma_\tau}}{\partial\sigma_\tau} &= 2\zeta_2\vartheta_\tau\\
&+ (15A^2\sqrt{2}c_0\zeta_4)/8 + \zeta_3 b_1 + a_1\zeta_2(-5k_0^2\vartheta_\tau^2\sigma_\tau^2 - 36/\sigma_\tau^2)/4\\
&+ a_1\zeta_2\sigma_\tau(10k_0^2\vartheta_\tau^2\sigma_\tau + 72/\sigma_\tau^3)/4\\
&+ (15A^2\sqrt{2}c_{X=Y}\zeta_{X=Y}(-k_0^2\vartheta^2\sigma^2 - 12/\sigma^2))/32,\\
\frac{\partial F_\vartheta}{\partial\sigma_\tau} &= 0,\\
\frac{\partial F_{\vartheta_\tau}}{\partial\sigma_\tau} &= -2A^2\sqrt{2}\zeta_4/(k_0\sigma_\tau^3) - 16\zeta_2 a_1\vartheta_\tau/\sigma_\tau^3\\
&+ 32\zeta_2/(k_0\sigma_\tau^5) - \zeta_{X=Y}c_{X=Y}A^2\sqrt{2}(8/\sigma^2 - k_0\vartheta)/(k_0\sigma_\tau^3),\\
\frac{\partial F_A}{\partial\vartheta} &= -A\zeta_1 k_0 + (75A^3 c_{X=Y}\zeta_{X=Y}\sqrt{2}k_0^2\vartheta\sigma^2)/64,\\
\frac{\partial F_\sigma}{\partial\vartheta} &= 2\zeta_1 k_0\sigma + (13c_{X=Y}\zeta_{X=Y}A^2\sqrt{2}k_0^2\vartheta\sigma^3)/32,\\
\frac{\partial F_{\sigma_\tau}}{\partial\vartheta} &= -(15A^2\sqrt{2}c_{X=Y}\zeta_{X=Y}k_0^2\vartheta\sigma^2\sigma_\tau)/32,\\
\frac{\partial F_\vartheta}{\partial\vartheta} &= -4\zeta_1 k_0\vartheta + (50\zeta_{X=Y}c_{X=Y}A^2\sqrt{2})/(9\sigma^2),\\
\frac{\partial F_{\vartheta_\tau}}{\partial\vartheta} &= -(\zeta_{X=Y}c_{X=Y}A^2\sqrt{2})/(4\sigma_\tau^2),\\
\frac{\partial F_A}{\partial\vartheta_\tau} &= A\zeta_2 + (35/4)Aa_1\zeta_2 k_0^2\vartheta_\tau\sigma_\tau^2,\\
\frac{\partial F_\sigma}{\partial\vartheta_\tau} &= -(7a_1\zeta_2\sigma k_0^2\vartheta_\tau\sigma_\tau^2)/2,\\
\frac{\partial F_{\sigma_\tau}}{\partial\vartheta_\tau} &= 2\zeta_2\sigma_\tau - 5/2a_1\zeta_2\sigma_\tau^3 k_0^2\vartheta_\tau,\\
\frac{\partial F_\vartheta}{\partial\vartheta_\tau} &= 0,\\
\frac{\partial F_{\vartheta_\tau}}{\partial\vartheta_\tau} &= 8\zeta_2 a_1/\sigma_\tau^2 - 4\zeta_2 k_0\vartheta_\tau.
\end{aligned}
\tag{A.41}
$$

References

[1] B.A. Malomed, D. Mihalache, F.W. Wise, L. Torner, J. Opt. B, Quantum Semiclass. Opt. 7 (2005) R53.
[2] Y. Kivshar, G.P. Agrawal, Optical Solitons: From Fibers to Photonic Crystals, Academic Press, San Diego, 2003.
[3] D. Suter, T. Blasberg, Phys. Rev. A 48 (1993) 4583.
[4] C. Rotschild, O. Cohen, O. Manela, M. Segev, T. Carmon, Phys. Rev. Lett. 95 (2005) 213904.
[5] W. Krolikowski, O. Bang, N.I. Nikolov, D. Neshev, J. Wyller, J.J. Rasmussen, D. Edmundson, J. Opt. B 6 (2004) S288.
[6] H. Tagwo, A. Mohamadou, C.G. Latchio Tiofack, T.C. Kofané, Optik 144 (2017) 246.
[7] O. Bang, W. Krolikowski, J. Wyller, J.J. Rasmussen, Phys. Rev. E 66 (2002) 046619.
[8] M. Peccianti, K.A. Brzdakiewicz, G. Assanto, Opt. Lett. 27 (2002) 1460.
[9] N.I. Nikolov, D. Neshev, W. Krolikowski, O. Bang, J.J. Rasmussen, P.L. Christiansen, Opt. Lett. 29 (2004) 286.
[10] Z. Xu, Y.V. Kartashov, L. Torner, Opt. Lett. 30 (2005) 3171.
[11] A.S. Desyatnikov, Yu.S. Kivshar, L. Torner, Prog. Opt. 47 (2005) 291.
[12] A.I. Yakimenko, Yu.A. Zaliznyak, Yu.S. Kivshar, Phys. Rev. E 71 (2005) 065603.
[13] D. Briedis, D.E. Petersen, D. Edmundson, W. Krolikowski, O. Bang, Opt. Express 13 (2005) 435.
[14] A.S. Desyatnikov, Yu.S. Kivshar, Phys. Rev. Lett. 88 (2002) 053901.
[15] A.S. Desyatnikov, A.A. Sukhorukov, Yu.S. Kivshar, Phys. Rev. Lett. 95 (2005) 203904.
[16] E. Desurvire, J.R. Simpson, P.C. Becker, Opt. Lett. 12 (1987) 888.
[17] G.P. Agrawal, Phys. Rev. A 44 (1991) 7493.
[18] M. Manousakis, S. Droulias, P. Papagiannis, K. Hizanidis, Opt. Commun. 213 (2002) 293.
[19] S.I. Fewo, T.C. Kofané, Opt. Commun. 281 (2008) 2893.
[20] S.I. Fewo, C.M. Ngabireng, T.C. Kofané, J. Phys. Soc. Jpn. 77 (2008) 074401.
[21] C.G. Latchio Tiofack, A. Mohamadou, T.C. Kofané, A.B. Moubissi, Phys. Rev. E 80 (2009) 066604.
[22] E. Ding, J.N. Kutz, J. Opt. Soc. Am. B 26 (2009) 2290.
[23] M. Soljacic, M. Segev, Phys. Rev. Lett. 86 (2001) 420.
[24] I. Towers, B.A. Malomed, J. Opt. Soc. Am. B 19 (2002) 537.
[25] M. Matuszewski, M. Trippenbach, B.A. Malomed, E. Infeld, A.A. Skorupski, Phys. Rev. E 70 (2004) 016603.
[26] Y.J. He, H.H. Fan, J.W. Dong, H.Z. Wang, Phys. Rev. E 74 (2006) 016611.
[27] A. Kamagate, P. Grelu, P. Tchofo-Dinda, J.M. Soto- Crespo, N. Akhmediev, Phys. Rev. E 79 (2009) 026609.
[28] M. Djoko, T.C. Kofané, Opt. Commun. 416 (2018) 190201.
[29] B.A. Malomed, L. Torner, F. Wise, D. Mihalache, J. Phys. B, At. Mol. Opt. Phys. 49 (2016) 170502.
[30] D. Zanga, S.I. Fewo, C.B. Tabi, T.C. Kofané, Commun. Nonlinear Sci. Numer. Simul. 80 (2020) 104993.
[31] C.B. Tabi, H. Tagwo, C.G.L. Tiofack, T.C. Kofané, Opt. Lett. 47 (2022) 5557.
[32] C.G. Tiofack Latchio, C.B. Tabi, H. Tagwo, T.C. Kofané, J. Opt. 25 (2023) 054001.
[33] C.B. Tabi, H. Tagwo, T.C. Kofané, Phys. Rev. E 106 (2022) 054201.
[34] K.S. Bezuhanov, A.A. Dreischuh, W. Krolikowski, Phys. Rev. A 77 (2008) 033825.
[35] S. Skupin, O. Bang, D. Edmundson, W. Krolikowski, Phys. Rev. E 73 (2006) 066603.
[36] W. Chen, Q. Wang, J. Shi, Q. Kong, Y. Chen, M. Shen, J. Phys. B, At. Mol. Opt. Phys. 50 (2017) 135401.
[37] D.J. Kaup, B.A. Malomed, Physica D 87 (1995) 155.
[38] A. Ankiewicz, N. Akhmediev, N. Devine, Opt. Fiber Technol. 13 (2007) 91.
[39] V. Skarka, N.B. Aleksić, H. Lebond, B.A. Malomed, D. Mihalache, Phys. Rev. Lett. 105 (2010) 213901.
[40] P.T. Dinda, A.B. Moubissi, K. Nakkeeran, Phys. Rev. E 64 (2001) 016608.
[41] B.G.O. Essama, J. Atangana, F.B. Motto, B. Mokhtari, E.C. Noureddine, T.C. Kofané, Phys. Rev. E 90 (2014) 032911.
[42] G.D. Montesinos, M.I. Rodas-Verde, V.M. Pérez-García, H. Michinel, Chaos 15 (2005) 033501.
[43] P.M. Morse, H. Feshbach, Methods of Theoretical Physics, McGraw-Hill, 1953.
[44] V. Skarka, N.B. Aleksić, Phys. Rev. Lett. 96 (2006) 013903.
[45] V. Skarka, N.B. Aleksić, D. Gauthier, D.V. Timotijević, PIERS Online 3 (2007) 83–86.
[46] V.M. Pérez-Garcia, V.V. Konotop, J.J. Garcia-Ripoll, Phys. Rev. E 62 (2000) 4301.
[47] V. Skarka, D.V. Timotijević, N.B. Aleksić, J. Opt. A, Pure Appl. Opt. 10 (2008) 075102.
[48] A. Djazet, S.I. Fewo, E.B. Nkouankam Ngompe, T.C. Kofané, Eur. Phys. J. D 74 (2020) 1.
[49] V. Skarka, N.B. Aleksi, V.I. Berezhiani, Phys. Rev. A 81 (2010) 045803.
[50] M. Djoko, T.C. Kofane, Commun. Nonlinear Sci. Numer. Simul. 68 (2019) 169.
[51] K.D. Moll, A.L. Gaeta, Phys. Rev. Lett. 90 (2003) 203902.
[52] M. Erkintalo, G. Genty, B. Wetzel, J.M. Dudley, Opt. Express 18 (2010) 25449.
[53] T. Hansson, D. Anderson, M. Desaix, M. Lisak, Opt. Commun. 284 (2011) 3422.
[54] J. Alexander, M. Grillakis, C. Jones, B. Sandstede, Z. Angew. Math. Phys. 48 (1997) 175.
[55] P. Grelu, N. Akhmediev, Nat. Photonics 6 (2012) 84.
[56] A. Djazet, S.I. Fewo, C.B. Tabi, T.C. Kofané, Appl. Phys. B 127 (2021) 151.
[57] T. Mayteevarunyoo, B.A. Malomed, D.V. Skryabin, Opt. Express 26 (2018) 8849.
[58] M. Abemgnigni Njifon, C.B. Tabi, T.C. Kofané, J. Opt. Soc. Am. B 37 (2020) A331.

[59] L. Megne Tiam, C.B. Tabi, T.C. Kofané, Phys. Rev. E 102 (2020) 042207.
[60] L. Tiam Megne, C.B. Tabi, J.A. Ambassa Otsobo, C.M. Muiva, T.C. Kofané, Nonlinear Dyn. 111 (2023) 20289.
[61] P. Otlaadisa, C.B. Tabi, T.C. Kofané, Phys. Rev. E 103 (2021) 052206.
[62] C.B. Tabi, P. Otlaadisa, T.C. Kofané, Phys. Lett. A 449 (2022) 128334.
[63] P. Legoya, A.S. Etémé, C.B. Tabi, A. Mohamadou, T.C. Kofané, Chaos Solitons Fractals 146 (2022) 112599.
[64] C.D. Bansi Kamdem, P.A. Ndjawa Yomi, C.B. Tabi, A. Mohamadou, Eur. Phys. J. Plus 138 (2023) 176.
[65] B.P. Edouma Biloa, C.B. Tabi, H.P. Ekobena Fouda, T.C. Kofané, Phys. Scr. 98 (2023) 115230.
[66] C.D. Bansi, C.B. Tabi, A. Mohamadou, Chaos Solitons Fractals 109 (2018) 170.
[67] C.B. Tabi, A.S. Etémé, A. Mohamadou, Physica A 474 (2017) 186.
[68] G.P. Agrawal, Nonlinear Fiber Optics, 5th edn, Academic Press, San Diego, 2013.
[69] Y. Kuramoto, Prog. Theor. Phys. 94 (1995) 321.
[70] D. Tanaka, Y. Kuramoto, Phys. Rev. E 68 (2003) 026219.
[71] Y. Kuramoto, D. Battogtokh, H. Nakao, Phys. Rev. Lett. 81 (1998) 3543.
[72] D.M. Abrams, S.H. Strogatz, Phys. Rev. Lett. 93 (2004) 174102.
[73] V. Garcia-Morales, K. Krischer, Phys. Rev. Lett. 100 (2008) 054101.
[74] H. Varela, C. Beta, A. Bonnefont, K. Krischer, Phys. Rev. Lett. 94 (2005) 174104.
[75] V. Garcia-Morales, R.W. Holzel, K. Krischer, Phys. Rev. E 78 (2008) 026215.